UNIVERSITY OF NATAL

THE DETECTION OF FIRES UNDER HIGH VOLTAGE TRANSMISSION LINES

by

CECIL RICHARD EVERT

Submitted in partial fulfilment of the requirements for the degree of Master of Science in Engineering, in the Faculty of Engineering, University of Natal, Durban, South Africa.

FACULTY OF ENGINEERING
King George V Avenue, Durban, 4001, South Africa

JULY, 2003

The whole text of this thesis, unless specifically indicated to the contrary in the text, is the original work of the author.

DECLARATION

I hereby declare that the material incorporated into this thesis is my own original and unaided work except where specific reference is made by name or in the form of a numbered reference. The work contained herein has not been submitted for a degree at any other university.

Signed : 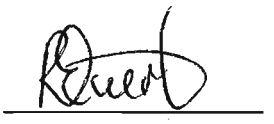

Cecil Richard Evert

Date : December 2003

ABSTRACT

Fires generate heat and propel burning material into the air above and around the core of the fire.

Fires under power lines reduce the breakdown strength of the air insulation due to the influence the heat and particles have on the electric field surrounding the conductors. The result can be flashovers and undesirable power supply interruptions in the electrical transmission network with a considerable impact on Eskom's 275 kV and 400 kV MTS (main transmission system) networks. Eskom typically experiences a loss in sales, a reduction in the quality of the power supplied to consumers and disgruntled consumers who in turn experience financial losses due to a loss in production.

In this thesis, the high frequency characteristics of corona and electrical discharges generated by the fire phenomena are studied. The influence of the operating voltages on the electric fields, the potential of different media to initiate ionisation and comparison of conductor construction (bundling and diameter) are all considered in the measurement of high frequency signals in the range of frequencies available in the tuned circuits connected to power lines.

The propagation of these high frequency signals is studied both in isolation of other sources of high frequency signals (within controlled laboratory conditions) and in the real environment adjacent to all other interfering sources.

Finally the fingerprinting of the varying high frequency signal patterns associated with fires is considered with a view to implementing an operational early detection device.

Early detection of a fire allows the utility to understand the source of a system fault, manage it effectively and if possible pre-empt possible failure by means of appropriately applied standard operating guidelines (SOG) to minimise the impact.

ACKNOWLEDGEMENTS

I acknowledge the support and guidance given in the first instance from the National Energy Council (NEC) in the early 90's and from those that were involved in the steering committee for this project at the time. They were Mr. J.L.M. Pretorius (NEC representative and lecturer at the University of Pretoria), Mr. R.K. Dell (Eskom), Prof. D.A. Swift (Chairman and Head of the Electrical Engineering department at the University of Natal), Prof. J.P. Reynders (Head of the Electrical Engineering department at the University of the Witwatersrand) and Mr. A.C. Britten (Corporate consultant at Eskom's research division "Technology Research and Investigations" now known as "Technology Services International" a division of Eskom Enterprises).

We acknowledge the support and guidance given from the Eskom Technology group and from the Technology Services International division (TSI) to reach the final stages of this research work. With the division's support, this work has culminated in a useful methodology and a practical detection mechanism. A similar document has been prepared for the NEC (Project reference number 219/89) and TSI (Project report number TRR/E/93/EL017).

To the support staff at the corona cage, thank you for the support provided and the additional work done in recording much of the data.

Thank you to Jan Esterhuisen and Bill Cloete from Eskom's National Control for approving the work performed on the Craighall / Lepini 275 kV quad-Zebra bundle. These results were the turning point between laboratory data captured in the corona cage at Eskom's high voltage test facility and the real field measurements.

In the second instance, a wide variety of Eskom personnel and colleagues and members in the sugar cane farming community are thanked for their valuable support. The work was staged in two phases with the second phase of work being completed in August 1997 with a series of sugar cane fires on Verbara Estates in Kwazulu Natal. Thank you to Gerhard van Niekerk (sugar cane farm in Mpumalanga – Tests in November 1992), Jean Roulliard and Howard Essery (Verbara Estates in August 1997) for allowing Eskom to become involved in your harvesting process, for

informing Eskom well in advance that you were planning to burn under the Eskom 275 kV lines and for being prepared to carry out the burning process at Eskom's convenience.

Thank you to the Telecommunications staff in the north eastern Transvaal, Hukkie Huckstead and Quinton Christie for your support and commitment. It was truly appreciated.

Thanks also to the Transmission management in Kwazulu Natal for supporting the extensive alterations to the network required to create the test line conditions under the Avon Impala feeders.

Thank you to the Eskom TSI library services staff for always being available to obtain documents and information from any corner of the globe. This gathering of information has played a large role in ensuring that we do not duplicate work done elsewhere and also helped eliminate outmoded hypotheses.

Thank you especially to A.C. Britten (Tony) for your continued support in this work and providing the ear to which I could speak when considering the new ideas and philosophies. Your feedback and differentiating criteria really assisted the process of understanding the fundamental aspects of the corona phenomena. Your help in using the RMS level detection really added value to the testing done in August 1997. Also thank you to Dr. John van Coller from the University of the Witwatersrand for providing me with a broader perspective of sometimes "tricky" concepts.

Thanks to my supervisor Dr Derek Hoch for his continued patience with the never-ending delays in producing this manuscript. A special thanks must also go to Prof Don Swift for his inputs over the first few years as supervisor of this work at the University of Natal and we wish him well with his health.

To my wife, Karen, who sacrificed much and had more than her fair share of sleepless hours while I documented this work, thank you for your patience and understanding. Without your love, kindness and support this work would not have been possible.

TABLE OF CONTENTS

LIST OF SYMBOLS

ΔW	= energy gained by an electron
e	= electron charge
E	= strength of the electric field
λ	= free path of a particle
λ_e	= free path of an electron
p	= gas pressure
T	= gas temperature
V_i	= ionisation potential
σ	= molecular cross-sectional area of intersection or collision cross-section
σ_i	= cross-section for ionisation
P_i	= probability of ionisation on impact
N	= number of particles per unit volume of gas
∇	= nabla, vector operator differentiating a variable in the x, y and z directions
Q	= point charge
g_v	= visual critical gradient on the conductor before ionisation starts
e_v	= visual critical voltage on the conductor before ionisation starts
g_0	= critical gradient of air (gradient at which air starts to breakdown)
E_{crit}	= electric field at which the probability of ionisation is high
α	= first ionisation coefficient (Townsend)
n	= number of electrons at a distance x from the cathode
I	= discharge current to distance x
I_0	= initial current leaving a cathode
d	= distance between two electrodes
γ	= second ionisation coefficient (Townsend)
η	= attachment of electrons in the travel path
r'	= GMR (geometric mean radius) of each conductor
r''	= overall GMR of the conductor bundle
r	= conductor radius

ε = permittivity of a medium

ε_0 = permittivity of a vacuum or approximately the permittivity of air ($\varepsilon_0 = 8.859 \times 10^{-12}$ F/m)

ε_r = relative permittivity, ratio of the medium's permittivity to the permittivity of a vacuum = $\varepsilon / \varepsilon_0$

μ = permeability of a medium

μ_0 = permeability of a vacuum or approximately of air ($\mu_0 = 1.275 \times 10^{-6}$ H/m)

μ_r = relative permeability for aluminium and copper, taken to be approximately equal to one

n = number of conductors in the conductor bundle

a = bundle radius calculated as a function of s

s = separation between the conductors in a conductor bundle

R = radius of the cylindrical cage (Eskom corona cage diameter = 3.5 m)

C = capacitance of a conductor bundle (in Farads per meter F/m)

L = inductance of a conductor bundle (in Henry per meter H/m)

Z_c = characteristic impedance of the conductor bundle

m_v = smoothness factor of the conductors

k = Boltzmann's constant = 1.3804×10^{-23} joules/°K

θ = ratio of ionised particles to the total number of particles

TABLE OF FIGURES

CHAPTER 1

Introduction

The research work described in this dissertation was performed to develop an aid in the prevention of fire induced high voltage power network failures. The researcher set out to determine the feasibility of identifying induced high frequency signals generated uniquely due to fires under power lines. The induced corona noise was studied as a conducted high frequency current source. The conducted signal had to be detected at existing filtering equipment. By using existing high voltage filtering equipment implementation costs could be kept to a minimum if the solution proved to be effective in eliminating the unwanted system disturbances.

1.1 THE PROBLEM

South Africa has a vast network of extra-high voltage (EHV) substations (more than 146) and transmission lines (over 22 000 kilometres) across the country implemented to supply power to industry and business (54% of total consumption), mines (26%), households (16%) and railways (4%) [a]. This transmission system is robust and must be capable of withstanding the loss of any single circuit without loss of supply to key customers. Quality of supply to large customers, such as Alusaf and Richards Bay Minerals and distributors such as the municipalities is particularly important. A circuit which is under threat of failure must be isolated as quickly as is realistically possible to minimise the depth of the voltage depression which will occur when a short circuiting event - such as a flashover between phases or phase to earth – takes place.

Fires burning under or near power lines are a potential hazard capable of disrupting the transmission and distribution of power. The lines most significantly affected by such disruptions in the Eskom network have been the transmission lines at 275 kV and 400 kV. In all cases including ring feeds, a system fault along a line causes a disruptive voltage-depression or

[a] Prior to the wide scale implementation of the electrification programme. It is understood that small households now consume a higher percentage of overall electricity.

voltage-sag. The net result is a voltage depression across all loads taken from these feeds including loads attached to all the associated step-down transformers. That is, customers across an entire region may experience the disruption to some degree.

Sugar cane fires and veld fires are the major sources of fire related power supply problems. Sugar cane fires occur principally in Kwazulu Natal and Mpumalanga whilst veld fires are found throughout South Africa. An additional source of fire is the Vynbos in the Cape provinces.

Tables are provided in appendix A showing the statistics of fires occurring in South Africa during 1989 to 1991 and the total number of outages occurring for the same period. A brief summary of that data is shown in the table below. On average, approximately 15% of total failures in the years 1989, 1990 and 1991 were due to fire induced faults. In these statistics, the data is reported information. That is, the minimum number of outages which have been caused by fires are reflected in this report. In many instances the source of a fault has been classified as unknown. Some of these may have been as a result of unreported fires. Therefore, a minimum of 346 fire-related incidents occurred in this 2-year-and-5-months period.

Table 1: Fire induced failure statistics

Year	Fire induced faults as a % of total faults	
	275kV network	400kV network
1989 (August to December)	13	17
1990	12	15
1991	15	23

Sugar-cane fires can be categorised into two groups: Fires which are planned by the farmer and fires which take place due to adverse weather conditions, vandalism, carelessness or sabotage. The burning of sugar cane is a common practice amongst the farmers of Kwazulu Natal because it assists in the harvesting process. Eskom has several hundred kilometres of high voltage transmission line in this region. Most of these lines supply key consumers with sensitive load requirements. An unscheduled disruption along these lines is highly undesirable due to the financial implications to both Eskom and its consumers. Eskom, therefore, initiated a programme known as "Operation Firebreak" to encourage co-operation between farmers and the utility.

Mpumalanga is the location for several power stations and many transmission lines leave this area to supplement the network supplying Gauteng, Kwazulu Natal, Free State and the Cape

Province. During the winter months, the fields become increasingly dry and so pose a hazard to the transmission network as fires in the region become more probable. As this is generally not an organised process, there is no way in which Eskom can be pre-warned of an approaching fire.

Earlier investigations showed that the disruptions were due to breakdown of the air about the conductors due to the proximity of the fire [1]. Changes in the composition of the air about the conductors implies a change in the corona activity about the conductors. This was confirmed by some preliminary tests using spectral measurements on the power line carrier (Performed in 1989 by A.C. Britten -Eskom, and T.R Reinertsen -formerly of Eskom, in collaboration with P. Naidoo - Eskom).

An additional strategy implemented by Eskom was the purchase of servitudes of high priority transmission lines. The cost was millions of rand and could not be implemented along all affected lines. A constraint in this approach was the "guaranteed servitude width" which would eliminate the risk of a fire fault. Some findings from the University of Queensland indicate that "any transmission line within 25 metres of a cane crop can be considered as subject to cane fire induced faults" [2].

1.2 RESEARCH OBJECTIVES

The research objective was to determine if fires could be detected so that appropriate action could be taken on the affected lines to minimise the influence of the fire on the power grid [b]. An appropriate action may be to de-energise the affected line before a fault occurs thereby preventing disruptive voltage depressions or to switch off the ARC only at the time of detecting a fire rather than operating entirely without an ARC aid.

Three major objectives were set out -

a) To investigate the nature and properties of electromagnetic noise on power lines arising from the presence of fires under those lines.

---

[b] From "Proposal for a National Energy Research, Development or Demonstration Project" as submitted by A.C. Britten in October 1989.

b) To establish the feasibility of discriminating between this noise and the intermittent presence of comparable levels of noise from other sources such as general conductor corona, electrical partial discharges within HV plant and discharges on polluted insulators.

c) To develop and implement a practical detection device for recognising the presence of fire induced noise. To verify the performance of the system under operational conditions.

1.3 SCOPE OF DISSERTATION

Chapter 2:
This chapter provides background information on the project. A layout of the Eskom main transmission system (MTS) network is presented. The type of customers Eskom is concerned about, the methods used to reduce electricity disruptions and previous research is covered.

What value exists in the higher frequency band of the frequency spectrum and how this can be used to improve the utility service to the customer is tabled. How the information at these frequencies can be extracted and what distortions exist are explained.

The order of priorities which dictated the approach used throughout the research is highlighted. Brief explanations cover the location where research was undertaken and the sources used to create the necessary physical parameters required for the experiments.

Chapter 3:
The mechanisms involved in the air insulation breakdown are explained. Detail is given to the physics and mathematical calculations from which the breakdown mechanisms are observed. Specific emphasis is given to the criteria for ionisation given the environmental components projected by fires and the operationally high voltages which induce high electric field stresses in the air gap between electrodes.

Attention is given to the corona phenomena, the modes which exist, the high frequency characteristics of corona, the Institute of Electrical and Electronic Engineers (IEEE) and the American National Standards Institute (ANSI) standards and the influence of the power line carrier (PLC) circuit on these frequencies.

The direct influence of rain and fires on corona is also examined.

Other potential sources of high frequency signals are listed and some discussion on these is given.

Chapters 4, 5 and 6:
These chapters cover the bulk of the research work carried out in laboratory conditions. Operational conductor bundles were used in a realistic, controlled environment with realistic environmental conditions simulating those experienced in the field.

A variety of hardware configurations (conductor types and bundle sizes) were tested to define the influence of system hardware changes on the measured signals generated by sources of high frequency signals.

Twin Zebra, Dinosaur, Wolf and Pelican conductor bundles are described here. Single, twin and triple conductor bundles were tested.

Both quasi-peak and instantaneous data was captured throughout the research with an attempt at keeping the work referenced to international standards.

Chapter 7:
This chapter provides a reference to the extensive work carried out at the University of Stellenbosch by staff and students from that university on a scaled model of the corona cage described in chapter 4. The work was carried out in contract to this project.

Chapter 8:
In this chapter the operational environment in an MTS network is explained. The existence of high voltage plant with insulation which can be utilised for extracting the high frequency signals and some limitations are detailed.

Chapter 9:

This chapter covers controlled testing with the specific emphasis on fires and the introduction of fire-induced corona into the operational environment. The signals which have been detected from within this environment are presented in this chapter.

The fires were prepared with veld grass and sugar cane assembled in scaffolding under the power lines at a point where the safety of both personnel and equipment was assured.

Chapter 10:

In this section the results from true operational conditions are conveyed. The fires were controlled sugar cane plantation fires in eastern Mpumalanga and Kwazulu Natal. In both regions the plantations are under 275kV transmission lines.

Chapter 11:

This chapter covers a variety of alternative detection algorithms, considered to detect and manage fire related high frequency signals. Due consideration was given to both practical application and operational implementation.

Specifications for and results from a detection device have been documented.

The research conclusions and recommendations have been presented in chapters 12 and 13 respectively.

CHAPTER 2

Background Information

2.1 ESKOM'S NETWORK

The main source of fire problems in South Africa has been along servitudes serving key customers. The fires cause line faults. These line faults are isolated via network protection protocols as soon as the fault is detected. During the fault, a fault current is initiated resulting in a proportionate drop in voltage. As soon as the line is isolated the fault current is extinguished and the voltage returns to the operating voltage. The voltage depression is experienced by different customers to a varying degree depending on their location and proximity to the line which had the fault. A series of reactionary measures is automatically initiated by industrial customers to minimise the impact of a loss of supply to their production processes. An example is the paper industry where materials move through rollers at a high rate and losses can be enormous if not addressed speedily. An additional factor influencing the severity of the voltage depressions is the load at the time of the fault (the higher the load the larger the impact).

One of the first geographic areas in South Africa where this impact was deemed unacceptable was in Kwazulu Natal. The region is a large consumer having Durban Electricity as the largest single consumer followed by large industrial users such as oil refineries (in Durban), paper mills and aluminium processing plants further to the north (Richards Bay and Empangeni). The Kwazulu Natal coastal and inland areas are extensively used for sugar cane farming. The harvesting process was deemed more efficient when first burning the debris on and around the sugar cane. All harvesting in Kwazulu Natal is done by hand. Transmission lines feeding the large consumers of electricity in this area cross over these farms.

The second region with a high impact is where the power has been generated, namely Mpumalanga. The power stations are surrounded by veld grass that dries out significantly in the autumn and winter months. In late winter, usually August, high winds are prevalent and fire is then a major risk.

Figure 2. 1 Transmission lines crossing sugar cane fields.

The Eskom transmission network is spread over the whole of South Africa. More than 22 000 kilometres of transmission line form the national grid [3]. Each power station is utilised to its maximum efficiency in order to supply the customer's electricity needs in the most cost-effective way. The quality of electricity used by the consumer is entirely dependent on Eskom's ability to maintain a constant voltage and frequency in the generation, transmission and distribution of electricity. Hence the affects of any disturbances in the network must be eliminated as rapidly as possible.

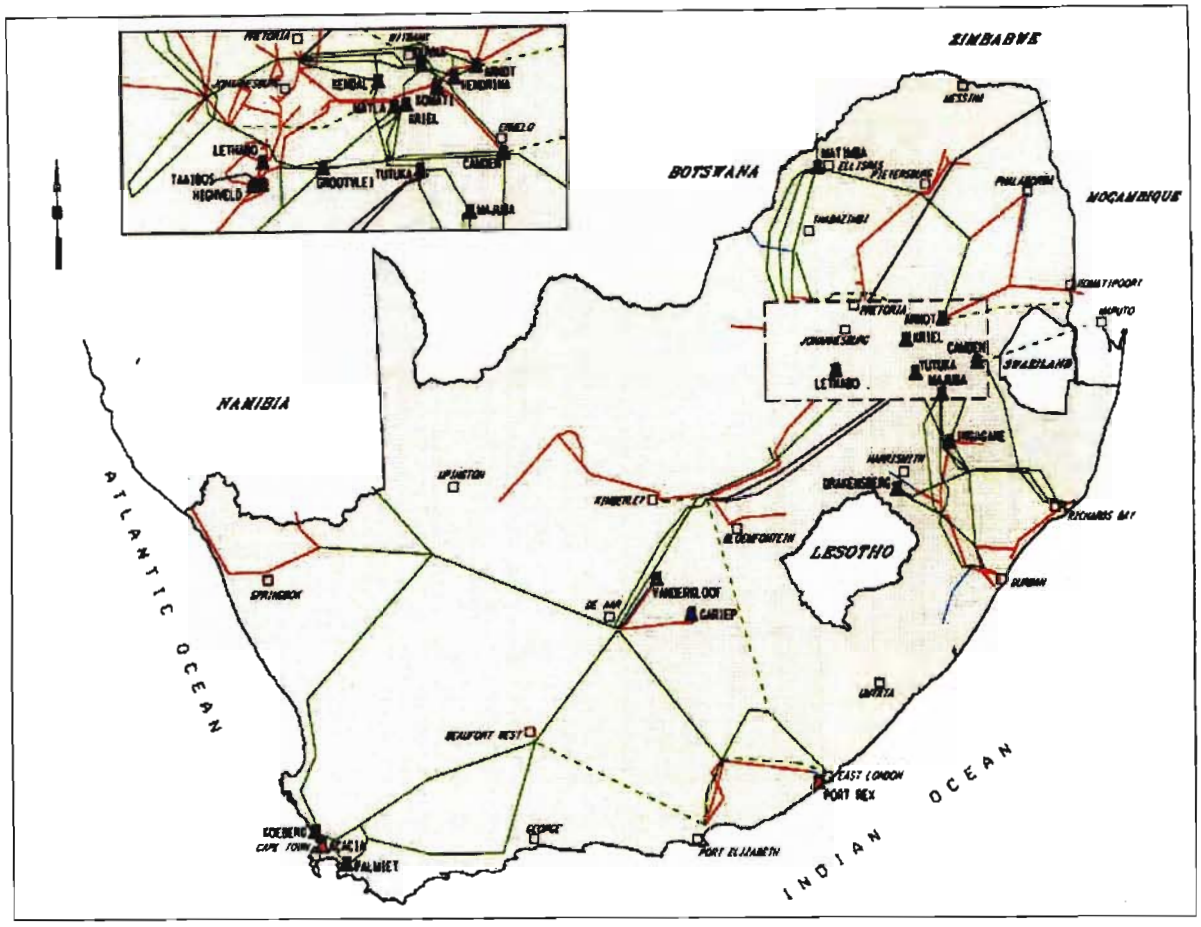

Figure 2. 2: Eskom HV / EHV / UHV network

2.2 MEASURES TO MINIMISE IMPACT ON ESKOM CUSTOMERS

In many instances, the voltage depressions have far-reaching effects with a fault in the north eastern reaches of Kwazulu Natal being visible in unacceptable levels of voltage depression as far south as southern Kwazulu Natal (an approximate distance of 350 km). All consumers sensitive to voltage fluctuations therefore become vulnerable to disruptions from incidents such as fire induced flashovers.

The industry in the north eastern Natal consume a significant proportion of the total Eskom supply (approximately 550 megawatts for RBM and Alusaf alone, which is approximately 1.5% of overall electricity generated by Eskom [c]) and hence are extremely vulnerable to disturbances

---

[c] On 4th September 1992, Alusaf was consuming 314 MW (MVA with a loading factor of 1.0), Richards Bay Minerals was consuming 210 MW and Eskom's overall installed generation capacity is 39 000 MW[1].

occurring. Similarly, any disturbances due to fires along the transmission lines in Mpumalanga jeopardise the supply of electricity from those power stations situated in Mpumalanga. Action then has to be taken under such conditions to redistribute the load to the remaining power stations. Thereby placing a higher burden on the remaining power stations. The result is that the overall network becomes vulnerable to any further faults occurring. The financial losses incurred when a voltage depression occurs affecting a major customer or several major customers can be in the region of millions of rand and are borne by industry. These losses cannot be afforded and every effort must and will be made to minimise the voltage depressions occurring.

Fault reports show that the overall number of voltage depressions occurring in the Eskom network have been decreasing. However, the total number of voltage depressions occurring due to fires were slowly increasing. In order to combat this problem Eskom implemented a "farmer awareness and co-ordination" program known as "Operation Firebreak". In the agreement, the farmer is expected to contact Eskom at a toll-free number to inform Eskom of any sugar cane plantation burning the farmer has planned. Eskom then sends out an Eskom official to establish visual contact at the point of risk. The official then maintains radio contact with the regional Eskom control centre. When the fire is to commence, the affected line is de-energised until the burning process is complete. This program does however, not take care of unplanned and unforeseen fires started due to weather patterns, sabotage, vandalism or carelessness. Eskom has spearheaded several research and investigation projects to identify parameters which could minimise the affects of fires on the transmission network [4], [5], [6]. The involvement of the industry in the research has increased with the National Energy Council (NEC) making funding available for this particular research in 1992 and also increasing interest shown by the affected industries.

2.3 PREVIOUS RESEARCH

Previous research work done by Eskom included defining parameters which may assist in the counteraction of the voltage depressions [1]. Utilising equipment to perform fast shunt compensation, development of a model by which to describe the cause of the breakdown of air insulation and laboratory research to determine the affects of the parameters and thereby clarify the mechanism leading to flashover during fires [5].

In the above work it was established that the fires may generate enough corona to in turn generate higher frequency noise.

As no measure of the activity of fires under power lines had yet been quantified, it was necessary to define the character of fire-induced corona noise with the aim of using this information for detection purposes. Therefore measurements had to be taken of the noise propagated along the transmission line rather than noise transmitted radially from the transmission line. Quasi-peak measurements are the more common means of measuring "radio noise" [d]. However, the measurement favours rapid repetitions of pulses as A.H. Davis [7] stated, the meter "must have an appropriate leak, for the loudness of a slow series of repetitions is less than that of a rapid series". Therefore the measurement of fire-induced corona noise cannot solely be measured with a quasi-peak meter only. Capturing data for further processing was therefore also an objective.

2.4 HIGH FREQUENCY NOISE AND HOW TO GET ACCESS TO IT

On the high voltage system, any high frequency noise (which is at low voltage) can only be observed with the aid of either filtering equipment or radio receivers. The filtering equipment can eliminate or significantly attenuate the 50 Hz high voltage signal and retain any higher frequency components conducted from the source to the filtering equipment. The power line carrier makes use of such filtering equipment.

---

[d] pp 206-207 in [35].

The detection device has to be incorporated into the current Eskom network and therefore the proposals were concentrated on the PLC (power line carrier) filtering system with the device being able to accurately identify fire over other noise sources.

The power line carrier (PLC) channel is a protection-signalling channel providing pilot protection communications to facilitate fast clearance and correct discrimination for faults anywhere within a high voltage power network. Pilot protection is a type of protection that compares electrical quantities at the two ends of a protected line. A pilot signal is coupled directly to the power line. Wave traps known as "line traps" are used to contain the signal to the line that is being protected. A transmitter and the associated receiver are coupled to the power line through line tuning equipment and a coupling capacitor. A radio frequency (rf) choke presents low impedance to the 50Hz but high impedance to the carrier frequency. The choke protects the electronic equipment from the 50 Hz high voltage power signal.

"High frequency signal transmission along the actual overhead power line offers advantages over the use of pilot links. It is robust and therefore reliable, constituting a low loss transmission path that is fully controlled by the power authority" [8]. Similarly the same path will serve as a conduit for any repeatable signals generated due to potentially repeatable conditions when a fire is present under a power line.

In Eskom, the PLC has an operating band from 50 kHz to 500 kHz. Each PLC then uses 4 kHz for transmitting signals to and another 4 kHz for receiving signals from the other PLC at the opposite end of the transmission line via modulation and demodulation. Similar to many European utilities, Eskom have in the past also utilised the PLC for voice and data communications. In the USA, pilot protection with PLCs has typically been dedicated to the protection of a particular circuit only with no additional voice or data facilities. Worldwide, the move has been to dedicated circuits to eliminate false triggering.

Any noise being generated on the transmission line (such as fire induced corona) is expected to have a considerably lower signal strength than the main communication signals between PLCs and it was therefore essential to avoid the PLC frequencies. The figure below illustrates the presence of controlled plc channels containing the pilot, voice and data components across the frequency spectrum.

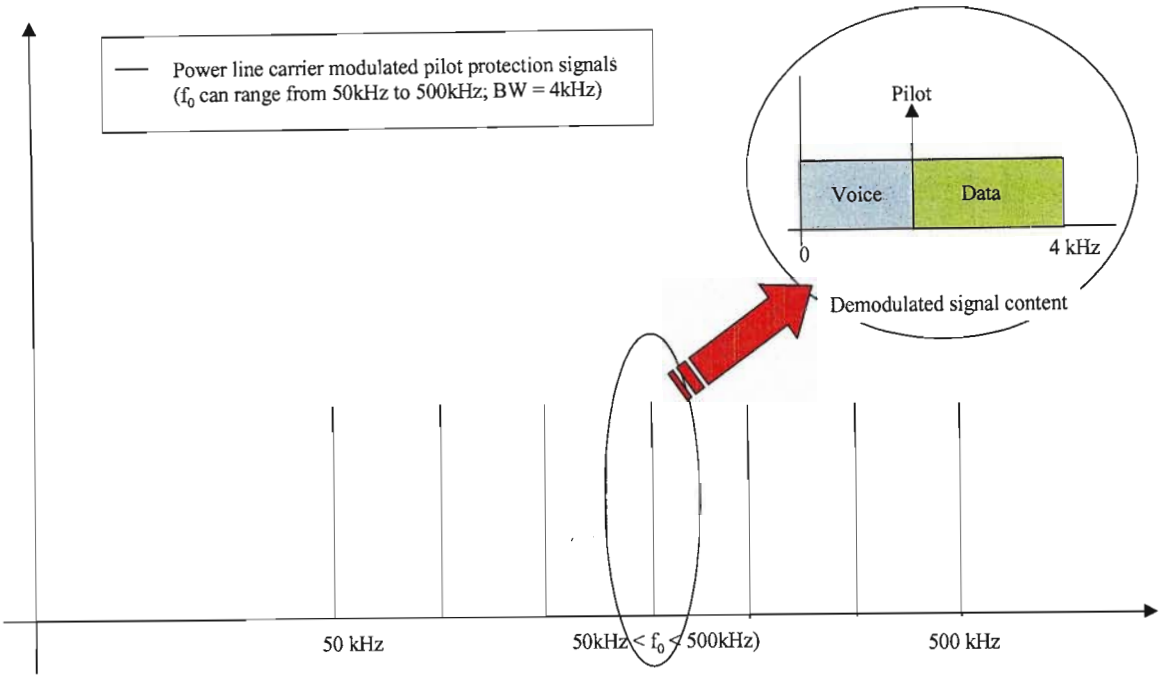

Figure 2. 3: Frequency spectrum of PLC signals.

Of concern was the attenuation of the noise signal along the transmission line. However, at the frequencies of interest in the PLC band (50 to 500kHz), the attenuation is typically 2 dB/100 km at 100 kHz and 5 dB/100 km at 500 kHz. The longest lines are typically of the order of 100 km in length and hence a maximum attenuation of around 5 dB can be expected on the longer lines at the higher end of the frequency range in the PLC system.

2.5 CORONA, CONDUCTOR DIMENSIONS AND FIRES

As the induced noise is a function of corona activity, the generation of fire-induced corona noise is dependent on the generation of corona.

The corona phenomena is a function of the local electric field existing about the conductors. If the local electric field increases above the critical electric field for ionisation to occur, ionisation starts and results in the generation of streamers which in turn, if the high local field persists, results in corona formation.

The field about a conductor bundle is dependent on many factors. The most significant factors are firstly, the applied voltage and secondly the conductor and conductor bundle diameters. Increasing the applied voltage increases the local electric field. Reducing the diameter of the

conductor or the overall bundle diameter whilst maintaining a constant applied voltage will increase the electric field about that conductor or bundle of conductors.

These parameters are taken into account when transmission lines are designed for transmission of large amounts of power, and for any particular operational line these parameters are constant. The additional parameters which change and cause an increase in the local electric field and hence an increase in the corona to above designed levels are those factors which change the air density and introduce high local fields due to near-point charges.

Fires introduce particles into the electric field. The particle becomes charged and forms part of a high localised field. Simultaneously, the higher temperatures from the fire causes an expansion of the air and hence a reduction in air pressure. The critical electric field within the lower air density pockets decreases.

Each particle and air density pocket contributes to the development of a higher local field and lower critical fields respectively, with resulting growth in the streamers occurring, developing into corona regions. The further the corona regions develop, the smaller the gap becomes between the highly stressed electrode and either ground or the other phases.

The result is a growing electric field at the head of the corona region and sufficient criteria for a self-sustaining passage of ionisation until flashover occurs.

2.6 OTHER SOURCES OF CORONA

Other parameters which influence the electric field and the generation of corona include the formation of water droplets on the underside of the conductors, movement of droplets past the conductor, change in the humidity, change in wind speed and pollutant on insulators.

2.7 RESEARCH PRIORITIES

The first priority was to measure the levels of induced corona noise at appropriate frequencies to categorise the characteristics of different influences. The goal was to establish whether fire-induced corona was significantly different from all other induced corona noise sources. Several options were available and decisions had to be made with regard to selection of environment

(operational lines or laboratory type testing), selection of fire (real or simulated quasi-repeatable), selection of domain (frequency related data or time data) and selection of format (instantaneous, average, quasi-peak, rms or some combination of these).

By the goals set it was necessary to select an environment where even the influence of the geometry of the surrounding structures were minimised. The environment also had to be able to simulate both fire and the other main corona generation parameter, namely "rain" [e].

Rain is a well known source of corona noise and may mask out any components of the fire-induced noise and therefore was selected as the prime component to which the fire-induced noise would be compared.

The effect of an isolated environment then had to be taken into consideration. Using the generation function, also known as the "excitation function", the radio noise measured in one environment with a known electric field can be extrapolated to another environment with a known electric field [9]. Likewise, when using a simulated fire, the relative difference between that fire and the typical fires experienced under operational transmission lines had to be quantified. The difficulty with a real fire is the spontaneous combustion or lack of it. For results to be quantified the conditions need to be repeatable in order to make several measurements and hence improve the level of confidence in the measurements made (as no international documented experience exists with such measurements). The choice of time versus frequency domain information was made by capturing data using a quasi-peak detector and with a digital storage oscilloscope. The time-domain data in digital form could then be processed and with the aid of Fast Fourier Transforms, the frequency domain information could then also be evaluated.

The final detector will be required to conform to the system in which it will be used. The measuring point will be in the substation between the power line carrier unit and the filtering circuitry. The filtering circuit being that circuit connected directly to the high voltage transmission line. The laboratory environment selected had to have a similar measuring system to that into which the final detector will be applied. The corona cage at Eskom's high voltage test facility is designed to house typical conductor bundles utilised on operational transmission lines

---

[e] See [33] and [35] as cited in [31].

and has the voltage supply to duplicate typical gradients experienced on those transmission lines. The cage measuring circuits are tuned to 500 kHz and will therefore be particularly sensitive to 500 kHz noise components. With a relatively large bandwidth on the receiving circuits, it was also possible to process lower frequency components.

2.8 RESEARCH LOCATION

The fundamental differences between rain and a particle-free flame were researched in the corona cage described above. A cage of much smaller dimensions and similar to the described corona cage has been built up at the University of Stellenbosch and the influence of the fundamental components of a fire - particles, smoke, etc. - were researched. The work performed by the university has been documented separately [10] under a post graduate dissertation from that university.

2.9 SOURCE OF FIRES FOR THE TEST OBJECTS

The fires used in the corona cage were from a gas fuelled burner normally used for driving hot-air balloons and fire fuelled by sugar cane. The gas for combustion is a liquid petroleum gas (LPG). With the burner as a standard unit, the temperatures generated were far higher than a sugar cane or grass fire which is typically around 110°C to 250°C at the conductors with short term peak temperatures estimated at between 800°C and 900°C [11]. Instances of temperatures as high as 1200°C [12] have however also been measured. The temperatures generated by the burner is dependent on the rate of combustion, but the flow of gas through the feeder pipes to the jets is also dependent on the rate of combustion. A minimum rate of combustion is required to prevent freezing of the gas whilst the rate of combustion must be controlled to ensure that the temperature of the flame remains realistically low. Hence the burner was modified to generate the lowest possible temperature. The temperature directly above the visible portion of the flame ranged from 450°C to 550°C [f] and this was also the temperature at the conductors when the flame was directed at the conductors (wind condition dependent). Cane fire temperatures have

---

[f] As measured on the reef (altitude 1500 meters above sea level) with an Agima thermovision temperature sensitive video camera.

been recorded by the author and found from a variety of fire tests that statistically a high percentage of fires produce heat of the order of no more than several hundred degrees Celsius.

The corona cage is equipped with a rain generating facility producing rain at a rate of 2 mm/min. Measurements were done recording quasi-peak (noise in dB vs gradient in kV/cm) and time domain (noise and power signals in volts vs time in ms) data. The full length of the cage is equipped with the rain generator and therefore the length of conductor bundle exposed to the rain was forty meters. The section of line exposed to the fire was approximately one meter. Triple Wolf, twin Wolf, single Wolf, twin Dinosaur and twin Zebra conductor bundles were tested in the cage. (All conductors are described according to their diameters and are allocated names accordingly, these conductors are described in appendix B).

The quasi-peak measurements showed in each case that the fire-induced corona noise generated was higher than the rain-induced corona noise. The time domain measurements indicated several differences in the noise patterns and helped explain why the quasi-peak fire-induced noise measurements were higher than the rain-induced noise measurements. The occurrence of a streamer can be seen to generate a large pulse of noise propagated down the line to the measurement point. The major differences seen in the time domain measurements were related to the pulses observed and thereby related to the physical occurrence of the streamers at the conductors. The two most significant differences in the fire-induced corona noise pulses and the rain-induced corona noise pulses were the amplitude and the time between pulses. The fire-induced corona noise pulses were much larger and the time between pulses was more irregular (whilst still a function of the gradient, the presence of some inconsistent catalyst - reduced air density in this case - was stimulating the corona activity).

Rain-induced corona noise was generated as a result of many droplets attached to the conductors. The end of each droplet constitutes a large localised field. With a constant rain rate, these droplets attached to the conductor are perpetually present during the test. The transition of applied voltage between positive and negative half cycles, increases and decreases the electric field and hence the localised fields at the droplets. It is therefore evident that the localised fields at the droplets will exceed the critical field - for ionisation to occur - only when the applied voltage is above a certain threshold and will remain so until the applied voltage falls below that threshold. Also, once the local field is greater than the critical field, any further increase in the applied voltage will increase the local field and increase the amount of ionisation occurring until

some saturation point is reached. The rain results were then as expected. Once an inception threshold voltage was reached, pulses were observed to be occurring continuously, rising and falling with the applied voltage and then at some extinguishing threshold voltage the pulses disappeared.

Fire-induced corona noise was generated due to the reduction in air density. The electric field here is also dependent on the applied voltage and will therefore also experience a cyclical increase and decrease in the local electric field in pockets where the air density has decreased. However, unlike the constant existence of droplets on the conductors, these air pockets are at the mercy of air movements which are constantly changing. The pocket of air has a lower air density due to the expansion of the air in that pocket which in turn is due to the increase in temperature. However, hot and cold air have preferable energy levels for equilibrium and the air will move in an attempt to reach that equilibrium. The final result is a continuously changing scenario where the source of the localised electric field is not always present. With the above reasoning the results obtained can be understood. Large pulses occur due to the very high localised fields occurring and large and irregular time periods occur between pulses due to the movement of the heated air about the conductors.

Tests were performed in the operational line environment on a 275 kV horizontal configuration transmission line at 1500 meters above sea level. The measurements were made at the point described previously, between the filters and the PLC equipment. In order to avoid the PLC communication frequencies and adjacent line PLC communications, it was necessary to filter the signals received. A 52 kHz BBC carrier passive bandpass filter with a 4 kHz bandwidth was used to do this. The test included using the abovementioned gas burner, a sugar cane fire and a grass fire. The gas burner generated large amounts of fire-induced corona noise due to the controllability of this fire. The sugar cane and grass fires were not controllable (other than being able to extinguish them) and were totally dependent on the elements. The wind occurring at the time undermined the sugar cane and grass fire tests. The results of a gas fire show a clear and substantial increase in the background noise measured about 52 kHz.

Similar measurements were also performed on a long 275 kV transmission line with a sugar cane plantation fire present under the line. The development of the fire was monitored on site and its progress was communicated back to the substation some 70 km from the site. The noise induced on the transmission line by the fire was recorded and showed an extremely clear increase in the

noise levels. The progress of the fire was also visually recorded and correlated with the fire-induced noise measured on the digital storage oscilloscope.

Another significant form of noise on the transmission lines is that of polluted insulators. Earlier work done by Eskom showed the possibility of very large components of polluted insulator-induced corona noise existing. Both the clean and the salt fog tests were performed and unfortunately both showed no significant increases in noise levels when there should have been and the conclusion was that whilst the data may be correct due to doubt cast on alternative data available, it was improbable and the tests were unsuccessful. The required fog density for these tests to succeed is high whilst at the same time the droplet size in the fog is also required to be small. Thereby droplets accumulate on the insulators and the insulators are moistened rather than drenched. In the corona cage the above affect can only be duplicated if the droplets are allowed to accumulate around the insulators and this can only be made possible if a closed environment were built up around the insulators to seal off any air movement. The air movement causes the droplets to drift in an unrepeatable manner, usually away from the insulators.

The results obtained thus far bear sufficient evidence to state that the detection of a fire under a high voltage power line is plausible. Hence it is appropriate to present a proposal for a first pass prototype detector. The results must be taken in perspective including all constraints of the laboratory environment and extrapolating their affects. An example is the lack of particles in the simulated fire. From previous work done locally and abroad, particles reduce the breakdown strength of air. Therefore the corona activity with particles will increase and make the detection of fires above other noise sources more effective.

Proposals for a prototype detector are described in terms of the approach rather than the specific design of a "black box". Several alternatives exist by which to detect the fire-induced signals and can either be used separately or in combination, that is, in parallel and thereby reducing the probability of a false indication. The use of more than one processing method can then be used to provide "intelligent" detection processing. The following are proposed outputs from the detector: A threshold measurement to detect voltage levels above a specified level, ac positive and negative half cycle activity monitor, ac zero-crossover voltage monitor, monitor of frequency of pulses within a specified time limit (usually in reference to the ac cycle) and timed monitoring of corona activity. More detail of these proposals are given in the body of the report.

The first pass prototype detector was tested in the corona cage with sugar cane fires and then in the operational line tests described above involving the sugar cane plantation fire. The results of this first pass prototype device were extremely positive.

CHAPTER 3

Basic insulation breakdown process

3.1 BREAKDOWN OF THE AIR INSULATION

The spacing between power system electrodes (between phases, phase-to-overhead-earth-wires and phase-to-ground) is designed such that the air gap between them will not become conductive under normal operating conditions. The applied voltages, electric and magnetic fields and several other parameters are taken into account to ensure that the air insulation remains intact. In addition, the power losses due to the high electric field stresses in the air gap are also considered. If the surface gradients on the conductors are too high for any typical conditions, the 50Hz power losses will be higher and reduce the overall efficiency of that particular section of the power network.

Breakdown of the air gap is a progressive process from partial to complete breakdown. Continuous partial breakdown of the air gap leads to system power losses without a network failure taking place.

In an alternating current (AC) power system the alternating voltage (from a positive polarity to a negative polarity and back to a positive polarity) forces the electric fields through the same alternating pattern which in South Africa is at a rate of 50 cycles per second or one cycle every 20ms.

The electric field will force free electrons and positive ions to move in a direction dictated by the polarity of the field and at a speed dictated by the intensity of the field. Either objects such as molecules, will stop these free electrons or the electron will move to a point where the electric field no longer has an influence on the electron. In higher electric fields, free electrons may gain sufficient energy between collisions with atoms to cause ionisation on impact with neutral molecules resulting in ion pairs. That is, an electron is knocked out of the outer layer of the molecule by the travelling free electron, resulting in the creation of another free electron under the influence of the same electric field and leaving behind a positive ion. Whether ionisation

takes place depends entirely on how much energy the electron gains before it makes contact with a neutral atom.

For a given volume of gas within which these free electrons and the molecules exist, the typical distance an electron can travel before colliding with another molecule is known as the mean free path.

The energy gained by an electron over the mean free path, is given by

$$\Delta W = eE\lambda_e \tag{1}$$

where λ_e is the mean free path in the direction dictated by an electric field of strength E. The electron charge, e, is -1.6 x 10^{-19} coulombs. Ionisation will take place when ΔW is at least equal to the ionisation energy of the molecule with which the electron is colliding, which is eV_i where V_i is the ionisation potential. In addition to the electric field, the mean free path λ_e is therefore also an influencing parameter and is directly proportional to temperature (T) and inversely proportional to the gas pressure (p) [13]:

$$\lambda(p,T) = \lambda_0\left(\frac{p_0}{p}\right)\left(\frac{T}{T_0}\right) \tag{2}$$

where λ_0, p_0 and T_0 are constants. Hence λ_e is inversely proportional to the density of the gas. Any fires under the power lines can be expected to both increase the temperature of the air about the conductors and decrease the gas density (or air density), hence the mean free path of electrons in the air about the conductors can be expected to be longer. Therefore a larger value of energy ΔW gained by the electron as a direct result of the fires under the conductors, can be expected. However, ionisation by collision or electron impact, as are all other processes in gas discharges, is a probability phenomenon usually expressed in terms of cross-section for ionisation, denoted by σ_i which can be defined as the product of P_i, the probability of ionisation on impact, and σ, the molecular cross-sectional area of intersection or simply the collision cross-section. That is:

$$\sigma_i = P_i\sigma \tag{3}$$

where the collision cross-section is:

$$\sigma = \frac{1}{N\lambda} \tag{4}$$

and N is the number of particles per unit volume of gas. Therefore the event of a fire under a power line will increase the probability of an increase in corona activity which should be measurable. In order to develop a high level of confidence in results, the number of samples must be as high as is reasonably possible.

Since λ is proportional to 1/p in equation (2), then from equation (1) ΔW is proportional to E/p. Decreases in gas pressure as previously stated and increases in electric field (gradient), will increase the energy gained by an electron. The gradient on a conductor or conductor bundle is dependent on the applied voltage on the conductors

$$E = -\nabla V \tag{5}$$

where nabla ∇, is a vector operator differentiating V in the x, y and z directions. Increasing the applied voltage on a conductor or conductor bundle will increase the gradient on the conductors and increase the energy ΔW gained by the electron.

The gradient on a conductor or conductor bundle is also dependent on the dimensions of the conductors or of the overall conductor bundle. From fundamental electromagnetic theory [14] the analysis of point charges can be used for the influence of conductor dimensions

$$E = \hat{r}\frac{Q_1}{4\pi\varepsilon r^2} \tag{6}$$

where for a given point charge Q_1 in medium with permittivity ε, the electric field in direction of the unit vector is inversely proportional to the square of the distance from that charge. The dielectric constant or permittivity is often conveniently expressed as the relative permittivity ε_r which is the ratio of the medium's permittivity and that of a vacuum. This is confirmed by work done by Peek [20], [22], [26].

$$g_v = \frac{e_v}{r\log_e\frac{s}{r}} \tag{7}$$

where g_v is the visual critical gradient on the conductor before ionisation starts, e_v is the visual critical voltage, r is the conductor radius and s is the separation between conductors. The air density factor δ, was taken here as 1. That is, the barometric pressure was 76 cm of Hg and ambient air temperature was 25 °C [from equation (16)]. Therefore the larger the radius of the conductor or conductor bundle is, the smaller the field will be for the same applied voltage and the lower the energy ΔW gained by the electron.

In summary of the above statements, increasing the applied voltage on a given conductor bundle will increase the extent to which ionisation is occurring and likewise decreasing the conductor and/or conductor bundle diameter for a given applied voltage will also increase the electric field and hence the probability of ionisation occurring. Townsend [15] found that when gas is under a sufficiently high electric field, the current in the gas increases proportionately with the applied voltage, then at some voltage (A) in figure 3.1 below, remains constant and again at some higher voltage (B) the gas current increases exponentially.

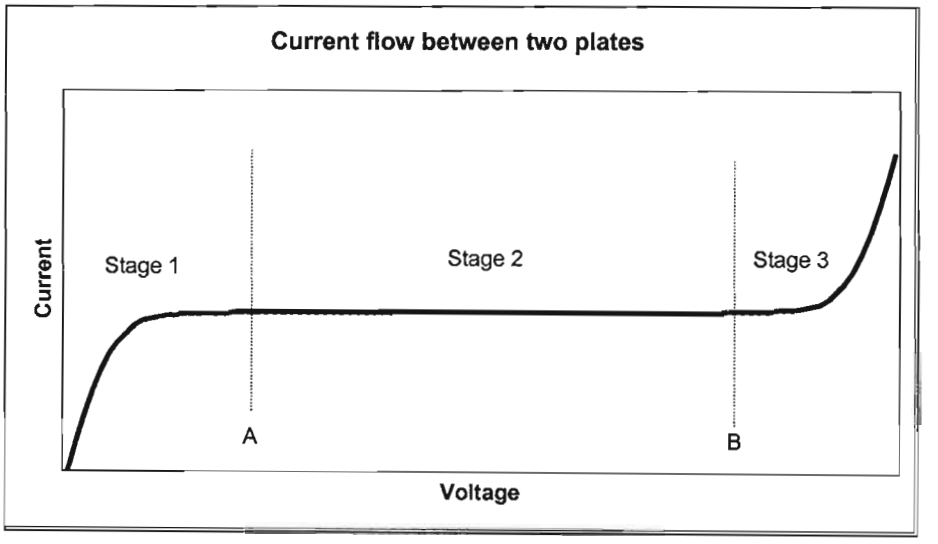

Figure 3. 1: Current flow between two plates due to applied voltage (and electric field)

This final exponential increase in stage 3 is as a result of ionisation of the gas by electron collision. Townsend introduced the *first ionisation coefficient* α, to explain this increase in current. Where α is the number of ion pairs (new electron and the remaining positive ion) produced by an electron per unit length of path in the direction of the applied electric field:

$$dn = \alpha n dx \tag{8}$$

where n is the number of electrons at a distance x from the cathode. These electrons increase by dn at a distance x+dx from the cathode.

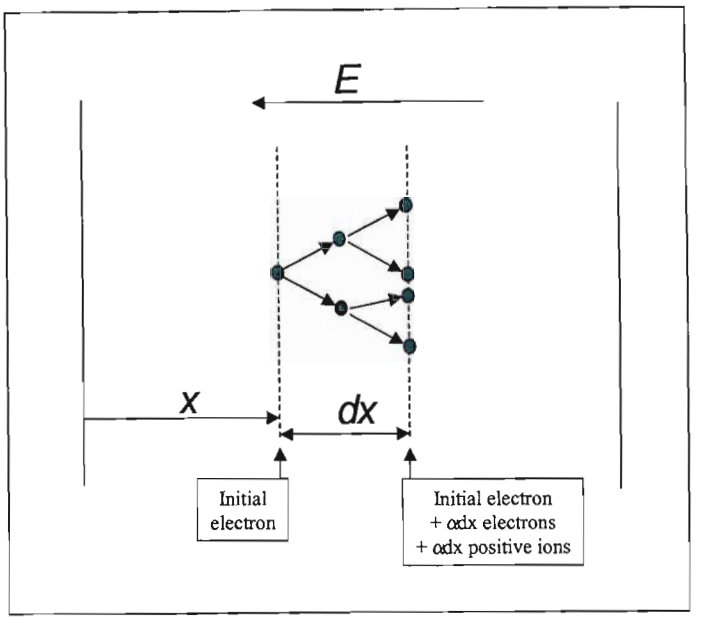

Figure 3. 2: Electron collisions with stationary molecules producing electrons and ions.

If n_0 is the primary number of electrons generated at the cathode (at x=0), then at x=d:

$$n = n_0 e^{\alpha d} \tag{9}$$

The discharge current to distance x is then

$$I = I_0 e^{\alpha d} \tag{10}$$

Here $e^{\alpha d}$ represents the number of electrons produced by one electron travelling in an electric field with a separation of d between electrodes and I_0 is the current leaving the cathode. A *second ionisation coefficient* γ, was introduced for cathode secondary processes. The electrode current at the anode becomes

$$I = I_0 \frac{e^{\alpha d}}{1-\gamma(e^{\alpha d}-1)} \tag{11}$$

Mathematically, the first ionisation coefficient can be described as follows [g]

$$\alpha = pf\left(\frac{E}{p}\right) \tag{12}$$

with dependence on E and p. Similarly γ is dependent on E and p. The ionisation by electron impact results in an avalanche as more collisions generate more ions and electrons. As the applied voltage increases, the ratio E/p increases and so α and γ also increase. Therefore the

---

[g] See p 279 [15].

denominator in equation (11) will decrease and I will increase. For breakdown to occur, I becomes self-sustaining and indeterminate. The criteria for self-sustained discharge (current flow tends to infinity) is when the denominator will be zero and is

$$\gamma(e^{\alpha d} - 1) = 1 \tag{13}$$

Provided the local electric field continues to be greater than the critical field for ionisation, further ionisation will occur at greater distances from the cathode resulting in streamers occurring. This is the development of additional avalanches at the "head" of the previous avalanche due to a high local field still present. From equation (9), the number of electrons is dependent on $e^{\alpha x}$ where x is the distance from the cathode to the streamer head. The criteria for the initiation of streamers were initially developed, independently, by Raether [16] and Meek [17] and as a result of subsequent research, they have been merged into the formulation:

$$\int_{x_{cathode}}^{x_{streamer}} (\alpha - \eta) dx = 18 \tag{14}$$

where η represents the attachment of electrons in the path. The above criterion will be met when a sufficiently high applied voltage increases the local electric field E_{local} to exceed E_{crit} in the volume of air about the conductors. E_{crit} could be defined as that field at which the probability of ionisation by electron impact is high. The avalanche process will result in filamentary streamers propagating beyond the limits of the critical volume. Excitation and recombination by the initial avalanches generate photo-ionising quanta triggering streamers at other locations about the conductors. A web of streamers then develops out of the critical volume into the "first corona" region. As the "tip" of the streamers move further from the conductor, E_{local} decreases until $E_{local} < E_{crit}$ and the streamers halt. The electrons from the streamers then rapidly combine to produce a channel of positive and negative ions. During the corona propagation phase (streamers) the channels have experienced thermal expansion and the positive and negative ions generated then drift apart and generate space charge filaments in the field.

3.2 THE CORONA PHENOMENA

3.2.1 Corona Modes

Corona is a fundamental component of the breakdown process as mentioned in the previous section with the corona regions existing as a web of streamers originating from the conductor,

where the conductor is usually the highest point in the electric field. The breakdown of the air by the corona generates light, audible noise, radio noise, conductor vibration and ozone with a dissipation of energy. Corona as a phenomena is well discussed in many journals and books with significant work done by people such as L.B. Loeb [18] (1965) and F.W. Peek [19],[20],[21],[22] (1911-1913, 1929)

For the positive and negative polarities, several "modes" of corona exist [h]. All corona modes are directly dependent on the voltage applied to the conductor. Negative applied voltages cause the following corona modes to occur (in order): "Trichel pulses" are the first to occur with rise times of between 25 and 50 ns and amplitudes of up to 20 mA on some electrodes. Increasing voltage increases frequency and decreases current amplitude, with a typical maximum frequency of 2 kHz. Upon reaching the maximum frequency, higher voltages result in "pulseless glow" forming - described as a "luminous area with a bright spherical glow". Further increases in voltage result in "negative streamers" and little branches start developing from the spherical glow - pulses with rise times of the order of 0.5 μs.

Positive applied voltages cause the following corona modes to occur (in order): "Onset pulses" are the first to occur appearing as streamers in a stem with some branching - rise times of 30 ns and amplitudes of up to 250 mA on some electrodes and maximum frequencies of 200 Hz on large electrodes. Note that a high repetition rate of these pulses (and hence branching) generates a brush-like appearance. "Hermstein's glow" forms gradually into an ionising layer with increasing voltage - discharge with small ripples up to 2 MHz. "Positive streamers" are the final mode in this polarity resembling the onset streamers and displaced by the negative space charge - rise times in the nanosecond range with velocities from 20 to 2000 cm/μs, faster than the negative streamers due to photo-ionisation. Repetition rates of the pulses can be up to 240 000 pulses per second [23].

3.2.2 AC Corona

The transition of the applied voltage from positive to negative to positive polarities - has all of the above modes of corona, but the transition time from one polarity to the next has an influence

---

[h] Transmission Line Reference Book - 345kV and Above; pp 170 - 175

on the development of the different modes. For the 50 Hz power cycle, the rise time of the power cycle is 5 ms. Hence, if the applied voltage (RMS) is high enough, the transition from one mode of corona to the next will occur milliseconds apart and may or may not influence the onset of the next mode. Note that the positive corona pulses are larger than the negative corona pulses and that the positive corona modes are initiated at a lower gradient than their respective negative corona modes. In particular, the Hermstein glow and breakdown or positive streamer modes commence at a lower voltage than their negative corona mode counterparts [i]. The modes are illustrated in the figure below. For the positive modes, inception occurs on the rising edge and will extinguish on the falling edge, and vice versa for the negative modes.

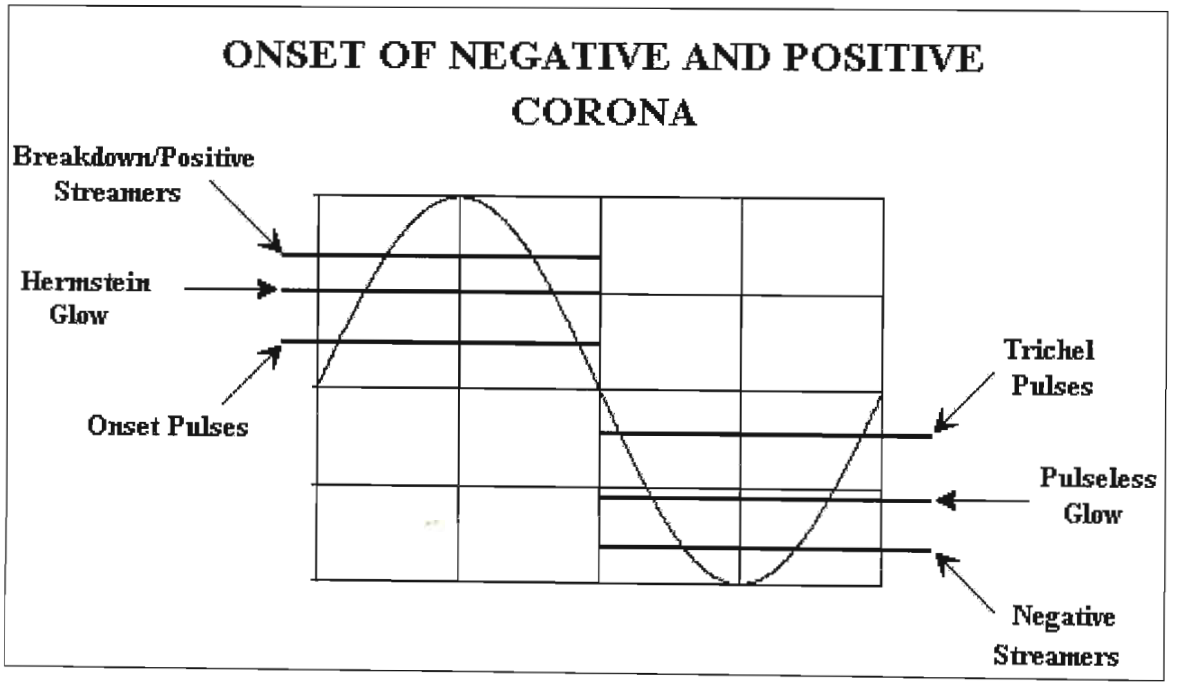

Figure 3. 3: AC corona modes

From the previous section, the breakdown process was shown to be dependent on the electric field stresses experienced at the conductor. Onset of corona defined in terms of voltage on a given conductor or conductor bundle can be calculated by results obtained from work done by Peek and previously discussed with equation 7:

$$e_v = g_v \delta r \log_e \frac{s}{r} \tag{15}$$

[i] "Transmission Line Reference Book - 345kV and Above"; p 175

δ represents the air density which is a function of the barometric pressure and the ambient temperature. From Peek's work δ is directly proportional to the barometric pressure (b) in cm of Hg and inversely proportional to the ambient temperature (T).

$$\delta = \frac{3.92b}{273+T} \tag{16}$$

From experimental data Peek found that

$$g_v = g_0\left(1+\frac{k}{\sqrt{r}}\right) \tag{17}$$

assuming δ is 1. g_0 is the actual critical (or "rupturing") gradient of air, that is, the gradient at which the air as an insulator starts to breakdown. g_0 is a constant for all diameters of conductors and all spacing [j] and has a peak value of 30kV/cm peak or an RMS value of 21kV/cm (for parallel wires) for air at 25°C with a barometric pressure of 76 cm of Hg. The value "k" is a constant with a value of 0,3. The term "r" is the radius of the conductor. For different electrode configurations, g_0 and k will change marginally [k]. The smoothness factor of the conductor m_v, and the air density δ, must also be included to provide a value for the critical gradient E_{max} where $E_{max} = g_v$ on a conductor bundle [l].The gradients for different conductors and conductor bundles can be calculated from Peek's law:

$$E_{max} = g_0 m_v \delta\left[1+\frac{0.3}{\sqrt{\delta r}}\right] \qquad \text{(in kV/cm)} - \textbf{\textit{Peek's Law}} \tag{18}$$

where g_0 = 31kV/cm for a wire in a cylinder,
and g_0 = 30kV/cm for parallel wires.

3.2.3 Thermal Ionisation and Thermal Impact

Thermal ionisation has been considered a possible contributing factor to the increase in corona when fires are under the transmission lines. With a sufficient increase in temperature, thermal ionisation could be a source of additional free electrons in the breakdown process. The additional

---

[j] See pp 1934 –1935 [19]

[k] See p73 [22]

[l] See p64 [22]

ions available due to the increased temperatures would then be available in the electric field for the onset of the corona avalanche and for further ionisation by electron impact.

From Saha's equation, thermal ionisation becomes a significant contributor at temperatures above 1000°K [13].

$$\left(\frac{\theta^2}{1-\theta^2}\right)p = 2.4\times10^{-4}T^{5/2}e^{-eV_i/kT} \quad \textbf{\textit{– Saha's Equation}} \tag{19}$$

θ represents the ratio of ionised particles to the total number of particles, eV_i the ionisation energy of the gas, k is Boltzmann's constant, p the pressure in Torr (or mm Hg) and T the temperature in °K[24].

Measured temperatures done on fires in South Africa under power lines have revealed temperatures in the region of 150 to 250°C at the conductors. As temperatures higher than 800°C are required for a change of only one volt [25], it appears unlikely that thermal ionisation plays any major role in the inception of the breakdown process. The contribution of thermal energy may rather be considered in the increase of energy in molecules. Neutral atoms or molecules may absorb the energy from the high temperature in such a way as to cause electrons within them to be displaced to outer orbits. The excited atom or molecule is now in an unstable state and the electrons may then be more easily dislodged by collision and ionisation follows [m].

3.2.4 Corona and Radio Frequencies

The breakdown of the air by the corona as previously stated, generates radio noise [n] which is of particular interest for the detection of corona. This "noise" is defined in the ANSI/IEEE Std 430-1986 as "any unwanted disturbance within the radio frequency band, such as undesired electric waves in any transmission channel or device" [26]. The radio frequency band within which radio noise is generated extends from 3 kHz to 30 GHz. The IEEE standard procedures used for measurements of radio noise from power lines and in substations apply to the frequency range 10 kHz to 1 GHz, with particular emphasis on the amplitude-modulation broadcasting (535 kHz to 1.605 MHz) and television broadcasting (54 to 72 MHz, 76 to 88 MHz, 174 to 216 MHz

---

[m] See p46 [22]

[n] See p205 [35].

and 470 to 906 MHz) bands. This information has particular bearing on the frequencies available in the power line carrier filtering equipment available in Eskom's transmission system.

The radio noise component of the corona is a measurable entity and is both transmitted radially from the conductors (causing radio and television interference) and propagated along the conductors (to be terminated in the substation at either or both ends of the line). The propagated radio noise is therefore of primary interest in the detection of fires.

Corona is a current source. Any pulses occurring due to corona activity consumes energy [o] and at a constant voltage at 50 Hz the changes in current is measurable.

3.3 RAIN AS A CATALYST FOR CORONA

When rain falls onto a conductor, the droplets are pulled by gravity down the strands to form along the bottom of the conductors. Under stress, the conductor now has several non-uniform surfaces where the droplets have settled. The droplets become ionised and form part of the conductors surface with the field increasing accordingly about the droplets. The net result on the high voltage transmission lines is that where there was no corona before, it is now stimulated by the increased local electric field to a value above the critical field ($E_{local} > E_{crit}$).

Rain drops passing close to the conductors also become ionised due to the field and temporarily become an extension of the conductors greatly increasing the corona activity. The increased corona activity also results in a reduction in the spark breakdown potential of normal air. Work done by Macky [27] (1931) showed that water drops falling in a uniform field in excess of 8 kV/cm became distorted and lowered the spark breakdown potential of the normal air from 30 kV/cm to 8 kV/cm (depending "slightly" on the droplet size).

According to G.W. Juette and L.E. Zaffanella [28], at rain rates above 0.1 inches/min (2.5 mm/min), the generated radio noise was virtually uninfluenced by the rain intensity [p]. This

---

[o] See pp 1940 -1942 [19]

[p] The rain rate per "hour" seems to be an error, possibly the intention was 2.5 mm/min or 0.1inches/min.

characteristic of rain-induced corona noise provides a repeatable test which can be compared for results obtained at different altitudes.

L. Boulet and B.J. Jakubczyk of the Université Laval, Faculté des Sciences, Quebec, Que., Canada completed work on AC corona in foul weather conditions and presents the phenomenon in an overall picture "in the range which may be of interest to engineers" [29].

3.4 FIRE AS A CATALYST FOR CORONA AND BREAKDOWN.

3.4.1 Flame Temperatures

Fire has the fundamental component of high temperatures. The temperatures of the sugar cane fires in the proximity of the conductors has been estimated to be in the region of 110°C to 250°C. Flame temperatures have been measured up to 800°C and 1200°C, but it appears that no accurate measurements have been made to date. In limited measurements made in this project with advanced thermal detecting visual equipment, temperatures greater than 162 C were recorded at the conductors in a genuine sugar cane plantation fire. Further temperature recordings should be made to capture more information about the actual temperatures under which corona is being generated at the conductors. It is however, not expected that the temperatures would be high enough for thermal ionisation to play any major role in the corona process. As explained previously (section 3.2.3), work done by K.T. Compton [25] showed that temperatures of over eight hundred degrees are required to reduce the breakdown strength of air by even a small amount with the assistance of thermal ionisation.

3.4.2 Flame Lengths

The heat generated by the fire is a continuous "plasma" frequently releasing large pockets of heat from the main body of the flame. Depending on the environmental elements, flames of a sugar cane fire may reach the conductors from many meters away. Sugar cane fires have now been visually recorded with flames reaching heights of several meters above the earth wires on a triangular line configuration. With no wind present, the vertical heights obtainable from a continuous flame should therefore not be underestimated. Recordings have captured flames at heights of 25 to 30 meters. In the environment, humidity will also influence the eruptive nature of the fire. In very dry conditions the turbulence created by the fire will be extremely explosive

with the thermal vertical ascent being very much less limited. Likewise in windy conditions, the horizontal distances across which the flames could be distributed is at times extremely far (unexpectedly far for the inexperienced since J.T. Bird refers to distances of up to 25 meters).

3.4.3 Air Density / Air Pressure

The fundamental activity occurring due to the presence of higher temperatures, is the decrease in air density. From equations (1) and (2), substantial increases in temperature (T) and decreases in pressure (p) will substantially increase the mean free path experienced by electrons under the influence of an external electric field. Hence the energy gained by those electrons will also increase substantially. The probability of ionisation, P_i, will therefore be higher and the rate of electron avalanche will increase. The nett result then follows that for fire-induced corona the voltages at which the different modes of corona start to occur should be lower than is the case for rain-induced corona. However, unlike rain, the flames of the fire are not continually in the same physical position in the column below the conductor (figure 3.3) but rather will shift and move around in that column touching and covering the conductor surfaces sporadically. Hence large streamers can be expected at lower voltages but due to the varying position of the flames at the conductors, these large streamers will not be continuous, as can be expected in the case of rain-induced corona.

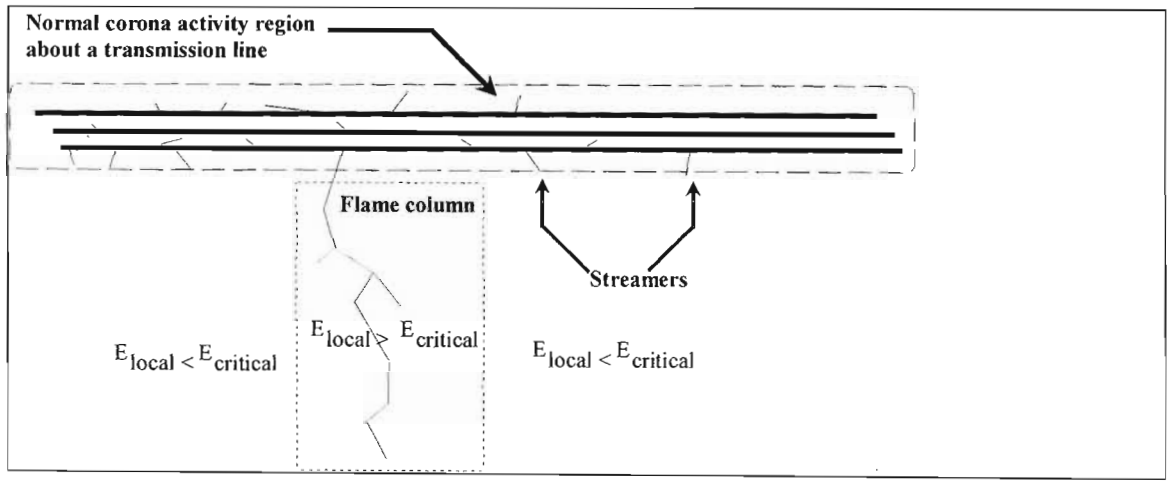

Figure 3. 4: Development of a streamer with the aid of reduced air density

In some instances, flames will also pass by the conductors in pockets dislocated from the main body of the flames.

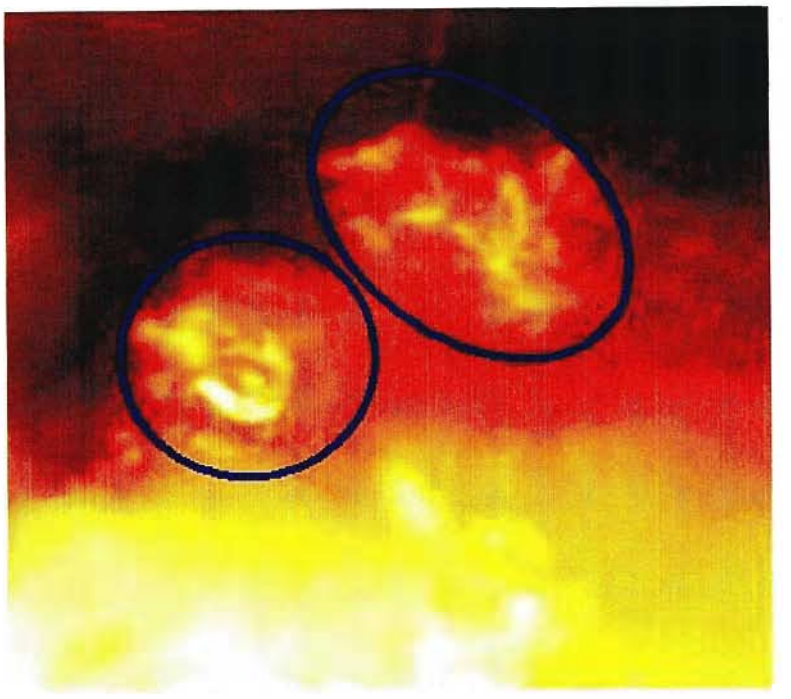

Figure 3. 5: An example of pockets of flame.

3.4.4 Particles

The presence of carbon-based particles in sugar cane fires is another factor which will severely influence the electric field about the conductors. The distortions caused by conducting particles to electric fields are well understood [30]. Sadurski postulated, "the presence of particles in bush fire flames are responsible for the flashover of transmission lines" [5]. In the proximity of the conductors the particles become dipoles (figure 3.4), ionised by the electric field and becoming part of the field lines emanating from the high voltage conductors.

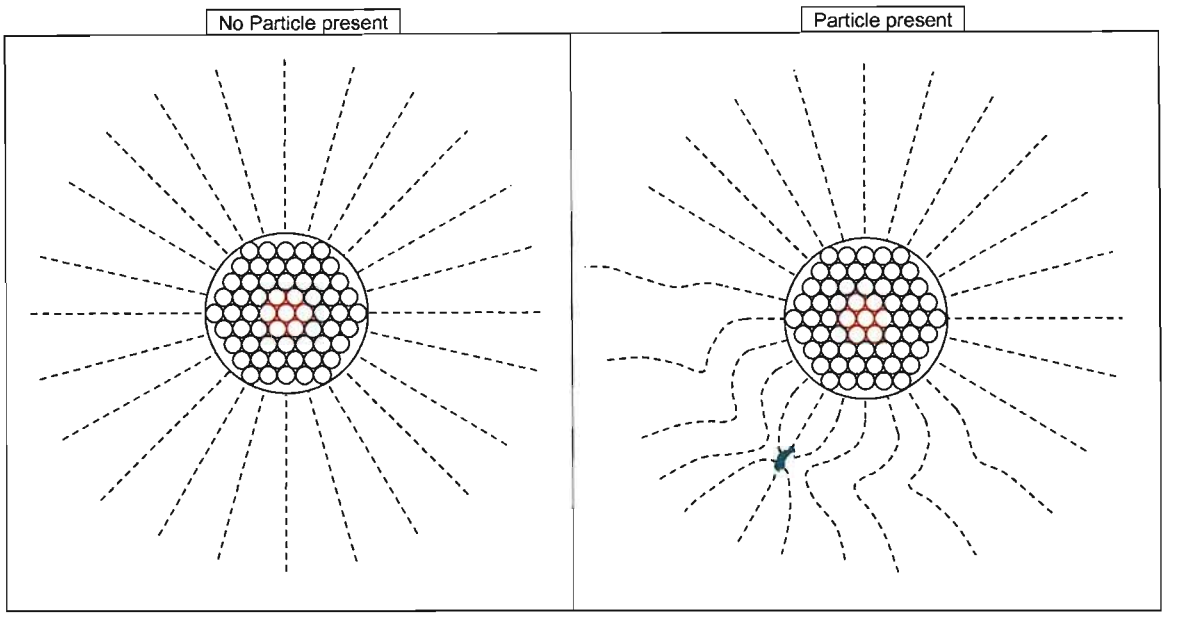

Figure 3. 6: Deformation of electric field about a conductor due to presence of a particle

The increased local field due to the particle will start the process of ionisation by electron impact, and provided the electric field is high enough, the gap between conductor and particle will be bridged with streamers then emanating from the particle.

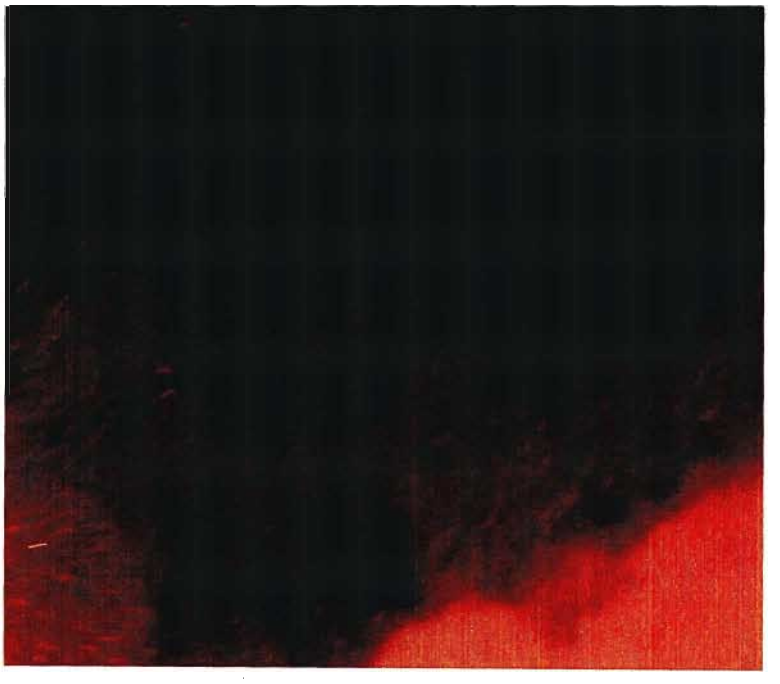

Figure 3. 7: An example of particles in and above flames during a night-time fire.

Should there be sufficient particles in the gap between electrodes, the bridging affect from conductor to particle to particle will finally result in the bridging of the entire gap.

The final bridge to flashover may not necessarily be a particle bridge but rather the increased electric field stresses across the reduced gap between the last particles (front of the leader) and the other electrode. More research is being carried out in this field to determine the process by which particles bridge the gap and the requirements for such a flashover to occur due to the sugar cane particles. Also the role which particles play in the breakdown of the air insulation in the event of a sugar cane plantation fire under power lines [q].

3.4.5 Chemical Reactions

The research work performed here does not consider the influence of different flammable materials and as such does not compare the chemical reactions resulting from different combustion processes. For any given flammable material, combustion of the material will result in the release of electrons and ions according to the chemical reactions. The number of free electrons available for ionisation by collision will therefore vary from flammable material to flammable material. Any material producing more free electrons through the combustion process may induce higher corona intensities. The conductor and bundle dimensions and the applied electric field stresses are critical components which will influence the degree to which that corona intensity will exist further from the conductor surfaces.

3.5 POLLUTION ON INSULATORS

In order to simulate the affects of polluted insulators on the transmission system, two high-voltage tests are universally accepted [r]. The salt-fog test requires a string of clean insulators stressed between a high applied voltage and ground. A mixture of salt and water is then sprayed onto the insulators in a fine fog under operating conditions. The result is an increase in the leakage current (at 50Hz) through the conducting layer of the mixture of salt and water. The

---

[q] Previously by Professor D. A. Swift, Head of Electrical Engineering Department, and now by Dr D.A. Hoch, Head of High Voltage Engineering both from the University of Natal, Durban, South Africa.

[r] Artificial pollution tests on high-voltage insulators to be used on a.c. systems, IEC Publication 507 revised edition, 1987, stipulates the procedures for the salt-fog method and solid-layer method of testing polluted insulators.

current flow warms the layer and the layer starts to dry out, thereby developing dry bands. The current flow generates an arc across this dry band and the band increases in width due to further heating. This continues until either the gap is fully bridged by the arc and flashover results, or the overall flow of leakage current is stemmed as not enough current flows to sustain the arc. When the dry bands are sufficiently wetted again, leakage current will flow. The second test is a clean fog or solid-layer test. Here insulators are pre-polluted with a mixture of kaolin, salt and water. Ensuring a uniform layer of pollutant is applied, the solution is then baked until a crystalline layer is formed. The string of insulators are then stressed to a high voltage and tap water is sprayed onto the conductors in a fine fog. The layer of pollutant becomes conductive and the process as for the salt fog test occurs. In both cases the arc occurring generates high frequency components and can be seen as a source of noise measurable at the circuit measuring point. In addition, where the insulators are not entirely bridged by the conducting medium, a region of high stress exists across the gap and the local field at this point is higher than the critical field with corona resulting. Corona electrical discharges can also be seen about the underside of the insulators when the local fields are equal to or higher than the critical field. The resulting ionisation leads to streamers and corona if the fields are large enough. The changing field will influence both these parameters, the higher the fields the larger these affects will be.

3.6 SURGES

Lightning and switching surges exist due to specific activities which, with closer scrutiny, will show that these characteristics can be defined, and with appropriate measures, can be excluded from any detection system. An example is the existence of high levels of noise on the line irrespective of the phase orientation of the 50 Hz supply. Hence noise may be present at the 50 Hz zero cross-over point. From figure 3.2, no modes of corona activity exist at the zero cross-over point of the power cycle.

3.7 INFLUENCE OF OTHER SPURIOUS SIGNALS AND NOISE

Noise on a channel was defined as "any unwanted disturbance within the radio frequency band, such as undesired electric waves in any transmission channel or device". By this definition it would be unwise to predict that ALL incidents of noise have been adequately defined and therefore it will be necessary to monitor the progress of the detection device and to develop a reliable database of noise patterns on an ongoing basis. The more significant influences on the

system will be those that are first identified. A dedicated research schedule will be required to further investigate the factors which may influence the performance of the fire detection device and may be used to further improve the performance of the network. In addition, corona has many components which are not entirely understood and such additional research via the analysis of corona noise on the high voltage lines may help clarify scientific facts from fallacies.

CHAPTER 4

Laboratory – Large Corona Cage: Set-up and method

The research work reported in this dissertation covers three of four measurement configurations and testing sites. The fourth, a small corona cage, is referred to in chapter 5 for completeness of all the work carried out at the time.

This chapter describes the large full size corona cage (figure 4.1) and its operation, the conductors tested, the test methodology, test procedures and finally the measurement methodology (circuit layout, etc.). Chapters 5 and 6 contains the results and conclusions obtained from this large corona cage.

4.1. BACKGROUND

Eskom has a high voltage test facility which includes a corona cage shown in figure 4.1 below.

Figure 4. 1: Eskom corona cage

Performing measurements in the corona cage provided the author with the opportunity to isolate the fire-induced corona noise from all other major noise sources. In addition, the facility eliminated background noise which is always present on an operational transmission line. Finally, the facility provided an environment within which the research work could proceed without delay. In the operational environment, network operations dictate what can and cannot be done and when it can be done.

The cage is made up of three wire mesh cylinders 7 meters in diameter. Figure 4.2 shows an internal view of the construction of the cage. In the photo, a twin Zebra conductor bundle was in position strung between the two sets of corona rings at each end of the cage. The red circular beams are the ends of the three cylinders. The horizontal pole visible to the left of the picture is an incoming aluminium bus bar carrying the supplied power to the conductor under test. The aluminium pole has a smooth surface to eliminate any possible sources of corona from the supply to the conductor under test.

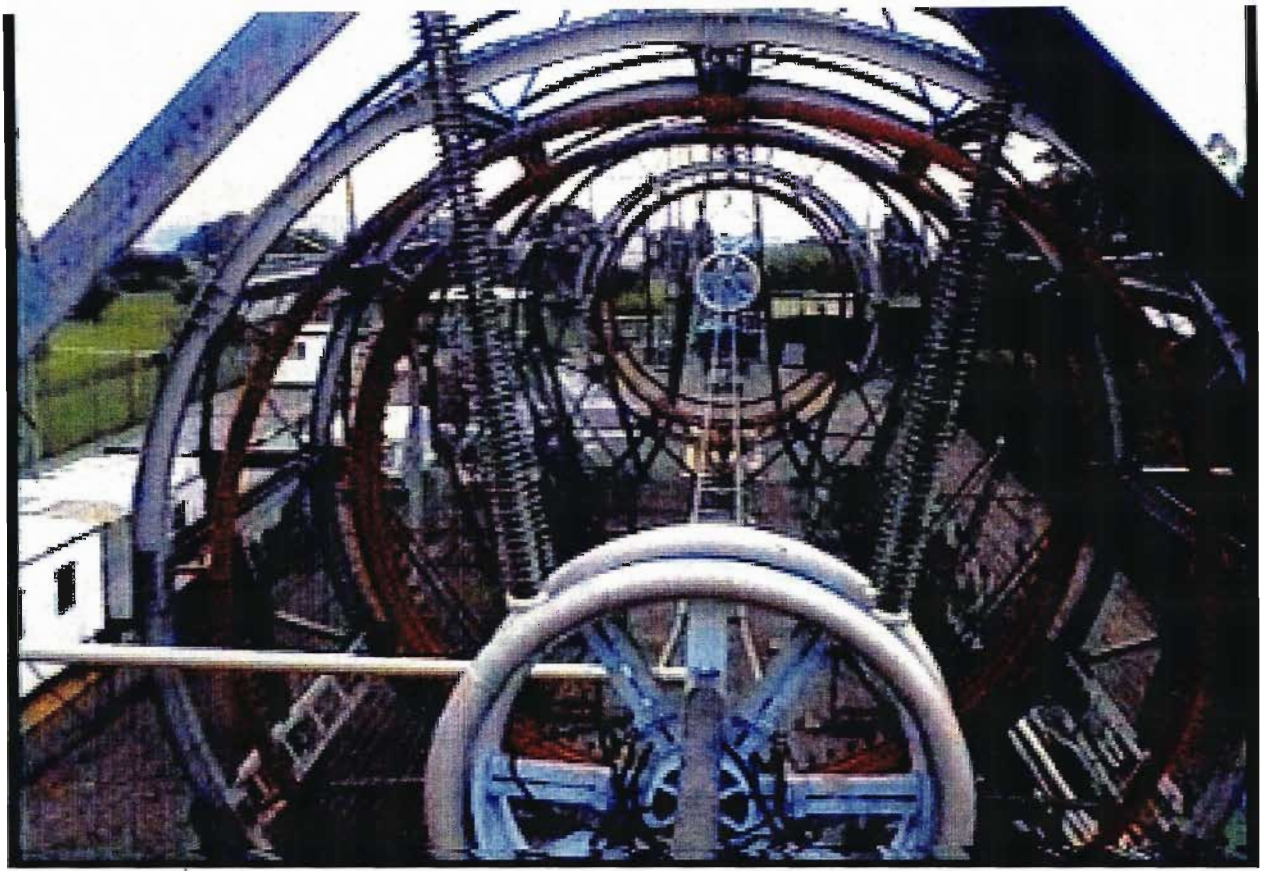

Figure 4. 2: End view of the corona cage

Figure 4.3 shows one of the two end cylinders to the left of the coupling capacitor. Each of these cylinders are 5 meters in length. These cylinders eliminate end effects from the section of conductor exposed to the test conditions. Rain is generated in the cage only on the centre cylinder which is 30 meters long.

Figure 4. 3: End effects segment and rain nozzle structures

Figure 4. 4: High frequency filtering coupling capacitor

Figure 4.4 shows the coupling capacitor (CC) with the additional filtering included in the box at the base of the CC also illustrated in figures 4.5 and 4.6.

Figure 4.7 shows the hardware in the box which

(1) drains the residual 50Hz current to ground through the inductance at the top of the box,

(2) compensates for capacitive phase shift caused by the coupling capacitance with the inductance in the right lower half of the box,

(3) matches the line impedance of the installed conductor bundle with a potentiometer in the lower left side of the box, and finally

(4) matches the 50Ω instrument impedance with components on a (barely visible) printed circuit board in the bottom half of the box.

The overall circuit diagram for the above mentioned components is shown in figure 4.13 in section 4.7.

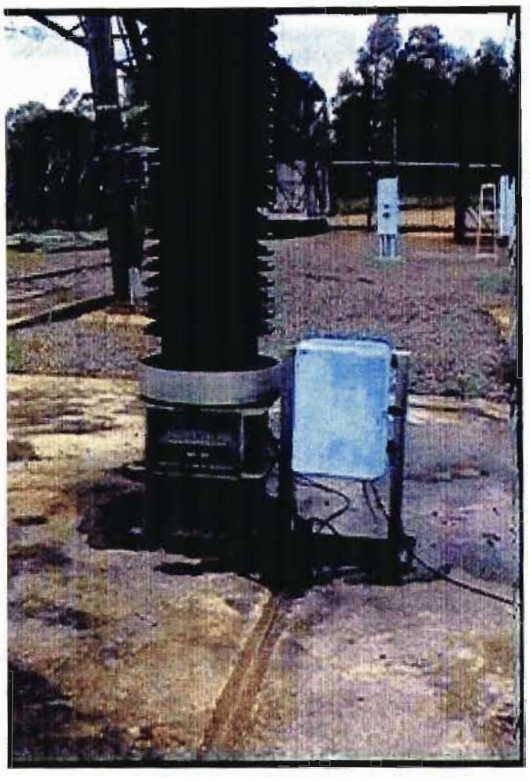

Figure 4. 5: Filtering unit

Figure 4. 6: Filtering unit open

The additional filtering circuits for the high frequency signals are shown in the figures above.

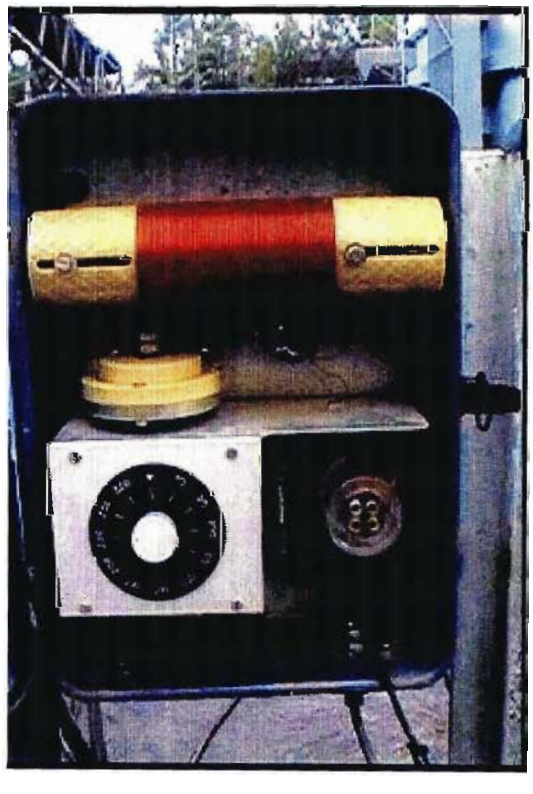

Figure 4. 7: Filtering unit components

Figure 4.8 shows the coupling capacitance that is used to provide the voltage applied to the test circuit. The unit is calibrated to provide an accurate 50Hz voltage division and a further

90° phase shift unit is used to provide angle compensation from this capacitive voltage measurement that induces a phase shift between the primary voltage and the current flowing through the device.

Figure 4.9 shows the 6kV/400kV step up transformer that supplies the power to the test circuit.

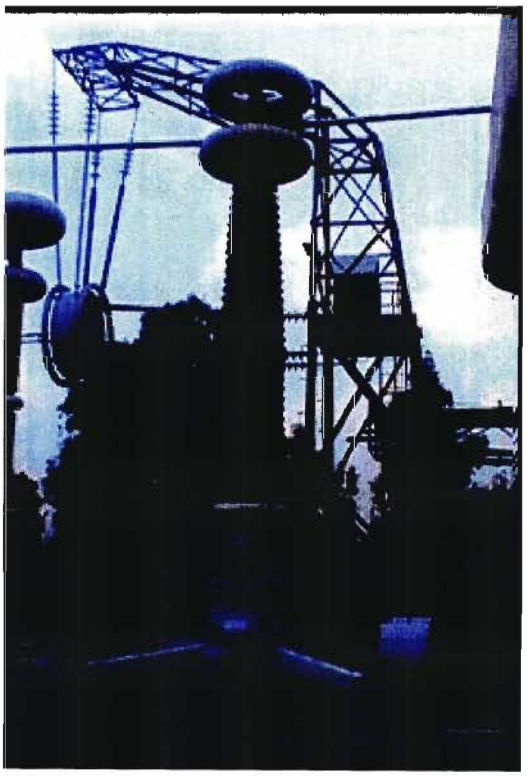

Figure 4. 8: Calibrated coupling capacitor - line voltage measurement

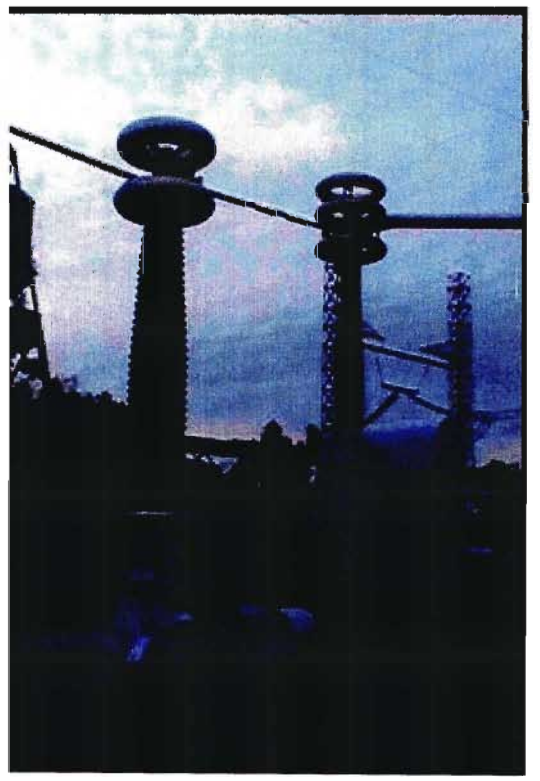

Figure 4. 9: Voltage divider and supply transformer

Figure 4. 10: All equipment connected between the supply transformer and the corona cage

The power supply to this facility can supply up to 400 kV at a maximum of 2 ampere. Limited by the power transformer. Figure 4.11 shows the power supplies to the test facility.

Figure 4. 11: 6kV Low voltage (LV) source of supply to the step-up transformer

The 6kV supply is regulated to provide the required voltage on the test conductors within the corona cage. The appropriate surface gradient for a particular conductor bundle under test can be

provided by calculating the required voltage for that gradient given the dimensions of the corona cage and the conductor bundle under test..

Further details of the corona cage can be obtained from a document by A.C. Britten and C. van der Westhuizen, in which the complete function of the corona cage is described as follows: "*To allow the main corona parameters of conductors to be measured as a function of the applied voltage (and hence conductor surface gradient)*" [31].

4.2. OBJECTIVES

The main goals at this test station were to:

(a) establish the noise levels and pattern generated by the fire-induced corona noise,
(b) determine whether or not the fire-induced noise could be identified when observed directly, and
(c) determine whether or not this noise was distinguishable from other major noise sources such as rain.

4.3 OPERATION

The conductors under test are strung through the corona cage made up of the three horizontal cylinders of wire mesh, 7 m in diameter and 40 m in overall length. All environmental test conditions were applied to the central 30 m section of the cylinder. In this way, all corona occurring will be generated in uniform electric field conditions applied to the conductor rather than due to any irregular shape of the field about the conductors which may be caused by fixed installations in the proximity of the conductors. The conductor or conductor bundle is terminated at both ends on corona rings to minimise corona "end affects".

Figure 4.12 shows the block diagram of the band-stop filter in series with the power supply to block any high frequency components from passing from the bundle to the power supply. A bandpass filter is placed in parallel with the supply and band-stop filter to extract the high frequency components generated from the conductor bundle. In this way any propagated noise generated due to induced corona should be measured in the stage following the bandpass filter. In the corona cage, both filters were tuned to a centre frequency of approximately 500 kHz.

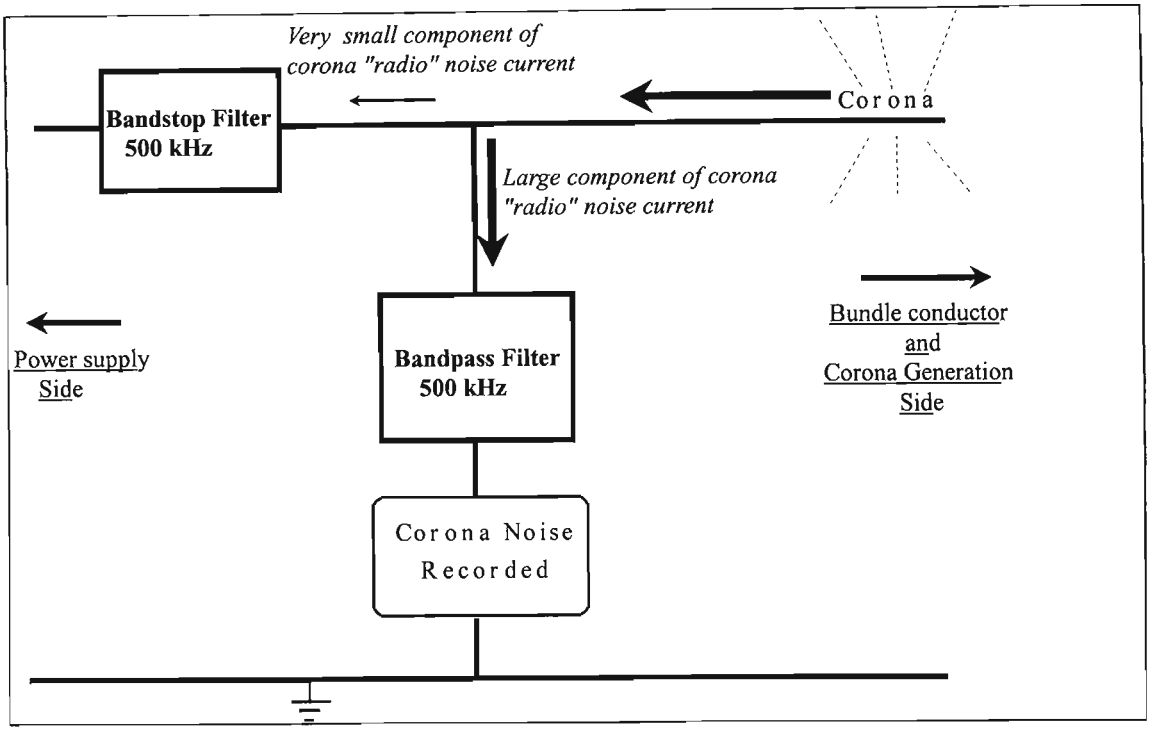

Figure 4. 12: Block diagram of the corona cage with filtering

4.4 CONDUCTORS UNDER TEST

The corona cage is large enough to test any of the largest conductor bundles in use in South Africa including that used for the 765kV transmission feeders. The 275 kV and 400 kV networks have specifically been identified due to their impact on the country's economy and the high exposure to potential fire induced outages. The 275 kV network typically uses the twin Zebra conductor bundle and the 400 kV network typically has the twin Dinosaur bundle.

The Zebra conductors have an overall diameter of 28.56 mm with 54 aluminium strands and 7 steel strands each with a diameter of 3.17 mm. In the Eskom main transmission system (MTS), this conductor is used in a twin conductor bundle configuration. The feeder configuration is usually a horizontal alignment where the phases are in line several meters apart with two single earth wires overhead providing lightning protection. The line is then designed for a surface gradient in the region of 14kV/cm at maximum voltage.

The Dinosaur conductors have an overall diameter of 35.56 mm with 54 aluminium strands each with a diameter of 3.95 mm and 19 steel strands each with a diameter of 2.36 mm. As for the Zebra, the Dinosaur is also used in a twin bundle with the same feeder configuration. Here the line is designed for a surface gradient in the region of 15 kV/cm at maximum voltage.

Other conductors tested during the progress of this project were the Wolf conductor in single, twin and triple bundle configurations and the Pelican conductor in twin and triple bundle configurations. The Wolf conductors have an overall diameter of 18.13 mm with 30 aluminium strands and 7 steel strands each with a diameter of 2.59 mm. The Pelican conductors have an overall diameter of 20.67 mm with 18 aluminium strands and 1 steel strand each with a diameter of 4.13 mm.

4.5 TEST METHODOLOGY

Measurement in the corona cage is done in the more widely used fashion for Radio Influence Voltage" (RIV) which is by quasi-peak measurement. The implication here is that the "annoyance" level of the induced corona noise is measured. That is, the level of the output from the quasi-peak detector depends not only on the peak values of the noise pulses but also on the repetition rate of those noise pulses.

As the character of the fire-induced corona was unknown, an additional "time domain" measurement was included to define the specific corona activity at the pulse or impulse level where ionisation is initiated. This was possible by using digital storage oscilloscopes. Having digitised the electrical transient activity, it was possible to carry out a fast fourier transform (FFT) on each waveform of interest and hence describe the frequency characteristics specific to each observed activity. Note that although the quasi-peak measurement changes with time, the "averaging" affect it has creates a reasonably steady (recordable) value for a particular surface gradient relatively independent of time. Thereby it is no longer a "time domain" measurement to be interpreted with the instantaneous applied voltage and can only be specified at the frequency of measurement. The quasi-peak recording facility was available at the corona cage and hence was used in addition to the digital storage oscilloscopes for additional information and comparability to international measurements, an example being the measurements done in Italy for rain-induced corona.

4.6 TEST PROCEDURES

For each conductor bundle the following procedures were followed:

4.6.1. Dry Conditions

The tests required that the air about the conductors and within the corona cage cylinder remained dry and relatively free of moisture. No flames were required for this stage.

The voltage on the conductor bundle was raised to a point above the normal operating voltage and gradually decreased in steps of gradient (kV/cm). The gradient was then held at specific gradients to record both quasi-peak and time domain data. The voltage was therefore raised to a point where at least some corona activity was visible and from there decreased until no corona was visible.

A reduction in potential rather than an increase in potential ensures that the cut-off of the corona current is accurately measured since the cut-off (which is the threshold for the onset of corona current) will always occur at the same potential [s].

For each step, the induced corona noise propagated along the line was measured after a short period allowing the surface gradient on the conductor surface to "settle". In most cases the quasi-peak levels of that noise was recorded.

4.6.2. Rain Conditions

The acceptable rain rate required for tests of this nature was 2 mm/min which was classified as "heavy rain". No flames were required for this stage.

Again the voltage on the conductor bundle was first increased to a point where corona was clearly visible and then decreased from the higher gradient. This was done with the water sprayers above the corona cage providing the heavy rain conditions. The surface gradient was again reduced in steps with rain falling and paused at the required gradients. After a "settling" period in which the droplets on the conductor were in a steady state, measurements were taken.

---

[s] See p75 [18]

The test was stopped once no further corona was visible or the level of activity had dropped significantly.

4.6.3. Fire Conditions

Three sources of fire were considered:
(1) Gas fire (a fire source with no particles), (2) grass fire and (3) sugar cane fire.

The gradient (in kV/cm) on the conductor bundle under test, was increased from a low gradient up to gradients where either:
(1) flashover occurred, (2) very loud audible corona was generated or (3) until the voltage started deteriorating due to the limited power transformer supply capacity.

The increase in gradient was done in controlled steps in accordance with the observed activity. In contrast to dry air and rain conditions, flames do not present a uniform presence around the conductors within the corona cage. As such, the accuracy of the extinguishing gradient cannot be guaranteed and hence the benefits associated with reducing the gradient do not apply for the fire tests. In addition, the maximum gradient before flashover occurs cannot be guaranteed as the flames do not provide a singular plasma which remains stable. The transformers used to supply the power to the corona cage were both sensitive and expensive to replace - therefore it was preferable to avoid as many flashovers as possible. The decision was therefore to increase gradient rather than decrease gradient.

The gas fire was produced with a balloon burner requiring low pressure gas. The burner temperature was controlled to a lower temperature to prevent the conductors under test from melting. In the Eskom transmission network very little annealing is seen and as such no excessive temperatures were used in the simulation. In this manner a reasonably repeatable procedure was possible.

The challenge in the procedure was to ensure that the flame and resultant heat generated, remained near the conductors. Winds at very low velocities were capable of causing a deviation of the flame path from the conductors. The gas flames were nearly transparent in bright sunlight conditions where the sunshine matched the light frequencies emanating from the flames. The flames had to be described in both width and depth in order to guarantee that observed high frequency activity matched the physical dynamics present at the conductors.

The starting gradient was always considerably lower than would normally be experienced on the operational transmission lines. For each step the existing induced corona noise propagating along the line was measured and in most cases the quasi-peak levels of that noise was recorded as accurately as possible. A "settling" time with the fire tests were inappropriate as the flames were rarely steady.

The balloon burner had an activation switch which allowed the operator to remotely initiate a fire. The burner was then operated several times at each surface gradient selected. That is, the chamber was energised to the required gradient and only then was a flame without particles applied to the chamber. A large increase in the audible corona was considered as an early warning of imminent electrical breakdown in this test.

Sugar cane was also provided. The sugar cane fire tests in the cage were managed rather than controlled. The sugar cane was assembled vertically within metal scaffolding *below* the wire mesh cylinder in order not to interfere with the electrical characteristics of the applied gradients about the conductor bundles under test. The fuel was set on fire and personnel moved to safety before the line was then energised. At this point the flames start to build up and visual observations were matched to high frequency electrical activity observed on the monitoring equipment.

This process enabled the author to also monitor the influences of smoke and particles on the generated corona levels. No "settling" time was possible with these tests and the quasi-peak levels were not recorded as no steady state conditions were possible.

4.7 MEASUREMENT METHODOLOGY

4.7.1 Measurement Circuit

The critical component of the measurement method is the bandpass filter that provides the extraction process of the signals which contain information about the presence of the fire at the conductors.

The bandpass filter as shown in the block diagram in figure 4.12 is detailed in figure 4.13 below.

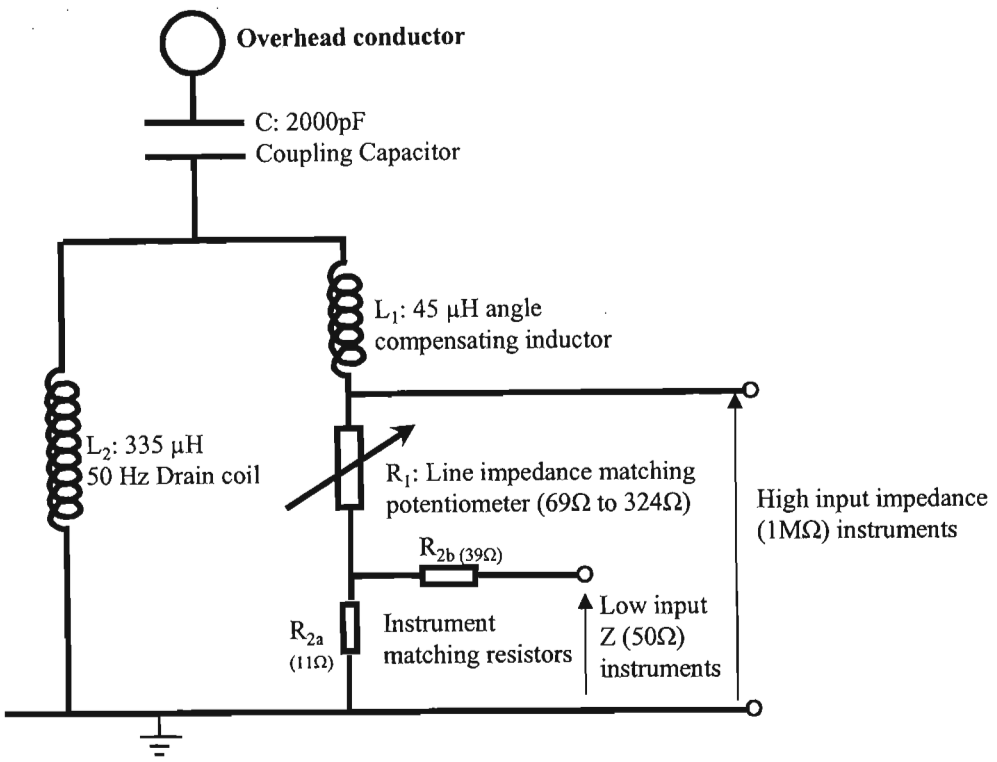

Figure 4. 13: Bandpass filter as configured at the corona cage

The filter contains 5 essential blocks:

1) C: 2000 pF (2nF) coupling capacitor;
2) L_2: 335 μH 50 Hz drain coil;
3) L_1: 45 μH angle compensating inductor;
4) R_1: An impedance matching variable potentiometer adjustable from 69Ω to 324Ω; and
5) R_2: 11 Ω impedance matching resistors for the quasi-peak instrument.

4.7.2 Impedance Matching

The impedance matching variable resistor was used to adjust the operating impedance to match the characteristic impedance of the conductor bundle tested in the cage. Thus any induced corona

noise from the bundle in the frequency range of interest would not be reflected back onto the bundle.

The characteristic impedance of the conductor bundle is calculated as a function of the capacitance and inductance of the conductor bundle and hence also of the overall radius of the conductor bundle. The geometric mean radius (GMR) of each conductor is given by

$$r' = e^{-\frac{\mu_r}{4}} r \tag{20}$$

where r is the conductor radius and
μ_r is the permeability. For the inductance calculation $\mu_r \approx 1$ for aluminium and copper.

$$r' = e^{-\frac{1}{4}} r \qquad \text{(20a) For inductance}$$

To calculate the capacitance, the GMR of the conductor is taken as

$$r' = r \qquad \text{(20b) For capacitance}$$

The overall GMR of the conductor bundle is given by

$$r'' = \sqrt[n]{n r' a^{n-1}} \tag{21}$$

where n is the number of conductors in the bundle and
a is the bundle radius calculated as a function of s, the separation between the conductors.

The capacitance and inductance can then be calculated. The capacitance of a conductor bundle (in Farads per meter) is calculated as

$$C = \frac{2\pi\varepsilon_0}{\ln \frac{R}{r''}} \tag{22}$$

where R is the radius of the cylindrical cage (Eskom corona cage radius = 3.5 m). ε_0 is the permittivity of a vacuum or approximately the permittivity of air ($\varepsilon_0 = 8.859 \times 10^{-12}$ Fm^{-1}).

The inductance of a conductor bundle is calculated as

$$L = \frac{\mu_0}{2\pi} \ln \frac{R}{r''} \tag{23}$$

where μ_0 is the permeability of a vacuum or approximately of air ($\mu_0 = 1.275 \times 10^{-6}$ Hm^{-1}).

Finally, from the capacitance and inductance, the characteristic impedance of the conductor bundle can be calculated:

$$Z_c = \sqrt{\frac{L}{C}} \tag{24}$$

The calculations for each conductor bundle have been done and are recorded in appendix B.

4.7.3 Circuit explanation

a) High frequency filter: The coupling capacitor in figure 4.13 virtually eliminates the high voltage, low frequency 50 Hz component.
b) Capacitive phase shift: However, due to the capacitance, it also causes a phase shift in the current passing through the coupling capacitor. The 45 μH inductor compensates for that phase shift.
c) 50 Hz leakage current: The coupling capacitor does not completely eliminate the 50Hz signal. The 335 μH inductor shunts the balance of the 50 Hz current component to ground and away from the measuring circuit.

4.7.4 Measurements

Quasi-Peak measurements: The quasi-peak measurement is taken, as indicated in figure 4.13, directly from this circuit with a CISPR-approved Mod. SE 133 receiver [32].

Time domain measurements: The digital storage oscilloscope was connected across the entire resistor bank. The oscilloscope used has a high input impedance (1 MΩ). The connection between the measurement point on the resistor bank and the oscilloscope was made with approximately a 10m length of RG58 coaxial cable of characteristic impedance 50 Ω. For very

high frequencies this may result in reflections occurring due to the impedance mismatch between the coaxial cable and the input impedance of the oscilloscope. However, the signals being measured were of relatively low frequency (50kHz to 500kHz) such that the coaxial cable is electrically short. No reflections were observed in the measurements for these frequencies. The resultant burden on either the Quasi-peak detector (50Ω input) or the line impedance (69 to 324Ω) was negligible. The measurement is therefore a voltage measurement of a current source. Due to the available equipment the voltage measurement was more convenient than the direct measurement of current using a Rogovski coil or similar arrangement.

In order to accurately interpret the noise patterns captured with the digital storage oscilloscope, it was necessary to also capture the 50 Hz applied voltage waveform. As the conductor surface gradient is directly proportional to the applied voltage [equation 5] the observed corona pulses can be interpreted in terms of the corona modes presented in figure 3.3 with greater accuracy and confidence.

4.7.5 Sampling frequency theory and selection

The measurement electrical circuit had a centre frequency of 500kHz. A minimum sampling frequency of 1MHz (Nyquist frequency) was therefore necessary to accurately document all the measurable signals from this system.

Fire-induced corona pulses and their characteristics were entirely unknown at the time of this project. For accurate comparisons between fire-induced corona and other sources, the recorded data needed to be more descriptive than the minimum requirement for correct definition of the signal.

Fire-induced corona was expected to be more sporadic than more consistent signal sources such as rain and rain droplets. The flame is influenced by several parameters such as convection due to the heat generated in the flame. Due to these parameters, flames will typically be volatile and not remain constant at the conductors.

An exception to this statement would be when a very large fire engulfs the conductors. In this instance the size of the flame (width and depth) dictates that the conductor remains within the flame despite the flame's volatile movement. In the gas fire experiments the flames will not be large enough to engulf the conductors at all times.

In order to eliminate any uncertainty, the sampling frequency was selected at a higher level of between 5 and 10MHz, rather than remain at Nyquist.

It must be understood that the actual electrical discharges, electrical discharges in air in this case, have faster rise times than would be detectable with the proposed 10MHz sampling frequency. Expected rise times of an air discharge was in the vicinity of 10ns which requires a sampling frequency of at least 200MHz (preferably higher) and a different sampling circuit than is already available in the power transmission network and its associated high voltage apparatus. Hence the measured signals here are being observed for their changes as the energy from each discharge passes through the available filtering circuits through their periods of rise time and dissipation time.

4.7.6 Sampling duration and selection

Rain-induced corona noise has been researched in detail and as a result the trends are well known. The same is not true for fires. Given the theoretical knowledge available, fires need to be tracked for longer periods to understand how the fire-induced corona will fluctuate over time.

In order to capture the signals in relation to a full power cycle, a minimum of 20 ms of data was necessary. Any deviations as a result of the changing alternating current power cycle waveform could then be defined. With a sample rate of 10 MHz (10,000,000 cycles per second) the duration between samples is 100 ns. For a period of 20 ms a total of 200 000 samples was necessary.

The changes in a single power cycle should present increases in field, decreases in field, possible increases in electric field exceeding the critical electrical field (E_{crit}) for ionisation, and possible ways in which the fire induced corona may change. However, one cycle is insufficient to define how the corona activity has changed due to variations in the flames at the conductor. An increase in corona activity is expected as the flames move towards the conductors. As the flames engulf the conductors (on average), the corona is expected to be at a maximum and then the flames will move away from the conductors and the associated corona will decrease. In addition the volume of degraded air insulation will also influence the overall activity levels especially when that volume tends towards bridging the entire gap between electrodes. Therefore the fire-induced

corona must be monitored for more than one power cycle to observe these changes and to define the level of confidence in observed fluctuations.

A compromise was necessary between the cost involved in more measurements and amount of information in the captured waveforms. It was assumed from theory and experience of specialists in the field of corona that the induced noise generated due to fires would be in the form of pulses. Hence very fast rise times could be expected and if the digitising points (sample point separation) were too far apart, some of these pulses may be omitted. The character of a fire is both volatile and unreliable. Adding this fact to the fact that ionisation by collision is a probability phenomenon (page 21), costs would be higher if the sample rates were reduced.

The concept of detecting fires under power lines could fail, not because the concept was at fault but because the measurement technique was limited. The rewards of being able to detect fires and act on that knowledge far outweighed the sacrifice of time and money. Based on this knowledge, the first oscilloscopes used in this project were inadequate. The best oscilloscopes accessible to the project had sample length capacities of 8000 and 16000 samples. Clearly lower sampling rates had to be used with this equipment or the 50 Hz applied voltage had to be ignored. Other equipment such as tape recording devices were also inadequate. These instruments were tested and at frequencies of 500 kHz were found to generate unacceptably high levels of background noise introduced by the equipment. Whilst the dynamic range of the instruments was important, the availability of suitable instrumentation was non-existent. Hence the initial work was done in two categories or stages. One of lower sampling frequency (to track the power cycle) and the other of higher sampling frequencies for corona noise only. The lower sampling rates were preferable since the variation in corona cannot be discerned without knowledge of the field stresses.

Eskom T-S-I then acquired digital storage oscilloscopes with very large storage capabilities and the corona and 50 Hz voltage for at least one 50 Hz cycle was recorded for the different conditions on the remaining conductor bundles.

CHAPTER 5

Laboratory – Large Corona Cage: Quasi-Peak Experiments

5.1 RESULTS - REFERENCED TO GAS FIRE

5.1.1 Overview

This chapter covers the quasi peak test results captured at the corona cage. The configurations for which quasi-peak data was recorded included the following conductor bundles:

a) Twin Dinosaur;
b) Twin Zebra;
c) Triple Wolf;
d) Twin Wolf, and
e) Single Wolf.

For each bundle the measurement circuit had to be adjusted such that the measuring impedances (R_1 and R_2 in figure 4.13) matched the characteristic impedance of the conductor bundle under test. This eliminated the presence of any reflections that may have occurred as a result of mismatching.

The results are reported with a graph for each set of comparisons between dry conditions, rain conditions and fire conditions. The fire condition for this set of data is restricted to the gas fire test results. The gas fire as a source was sufficiently controllable to obtain reliable readings from the instrumentation. This was not possible from sugar cane and grass fires as these tests were not controllable but simply manageable.

Here fluctuations for the differing conditions will be discussed as a radio interference voltage (RIV) signal in relation to the applied electrical stress conditions in that central cylinder of the corona cage (in kV/cm).

5.1.2 Twin Dinosaur conductor bundle

5.1.2.1 Filtering circuit configuration

From the calculations in appendix B, $Z_c = 232.39\Omega$. The variable resistor R_1 in figure 4.13 can be set accordingly.

5.1.2.2 Test Results

In the figure below, the noise levels under dry conditions increase dramatically between 12kV/cm and 14kV/cm. Further increases in surface gradient results in a more gradual increase in RIV. In rain conditions the RIV is considerably higher from onset at 9kV/cm at approximately 50dBμV above dry conditions. The RIV then increases gradually towards a point at around 24kV/cm where the dry and rain conditions have very similar RIV values of approximately 85dBμV. In fire conditions the RIV levels approach the extreme levels reached in dry and rain conditions almost from the onset at the surface gradient of 9kV/cm with an RIV value of approximately 80dBμV. At 11kV/cm the RIV values for the gas fire exceeds the dry and rain conditions at 25kV/cm. At the normal operating gradient of around 15kV/cm the RIV values are approximately 50dBμV, 75dBμV and 95dBμV for dry, rain and gas fire conditions respectively.

Table 2: Quasi peak test data for twin dinosaur conductor bundle

Surface Gradient (kV/cm)	RIV Measurement (dBμV)		
	Dry Conditions	Rain (2 mm/min.)	Fire (In dry condition)
9	4	53	80
10	5	57	85
11	7	61	90
12	11	65	95
13	47	68	95
14	44	72	98
15	50	75	95
16	55	77	95
17	58	79	Flashover

(A complete table is given in appendix C).

The RIV readings for the gas fire conditions increased to 95dBμV at 12 kV/cm and then remained at this level through increasing surface gradients to 16kV/cm. This implies a level of saturation may have been reached. The air insulation was breached when the surface gradient was increased to 17kV/cm.

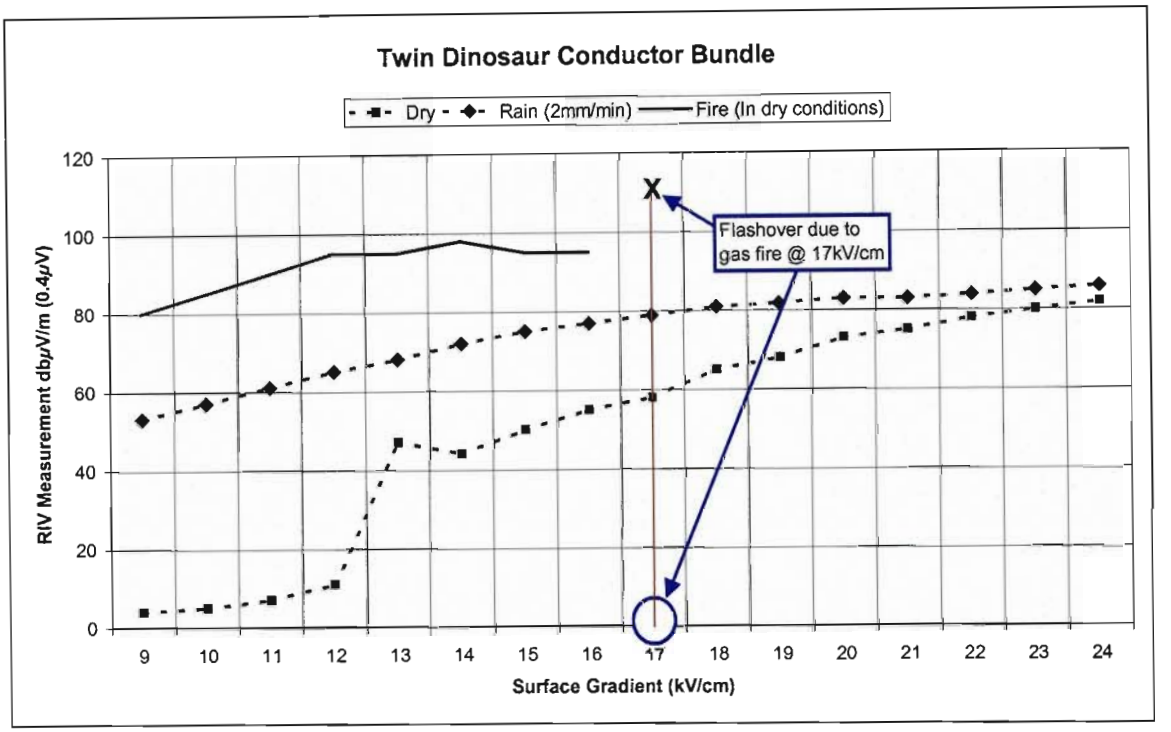

Figure 5. 1: Quasi-peak data of corona noise in dry, wet and fire conditions (twin Dinosaur).

As per the objectives given in section 4.2, (a) the noise levels generated by the gas fire induced corona is 95dBμV at the normal operating surface gradient for this conductor bundle of 15kV/cm. (b) The fire-induced noise can be observed directly as the levels exceed dry conditions RIV levels by 45dBμV at 15kV/cm which is nearly double the levels in dry conditions. (c) The fire-induced RIV is 20dBμV higher than the levels generated due to heavy rain conditions at 15kV/cm which is an increase of 27% from heavy rain levels.

The results are therefore positive in every aspect and fires can be detected with a CISPR-approved Mod. SE 133 receiver. However, the gas fire was carefully controlled to produce a stable flame at the conductors. A flame under natural conditions will not continuously envelope the conductors and as such the state at the conductors will fluctuate between dry and fire conditions as the flames move back and forth about the conductors. This may result in a fluctuation in the RIV readings between 50dBμV and 95dBμV at 15kV/cm.

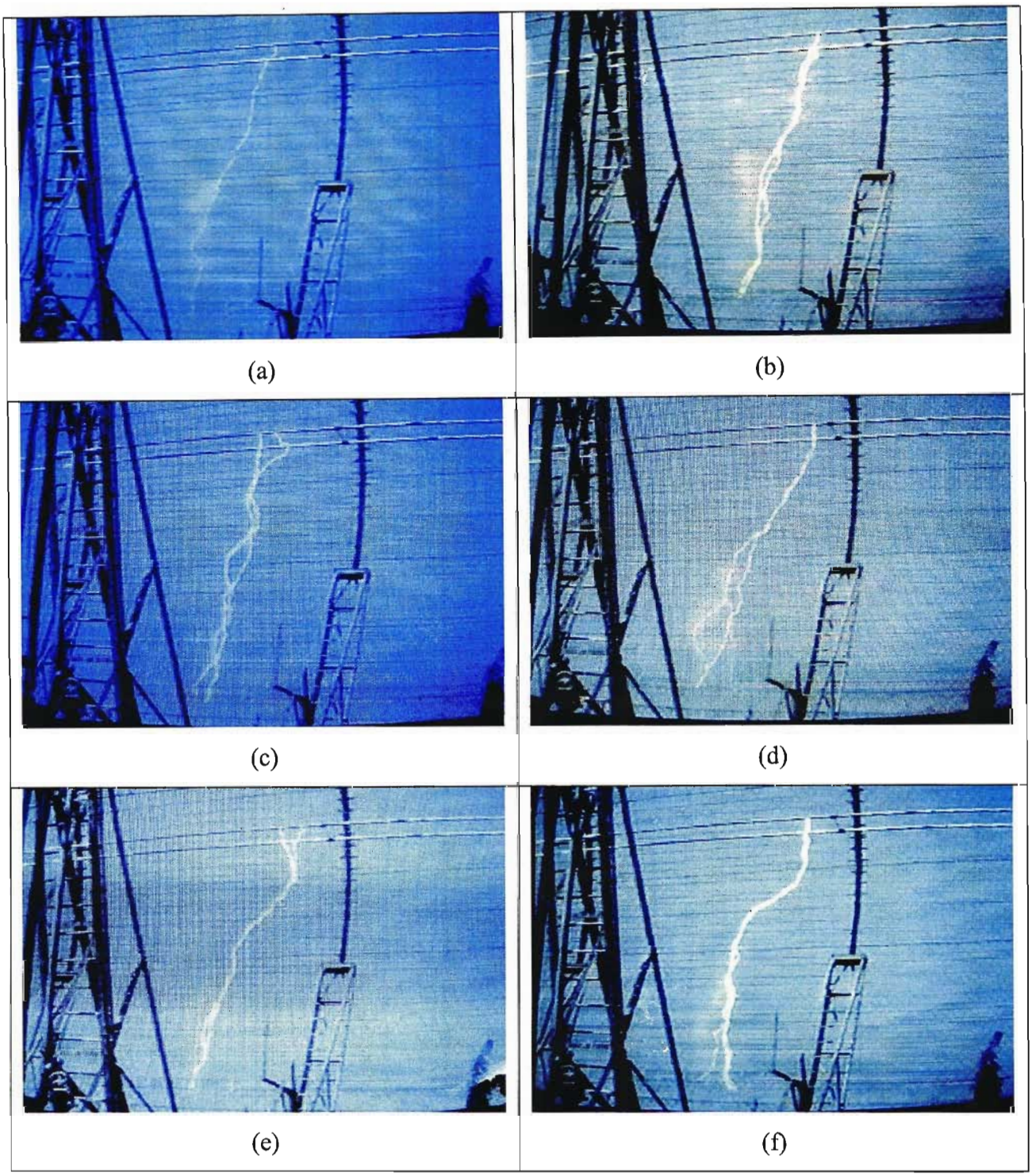

Figure 5. 2: Repeatable flashovers at 17kV/cm – Twin Dinosaur in controlled gas fire

5.1.3 Twin Zebra conductor bundle

5.1.3.1 Filtering circuit configuration

From the calculations in appendix B, $Z_c = 239.01\Omega$. The variable resistor R_1 in figure 4.13 can be set accordingly.

5.1.3.2 Test Results

The dry condition test results show a gradual increase in RIV levels from 45dBμV at 11kV/cm to 74dBμV at 19kV/cm. This is a step up from the dry conditions readings for the twin dinosaur conductor bundle of 7dBμV at 11kV/cm and 58dBμV at 17kV/cm. In rain conditions the readings are approximately 1 to 4dBμV lower than the twin dinosaur conductor bundle but a gradual increase is also evident with RIV readings of 60dBμV at 11kV/cm and 77dBμV at 19kV/cm.

Table 3: Quasi peak test data for twin dinosaur conductor bundle

Surface Gradient (kV/cm)	RIV Measurement (dBμV)			
	Dry Conditions	Rain (2 mm/min.)	Fire (Measured)	Fire (Adjusted)
11	45	60	59	65
12	54	63	69	69
13	54	66	69	72
14	61	68	69	75
15	63	71	65	77
16	65	74	79	79
17	67	75	66	83
18	71	76	85	85
19	74	77	75	90

The gas-fire conditions were difficult to control resulting in the phenomena considered in the previous section. At certain gradients the RIV readings matched those of the dry conditions as can be seen when comparing the values at 11kV/cm, 15kV/cm and 17kV/cm. It is clear that at these gradients the flames were not present at the conductors for a sufficient period to provide a stable reading of the flame induced corona. As a result a series of projected data was created

from the data obtained at other gradients and is shown in the column "Fire (Adjusted)" in the table above.

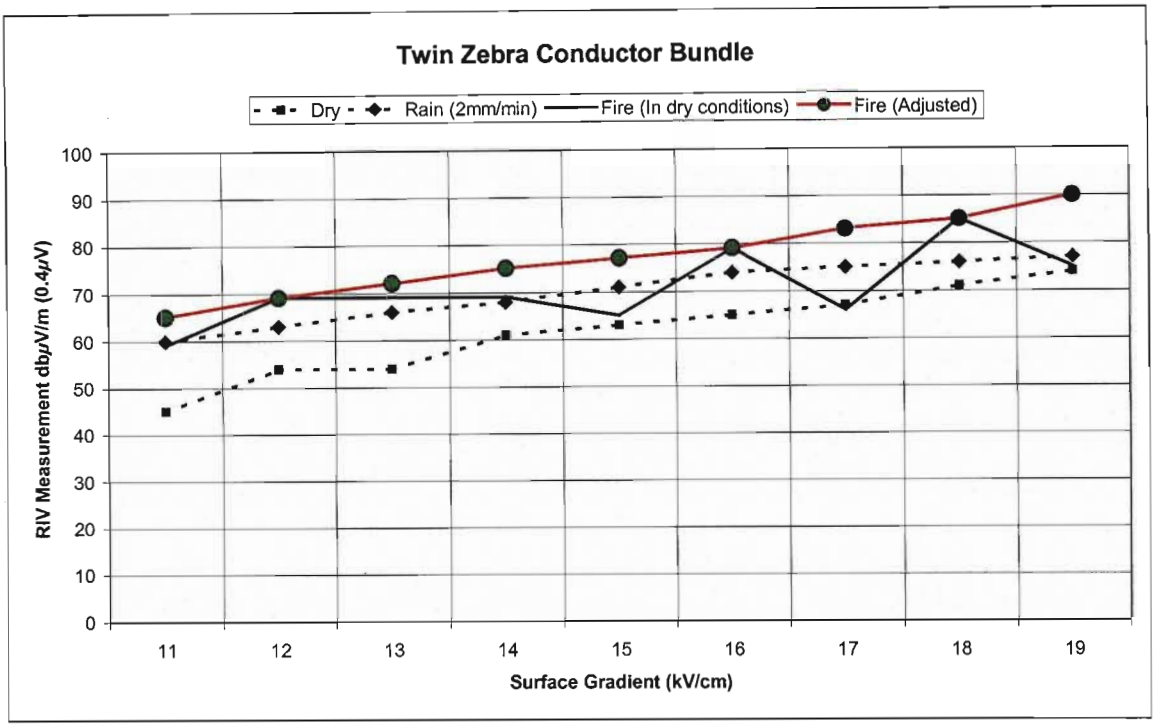

Figure 5. 3: Quasi-peak data of corona noise in dry, wet and fire conditions (twin Zebra).

At 12kV/cm, 16kV/cm and at 18kV/cm the RIV readings for the fire conditions are only 6dBμV, 5dBμV and 9dBμV respectively greater than the readings for heavy rain conditions.

As per the objectives given in section 4.2, (a) at 14kV/cm the RIV levels for the gas fire induced corona are 69dBμV (measured) and 75dBμV (projected). (b) The fire-induced noise levels are higher than that experienced in the dry conditions with a minimum increase of 8dBμV and a projected increase of 14dBμV at the operating surface gradient of 14kV/cm for the twin zebra conductor bundle. Therefore under steady conditions, the fire will be directly observable. (c) At 14kV/cm the measured levels of RIV for rain and fire were at the same level but 7 to 8dBμV above dry conditions. Some fire induced corona must have been present to push the fire RIV values above dry conditions but not sufficiently to rise above the rain condition RIV values. The projected fire induced RIV value of 75dBμV is 7dBμV above the rain conditions value. This was an increase of only 10% and not sufficiently high to conclude that fire is distinguishable from rain using the RIV quasi peak method of detection.

5.1.4 Triple Wolf conductor bundle

5.1.4.1 Filtering circuit configuration

From the calculations in appendix B, $Z_c = 227.94\Omega$. The variable resistor R_1 in figure 4.13 can be set accordingly.

5.1.4.2 Test Results

The power supply had to be switched between two taps to provide a sufficiently high voltage to produce the surface gradients shown in the graph below. All three conditions were tested at the higher tap and the fire tests were continued on the lower tap to complete the trend of corona development in this condition.

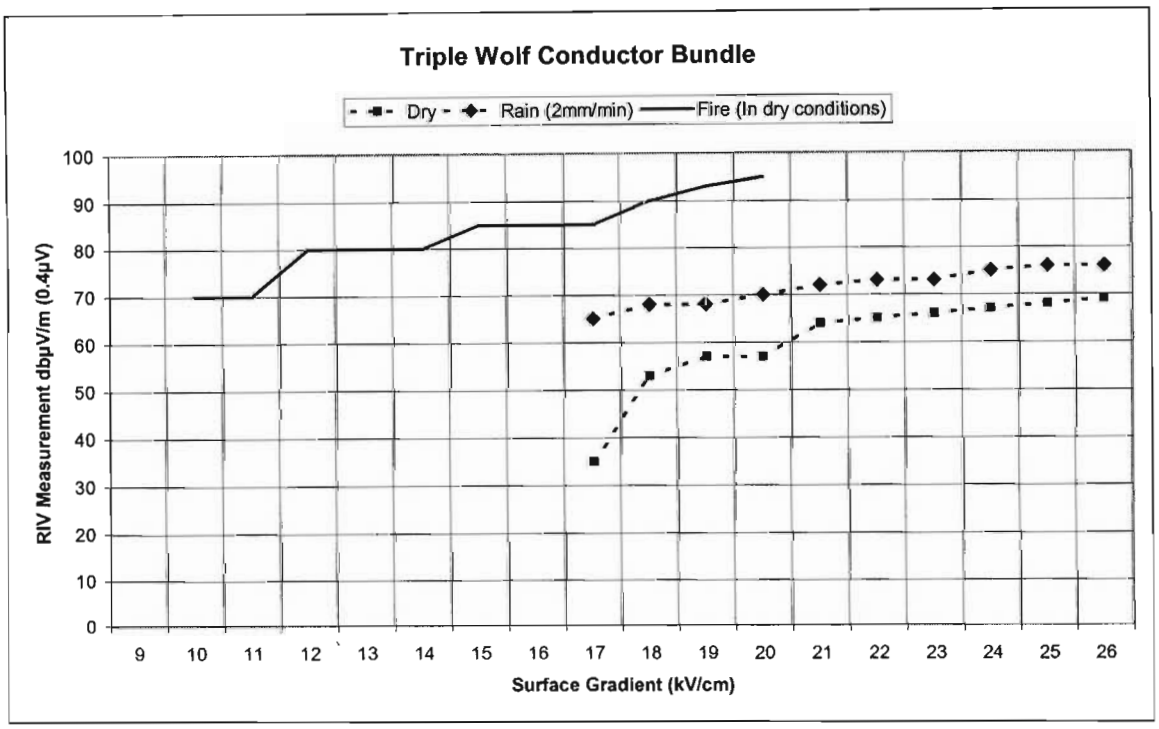

Figure 5. 4: Quasi-peak data of corona noise in dry, wet and fire conditions (triple Wolf)

At 17kV/cm, the dry condition RIV levels were very low at around 35dBμV rising rapidly to the mid-fifties and finally levelling out towards 70dBμV at 26kV/cm. In the heavy rain conditions the RIV levels were at around 65dBμV at 17kV/cm and gradually rising to 75dBμV at 26kV/cm.

Significantly, in fire conditions, the RIV levels were already exceeding the highest dry condition levels at 70dBμV at the very low surface gradient of 10kV/cm. At 17kV/cm, the fire conditions

generated RIV levels of 85dBμV, 20dBμV higher than heavy rain conditions and 50dBμV higher than dry conditions.

Increasing the surface gradient to 20kV/cm resulted in further increase in RIV levels to 95dBμV 25dBμV higher than heavy rain conditions and 39dBμV higher than dry conditions at the same surface gradient.

As per the objectives given in section 4.2, (a) the noise levels generated by the gas fire induced corona is 90dBμV at the surface gradient of 18kV/cm. (b) The fire-induced noise can be observed directly as the levels exceed dry conditions RIV levels by 37dBμV at 18kV/cm. (c) The fire-induced RIV is 22dBμV higher than the levels generated due to heavy rain conditions at 18kV/cm.

The results are therefore also positive in all three areas and fires can be detected with a CISPR-approved Mod. SE 133 receiver. However, as previously discussed for the Twin Dinosaur bundle, the gas fire was carefully controlled to produce a stable flame at the conductors. A flame under natural conditions will not continuously envelope the conductors and as such the state at the conductors may fluctuate between dry and fire conditions as the flames move back and forth about the conductors as was seen with the twin Zebra test results. This may result in a fluctuation in the RIV readings from around 50dBμV to 90dBμV at 18kV/cm.

5.1.5 Twin Wolf conductor bundle:

5.1.5.1 Filtering circuit configuration

From the calculations in appendix B, $Z_c = 252.68\Omega$. The variable resistor R_1 in figure 4.13 can be set accordingly.

5.1.5.2 Test Results

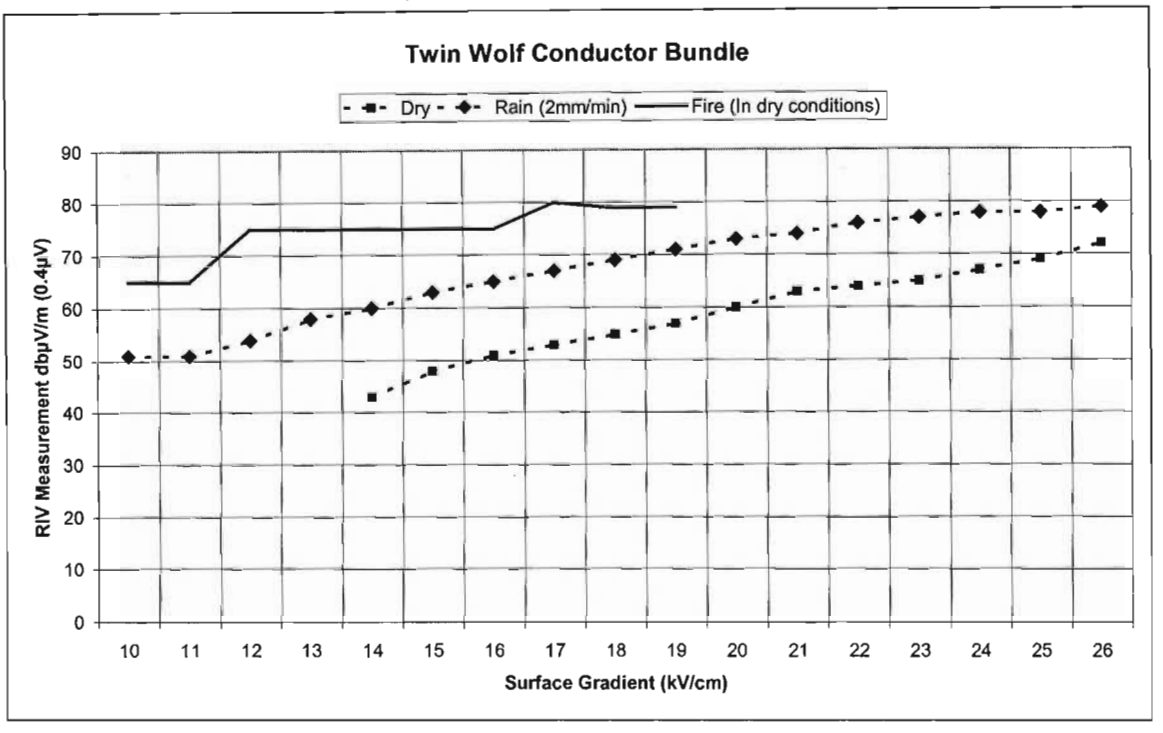

Figure 5. 5: Quasi-peak data of corona noise in dry, wet and fire conditions (twin Wolf).

In dry conditions the RIV increased from 44dBμV at 14kV/cm to 72dBμV at 26kV/cm. The heavy rain produced RIV levels of 51dBμV from as low as 10kV/cm which also gradually increased to just below 80dBμV at 26kV/cm. At the low end of the applied surface gradient scale RIV levels in the fire conditions started at around 65dBμV (14dBμV above RIV levels for rain conditions) and increased to around 80dBμV at 17 to 19kV/cm. Again, as for the twin Dinosaur bundle, the corona activity appeared to saturate or settle at the higher surface gradients.

At 18kV/cm there is a 25dBμV and 10dBμV increase in RIV levels from dry and rain conditions to fire conditions respectively.

The fire conditions under the twin wolf conductor bundle produced RIV levels of 80dBμV at 18kV/cm. RIV levels will make it possible to directly observe and identify a uniform fire or

flame below the transmission line. With a 10dBμV separation between fire and rain induced RIV, a constant fire or flame will be distinguishable from the heavy rain conditions.

5.1.6 Single Wolf conductor bundle:

5.1.6.1 Filtering circuit configuration

From the calculations in appendix B, $Z_c = 371.8\Omega$. The variable resistor R_1 in figure 4.13 can be set accordingly.

5.1.6.2 Test results

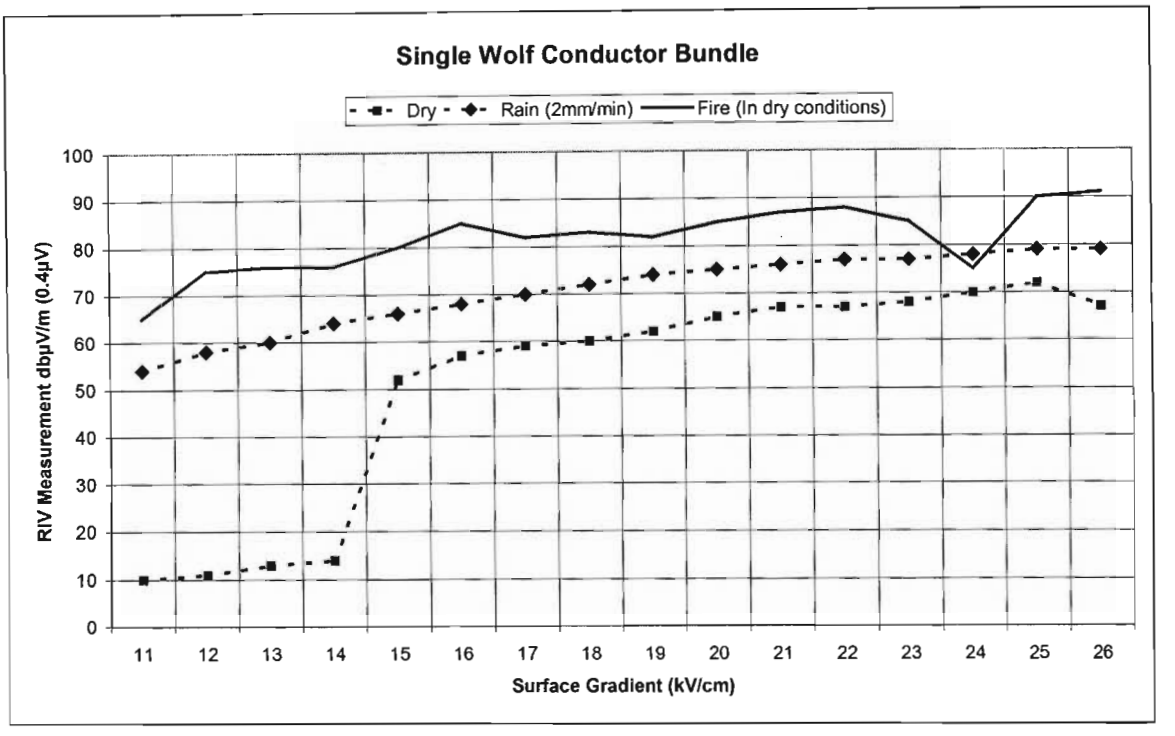

Figure 5. 6: Quasi-peak data of corona noise in dry, wet and fire conditions (single Wolf).

The test result for the fire conditions at 24kV/cm appear to be a sample taken when the flames deviated away from the conductors sending the RIV levels down towards that recorded for dry conditions. For all other surface gradients dry conditions increased from approximately 10dBμV at 11kV/cm 65dBμV at 25kV/cm and a steep increase at around 15kV/cm to 50dBμV. The RIV for rain conditions climbed from 52dBμV at 11kV/cm to 80dBμV at 26kV/cm. The fire induced RIV commenced at approximately 62dBμV at 11kV and increased reasonably consistently up to 90dBμV at 26kV/cm just 10dBμV higher than the rain condition levels.

a) RIV for a single wolf conductor at 15kV/cm is around 80dBμV, b) lines under fire will produce marginally detectable signal levels which can be observed directly and c) these fires will be distinguishable from heavy rain at a marginal 10dBμV at 15kV/cm.

The term "marginal" is applied in this context as a heavy rain storm would not be limited to a short section of line resulting in potentially higher levels of corona with longer exposed lengths. In addition a fire does not typically remain static and stable at the conductors as has been controlled in these experiments, resulting in lower quasi peak levels in reality at the points of individual exposure.

5.2 ANALYSIS OF THE QUASI PEAK DATA

5.2.1 Overview

All the tests produce some degree of clarity on the three corona cage research objectives raised in section 4.2 namely:

a) noise levels generated by the fire-induced noise

- Twin Dinosaur: 95dBμV at 15kV/cm;
- Twin Zebra: 75dBμV at 14kV/cm;
- Triple Wolf: 90dBμV at 18kV/cm;
- Twin Wolf: 80dBμV at 18kV/cm;
- Single Wolf: 80dBμV at 15kV/cm;

b) In each set of tests the fire-induced noise can be identified when observed directly although certain conditions are required;

c) In each set of tests the fire-induced noise was distinguishable from rain as a major noise source by

- 20dBμV at 15kV/cm for the twin Dinosaur;
- 7dBμV at 14kV/cm for the twin Zebra;
- 22dBμV at 18kV/cm for the triple Wolf;
- 10dBμV at 18kV/cm for the twin Wolf;
- 10dBμV at 15kV/cm for the single Wolf.

Fire in its natural development does not exist in the same manner as produced in these corona cage tests. In these tests the fire has been forced to exist in a consistent and stable manner across the long gap between two electrodes. This was done to provide a best case condition when flames do bridge the long gap between phases or between the phase conductors and ground. The natural flame conditions will therefore influence the "annoyance" persistence energy accumulated in the quasi peak measurement. This consideration will again be addressed in section 5.4 "Conclusions: Quasi Peak Experiments".

5.2.2 Twin Dinosaur

At 25 kV/cm the rain-induced corona noise activity was tending towards a saturation point where further increases in surface gradient resulted in smaller increments in RIV levels. The noise generated in the normal dry conditions was tending towards the same saturation point as that of

the rain, supporting the concept of a saturation point at which very little additional ionisation by electron impact takes place on a particular conductor bundle in air. The fire-induced corona noise activity showed stepped increases in the noise level from the lowest surface gradient recorded at 9 kV/cm. The level of noise generated at 9 kV/cm due to the gas fire corresponded to the level of rain-induced corona noise generated at 17 to 18 kV/cm and was 27dBμV higher than the rain-induced corona noise at 9 kV/cm. The noise generated above 11 kV/cm is higher than the rain-induced corona noise at any gradient during the test. The audio noise at the time of these measurements was high and the ensuing flashover is an indication that no further increases in ionisation without a full breakdown across the existing 3.5m gap were possible. Instead, the corona region about the conductor had extended down the heat column (or "plasma") and developed from corona activity into leaders which then bridged the gap between the conductors and the earth plane. This was remarkably repeatable at 17 kV/cm, stressing the fact that when the surface gradient was high enough and the environmental conditions were appropriate for sustained heat conditions at the conductors, the transition from ionisation to corona to leaders was consistent and inevitable. However, as the environmental conditions are rarely stable, such "appropriate" conditions were unlikely to persist for all the work performed in the corona cage.

A significant result here (not directly related to the detection of fires) is the repeatable insulation breakdown across the air gap with no particles and no significant contribution of any additional chemical reactions from any flammable materials other than the flammable liquid petroleum gas (LPG).

5.2.3 Twin Zebra

The RIV noise recorded for the rain and normal dry conditions were as anticipated according to predictions and other measurements.

The fire-induced noise recorded on the analogue quasi-peak instrumentation was erratic. The measurements do not correlate with previous knowledge of this work and the optical alignment of the flame was identified as the fundamental cause for the irregular measurements. The operator was requested to ensure that the flames were directly below the conductors before recording the noise levels. The operators control room was situated at ninety (90) degrees with the burner and overhead conductor bundle. Therefore the flames would rise towards the conductors directly in front of the operator. However, due to the fact that the flame was sometimes not opaque, the third dimension of depth was lost and made it difficult for the

operator to determine the precise position of the flame. The result was that the flames were, on occasion, vertically behind the conductors though appearing to be directly below the conductors. As previously discussed, in such measurements, the level of noise should be similar to that recorded in the normally dry conditions. The "bad" data could easily be identified as that data in close proximity to the dry condition data. In order to gain an improved approximation of the fire-induced corona noise generated, a "predicted" curve from the original data was extrapolated. The predicted trend is illustrated in figure 5.6 below.

The fire-induced corona noise generated from the twin Zebra conductor bundle was recorded at increasing intervals and was not as vigorous as the fire-induced corona activity occurring on the twin Dinosaur conductor bundle. The fire-induced corona noise levels were approximately 5 to 13 dBμV higher than the rain-induced corona noise levels when using the predicted values. With or without the projected figures, the twin Zebra data was not as convincing as the twin Dinosaur data although the fact that the fire-induced corona noise was more active than the rain-induced noise was significant. Affects such as the length of conductor exposed to the specific condition may significantly change these results. This comparison of conductor types is discussed in a later section.

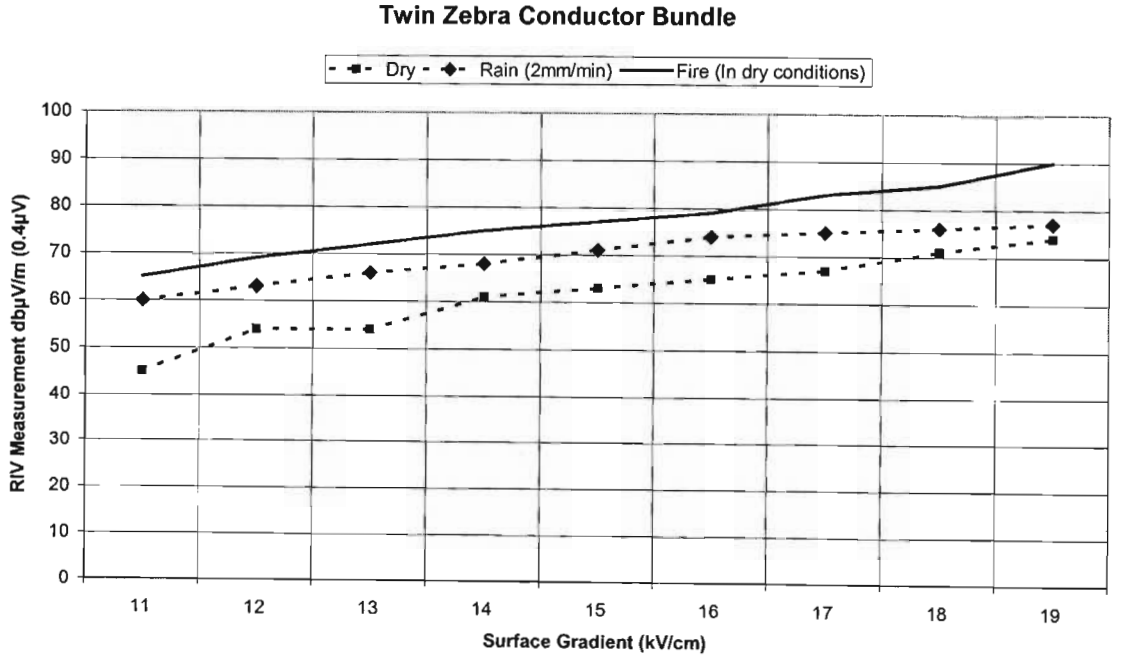

Figure 5. 7: Modified Twin Zebra quasi-peak data in accordance with theory.

5.2.4 Triple Wolf

At 12 kV/cm, the fire-induced corona noise activity was more vigorous than the highest level of rain-induced corona activity measured, which was at 26 kV/cm. The same trend towards what appears to be a saturation point was observed as the rain-induced corona noise had smaller increments with each kV/cm increase in the surface gradient. The rate at which the dry condition noise was increasing (relative to the surface gradient) indicated that the two curves were likely to intersect at some higher gradient. The fire-induced quasi-peak level corona activity was much higher. The results drew attention to the significant difference in quasi-peak levels. In the range in which a comparison was possible, the rain- and fire-induced RIV levels were separated by between 12dBμV and 25dBμV.

5.2.5 Twin Wolf

At 10 kV/cm the fire-induced corona noise activity was equivalent to the rain-induced corona noise activity generated at 16 kV/cm and 14dBμV greater than the rain-induced corona noise activity generated at the same surface gradient of 10 kV/cm. The trend was virtually the same for all three conditions. A maximum separation of 21dBμV between the rain- and fire-induced corona noise was recorded at 12 kV/cm. Again, further increases in the surface gradient for further tests may have resulted in a flashover taking place.

5.2.6 Single Wolf

As for the twin Zebra conductor bundle, the entire range of fire recordings made in the single Wolf tests, appeared to be "subdued", with typical dry condition levels recorded at 24 kV/cm. The fire-induced corona noise data was consistently higher than the rain-induced corona noise data (altering the 24kV/cm result as for the Twin Zebra test as illustrated in the graph below). The largest difference in quasi-peak noise levels was 17dBμV at 12 and 16 kV/cm. Over the entire range of surface gradients the results appear to have been very "smooth" even when taking the adjustment at 24 kV/cm into account.

On occasion the gas pressure from the gas burner dropped or the gas flow was reduced due to some freezing on the pipes taking place. This usually resulted in the reduction of the flame plasma height and a reduction in the thermal influences experienced at the conductors in the controlled conditions. That is, by restricting the flow of gas, the rate of combustion is slower and

the overall temperatures will be lower every time the gas burner is operated under these conditions. The results obtained on other conductors certainly did not support the "smooth" increase in fire-induced corona noise experienced here.

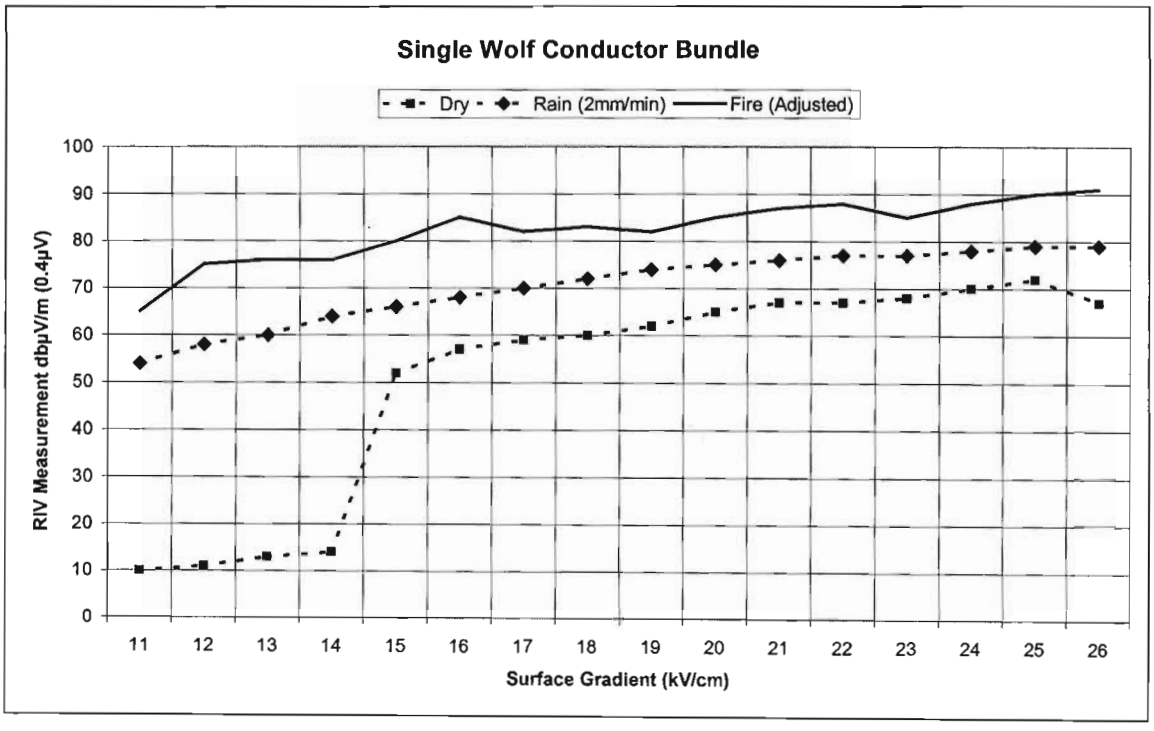

Figure 5. 8: Modified Single Wolf quasi-peak data in accordance with theory.

5.3 DIMENSION COMPARISONS

5.3.1 Affects of changing conductor dimensions in a given bundle

Of interest and of direct relevance to Eskom was the influence of changing the conductor diameter (that is, the type of conductor) in a bundle to determine the effectiveness of minimising air insulation breakdown due to fires. The quasi-peak data of the Wolf, Zebra and Dinosaur conductors in the twin conductor bundle were compared.

The overall geometric mean radius (GMR) for these three conductor bundles is:
Twin Dinosaur – 72.5mm;
Twin Zebra – 65.0mm; and
Twin Wolf – 51.82mm.

From Peek's Law, (section 3, equation 18), the larger the radius of a conductor, the lower the critical gradient for visual corona inception would be:

$$E_{max} = g_0 m_v \delta \left[1 + \frac{0.3}{\sqrt{\delta r}} \right] \qquad \text{(in kV/cm)} - \textbf{\textit{Peek's Law}}$$

For constant values of g_0, m_v and δ an increased r will decrease the value of E_{max}. Consequently, an increase in r translates to a higher RIV signal level.

5.3.1.1 Dry conditions

With equal spacing between the two conductors (namely 380 mm) in each case, the twin Dinosaur conductor bundle has RIV signal levels lower than the twin Zebra conductor bundle.

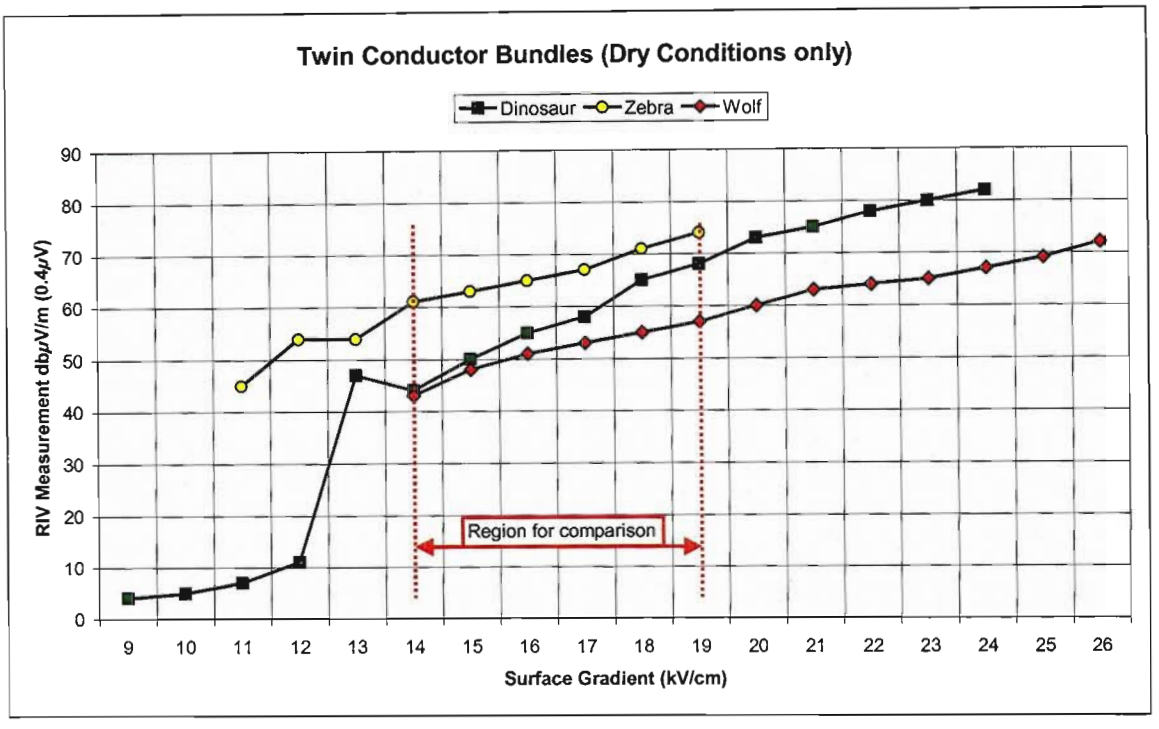

Figure 5. 9: Comparison: Conductor diameters (types) in dry conditions.

In the dry conditions existing on a power line there can be higher particulate matter and hence, when the line is operating near its corona limits, different levels of noise could be measured depending on the environmental conditions at the time.

The converse is also true. When the twin Dinosaur conductor bundle was tested, the conditions were ideal for testing with very little wind. At the higher surface gradients, the twin Dinosaur results can be seen to be increasing in relation to the slopes of the twin Zebra and Wolf, implying that at the higher gradients the influences of dust particulate, etc. in dry conditions is less significant.

5.3.1.2 Rain conditions

Unlike the normal dry conditions, rain is extremely repeatable. The droplets forming on a conductor will always be drawn to the underside of the conductor due to gravity and provided the conductors are similar in physical structure, will form on the underside of those conductors in a very similar fashion. The droplets are therefore quasi-permanent deformations on all the conductors and dominate other influences such as airborne particles.

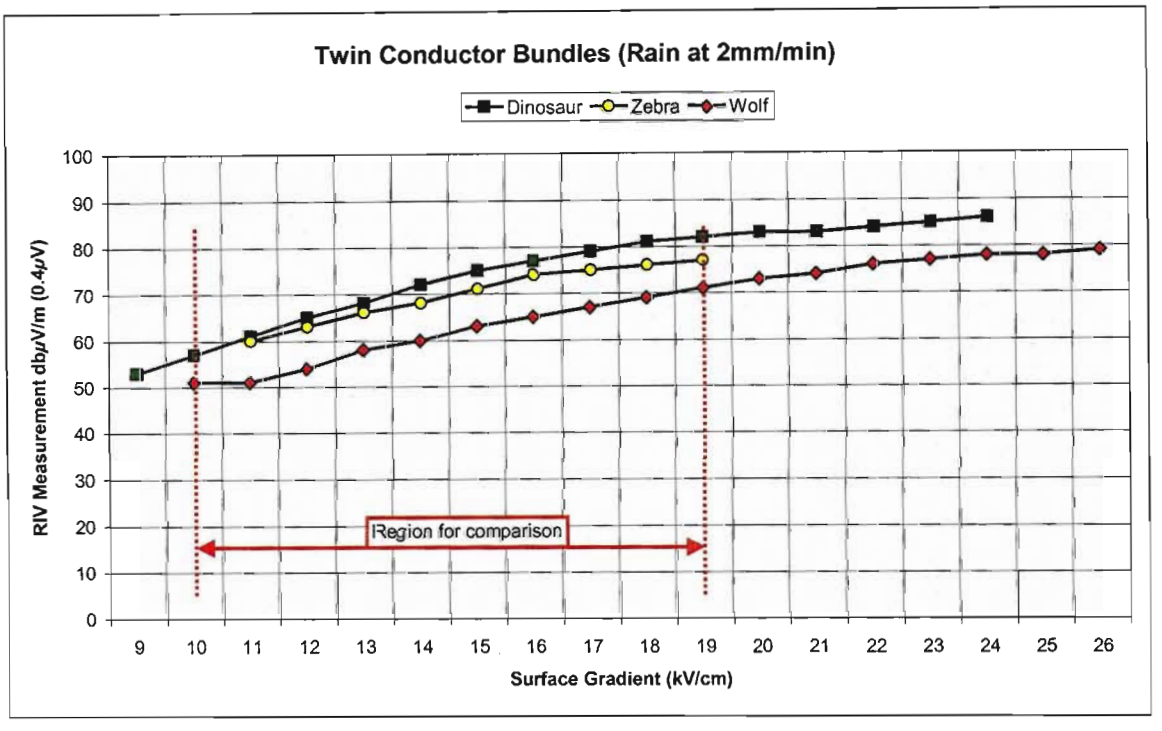

Figure 5. 10: Comparison: Conductor diameters (types) in rain conditions.

The RIV signals increased at very similar rates for the three conductor bundles. The smaller differential between the Zebra and Dinosaur may be due to the smaller overall GMR differential of 7.5mm between Zebra and Dinosaur versus 13.18mm between Zebra and Wolf.

5.3.1.3 Fire conditions

The results were less predictable but shows that for the same surface gradients the twin Dinosaur conductor bundle generates the highest level of corona noise.

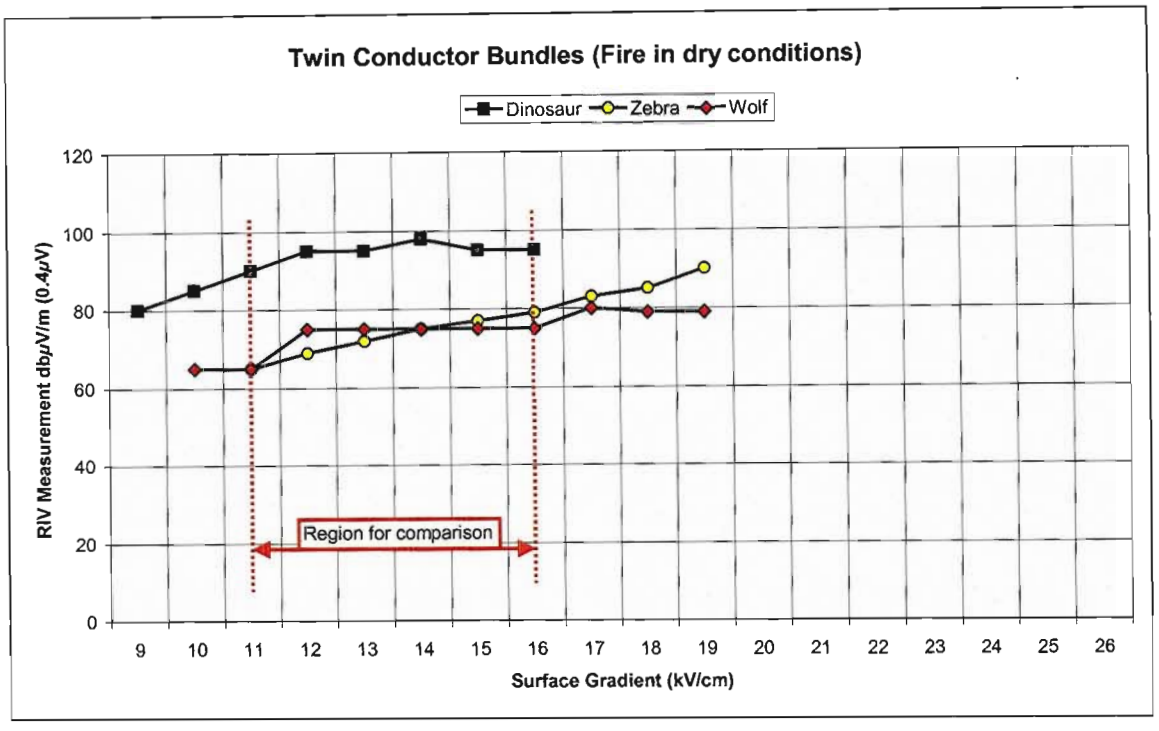

Figure 5. 11: Comparison: Conductor diameters (types) over fire in normally dry conditions.

Initially the reason for the large separation between the noise levels of the Wolf and Zebra conductors and that of the twin Dinosaur was considered to be some parameter of the applied voltage. However, this is unreasonable as the surface gradient is a function of that applied voltage and it is the surface gradient which influences the generation of the corona. By Peek's law, the RIV levels of the twin Zebra conductor bundle are too low when considering the levels of the twin Dinosaur and the twin Wolf conductor bundles. These differences can more than likely be attributed to the lack of repeatability of the fire tests and to the changing environmental conditions existing at the time as well as the variation due to the oscillations of the indicator needle in the analogue CISPR measurement. Any potentially higher actual RIV values for the twin Zebra would also therefore result in a higher differential between the rain and fire RIV values for this bundle.

5.3.2 Affects of changing the number of conductors in a given bundle

Of interest and direct relevance to Eskom was the affects of changing the number of conductors in a bundle to determine its effectiveness in minimising air insulation breakdown due to fires. The bundles compared were the single, twin and triple Wolf conductor bundles.

5.3.2.1 Dry conditions

In the normal dry conditions shown in the figure below, the triple conductor bundle shows marginally lower levels of noise at the lower gradients and virtually the same levels as the twin conductor bundle at the higher gradients. As the dry conditions are not entirely reliable these results should not be scrutinised too enthusiastically.

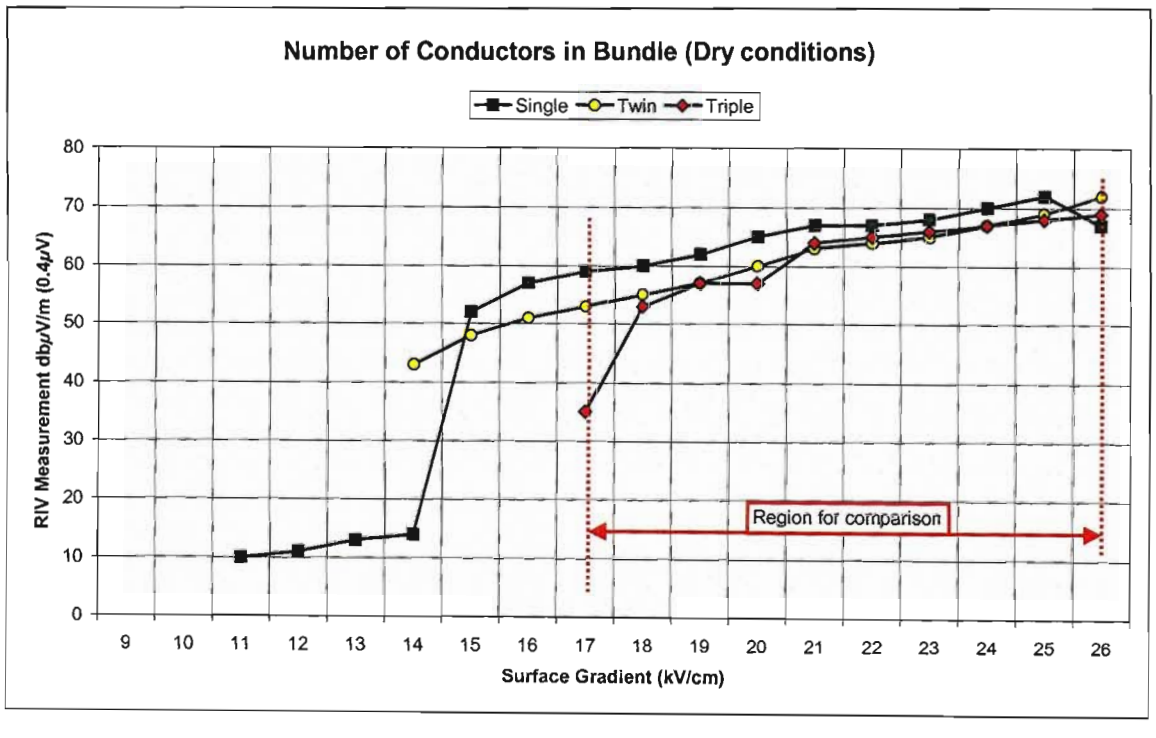

Figure 5. 12: Comparison: Number of conductors in dry conditions.

5.3.2.2 Rain conditions

The results obtained from the rain conditions as shown in the figure below indicated that these predictions were not totally inaccurate. At 19 kV/cm in rain conditions the triple conductor bundle generated 3 and 6dBμV, less noise than the twin and single conductor bundles respectively.

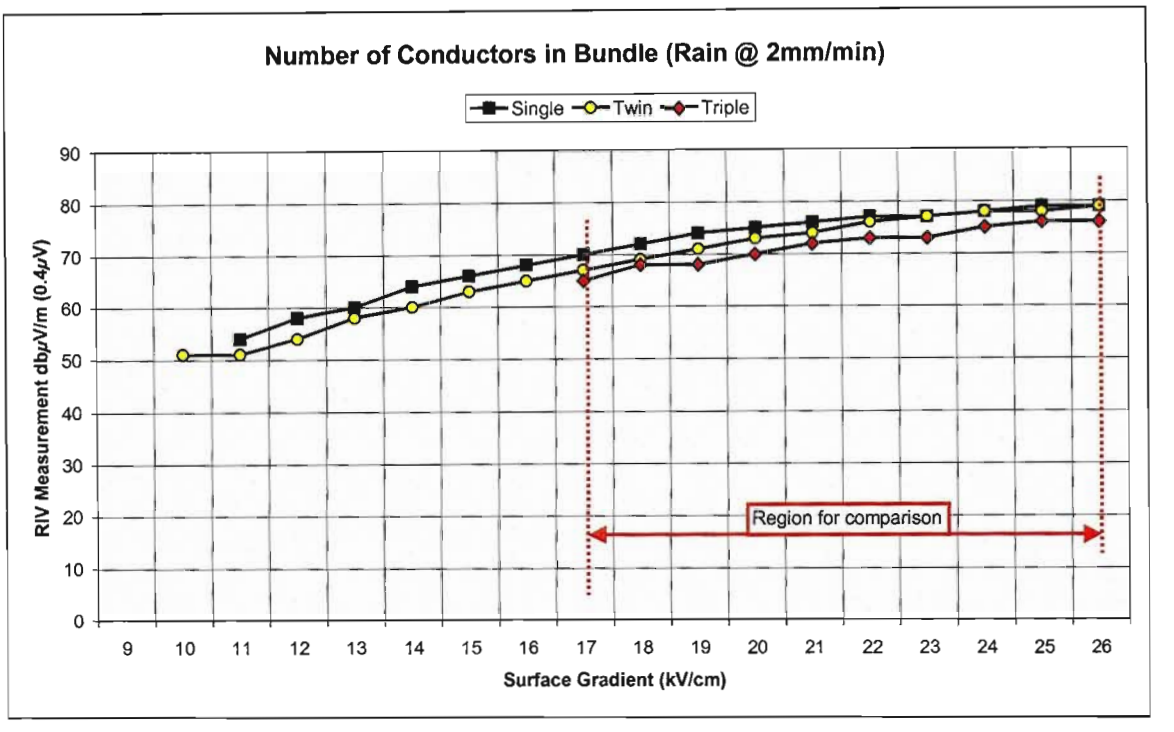

Figure 5. 13: Comparison: Number of conductors in rain conditions.

Using the excitation function, otherwise known as the radio noise generation function, Γ, the results for different conductor bundles can be compared to each other. The results obtained above match favourably when using equation 24 below as described by Gary and Moreau [33]

$$\Gamma_n = \frac{\Gamma}{\sqrt{n}} \tag{24}$$

The excitation function is related to the quasi-peak measurements done here by a constant which is dependent on the dimensions of the test environment. Γ = (RIV) - 25.87dB and n is the number of conductors in the bundle.

Table 4: Excitation Function at 17kV/cm

n	@ 17 kV/cm (in dB)			
	RIV	Γ_n	Γ_n- Γ_1	$-20\log\sqrt{n}$
1	70	44.13	0	0
2	67	41.13	-3.0	-3.01
3	65	39.13	-5.0	-4.77

Table 5: Excitation Function at 19kV/cm

n	@ 19 kV/cm (in dB)			
	RIV	Γ_n	Γ_n- Γ_1	$-20\log\sqrt{n}$
1	74	48.13	0	0
2	71	45.13	-3.0	-3.01
3	68	42.13	-6.0	-4.77

5.3.2.3 Fire conditions

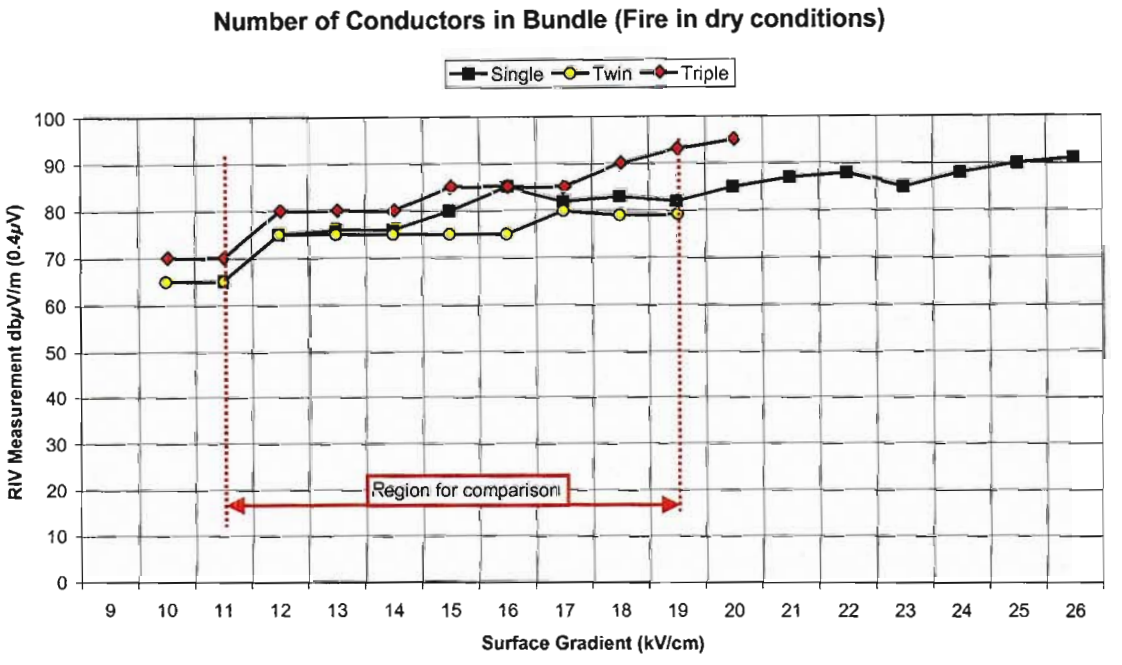

Figure 5. 14: Comparison: Number of conductors over fire in normally in dry conditions.

In the fire conditions, the results again became more unpredictable due to the influence that the environmental factors have on the test procedure and the activity of the flames due to the thermals within the flame boundaries.

The data recorded for n=3 appeared to be very high. In the light of previous discussions, these results were considered to be the typical results when a fire and its affects due to the heat are very close to the conductors. It was therefore concluded that the tests performed for the single and twin conductor bundles were done in conditions which were less stable and "ideal" than that for the triple bundle. Under environmental conditions similar to that for the triple conductor bundle the corona noise for the single and twin bundles were expected to be above that of the triple conductor bundle.

This uncertainty indicates that the measurement of fire-induced corona by means of a quasi-peak or averaging mechanism was possibly not sufficiently adequate to positively identify a fire under a power line.

5.4 CONCLUSIONS: QUASI-PEAK EXPERIMENTS

5.4.1 The Quasi-Peak values as a Measure

A "quasi-peak" measurement measures the "annoyance" level of the induced corona noise or signals. That is, the level of the output from the quasi-peak detector depends not only on the peak values of the noise pulses but also on the repetition rate of those noise pulses. Therefore, factors to consider when reviewing the quasi-peak data are:

1) Where two signals exist with impulses of equal amplitude, the signal with pulses with a higher repetition rate will have a larger quasi-peak value;
2) Where two signals exist with impulses of equal repetition rate, the signal with pulses with a higher amplitude will have a larger quasi-peak value;
3) Where two signals have a large differential between their respective impulse amplitudes, the repetition rate of those impulses will determine whether the signal with the larger amplitude has the higher quasi-peak value; and
4) Where two signals have a large differential between their respective impulse repetition rates, the amplitude of those impulses will determine whether the signal with the higher repetition rate has the higher quasi-peak value.

It is possible therefore, to have a signal with impulses at a lower amplitude than another but that occurs more frequently and therefore has a larger quasi-peak amplitude than the other signal.

5.4.2 Rain induced electrical discharges

For all five bundle configurations, the rain induced discharges quasi-peak values were higher than that observed in normally dry conditions as expected.

5.4.3 Fire induced electrical discharges

For all five bundle configurations, the quasi-peak values for fire induced corona is larger than the corona for heavy rain conditions at all surface gradients.

5.4.4 Fire detection using Quasi-Peak measurements

The extent to which the fire induced corona is larger is dependent on the amount of corona generated from the two sources. Larger lengths of conductor exposed to rain will increase the number of discharges generated due to rain. An increased number of discharges, even at low amplitude, will increase the quasi-peak readings measured on a power line.

More realistic fire conditions will reduce the sustained fire presence at the conductors. The number of fire induced corona discharges will decrease although the presence of particles will in turn increase the number of localised discharges associated with the presence of the particles. However, the tests completed here were focused on producing a flame bridge between the conductors and earth for 100% of the time during which the tests were being carried out. On this basis alone, the number of electrical discharges due to the presence of fires will be lower in the operational environment reducing the quasi-peak values recorded.

As a result the increased rain induced corona and the reduced fire induced corona conditions may combine to make it difficult to distinguish rain from fire with the quasi-peak measurement method.

CHAPTER 6

Laboratory – Large Corona Cage:

Time Domain Experiments

In this chapter, the high frequency noise signals are documented without any form of time domain filtering. That is, the individual corona pulses are observed in relation to the individual 50Hz power cycles in which they occur. The quasi-peak measurements are a measure biased towards "annoyance" levels. Any RMS and averaged measurements are measures biased towards moving average peaks. Here the measurements focus on actual events biased only by the filtering required to extract the signals from the high voltage conductors.

Section 6.1 reviews the tests similar to those in chapter 5 where a gas burner was used to generate the fire conditions. Section 6.2 documents the tests and results for sugar cane fire conditions. An analysis of the tests results for both fire sources is presented in section 6.3. The test results for polluted insulators and the possible interfering signals are discussed in section 6.4. In section 6.5 the author tries to put the corona cage test results in perspective by relating the results back to the operational main transmission system (MTS). Conclusions on the corona cage work are documented in section 6.6.

The corona cage provided an ideal facility to experiment with a variety of variables which may influence the interpretation of fire induced corona activity, namely changes in the number of conductors in a bundle and changes in conductor diameters. The different conductors have unique names and have specific numbers of strands, materials and diameters (see appendix B).

6.1 RESULTS - REFERENCED TO GAS FIRE

6.1.1 Overview

The results presented in this chapter cover time-domain instantaneous electrical discharge records detailing corona in dry air, corona generated due to the presence of rain on and around the conductors, and corona generated due to the presence of a fire with no significant particle content.

Section breakdown:
(6.1.2) Twin Dinosaur at 16kV/cm and (6.1.3) Twin Zebra at 17kV/cm.

Two different instruments were used to capture the data namely (in chronological order):

1) A Nicolet 2090 series digital storage oscilloscope (DSO) for the data on the Wolf conductor bundles; and
2) A Nicolet MultiPro 500 series digital storage oscilloscope (DSO) for the data on the Dinosaur and Zebra bundles.

Due to the limited capabilities of the Nicolet 2090 the data for the wolf bundles has been omitted from this thesis. The Nicolet 2090 had a very low sampling capacity and very little intelligent analysis was possible when interpreting the signals in relation to the 50Hz power cycle. Very little reliable correlation to the applied voltage and hence line electric field stresses was possible.

The Nicolet Multi Pro 500 series DSO had the ability to store data up to a capacity of 1 million samples in a waveform. Each sample contains two bytes of information and to be able to transfer the data onto 1.2 megabyte floppy (stiffy) disks, 600,000 sample points (1.2 Megabytes of data) was selected. At a sampling rate of 10 MHz, each channel could capture up to 60 ms of data. Sufficient channels were available to capture both the induced corona noise and the 50 Hz power cycle simultaneously. By cascading two sets of channels double the data was captured.

Therefore, each graph shown indicates both the high frequency waveform and the actual 50 Hz power signal. The equipment was able to record waveforms for 120ms which included a pre-trigger of 6 ms and a post trigger of 114 ms and six power cycles. The scales on the graphs were selected according to the maximum pulse amplitudes expected for the fire data. This allows a lucid comparison of each noise pattern with the noise patterns generated by the fire-induced corona.

6.1.2 Twin Dinosaur conductor bundle at 16 kV/cm:

The data shown in the following figures are enlarged in appendix E. In Eskom, the normal operating gradient for this conductor bundle is 15 kV/cm where the typical feeder phase orientation is horizontal with two ground wires overhead. The bundle was therefore stressed to 1kV/cm above the normal operating gradient during these measurements.

6.1.2.1 Dry conditions

Figure 6.1 shows the amount of electrical discharges present under dry conditions in the 6 power cycles recorded. Pulses in the second, fourth and sixth positive half cycles were visible whilst none were visible in the negative half cycles. These pulses translate to electrical discharges on the conductors.

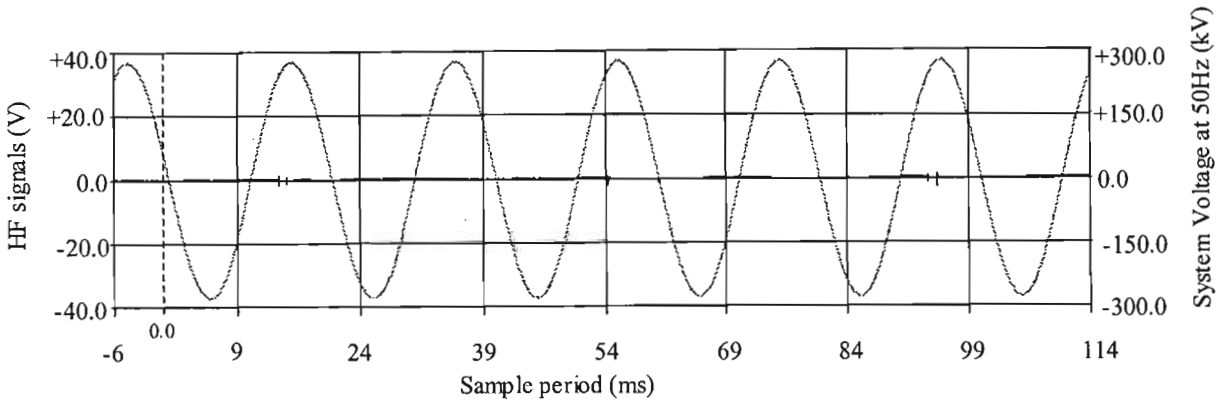

Figure 6. 1: Twin Dinosaur in normally dry conditions stressed to 16 kV/cm

The presence of discharges seen here translate to the very low quasi-peak values measured in chapter 5.

6.1.2.2 Rain conditions

Figure 6.2 shows the amount of electrical discharges present during rain conditions in the 6 power cycles recorded. Corona is produced in every positive half cycle. The point in the power cycle at which the discharges are both initiated and extinguished are reasonably constant.

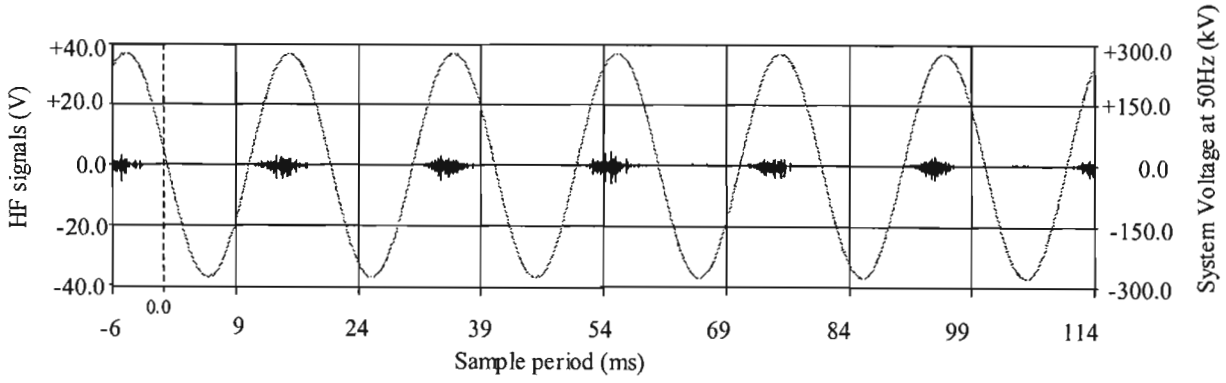

Figure 6. 2: Twin Dinosaur in rain conditions stressed to 16 kV/cm

The conductor bundle was therefore sufficiently stressed at this gradient and in these environmental conditions, to be in a region of continuous corona generation. A small number of discharges can be seen in two of the negative half cycles.

The state of corona appears to be that of streamer onset and Hermstein glow in the positive half cycle and marginal incidents of Trichel pulses in the negative half cycle (see figure 3.3 on page 28).

The peaks of the electrical discharges form a rough envelope tracking the shape of the applied electric field. The discharge repetition rate was sufficiently high to appear continuous. Signals peaked at values around ±4.5 volts.

6.1.2.3 Fire conditions (generated with a gas burner)

Figure 6.3 shows the amount of electrical discharges present during the gas fire conditions in the 6 power cycles recorded. Clearly a considerable increase in the amount of detectable electrical activity. Signals here peaked at values around ±20 to 30 volts with several pulses being clipped by the maximum voltage range set for the channel.

The electrical discharges were therefore of considerably larger amplitude than in rain and can be seen in the positive half cycle with discharges also taking place in the negative half cycle at a much lower amplitude.

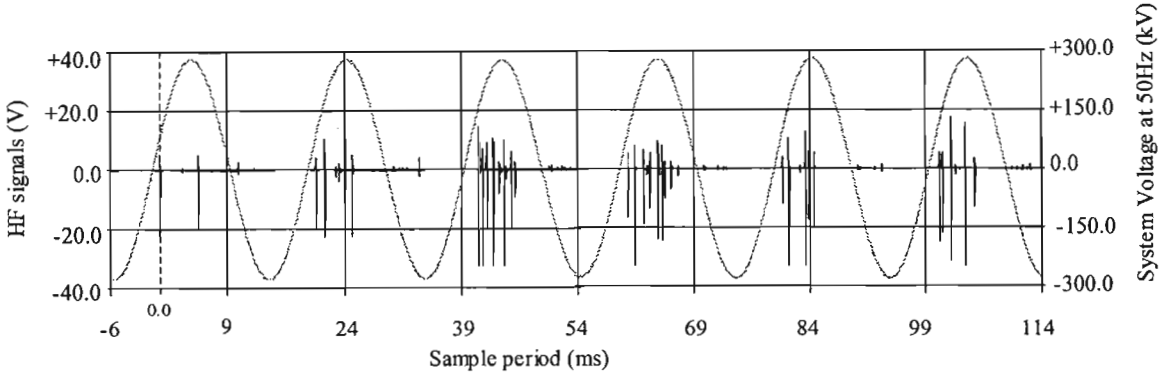

Figure 6. 3: Twin Dinosaur in fire conditions stressed to 16 kV/cm (Gas fire)

The point at which the discharge commenced in each power cycle varied. In some cycles the incipient point was at a lower voltage than that seen during the rain conditions.

The fluctuations were expected as the flame moved about the conductors. Even when constantly at the conductors, the heat content within the flame is not constant. Of interest is the amplitude of the electrical discharges taking place at these low incipient voltages. At approximately 42ms after triggering the signals in figure 3.2, the first discharges shown were already at a peak value of over 30volts. That is, there was no "envelope tracking" as was the case in the rain conditions.

Clearly the distortion in the localised gradients about the conductor in the flames significantly increases with the presence of the flames.

The author was not able to track the exact location of the flames per individual half cycle. Therefore more data was captured and circumstantial evidence was gathered to extract more knowledge about the probability of discharges. A second set of data is shown below which confirms that the electrical discharge activity shown is consistently stochastic.

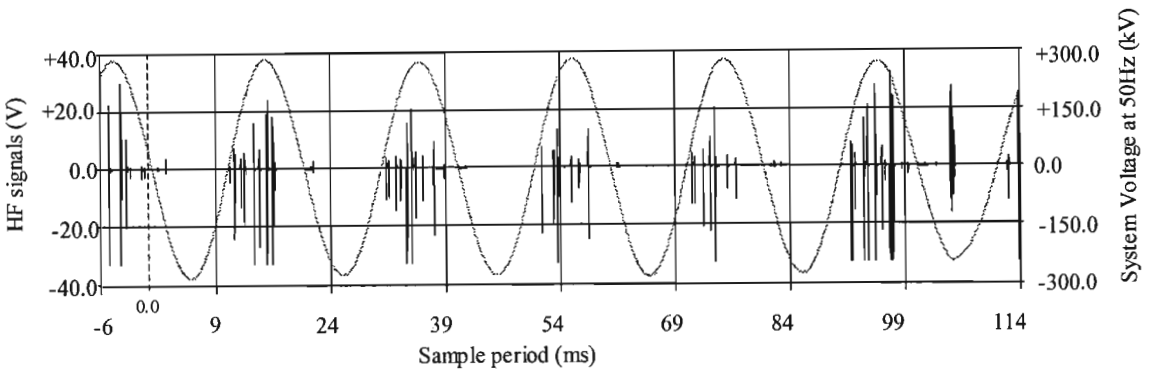

Figure 6. 4: Second sample - Twin Dinosaur in fire conditions stressed to 16 kV/cm

Figure 6.4 shows that at the time of the snapshot, corona activity was consistently induced in every positive half cycle. At the same time, large electrical discharges also started in the negative half cycle (refer to the last half cycle). With the exception of the last half cycle, the corona on the negative half cycles remain much smaller in amplitude than those in the positive half cycle. A flashover occurred shortly after this measurement was recorded. Recalling the modes of corona, the positive half cycles consistently produce very high amplitude pulses rather than any form of glow. Hence the discharges observed are most likely breakdown streamers. In the negative half cycle, small discharges can be seen in the early part of the half cycle and could be Trichel pulses. The large discharges in the final negative half cycle may be the onset of negative streamers prior to the reported flashover or breakdown incident. When viewing these results, early detection may be based on the occurrence of large negative half cycle streamers. However, the breakdown may be only a few cycles away and would not suffice as an early warning system. The extremely high amplitude positive half cycle streamers occurred much earlier and are significantly larger than the pulses present in the same window in heavy rain conditions.

In the last negative half cycle two important changes occurred.

1) As mentioned, the discharges in the half cycle were much larger than in previous half cycles, and
2) The 50 Hz power signal was distorted.

The second change is significant because the power supply is limited. In the VI relationship, an increase in current for a constant voltage will result in an increase in power consumed until the maximum available power is consumed. The voltage has started distorting indicating that the maximum power available had been consumed with still further increases in the current drawn through the electrical discharges into the gap between the conductor bundle and the wire mesh of the corona cage.

What is of particular interest is that, whilst currents of larger amplitude were being drawn during the positive half cycles, the power supply did not waver. The possibility exists that the discharges visible in the last positive half cycle were of such an extreme amplitude that the combination of both cycles contributed to the surge in demand for power. The actual peaks were not recorded here due to the clipping which took place.

Given the higher level of electrical activity, the repetition rate of the individual discharges appears to increase with the presence of larger amplitude discharges. This cannot be confirmed without further testing. What does appear clear is that with a continued presence of flames, the discharge repetition rate increases to the same intensity of the rain where a droplet is present on the line for the full duration of the tests. In the recorded samples, the number of large pulses in the negative half cycle were significantly less than those observed in the positive half cycles.

6.1.3 Twin Zebra conductor bundle at 17 kV/cm:

The data shown in the following figures are enlarged in appendix F. In Eskom, the normal operating gradient for this conductor bundle is 14 kV/cm where the typical feeder phase orientation is horizontal with two ground wires overhead. The bundle was therefore stressed to 3kV/cm above the normal operating gradient in the presented test results.

6.1.3.1 Dry conditions

Figure 6.5 shows some electrical discharges present in the positive half cycles under dry conditions in the 6 power cycles recorded. These pulses translate to electrical discharges on the conductors.

Firstly the gradient on the conductor bundle is 3kV/cm higher than the normal operating gradient for this conductor bundle and secondly the geometric mean radius (GMR) of the twin zebra is 65mm as opposed to the larger twin dinosaur at 72.5mm. In the dry conditions shown below, there are considerably more discharges taking place than is expected from a transmission line which has been correctly designed. The resultant corona activity translates to unnecessary power losses on the operational transmission line.

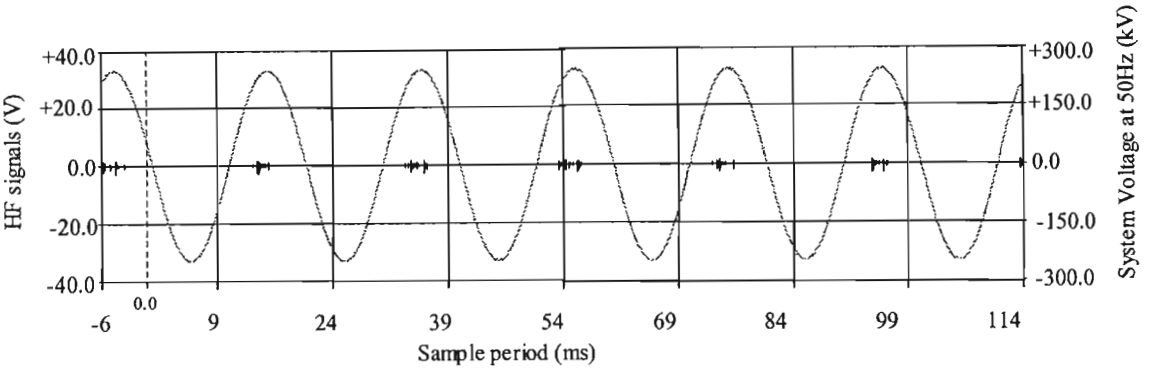

Figure 6. 5: Twin Zebra in normally dry conditions stressed to 17 kV/cm

The electrical discharges are visible in all the positive half cycles and do not have an envelope matching the applied line voltage. The activity is dependent on the air movement around the conductors and the associated fluctuations in air density. These fluctuations in air density will allow longer mean paths. These pulses correspond to positive streamer onset as discussed in figure 3.3.

The corona generated here was due to the higher electric field generating local fields higher than the critical field for ionisation by electron impact to take place ($E_{local} > E_{crit}$). As a result, the inception voltage for the induced corona activity may have been more steady than that shown for the dry conditions on the twin Dinosaur at 16kV/cm in figure 6.1 on page 85 where the discharges were more sporadic.

6.1.3.2 Rain conditions

In figure 6.6 the induced corona discharges had a higher repetition rate than in the dry conditions discussed previously. The development of electrical discharges was taking place continuously. The peaks of the discharges again formed an envelope matching the trend in the applied voltage as was observed in the twin Dinosaur test results.

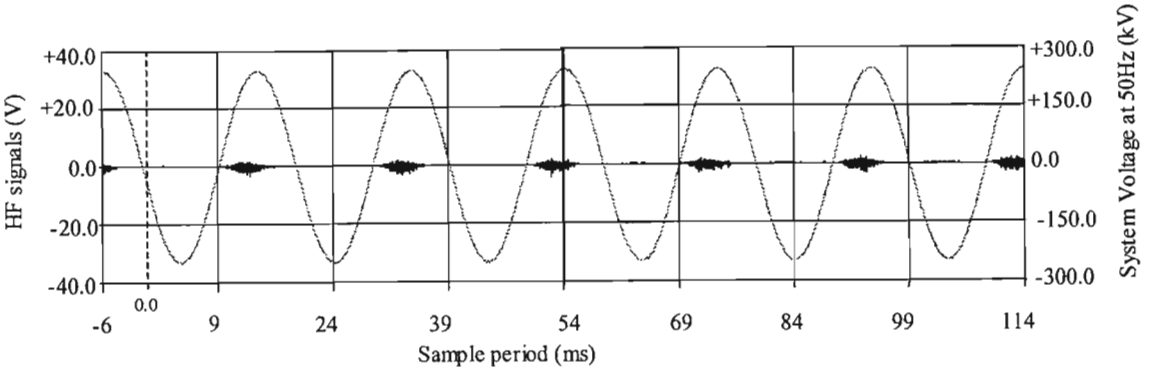

Figure 6. 6: Twin Zebra in rain conditions stressed to 17 kV/cm

Some individual pulses can be seen but the overall appearance is that of the Hermstein glow.

6.1.3.3 Fire conditions (generated with a gas burner)

In figures 6.7 and 6.8, the conductor bundle was again clearly stressed in a region of significant corona discharge. The intermittent display of corona activity was also clearly visible across all the positive half cycles in the two figures.

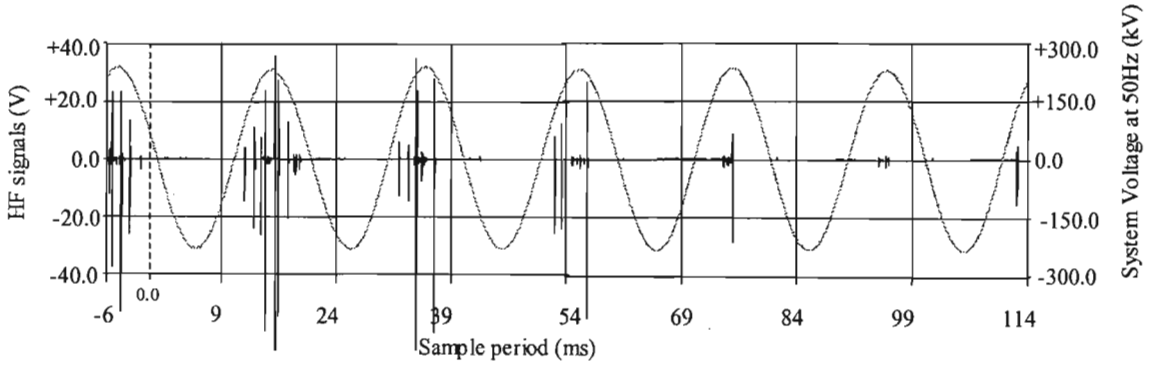

Figure 6. 7: Twin Zebra over gas fire conditions stressed to 17 kV/cm

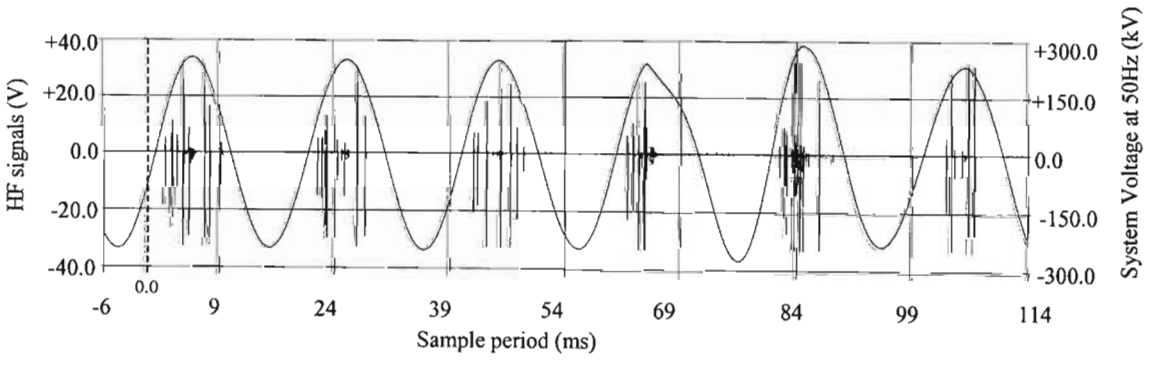

Figure 6. 8: Twin Zebra over gas fire conditions stressed to 17 kV/cm

The electrical discharges in the negative half cycles were here again seen to be very small even to the point where the discharges in the positive half cycle were sufficiently sustained to start

drawing excessive currents from the power source supplying power to the corona cage. The excessive currents result in distortion in the power frequency supply signal in the last three cycles shown in figure 6.8.

6.2 RESULTS - REFERENCED TO SUGAR CANE FIRE

6.2.1 Overview

The results are presented in order of

a) Twin Zebra at 15kV/cm in dry conditions and at 10kV/cm in rain and with a sugar cane fire;
b) Triple Pelican at 18kV/cm with dry air and rain and at 10kV/cm with a sugar cane fire ; and
c) Twin Pelican at 15kV/cm with dry air, rain and gas fire only and at 10kV/cm with a sugar cane fire only.

All measurements completed in this section were collected with the aid of a quasi-computer controlled Nicolet 490 digital storage oscilloscope with a maximum waveform capacity of 256 000 sample points per waveform.

For the controlled sugar cane fire tests, the sugar cane was loaded vertically into a squared off scaffolding structure. The tops of the leaves were kept below the cylinder of the corona cage structure.

The scales set in most of the following figures is set to ±4 volts versus the previous settings of ±40 volts.

6.2.2 Twin Zebra conductor bundle

In the normally dry conditions (at 15kV/cm) a sampled signal shown in figure 6.9 exhibited only one pulse at the point of triggering and no other activity above the background radio noise.

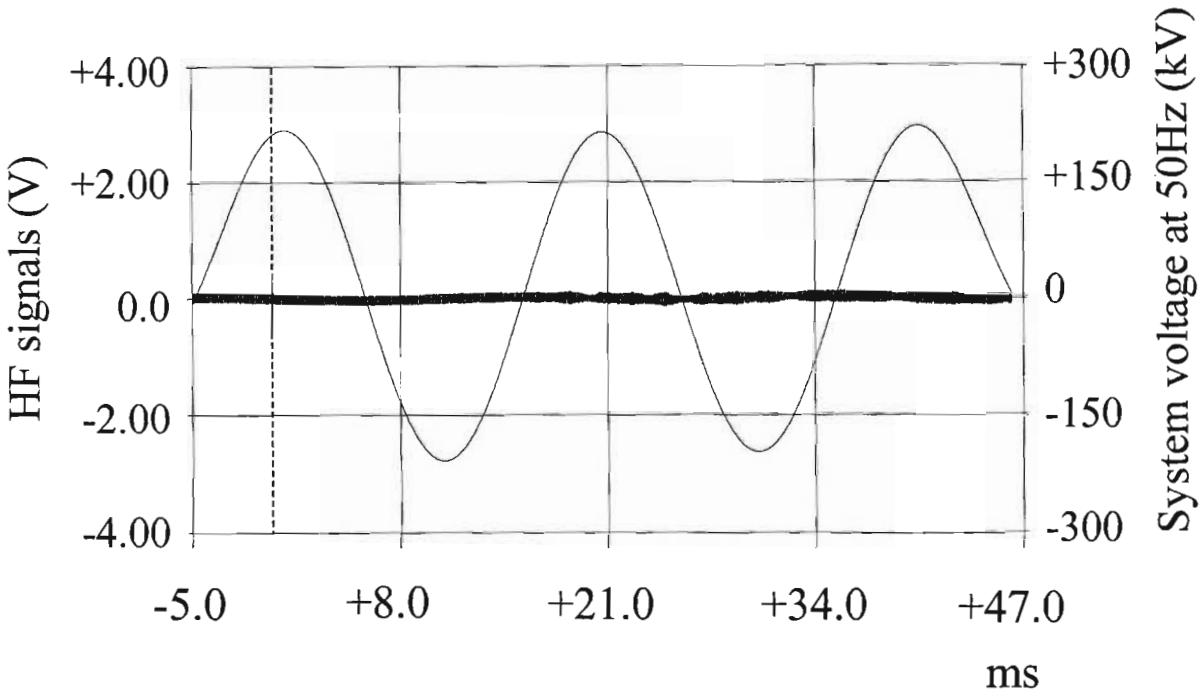

Figure 6. 9: Twin Zebra in normally dry conditions stressed to 15 kV/cm

During the heavy rain conditions also at 15kV/cm, the familiar envelope in the positive half cycles can be seen in figure 6.10 with marginal pulses in the negative half cycles.

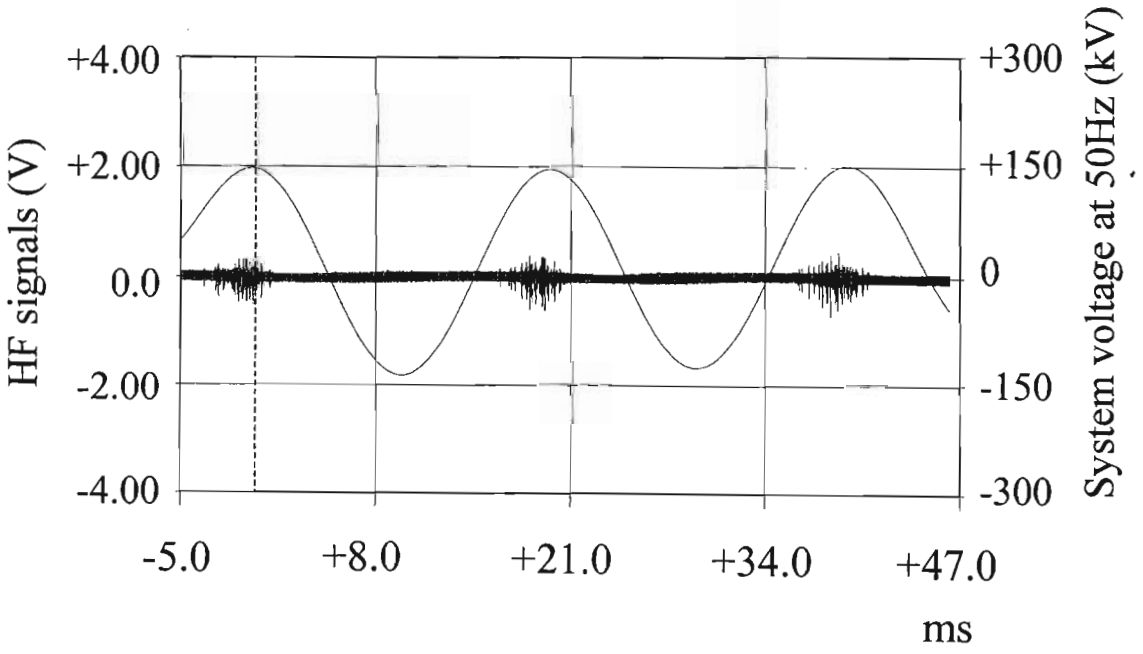

Figure 6. 10: Twin Zebra in rain conditions stressed to 10 kV/cm

The high frequency signals shown in figure 6.11 are those generated due to the presence of a sugar cane fire under the energised conductors. The sugar cane with its leaves as present in a

sugar cane plantation, was ignited. Then the conductors in the corona cage were energised and gradually increased up to 10kV/cm.

The power supply transformers could not provide a stable voltage at the higher gradients, hence tests at the low gradient of only 10 kV/cm were performed. At 10 kV/cm the amplitude of the pulses exceeded the dry and rain condition pulses. Compared to the rain induced corona, the fire induced corona pulses were more than 6 times greater, when they occurred.

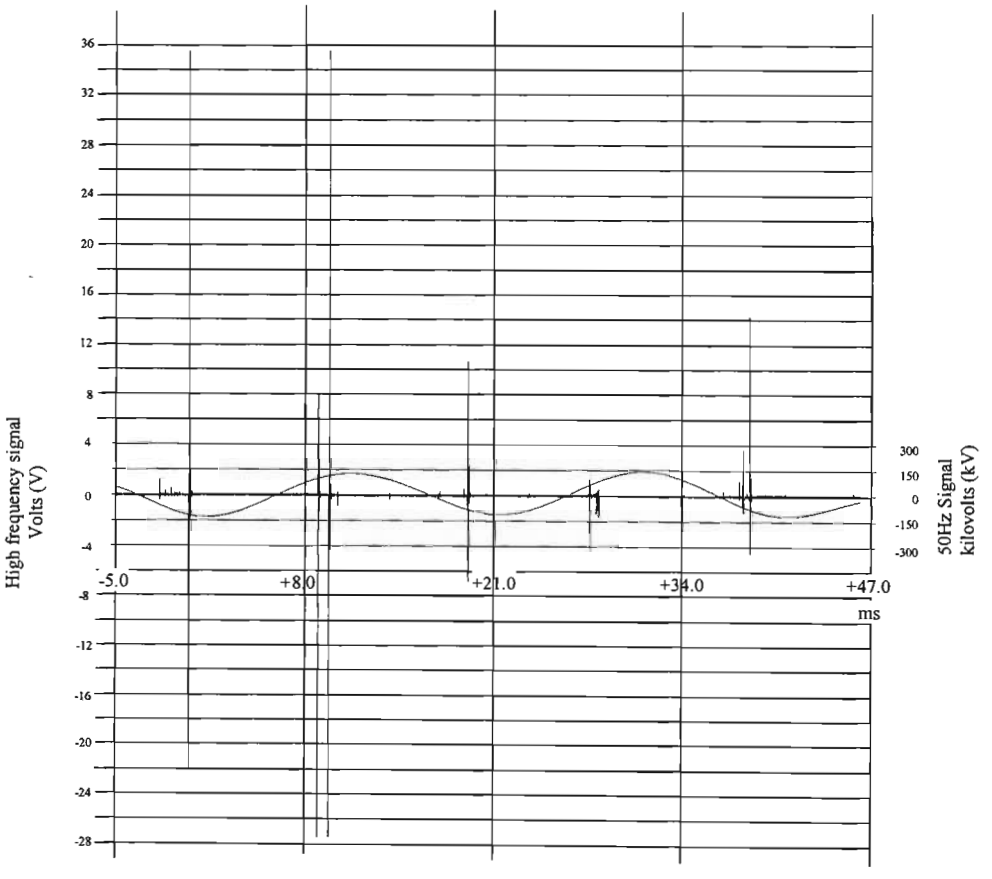

Figure 6. 11: Twin Zebra over sugar cane fire conditions stressed to 10 kV/cm

The corona was visible in both half cycles as opposed to being primarily visible in the positive half cycle for gas fire induced corona. Based on the comparative sizes of the corona in the two half cycles, it appears as though negative and positive streamers were now present at the conductors.

The presence of corona in both half cycles at 10kV/cm may be indicative of the significant impact of particles about the conductors. In section 6.1.3.3 the gas fire (generating heat only) produced highly repetitive corona pulses in the positive half cycle with very little corona in the negative half cycle at a gradient 7kV/cm higher than the test reported in this section. Here the corona pulses in the positive half cycle and the negative half cycles have similar repetition rates

considerably lower than observed in either the rain induced corona tests or the gas fire positive half cycle test results.

6.2.3 Triple Pelican conductor bundle:

Figure 6.12 below reveals only positive half cycle corona pulses for the high surface gradient of 18kV/cm in normal dry conditions.

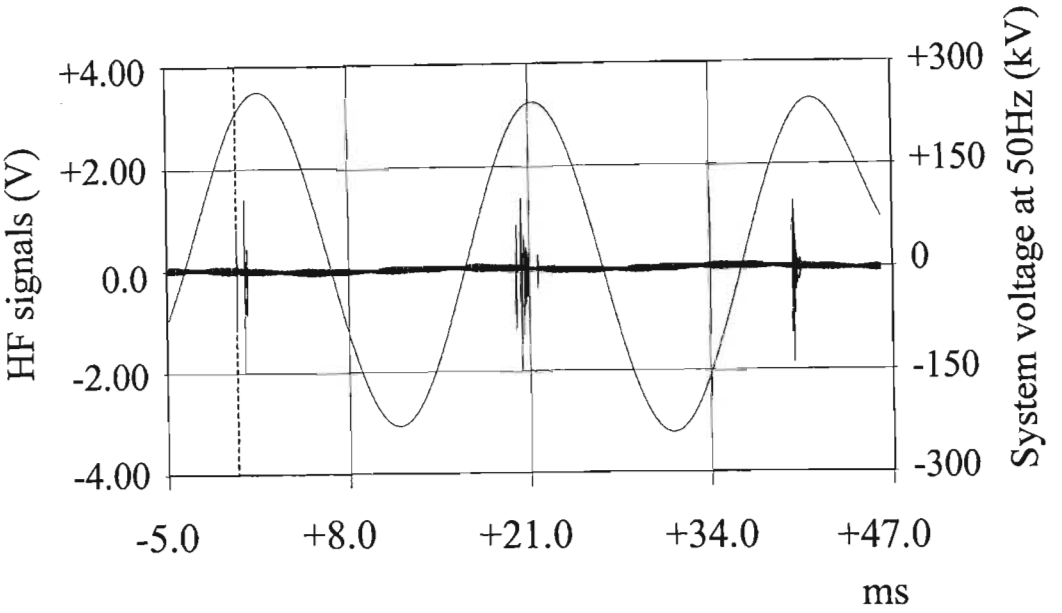

Figure 6. 12: Triple Pelican in normally dry conditions stressed to 18 kV/cm

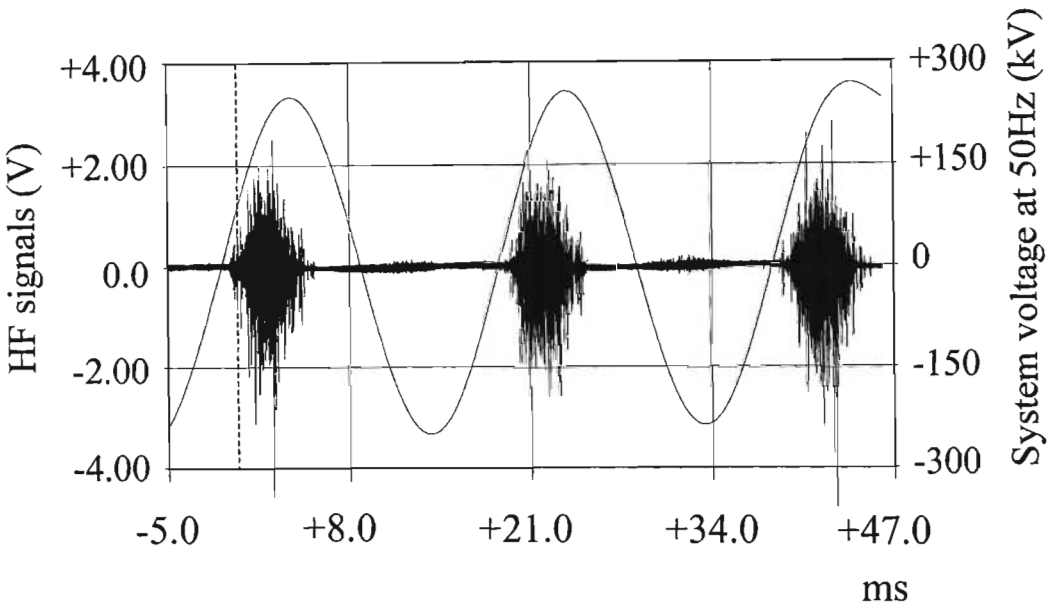

Figure 6. 13: Triple Pelican in rain conditions stressed to 18 kV/cm

At the same surface gradient under heavy rain conditions figure 6.13 reveals an increase in the corona pulses and amplitudes of up to twice the maximum amplitude observed in the dry conditions.

The sugar cane fire tests for the triple Pelican revealed a similar result to that observed for the twin Zebra conductor bundle. It was not possible to raise the gradient any higher than 10 kV/cm without deforming the 50 Hz cycle power signal which would introduce unrealistic frequencies into the energising power supply signal.

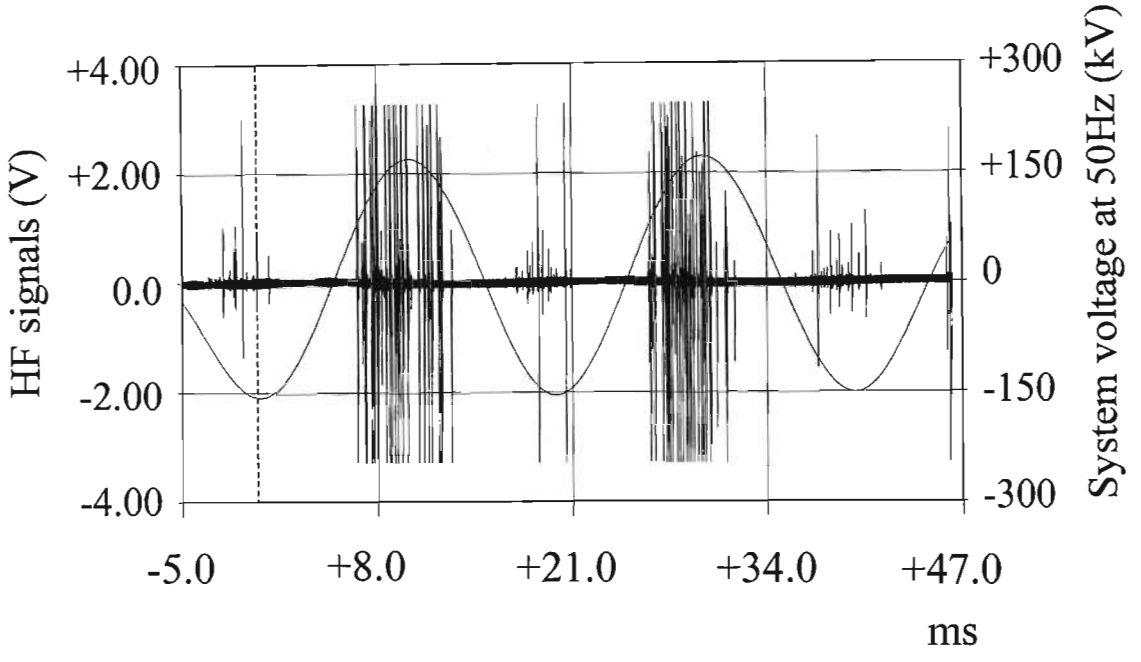

Figure 6. 14: Triple Pelican over sugar cane fire conditions stressed to 10 kV/cm

The phenomena seen in the tests performed on the twin Zebra were duplicated in this conductor bundle as seen in figure 6.14. The corona in the positive half cycles were clipped by the measurement range selected on the instrument but it can still be seen that there is a high number of pulses across each half cycle. Despite the relatively low surface gradient, negative half cycle corona pulses are clearly observed of similar amplitudes in each half cycle and with a similar repetition rate across the three half cycles shown.

6.2.4 Twin Pelican conductor bundle:

Figure 6.15 reveals corona pulses at in dry conditions at 15kV/cm in the positive half cycle only.

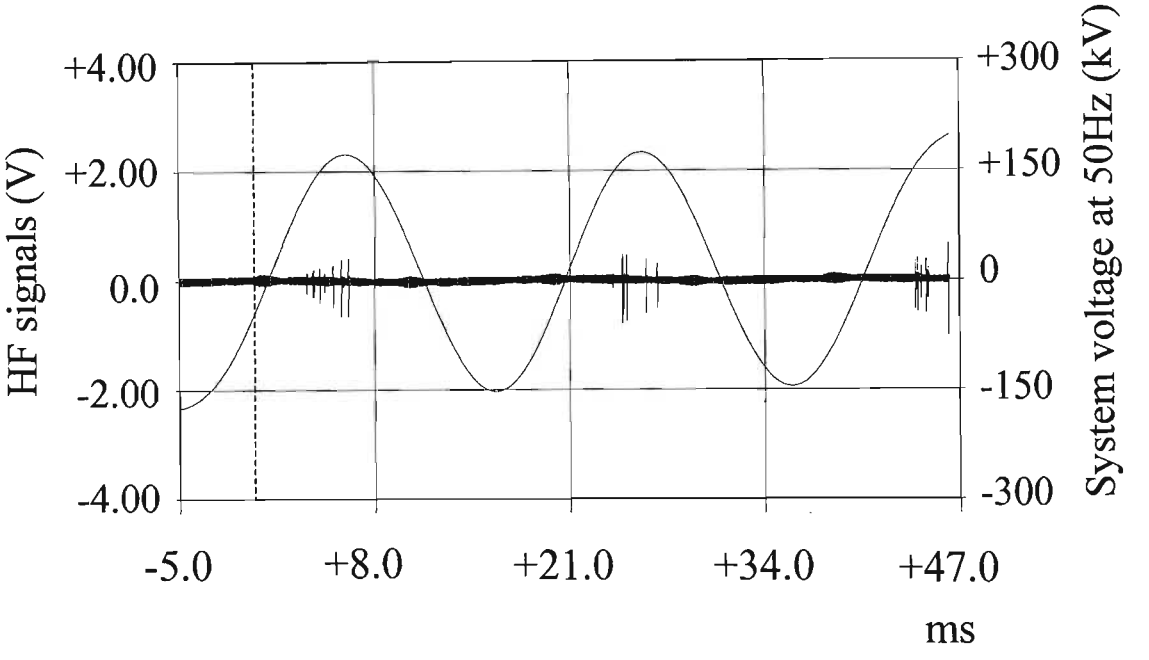

Figure 6. 15: Twin Pelican in normally dry conditions stressed to 15 kV/cm

The corona produced at 15kV/cm under heavy rain conditions as shown in figure 6.16 below demonstrate the repeatable nature of rain induced corona conditions.

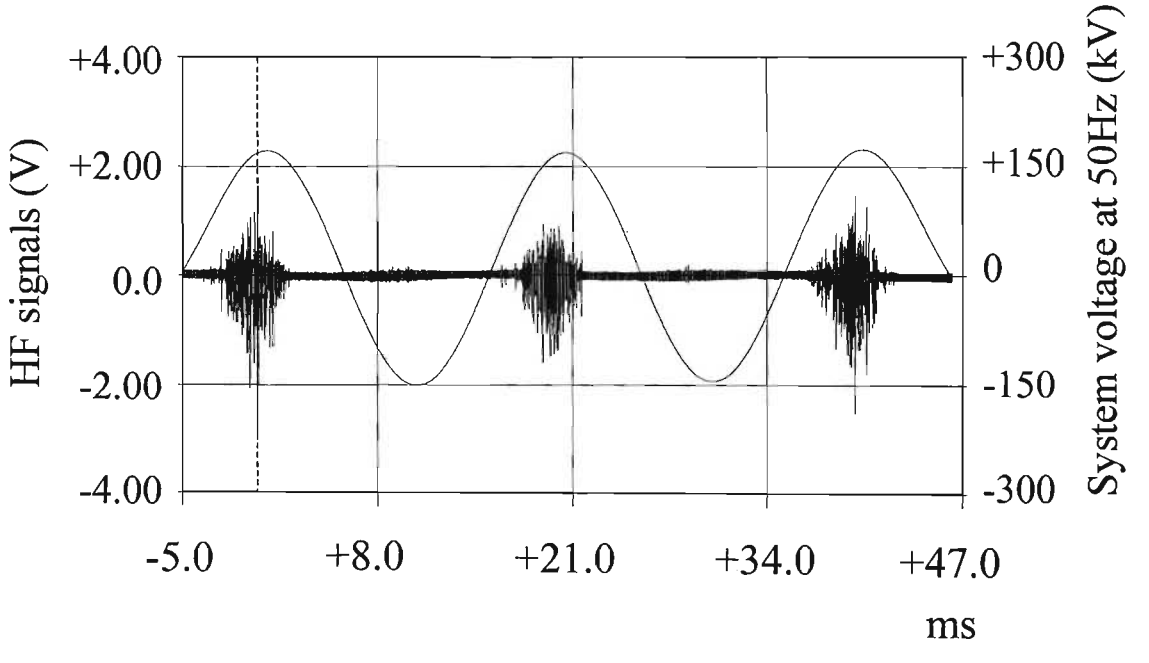

Figure 6. 16: Twin Pelican in rain conditions stressed to 15 kV/cm

Comparing figures 6.13 and 6.16 shows an increase in amplitudes for the higher surface gradients in figure 6.13 but the overall fingerprint is similar.

With the twin Pelican conductor bundle in the corona cage a gas fire test was also completed shown in figure 6.18 with the sugar cane test result shown in figure 6.17.

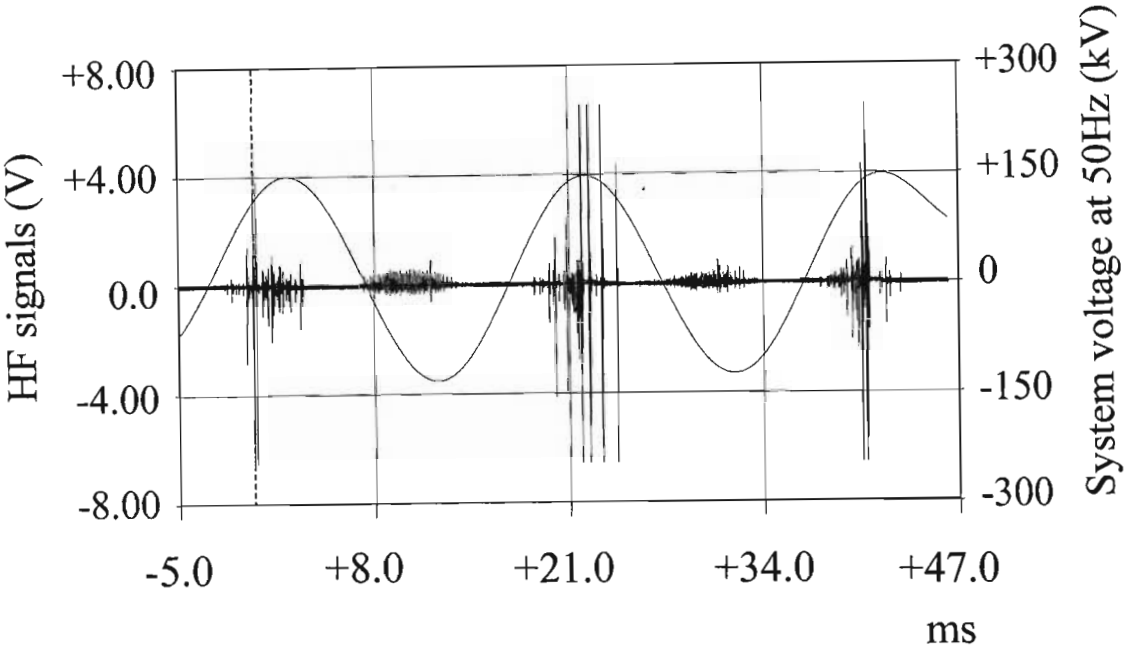

Figure 6. 17: Twin Pelican over sugar cane fire conditions stressed to 10 kV/cm

In figure 6.17 negative glow appears to be present whilst streamers appear to be present in the positive half cycles.

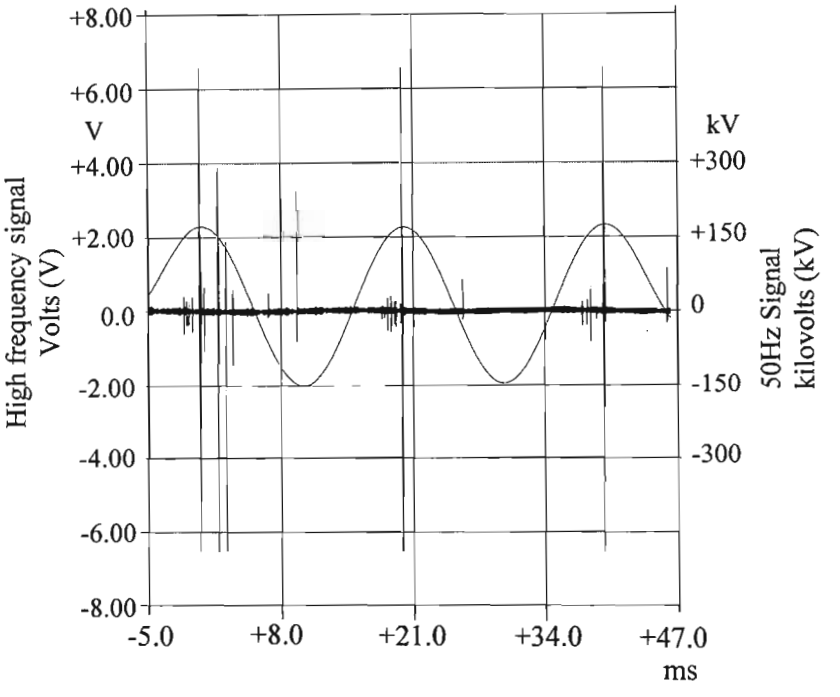

Figure 6. 18: Twin Pelican over gas fire conditions stressed to 15 kV/cm

At 1 5kV/cm t he n egative g low i s n ot v isible. T he streamers in the positive half cycle have a higher amplitude and may be the onset of breakdown streamers. The repetition rate of these streamers is also lower than that for the fire with particles.

6.3 ANALYSIS OF THE TIME DOMAIN DATA

6.3.1 Overview

The waveforms captured with the aid of the more sophisticated Nicolet 500 digital storage oscilloscope described the noise activity occurring due to the induced corona activity in great detail. The preferable sampling rate was 10 MHz. As the corona cage was tuned to 500 kHz, the minimum allowable sampling frequency was 1 MHz. However, this describes only two points of any 500 kHz component of the noise. Comparability was essential in the identification of fire-induced corona noise and hence two points at this frequency were not adequate. The sampling rate had to be at the maximum available whilst still being able to evaluate the affects of the corona activity. That is, a compromise had to be made between the sampling rate and the waveform length sampled based on the maximum 600 000 sample points available. The higher the sampling frequency, the shorter the overall waveform length would be. At 10 MHz, any relatively distinctive differences existing in the noise patterns between the rain-induced and fire-induced corona noise sources was expected to be detectable. The restriction was therefore set to a waveform length of 120 ms. The 6 cycles were sufficient to describe the relative changes in induced corona noise adequately.

The digital storage oscilloscopes reduce the data displayed in the frame when displaying larger volumes of data. By reducing the time span displayed in a frame, more detailed information becomes visible. The discussion here will therefore focus on the detail of figures shown in section 6.2 above. A half cycle will be identified which contains corona pulses. These pulses will then be displayed and their frequency response will be discussed and compared to pulses in the other conditions. Where more than one pulse is present in that half cycle, the frequency response is analysed with an individual pulse and with all the pulses present in that half cycle. Where the activity has a "no electrical corona discharge" zone, this zone is also analysed and compared to the frequency response of the activity outside this zone. The "no corona" zone also serves as a reference of background noise levels; interfering intermittent noise which may skew the interpretation; and a reference, namely the radio stations signal strength. Dry condition data was analysed for the background content present at any one time during the tests.

6.3.2 Twin Dinosaur conductor bundle (ref gas fire)

6.3.2.1 Twin Dinosaur Dry conditions

To identify the characteristics of the induced corona pulses as observed through the "filtered environment" of the corona cage, the pulse as generated in dry conditions was sufficiently isolated from abnormal conditions for evaluation. From figure 6.1 on page 85 the enlarged section of the waveform on the last full positive half cycle displayed two random pulses.

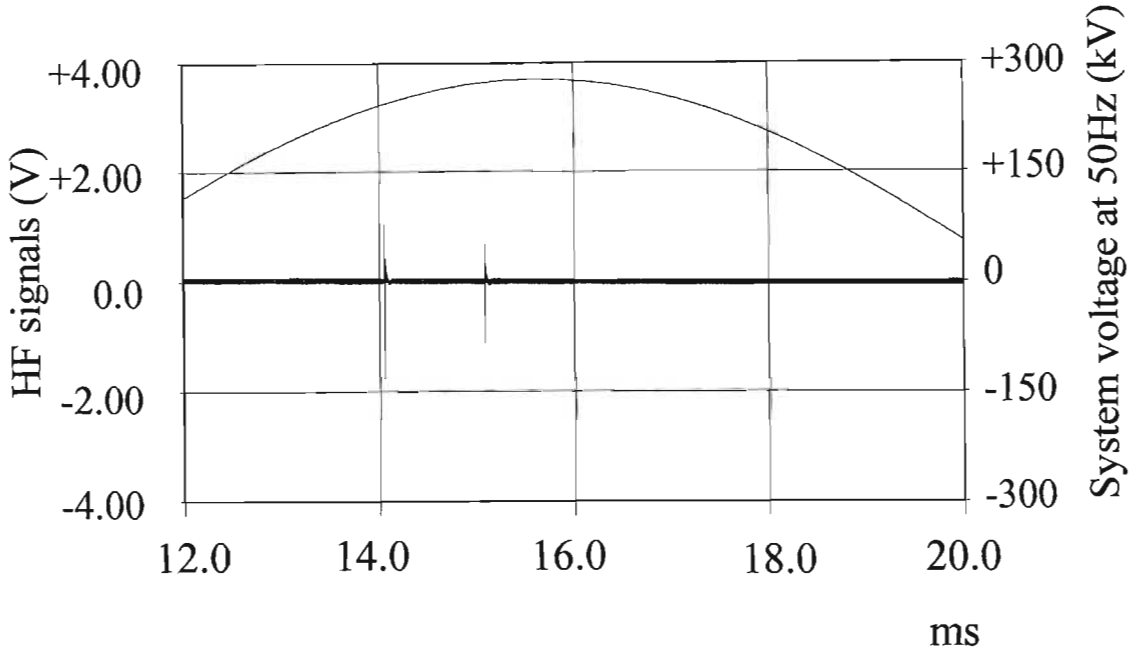

Figure 6. 19: Twin Dinosaur in dry conditions stressed to 16 kV/cm (one half cycle).

From the original waveform, these pulses were barely observable. These pulses were not repeatable in the sense that the two pulses did not regularly occur at the same position relative to the 50 Hz power signal. The occurrence may have coincided with the presence of some floating particles transported past or onto the conductors by the wind or may have been some insects (also considered to be of particulate nature) approaching the conductors. In either case the proximity of such particles are on a microscopic scale and could in no way be controlled in this environment. At the same time however, such particulate activity had no significant bearing in the final analysis, other than to describe the event when a streamer surges from the conductor.

Concentrating on a single pulse clearly demonstrated that more than a "simple" pulse was recorded by both the quasi-peak measuring equipment and the digital storage oscilloscope. An

impulse was recorded, which was generated as a result of the flow of current in a streamer, but noticeable ringing took place after that pulse as observed in figure 6.20 below.

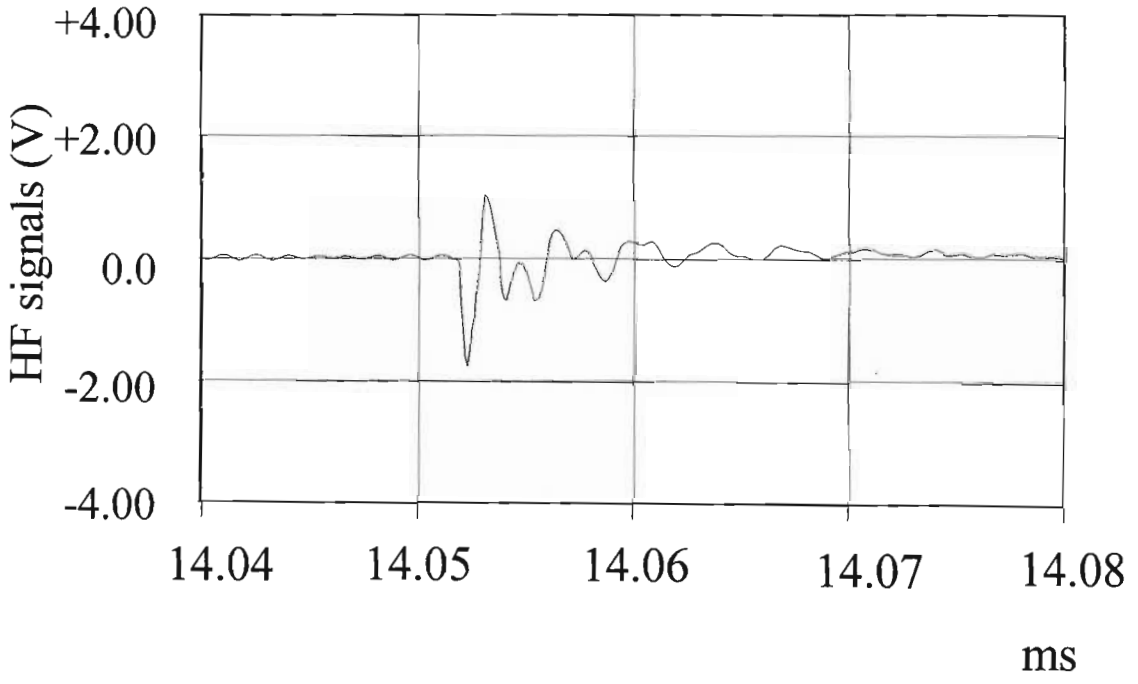

Figure 6. 20: First pulse in previous figure amplified.

Note that the voltage measured in the initial discharge was negative which was directly related to the direction of the applied electric field (which was positive at the time).

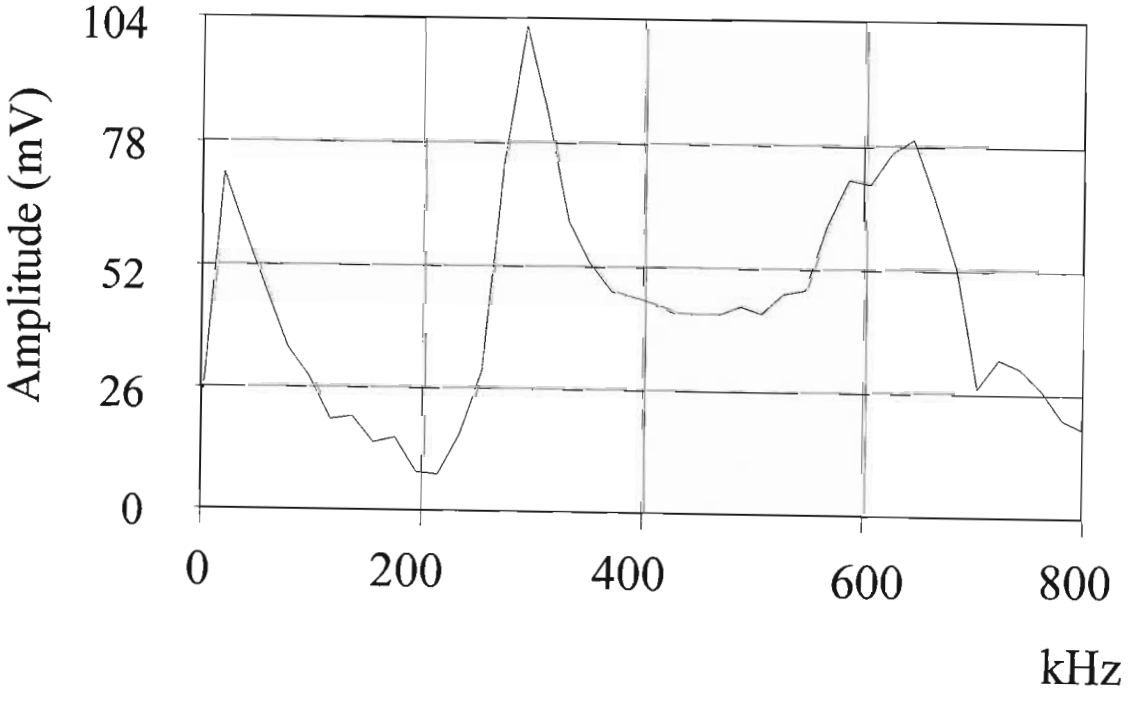

Figure 6. 21: Frequency spectrum of the recorded streamer pulse.

Figure 6.21 shows the spectrum of streamer activity over the frequency range of interest. The sample data used to obtain the above information was sampled at a rate of 10 MHz over 40.2μs

as shown in figure 6.20 and stored in a total of 402 sample points. The spectrum analysis was made with the assistance of a fast fourier transform (FFT) algorithm with rectangular window weighting criteria. The sampling frequency was high enough to adequately describe the activity occurring at the observed frequencies but the use of only 402 sample points was an impediment to the overall "picture". The maximum allowable sample size for the algorithm (16384 sample points) was selected and introduced an interesting overall "picture" of the results. The original waveform was cut over a longer section of the data and included both the observed pulses and the following was found:

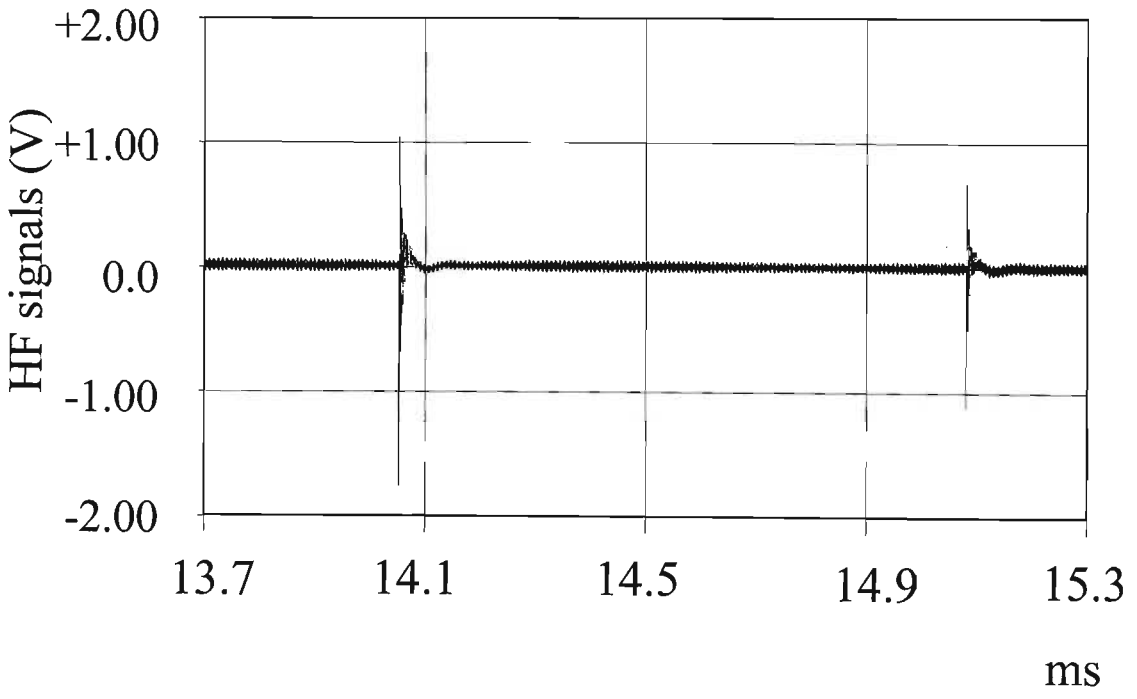

Figure 6. 22: Expanded view of the two streamer pulses.

The data shown in figure 6.22 contains a significant amount of background noise, with the two streamers occupying only a small proportion of the total data. The nett result was that the information in each of the two streamers was minimised due to the accumulative affects of the background noise (figure 6.23).

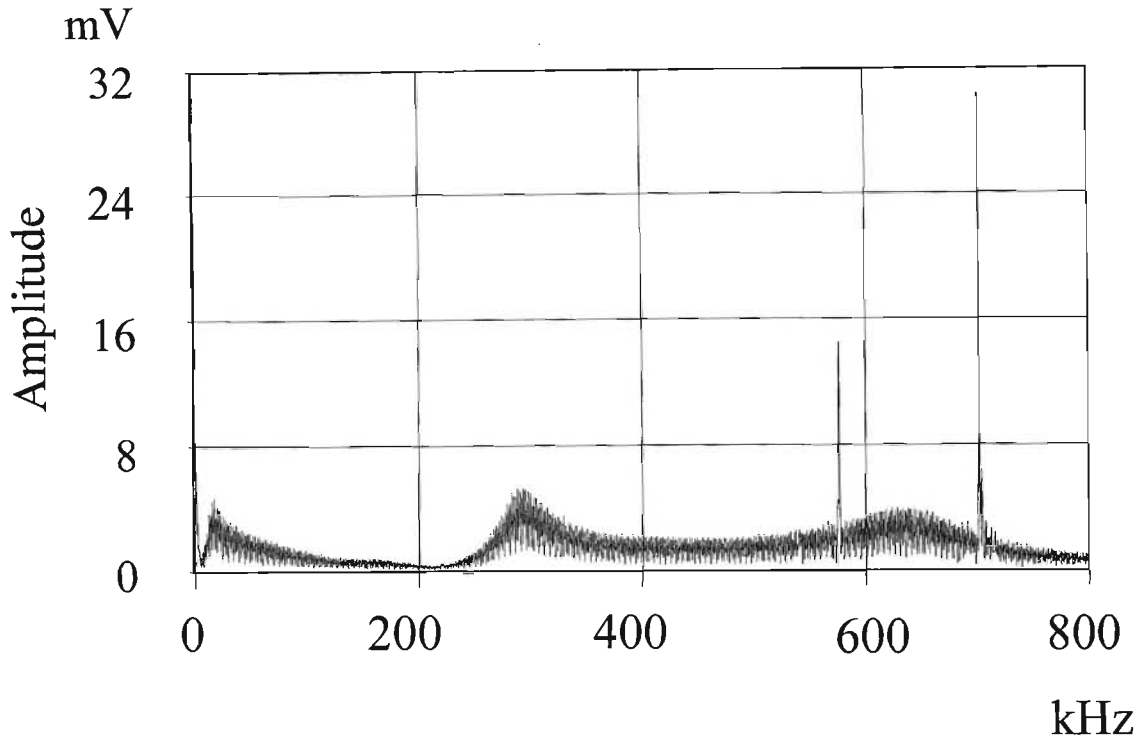

Figure 6. 23: Frequency spectrum of the two dry condition streamers and low level noise.

The total number of sample points taken for the calculation of the frequency spectrum shown in figure 6.23 was 16002 points. Excluding the two strong signals, the trend in the frequency spectrum was similar to that measured over the smaller number of points of figure 6.21. The significance was that the transfer function of the corona cage with parasitic capacitances and inductive affects included in the bandpass filter configuration was implicated with this result. In figure 6.24, the two spectra are superimposed and three observed peaks occurred at 19.6 kHz (point a), at 293 kHz (point b) and at 644 kHz (point c).

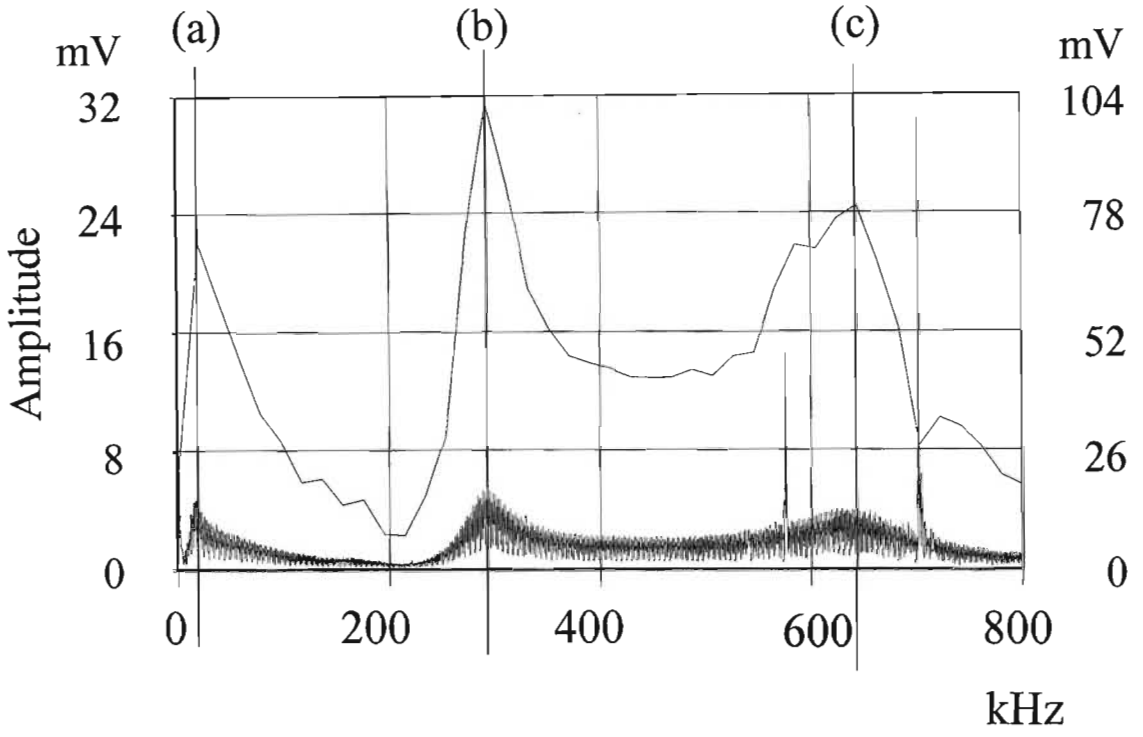

Figure 6. 24: Frequency spectrum comparisons (one and two pulses)

The time domain background noise data was isolated from the streamer impulses and illustrated in figure 6.25 below. The FFT of this data revealed that the previous trend in the filtering patterns could no longer be seen (figure 6.26).

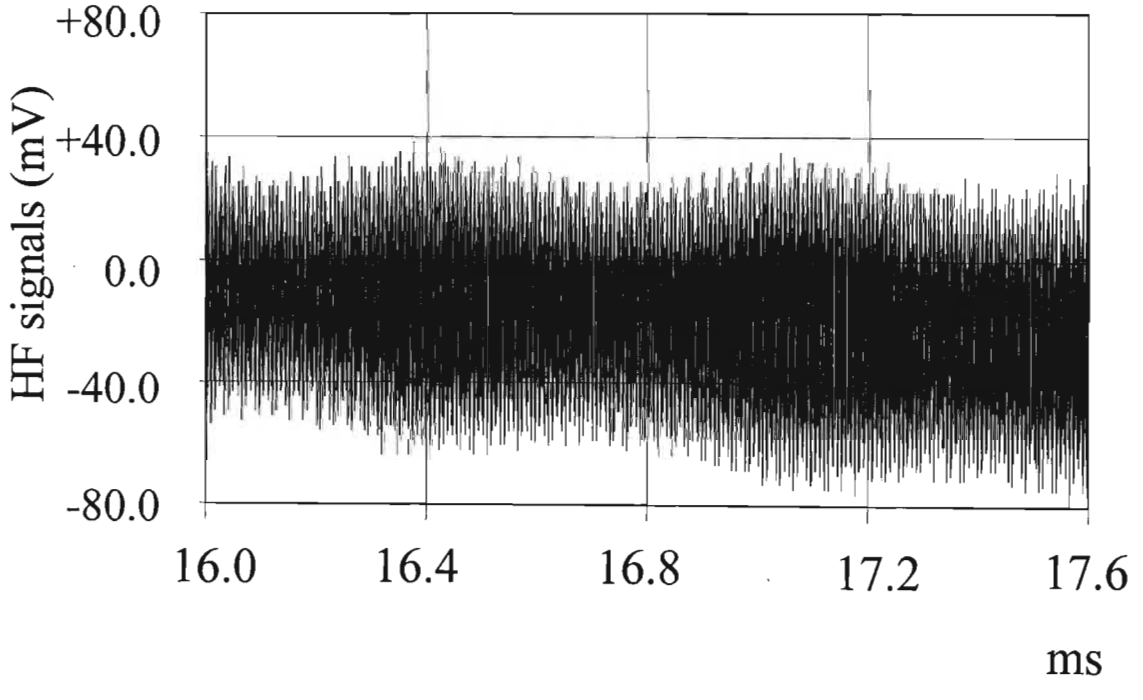

Figure 6. 25: Expanded view of noise with no streamers (dry conditions).

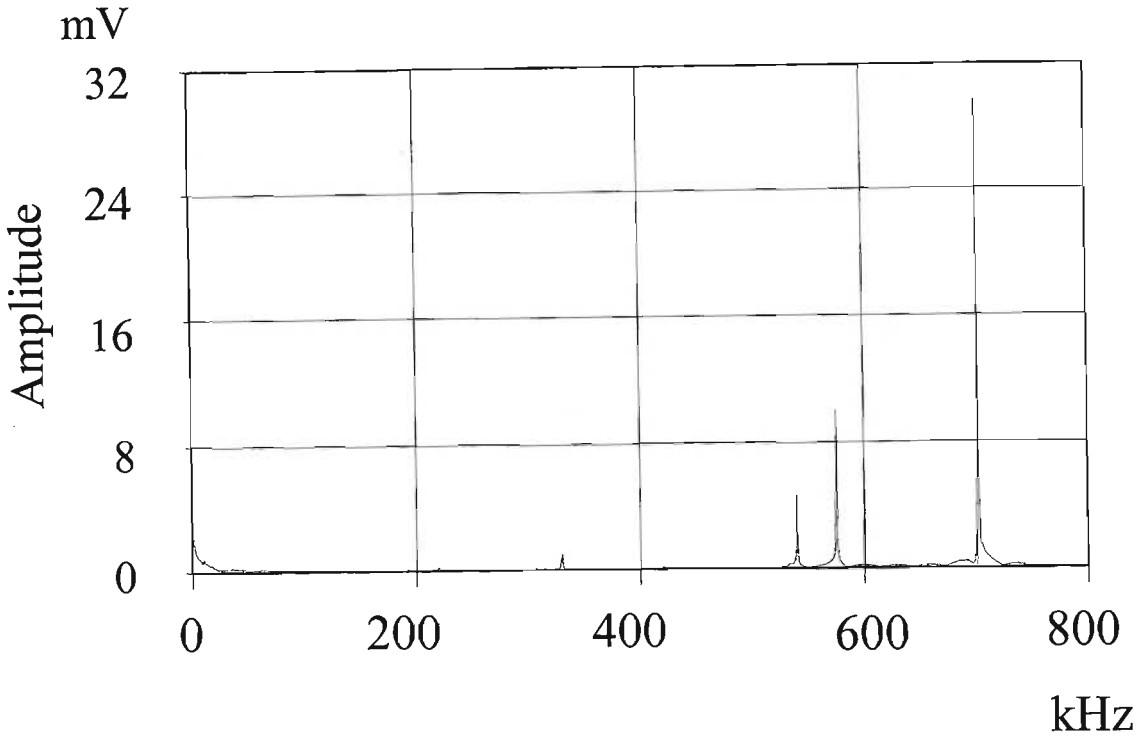

Figure 6. 26: Frequency spectrum of the background noise only.

The three high amplitude frequencies visible in figure 6.26 were investigated and found to emanate from radio station transmitters.

The local AM radio stations of Radio Bop, Radio Metro and Radio 702 could clearly be seen at 540 kHz, 576 kHz and 702 kHz respectively. This information was present on the transmission line at voltages much lower than the induced corona noise measured (± 80 mV as opposed to up to 1.8 volts).

In summary, the following has been concluded with respect to the existence of the pulses: The significance of these pulses was measured in terms of their overall affect on the system (as power loss usually defined as the 50 Hz "corona losses"). Over the fixed instant in which the streamer surges from the conductor the background noise was much less significant when considered over an instant of the same time duration. Therefore proportionately, much more power was present in the streamer impulses. However, over longer time periods, the frequency spectrum showed a stronger accumulative noise power due to the radio station transmissions. Therefore the outcome was a lower overall level of background noise as reflected in the quasi-peak measurements.

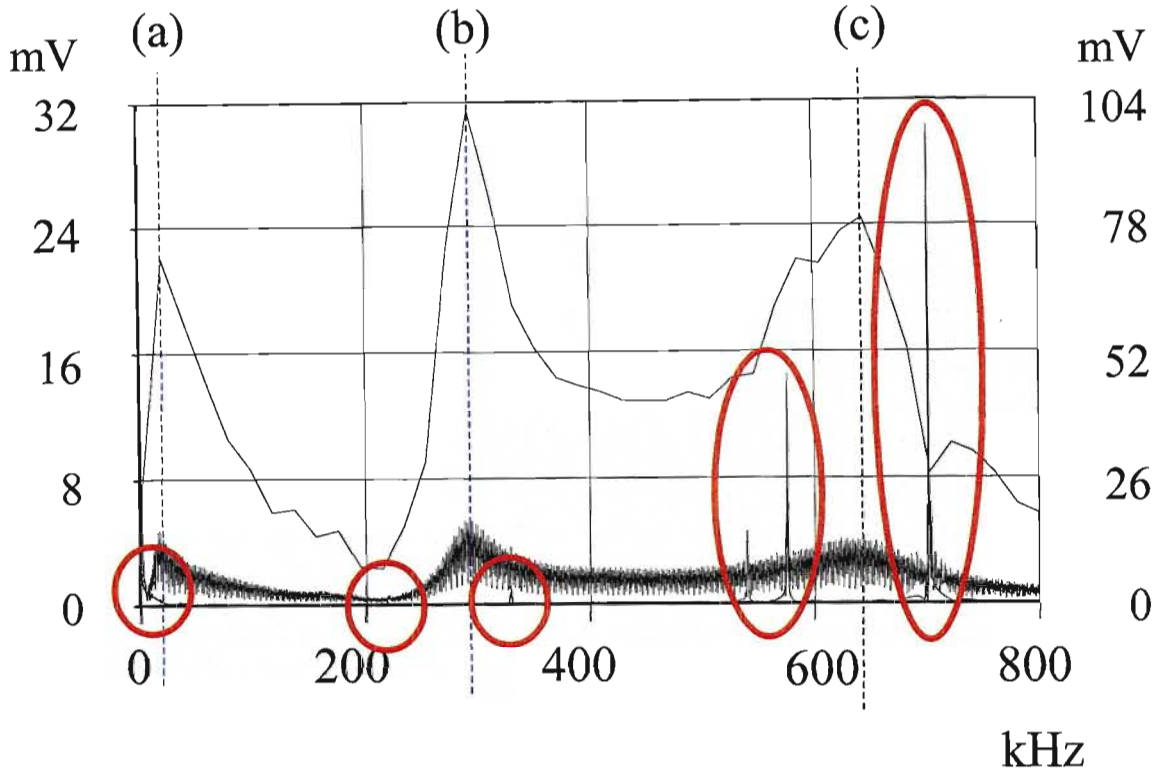

Figure 6. 27: Frequency spectrum comparisons (background, one and two pulses).

The frequency spectrum was seen as instrumental in the evaluation of the pulses and the mathematically determined data was summarised as follows: Figure 6.26 exhibited only the characteristics of the radio channel frequencies when no streamer impulses were included in the sample data from which the calculations were done. When the two streamers were included in the analysis, figure 6.23 indicated a rise in the level of noise over almost the entire spectrum with stronger nodes in the regions of 19.6 kHz, 293 kHz and 644 kHz. When only a single pulse was analysed, those three "nodes" were the only significant frequencies observable in figure 6.21 hinting at a white noise effect shaped by the transfer function of the corona cage circuit. The dominating frequency of Radio 702 (at 702 kHz) in figure 6.26 showed no change in magnitude when including the two streamers but was totally overwhelmed when analysed directly with the single streamer (figure 6.20). The streamer impulses therefore dominate the channel in the instant of time when they exist. Appropriate measurement techniques could highlight those events for correct and precise classification.

Figure 6.27 above have each of the background noise observable frequencies shown in figure 6.26, circled. The two pulse FFT is shown as the lower amplitude signal in that figure and the single pulse FFT is the large amplitude FFT.

Rain-induced and fire-induced corona streamers were expected to display similar but more powerful trends in the noise levels provided the physical processes by which they occur were similar to the streamers discussed. That is, provided they were generated via the same initiating physics of ionisation by electron impact.

6.3.2.2 Twin Dinosaur Rain conditions

In the macro view of figure 6.2 on page 85, there was a much larger number of streamers present which were on average only marginally larger than the streamers recorded in the dry conditions. The noise patterns generated under normal dry conditions (figure 6.1) and analysed from figure 6.19 onwards, were compared with the noise patterns generated due to rain in a similar single positive half cycle shown in figure 6.28 below. Without enlarging the graph any further, it was evident that many more streamers were generated in the heavy rain controlled conditions. When comparing with the dry conditions, the rain-induced corona noise was more consistent as a result of the uniform process of the layer of water forming about the conductors under the stresses of the electric field. The magnitude of most of the impulses observed in figure 6.28 were of the same order as that of the two dry condition impulses measured. The quasi-peak measurement method however, favours a "rapid repetition of pulses" and hence the marginally larger rain-induced corona had a much larger quasi-peak value since the rain-induced streamers occurred much more frequently than the streamers in the dry conditions.

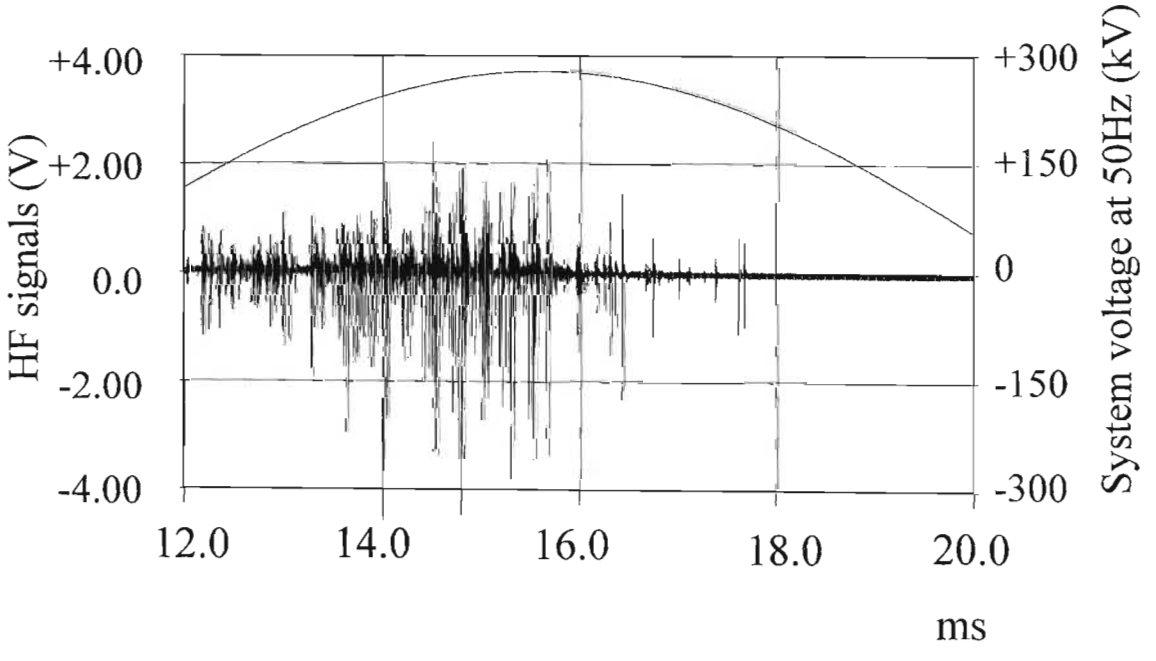

Figure 6. 28: Twin Dinosaur conductor bundle under rain conditions stressed to 16 kV/cm

To perform an accurate comparison of the data captured in the rain conditions with the results from the dry conditions, it was necessary to first observe the background noise levels to determine if any other abnormal activity was present. Figure 6.29 shows that background noise and figure 6.30 shows the FFT frequency spectrum of that background noise.

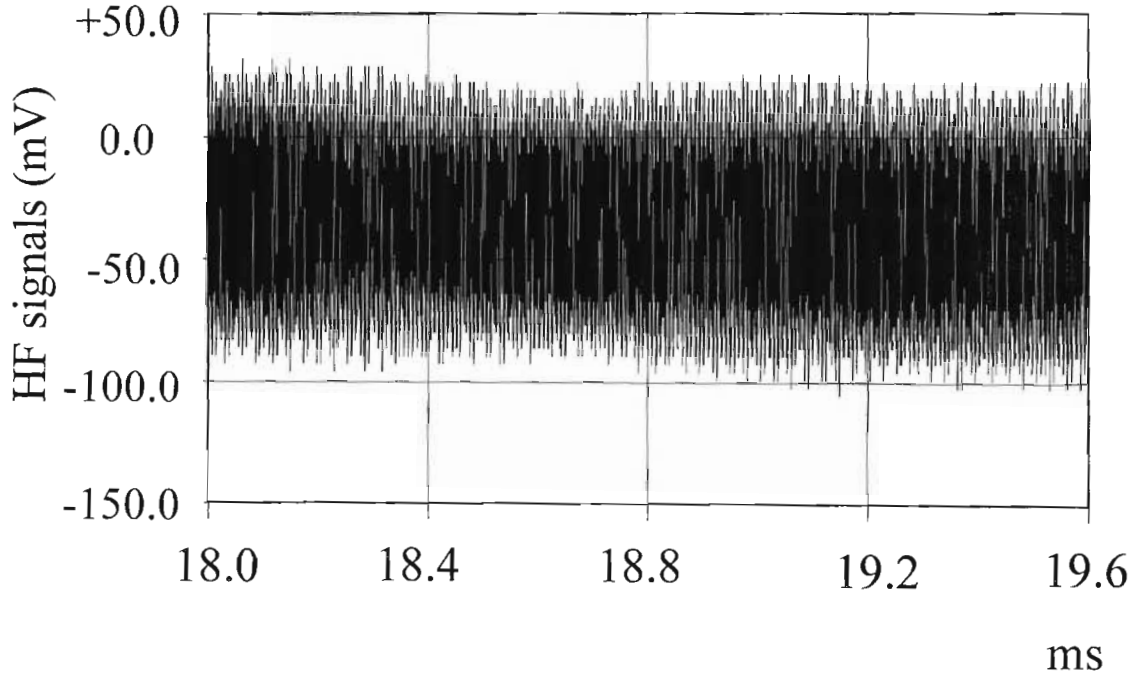

Figure 6. 29: Expanded view of noise with no streamers (rain conditions).

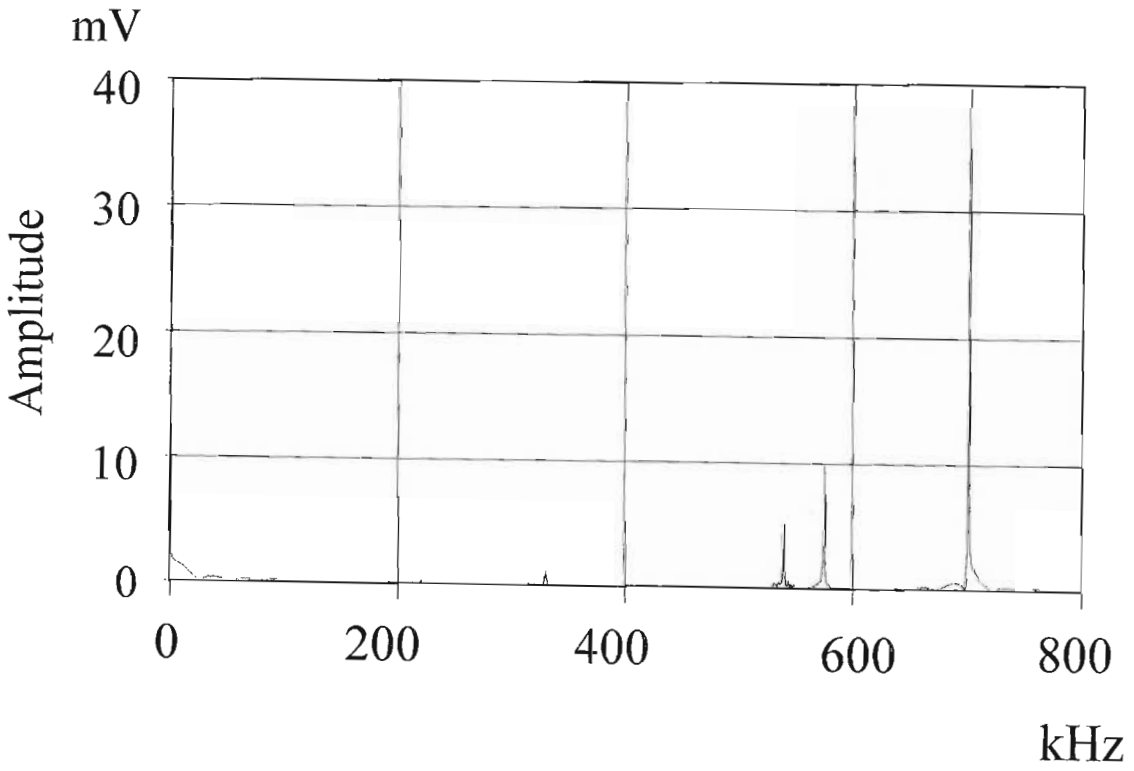

Figure 6. 30: Frequency spectrum of the background noise only (in rain conditions).

The only observable changes were the levels of the local broadcasting channels. Hence the channel was free of any other intermittent affects. An enlargement of figure 6.28, showing events

in the time domain in more detail, was necessary for evaluating the rain-induced streamers individually.

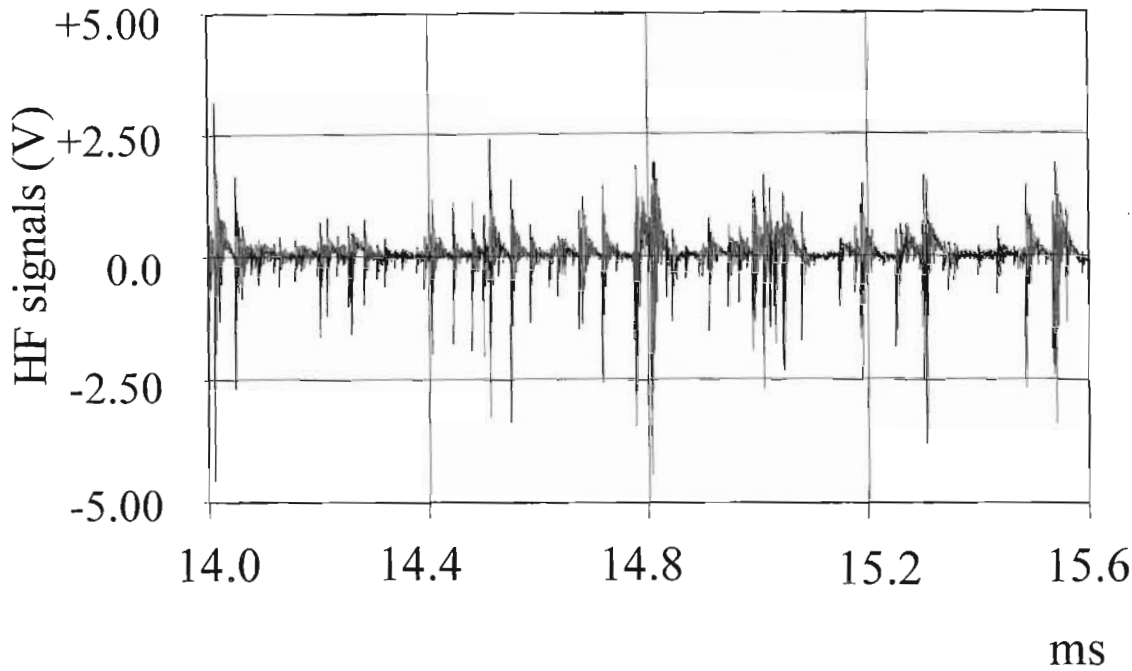

Figure 6. 31: An expanded portion of the rain induced corona in one half cycle.

The data (waveform data which was cut from 14 to 15.6 ms) demonstrated the clear distinction between rain and dry conditions.

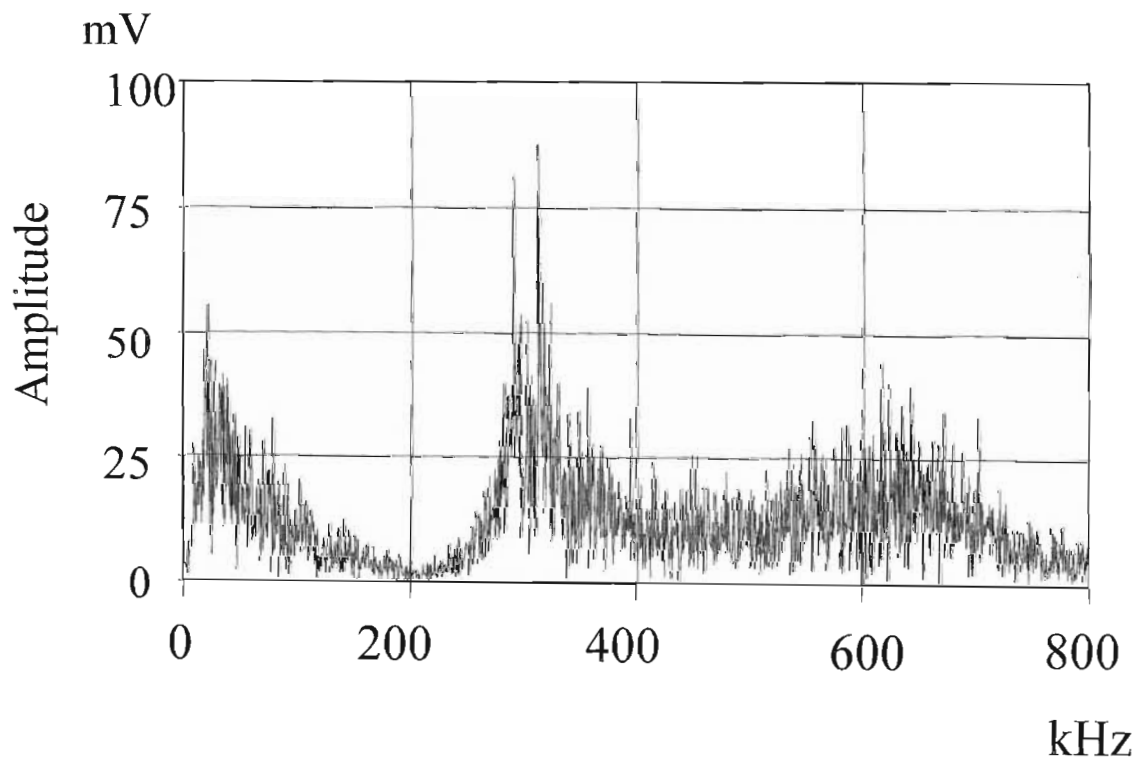

Figure 6. 32: Frequency spectrum of the rain induced corona activity (in rain conditions).

When rain was present on the conductors and the electric field on the conductors was high enough, the rain-induced streamers were continuous with the next impulse occurring before the ringing from the previous impulse had completely dissipated. On average the magnitude of the impulses recorded increased with the increase in the applied voltage and vice versa.

The frequency spectrum for the dry and heavy rain conditions are shown together in figure 6.33. The pulses in figure 6.31 occupied the greater proportion of the data sample and hence dominated the spectrum. The broadcast signals were totally engulfed by the rain-induced corona noise activity, an indication of the consequence of summing the components (in an averaging fashion - quasi-peak or otherwise). The centre node at approximately 293 kHz had jumped from about 6 mV to around 90 mV from having only two streamers to many respectively.

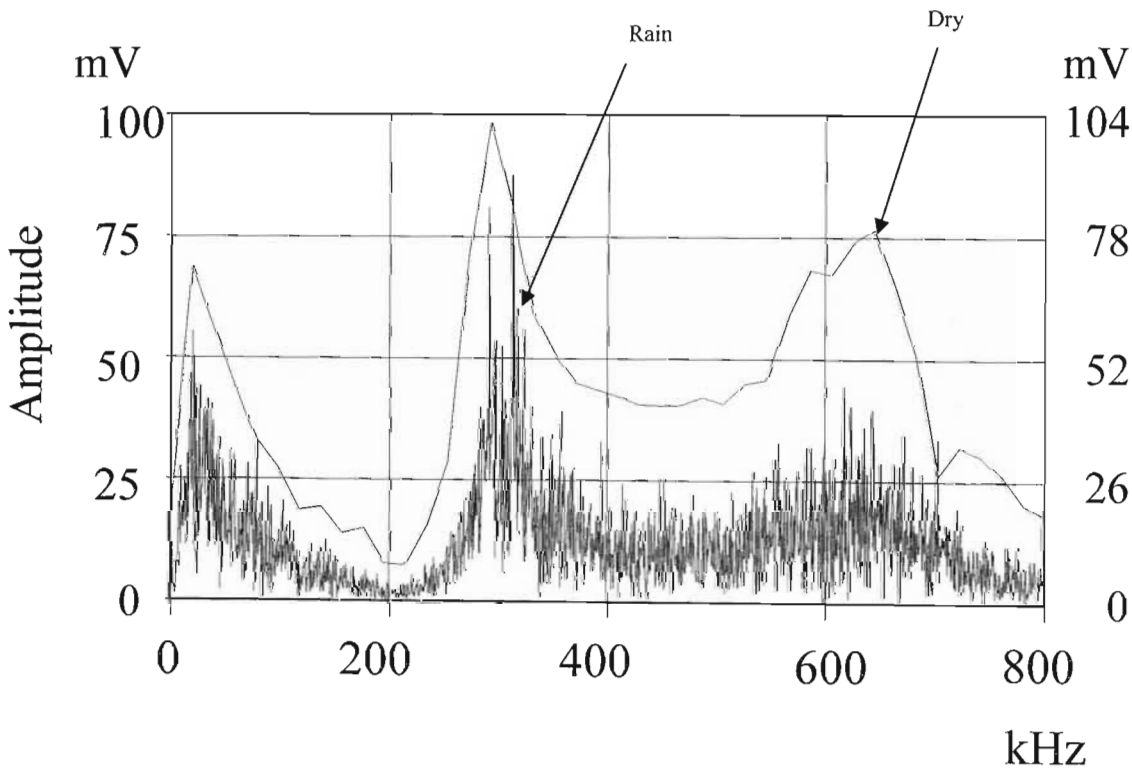

Figure 6. 33: Frequency spectrum comparisons (dry versus rain conditions).

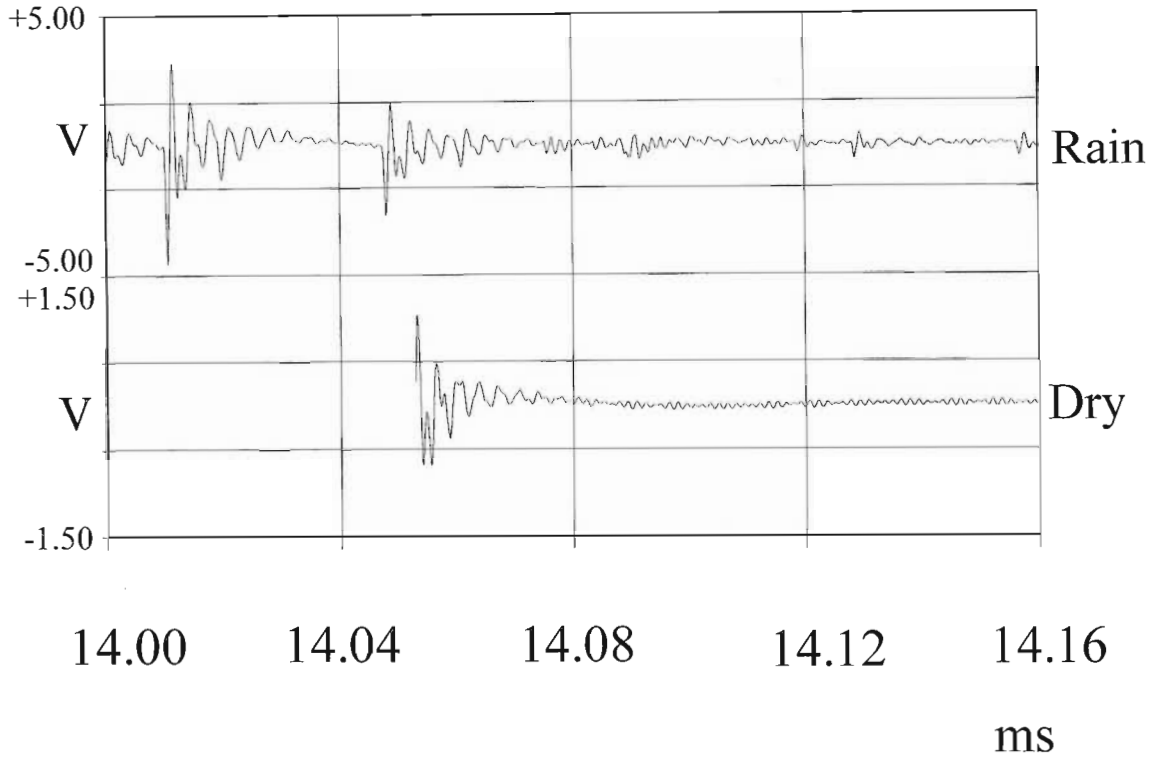

Figure 6. 34: Rain induced corona pulses versus pulses in normally dry conditions.

For a direct comparison of the induced corona noise activity from the dry conditions and rain conditions, additional focus was required on the rain-induced corona and in particular, focus on an individual pulse. A pulse from the rain and dry condition streamers are shown in figure 6.34 above.

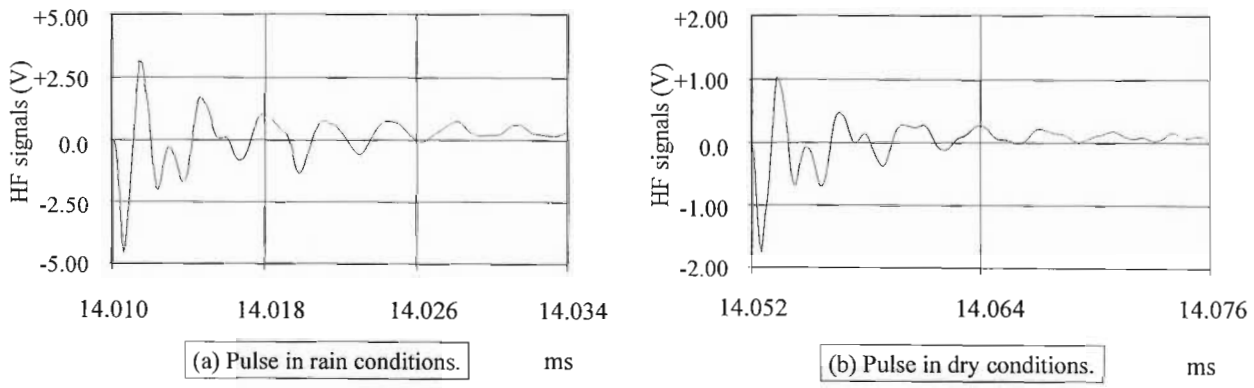

Figure 6. 35: Single rain induced corona pulse compared to pulse in dry conditions.

The pulses captured in both rain and dry conditions had the same character when comparing the dry pulse (and its related ring) with one of the rain-induced pulses directly above it. Hence it was safe to assume that they essentially existed due to the same influences, that is, the discharging

currents originated in the flow of charge due to ionisation by electron impact and observed through the same high voltage filtering circuit represented by the corona cage.

In conclusion of this analysis the important differences between the rain-induced corona pulses and the pulses under normal dry conditions, was the frequency at which the rain-induced pulses were repeated and the larger amplitudes of those pulses. The pulses captured in the normal dry conditions occurred at any time in space when the field was sufficiently and unpredictably distorted.

6.3.2.3 Twin Dinosaur Fire conditions

Where the rain-induced corona - or streamers - were only marginally larger than the random pulses occurring in the normally dry conditions, the fire-induced streamers visible in figure 6.36 below, were markedly larger than both the randomly generated dry streamers and the consistent rain-induced streamers. The repetition rates of the fire-induced corona pulses were however, less predictable than that of the rain-induced corona pulses. For the single gas fire source, the repetition rate of the fire-induced corona noise was lower than that of the rain-induced corona noise.

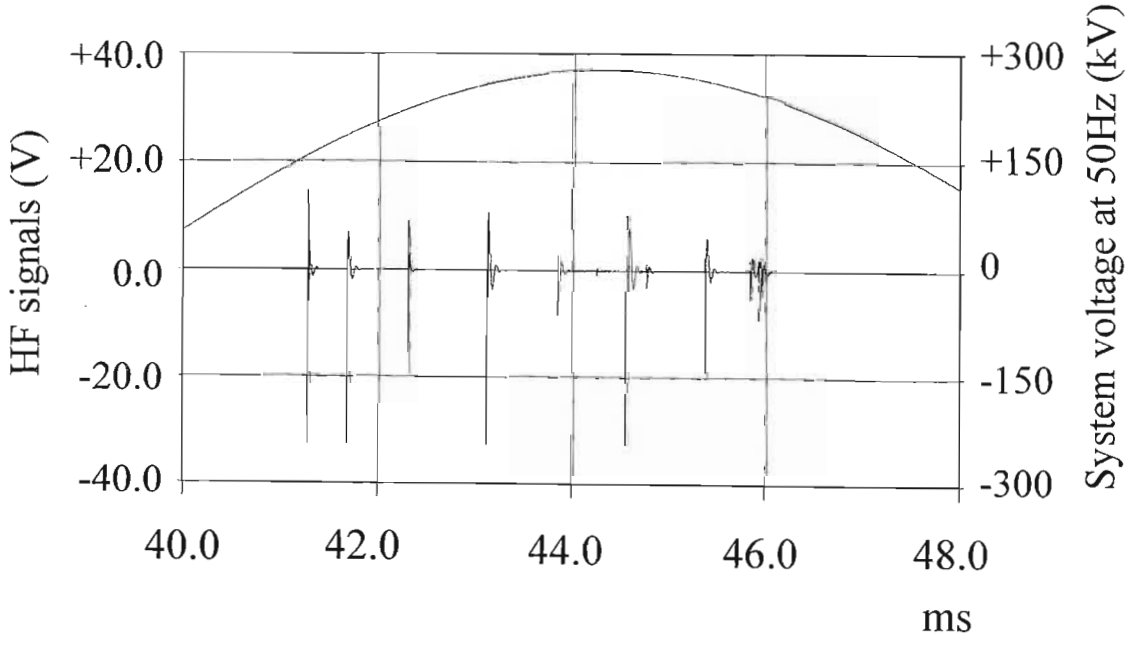

Figure 6. 36: Twin Dinosaur bundle over fire conditions at 16kV/cm.

The amplitude scales of the figures for dry and heavy rain condition data were ± 4.00 volts whereas the pulses observed in the figure above were clipped on scales of ± 40 volts. The dB

measurement of the factor of 10 change was therefore 20(log10) = 20 dB which was marginally higher than the quasi-peak data given at 16 kV/cm in figure 5.1 on page 60. For detection purposes, the above differences would be adequate to develop a detector. The criteria had to be firstly: positioning of an appropriate threshold voltage to identify the larger pulses and secondly: positioning of an appropriate threshold "frequency" to identify the lower repetition rate of the fire-induced corona noise activity. However, since the research work to date has not included all possible noise sources it was necessary to scrutinise the fire-induced corona noise in more detail.

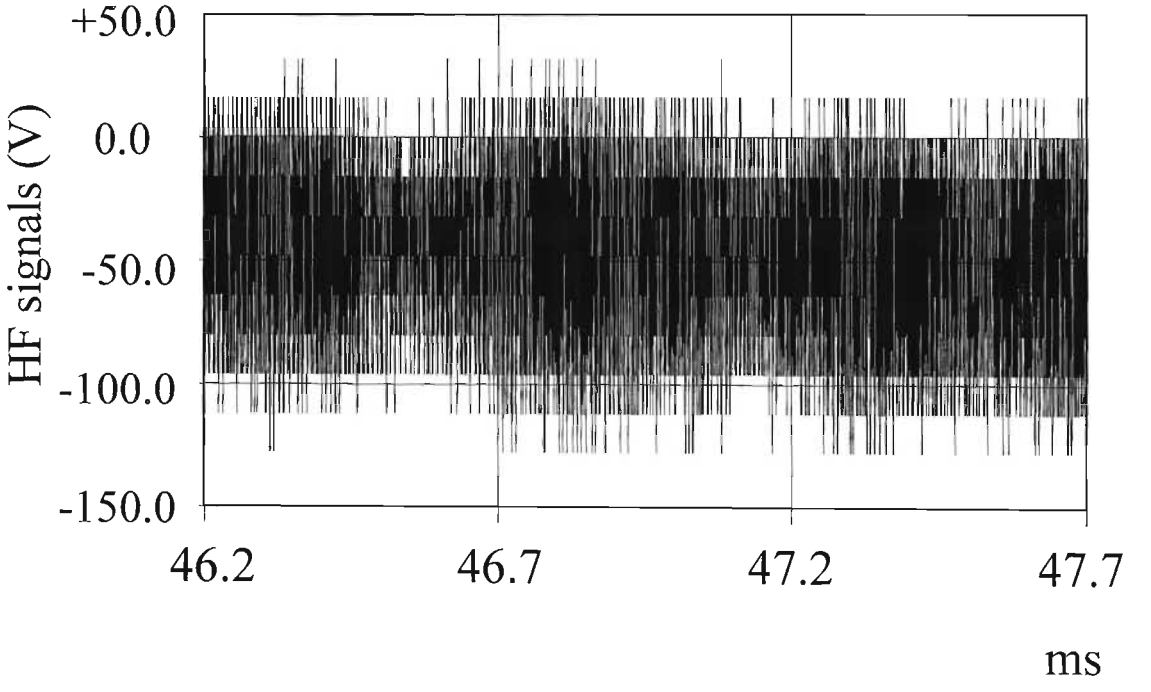

Figure 6. 37: Expanded view of noise with no streamers (fire conditions).

The background noise present on the system was shown in figure 6.37 above. It was virtually identical to the noise recorded for dry and heavy rain conditions.

The frequency spectrum in figure 6.38 below of the data in figure 6.37 showed the identical profile with only a few millivolts change in the signal strength of Radio 702 and Radio Metro.

Note that at the low voltage levels associated with the background noise measurements, the digitised signal (with 12-bit or 4096 divisions) suffers from some quantisation noise. The amplitudes are less than +50mV and more than -150mV. Since the signals do show increasing and decreasing trends, the frequency spectrum is not adversely influenced by this noise. Figure 6.38 shows prominent radio stations and verifies that lack of any significant signal content outside the radio transmission zones.

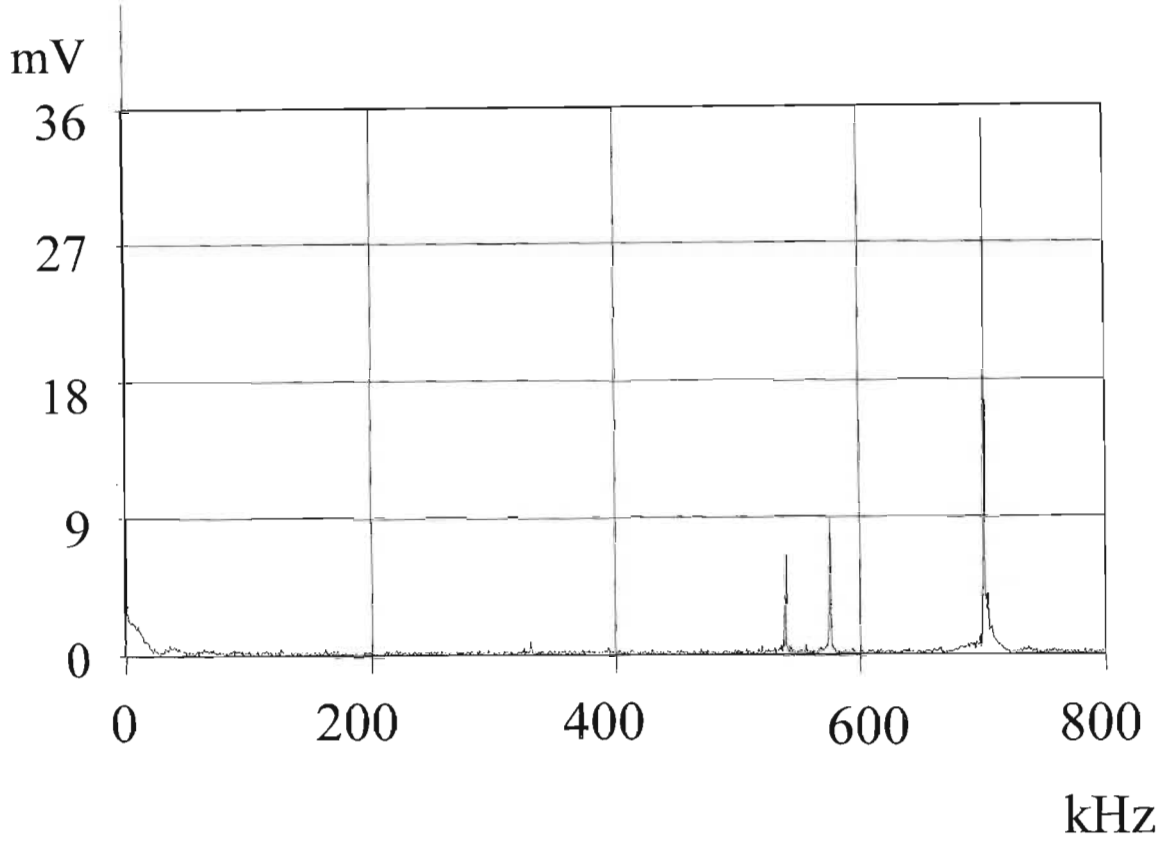

Figure 6. 38: Frequency spectrum of the rain induced corona activity (in rain conditions).

A segment of the fire induced corona waveform (again 1.6 ms in length) including two pulses was selected for analysis. Due to the larger magnitude of the fire-induced pulses the background noise was less significant – presenting a better signal-to-noise ratio.

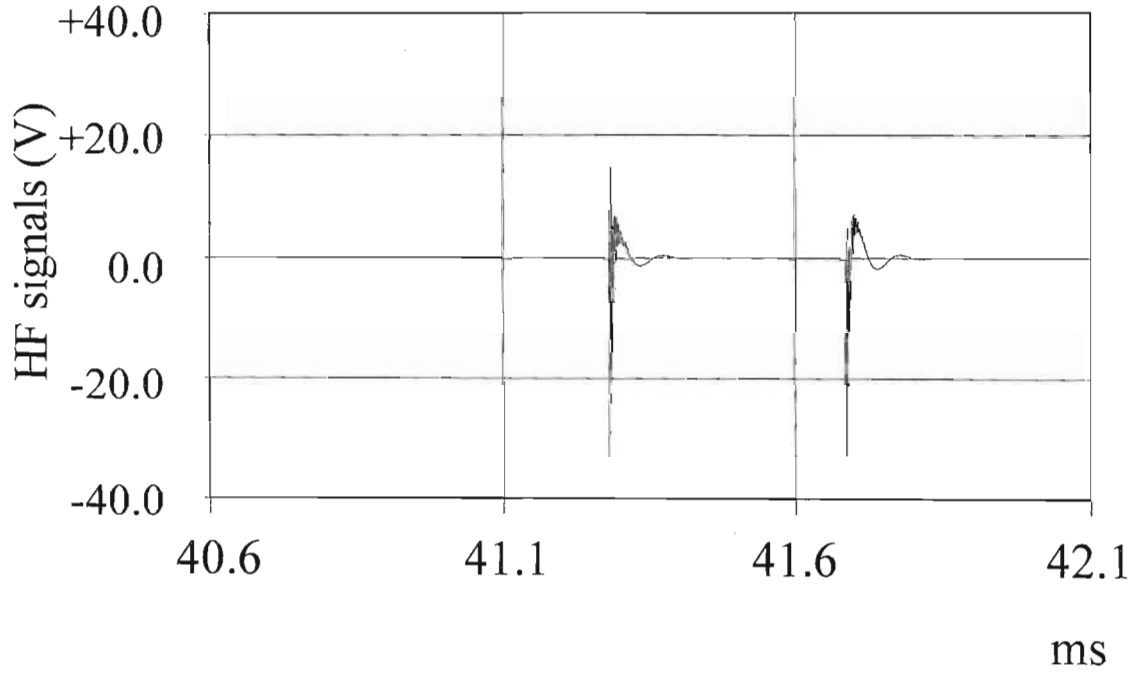

Figure 6. 39: Expanded view about two fire-induced pulses.

The FFT for the fire-induced streamers had a much larger amplitude across all frequencies.

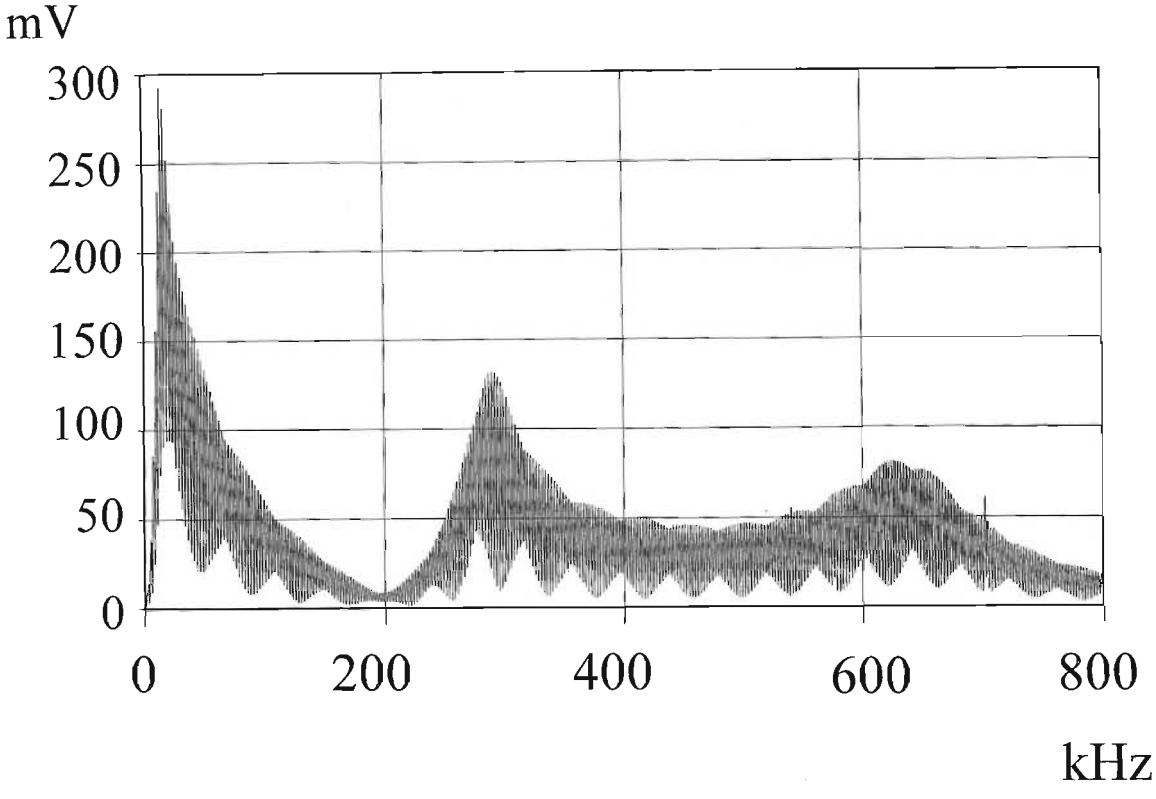

Figure 6. 40: Frequency spectrum of the two fire induced pulses.

In figure 6.40 above, the signal from Radio 702 was clearly visible. Apart from that signal, the broadband activity over the entire frequency range of just above zero to 800 kHz increased to the familiar shape of what appeared to be the transfer function of the corona cage with filters. When comparing the amplitudes across the whole spectrum, the fire-induced noise appeared to increase with decreasing frequency.

The rain-induced corona data of figure 6.31 on page 108 contained many more pulses but the frequency spectrum of that activity, figure 6.32 on page 108, showed a moderate increase in the noise levels with particular emphasis on the "node" at 293 kHz. The deduction therefore followed:

1) The fire-induced corona noise (with only a few streamers) contained stronger low frequency components than the rain-induced corona (with many streamers), and
2) The highest amplitude rain-induced corona frequency components (at 293kHz) were lower than the fire-induced corona components at the same frequency.

Figure 6.41 shows the two spectra superimposed for comparison.

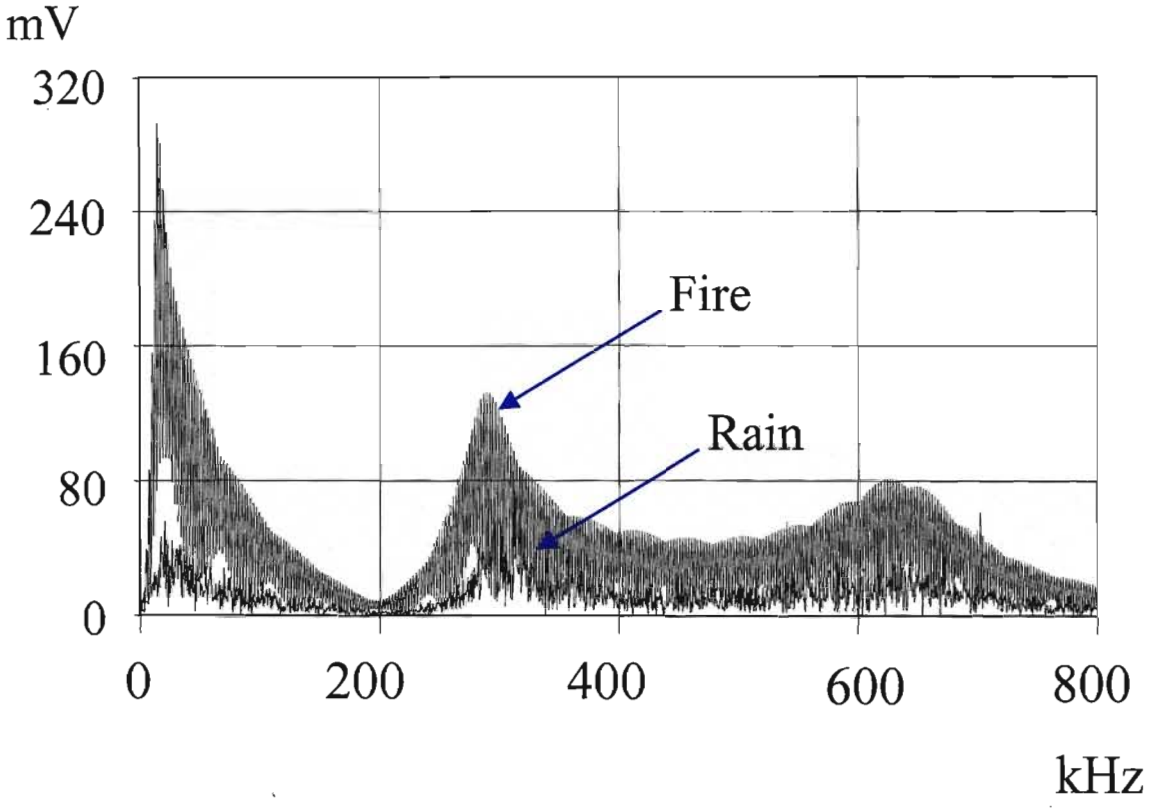

Figure 6. 41: **Frequency spectrum comparison: Rain versus fire induced pulses.**

6.3.3 Twin Zebra conductor bundle (ref gas fire)

The twin Zebra conductor test data was analysed in the same manner as that of the twin Dinosaur. Firstly a close-up view of the induced corona activity in the positive half-cycle was identified, followed by the background noise to establish that no abnormal activity was present and then finally the analysis of the corona activity in isolation.

6.3.3.1 Twin Zebra Dry conditions

Figure 6.42 below shows the discharges in a positive half cycle at 17 kV/cm in dry conditions.

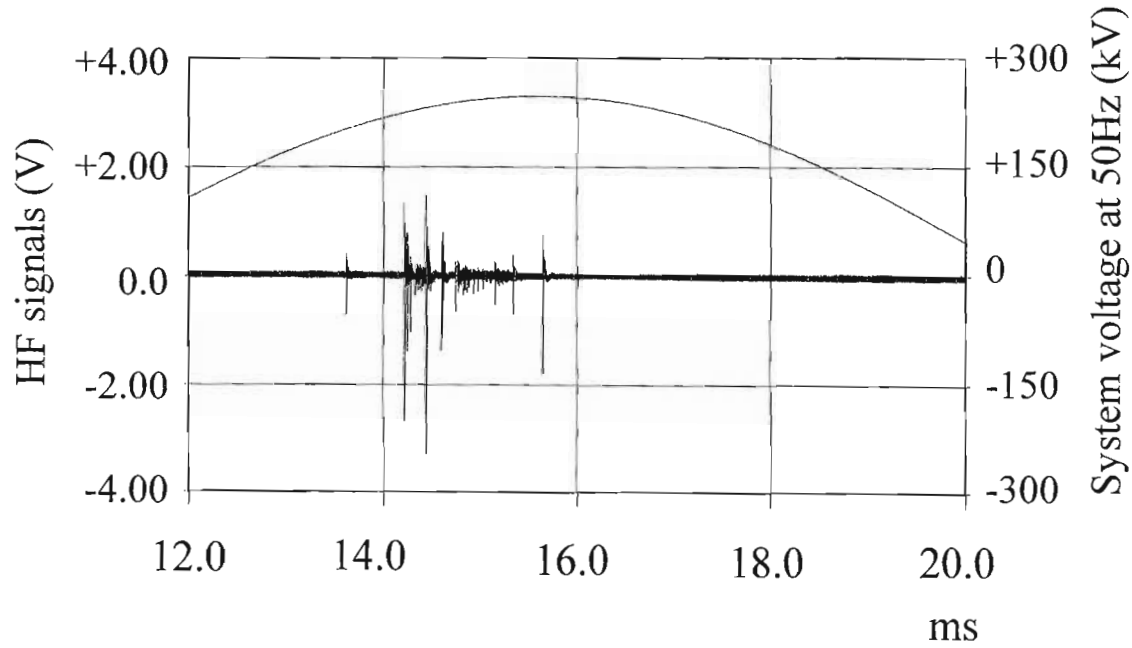

Figure 6. 42: Twin Zebra bundle in dry conditions at 17kV/cm.

The number of streamers occurring on a regular basis here in the normally dry conditions were higher than that recorded for the dry conditions on the twin Dinosaur bundle at 16 kV/cm (figure 6.19 on page 99).

The background noise in 6.42 displayed no affects from any abnormal activity in the frequency spectrum as seen in figures 6.43 and 6.44.

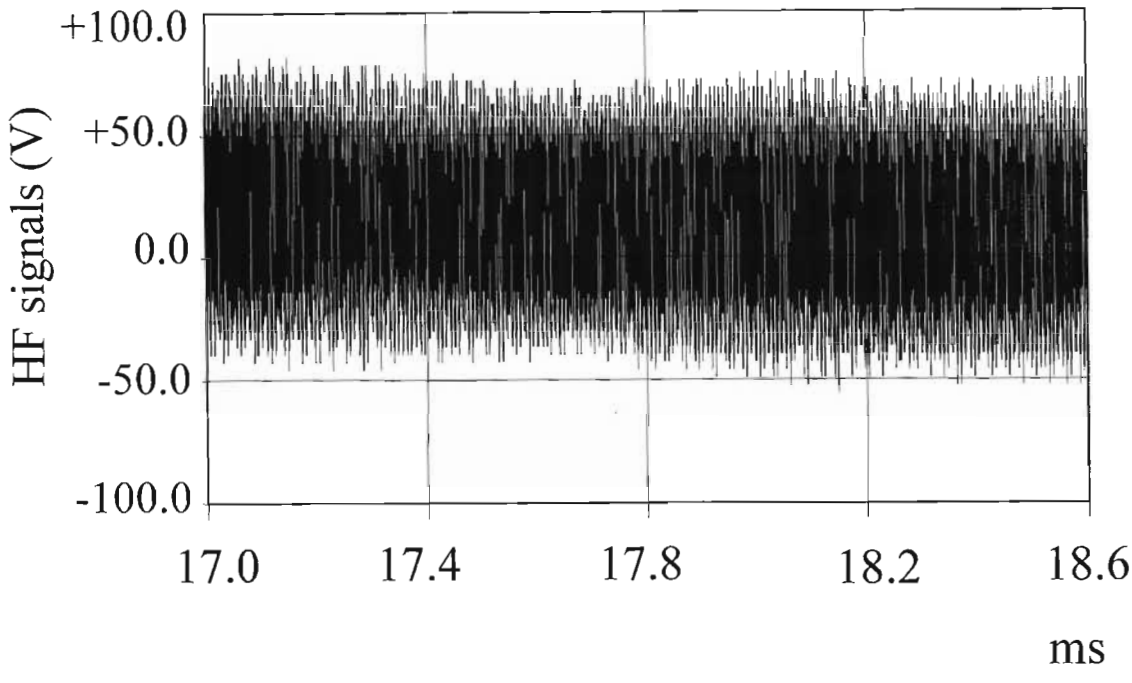

Figure 6. 43: Expanded view of noise with no streamers (dry conditions).

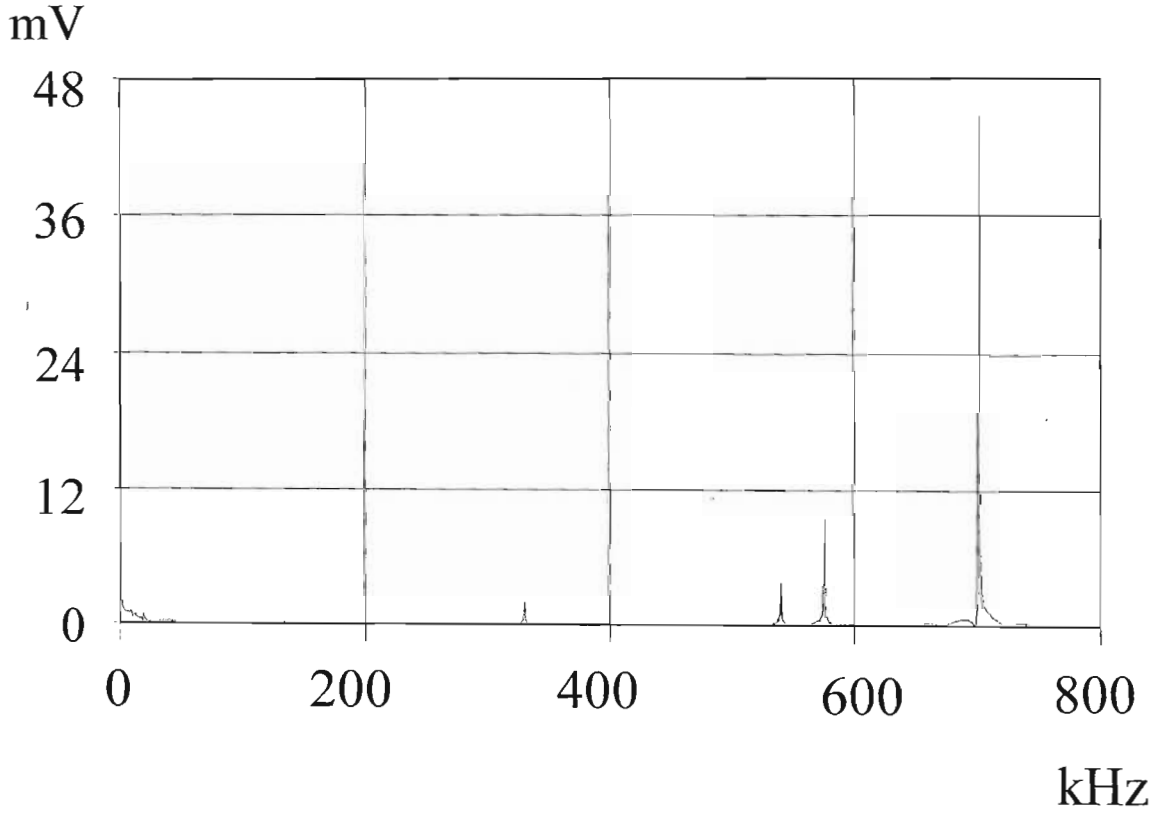

Figure 6. 44: Frequency spectrum of the background noise only.

The dry condition induced corona activity recorded in the positive half cycle of figure 6.42 was cut to fit the FFT algorithm (figure 6.45).

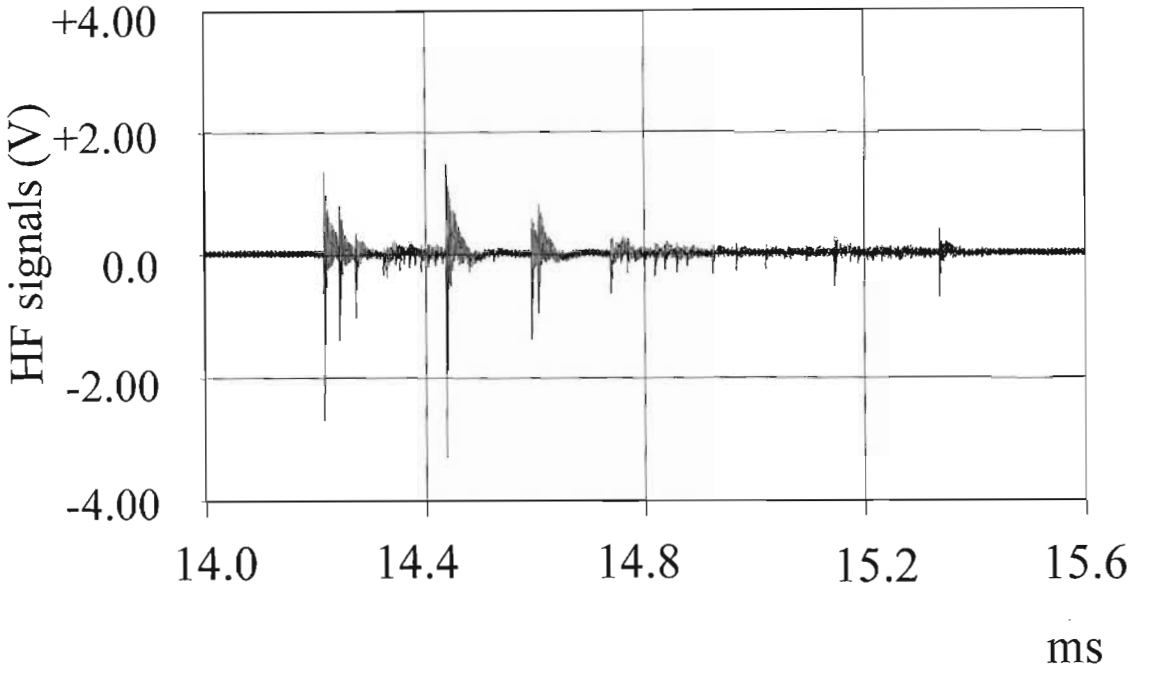

Figure 6. 45: Expanded view of the dry condition pulses.

Figure 6.46 below shows the frequency spectrum for that data.

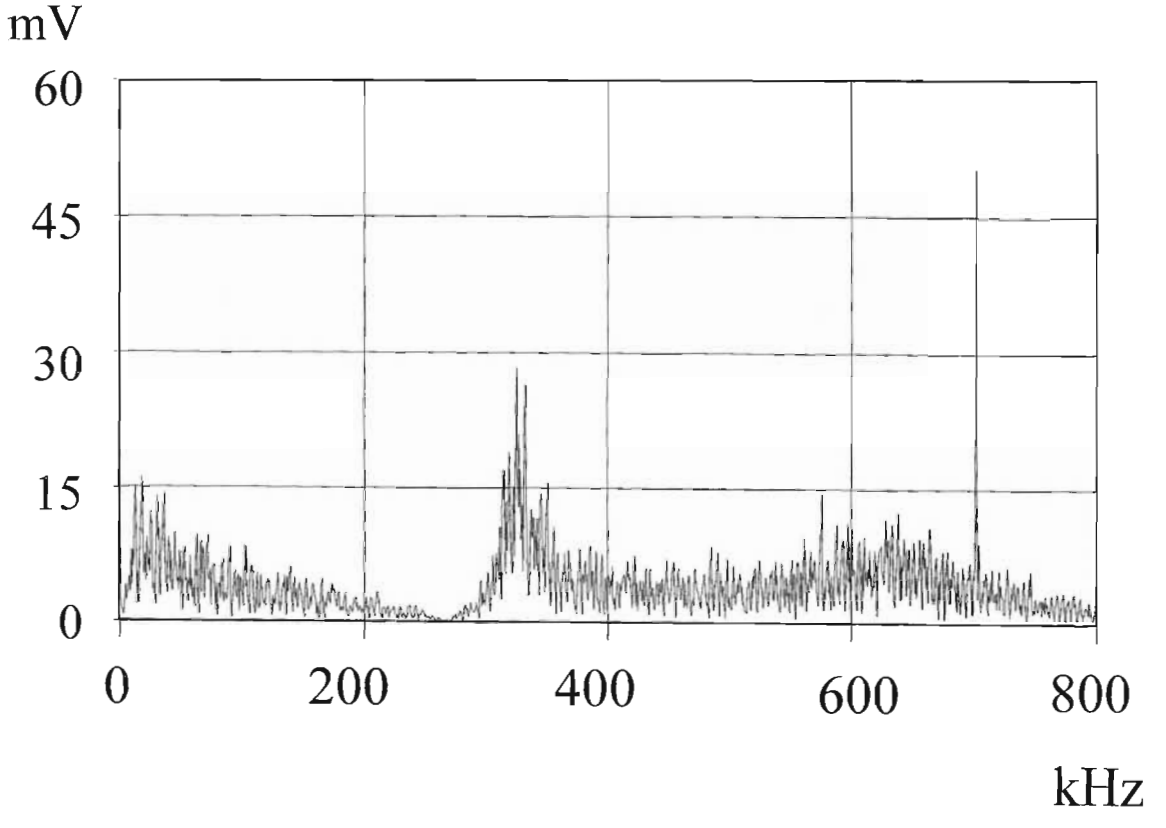

Figure 6. 46: Frequency spectrum of the dry condition pulses.

Using Radio 702 as an amplitude reference, the magnitude of the envelope over the entire twin Zebra data spectrum was higher than that calculated for the same conditions on the twin Dinosaur bundle and was due to the higher number of streamers present. The frequency spectrum profile was again similar to that of the twin Dinosaur bundle in dry conditions.

6.3.3.2 Twin Zebra Rain conditions

In the macro view of figure 6.6 on page 90, there was a much larger number of streamers present which were on average also only marginally larger than the streamers recorded in the dry conditions (similar to the results obtained on the twin Dinosaur bundle). The noise patterns generated under normal dry conditions were compared with the noise generated due to rain on the conductors and the rain data was shown in figure 6.47 below. Without enlarging the graph any further, it was again evident that many more streamers were generated under the controlled condition of the rain. When comparing this condition with the dry conditions, the rain-induced corona noise was more consistent as a result of the uniform process of the layer of water forming about the conductors under the stresses of the electric field. The magnitude of most of the impulses observed were of the same order as that of the dry condition pulses measured.

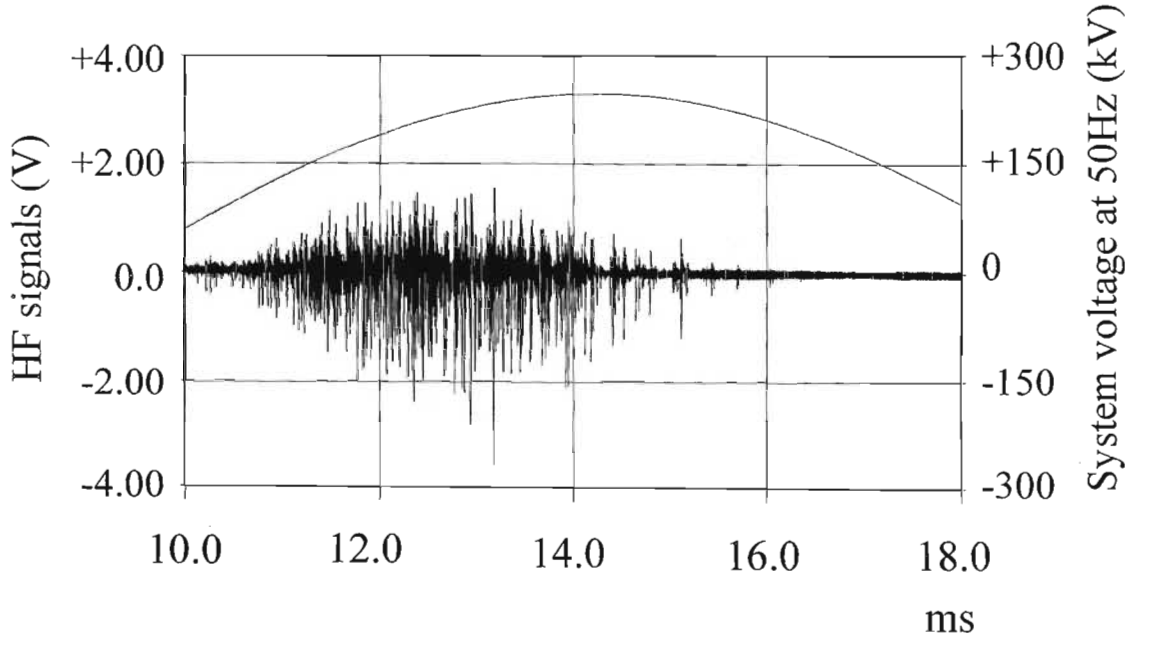

Figure 6. 47: Twin Zebra bundle in rain conditions at 17kV/cm.

The background noise (sample shown in figure 6.48) displayed no effects from any abnormal activity in the frequency spectrum as seen in figure 6.49.

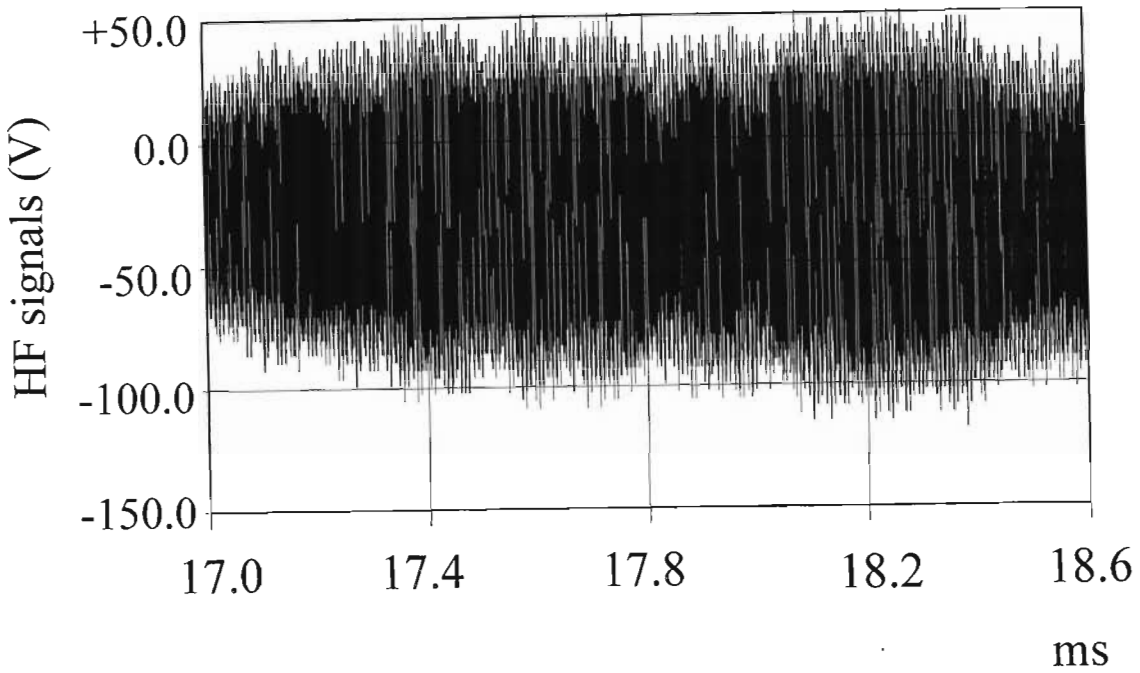

Figure 6. 48: **Expanded view of noise with no streamers (rain conditions).**

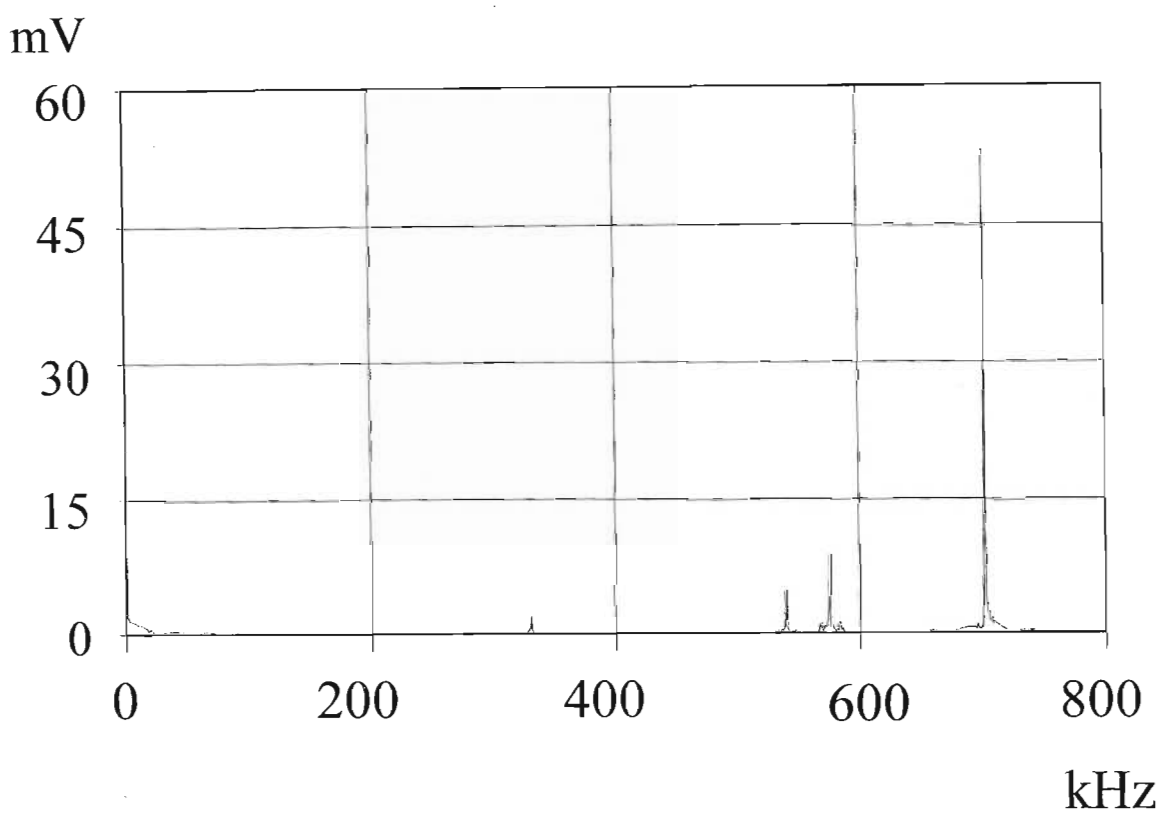

Figure 6. 49: **Frequency spectrum of the background noise only.**

The rain induced-corona activity recorded in the positive half cycle was cut to fit the FFT algorithm. The frequency spectrum of the rain-induced corona activity had equally high

components of noise at the 19.6 kHz and the 293 kHz nodes (of approximately 80 mV). The profile of the spectrum remained the same as previously observed.

6.3.3.3 Twin Zebra Fire conditions

Where the rain-induced corona pulses were only marginally larger than the random pulses occurring in the normally dry conditions, the fire-induced streamers were markedly larger than both the random dry streamers and the consistent rain-induced streamers. The repetition rates of the fire-induced corona pulses were however, also less predictable than that of the rain-induced corona pulses since these pulses were dependent on the presence of heat from the flames. For the single gas fire source, the repetition rate of the fire-induced corona noise was also lower than that of the rain-induced corona noise (compare figure 6.47 to figure 6.50 below).

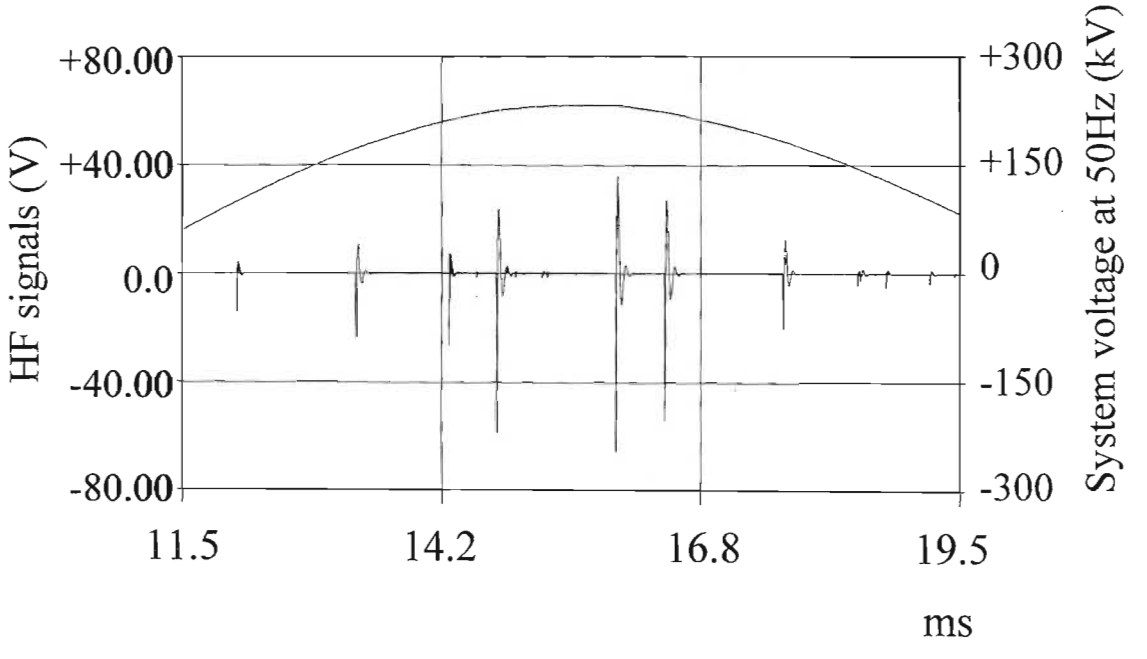

Figure 6. 50: Twin Zebra bundle in fire conditions at 17kV/cm.

The background noise during these measurements were consistent with the noise captured in previous tests (see figures 6.51 and 6.52 below).

In figure 6.51, the quantisation noise is more obvious as the overall signal has been raised up to +100mV from the previous level of +50mV.

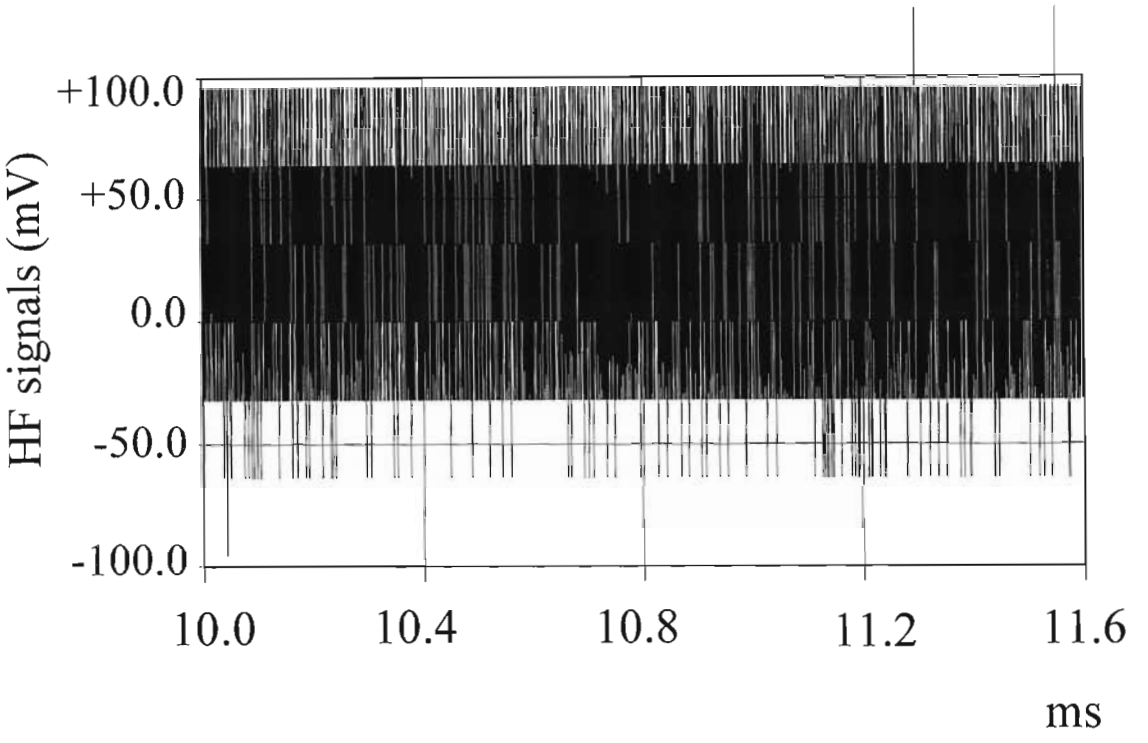

Figure 6. 51: Expanded view of noise with no streamers (fire conditions).

However, the signal has also moved up from –150mV to approximately –60mV. As a whole no significant change was observed from previous noise samples.

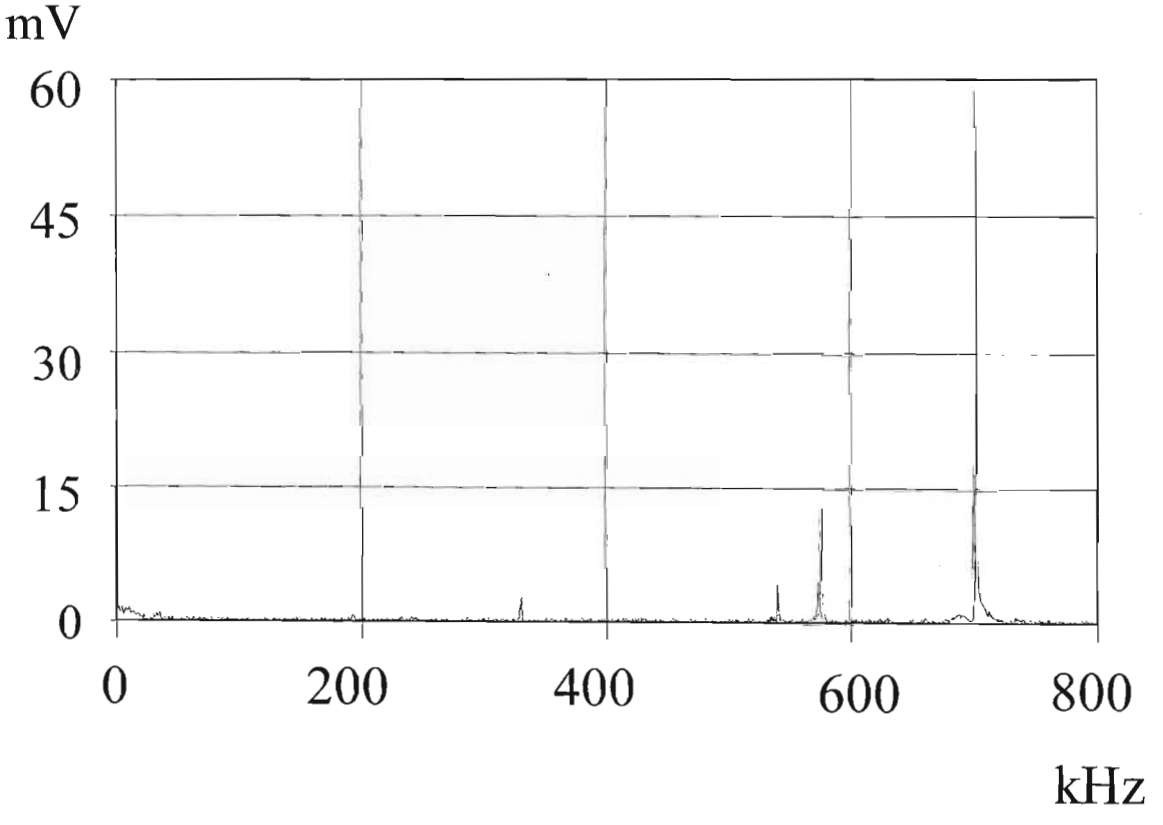

Figure 6. 52: Frequency spectrum of the background noise only (fire conditions).

The fire induced-corona activity recorded in the positive half cycle was cut to fit the FFT algorithm (figure 6.53).

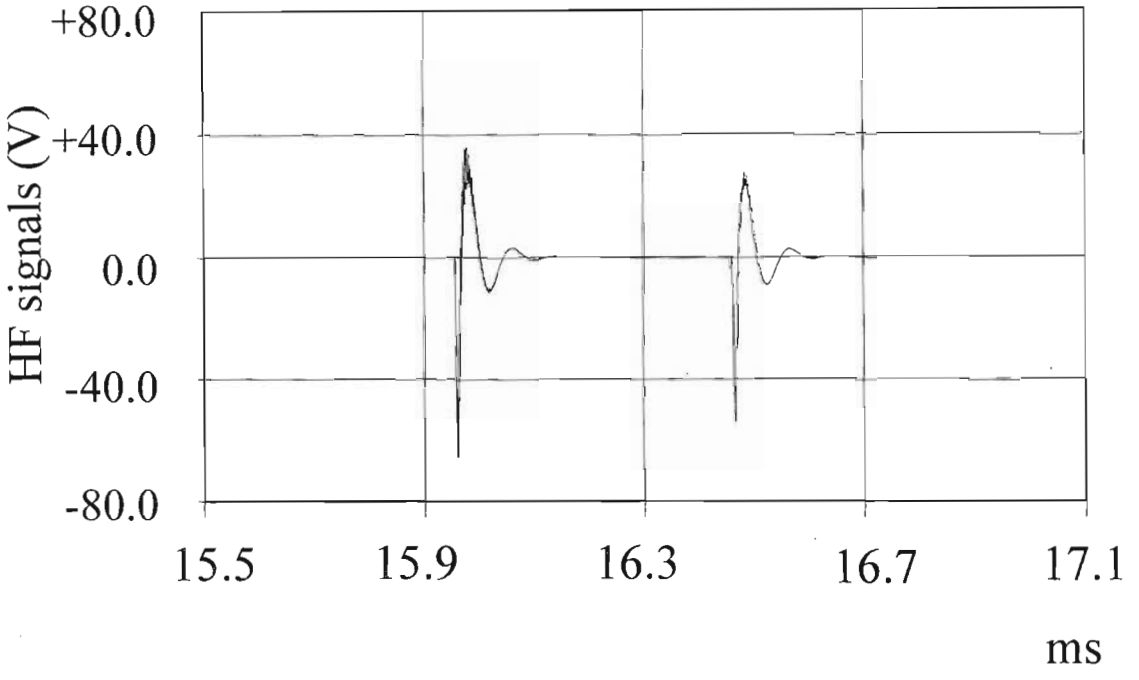

Figure 6. 53: Expanded view of the fire-induced pulses.

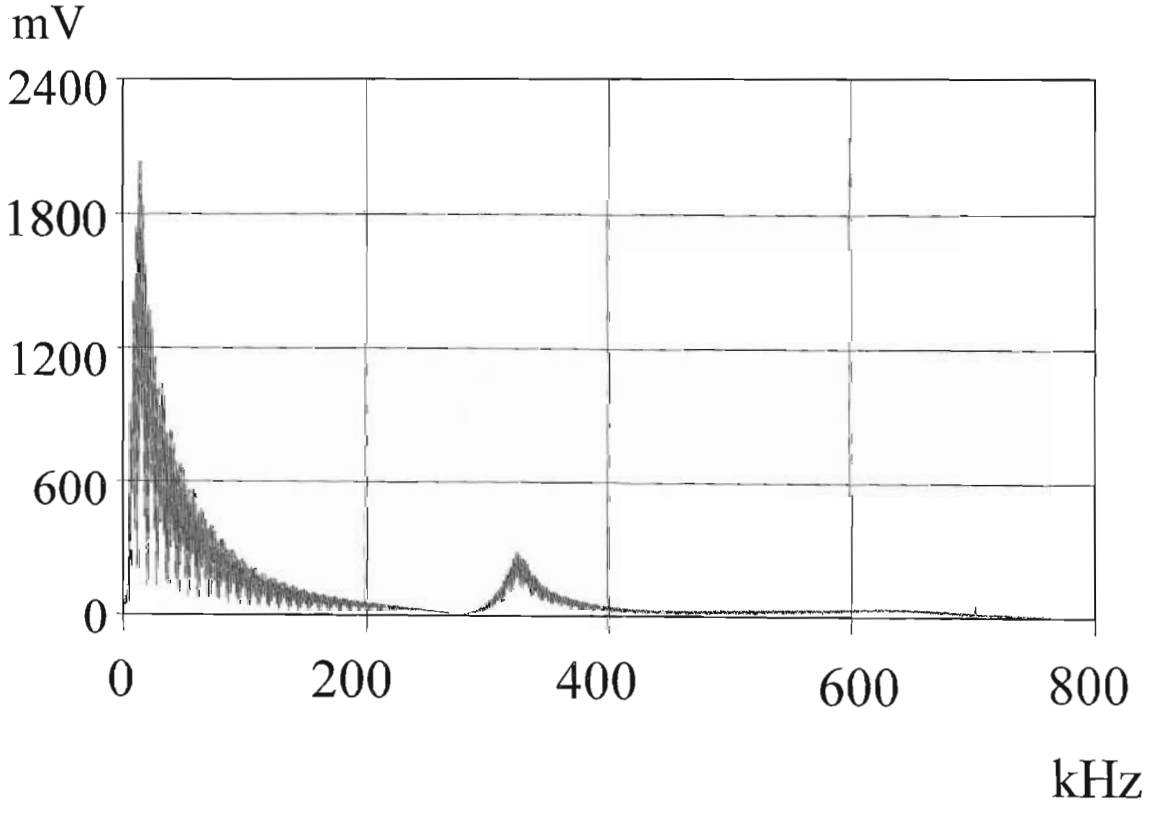

Figure 6. 54: Frequency spectrum of the fire related channel data recorded.

In figure 6.54 Radio 702 can be seen as a minuscule point.

From figure 6.55 below, the two fire-induced electrical discharges therefore contain a much larger amount of energy than that identified in dry and rain conditions

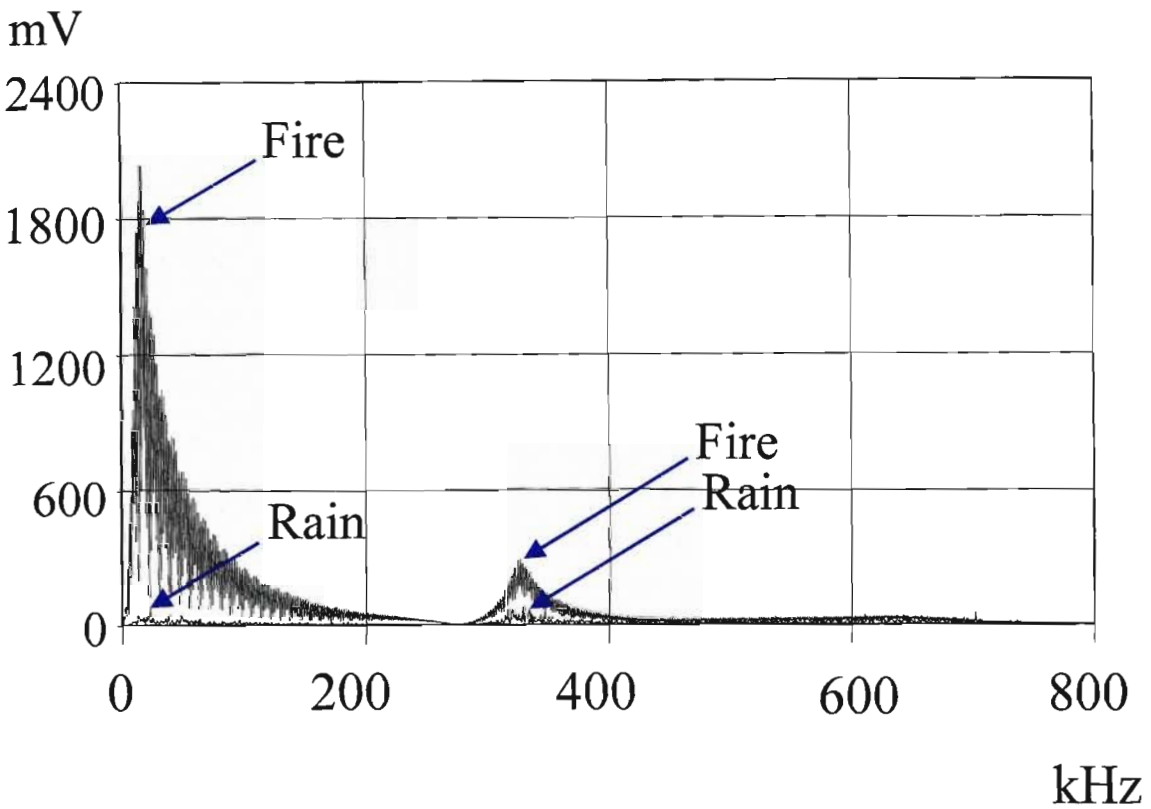

Figure 6. 55: Frequency spectrum comparison on Twin Dinosaur: Rain versus fire.

The magnitude of the frequencies around the 293 kHz node was much lower than at the 19.6 kHz node. However, the magnitude of the fire-induced pulses at this weaker node was still at least three times larger than the rain-induced pulses at the same frequency. Where the nodes in the rain conditions displayed approximately equal magnitudes at 19.6 and 293 kHz, the fire-induced pulses have a sharp rise from the higher node to the lower frequencies. At the lower frequencies, the fire to rain pulse magnitude ratio was approximately 26:1 with the fire-induced pulses therefore totally dominating the spectrum.

The large low frequency component present under fire conditions was also observed with the twin Dinosaur conductor bundle under fire conditions. However, these results were created with a gas fire which may have generated very specific paths for streamers in the reduced air density and high temperature plasma. A fire containing particles would generate more streamer paths and push up the rate at which the pulses occur (the gas fire was considered as having no particles of any size significant enough to play any role in the induced corona affects). In addition, the

FFT algorithm, limited to only 16 384 points out of 600 000 points, may have generated a distorted view of this result.

6.3.4 Twin Zebra conductor bundle (ref sugar cane fire)

The sugar cane fire tests were performed some time after the original gas fire tests (October 1992) and as a result the dry and rain condition tests were repeated to ensure that no abnormal conditions or any significant changes in the background noise went unrecorded.

6.3.4.1 Twin Zebra - Dry conditions

The results were documented on page 92 in figure 6.9. Analysing the data in the positive half cycle where the only pulse was captured, similar spectral information to the previous results were calculated.

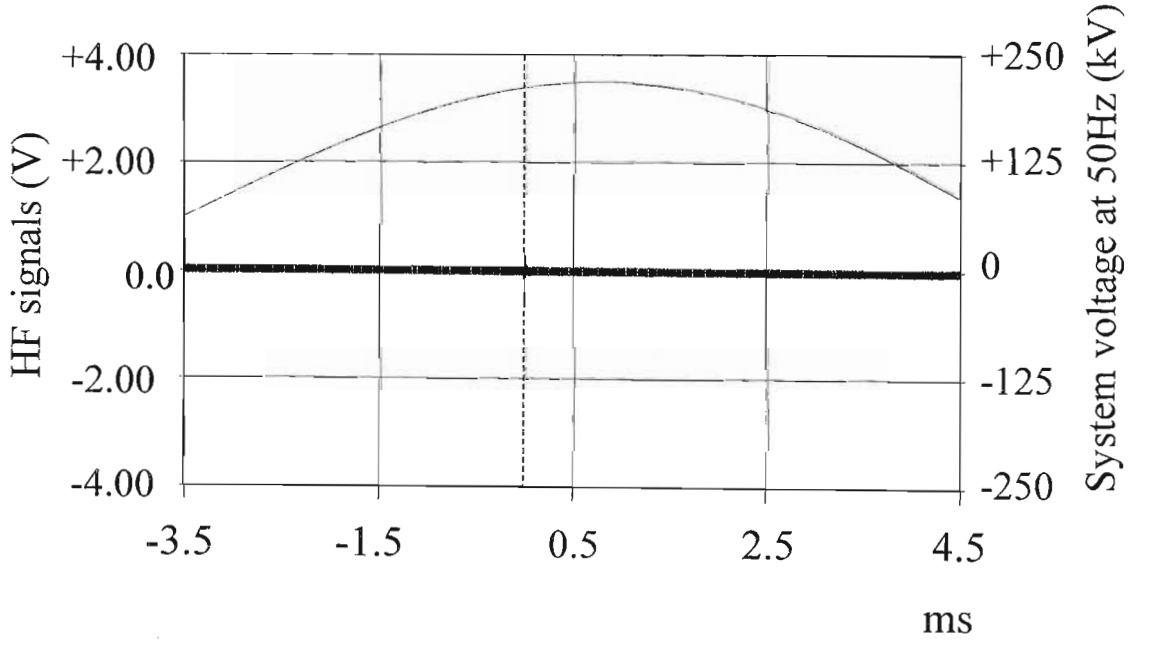

Figure 6. 56: Twin Zebra bundle in dry conditions at 15kV/cm.

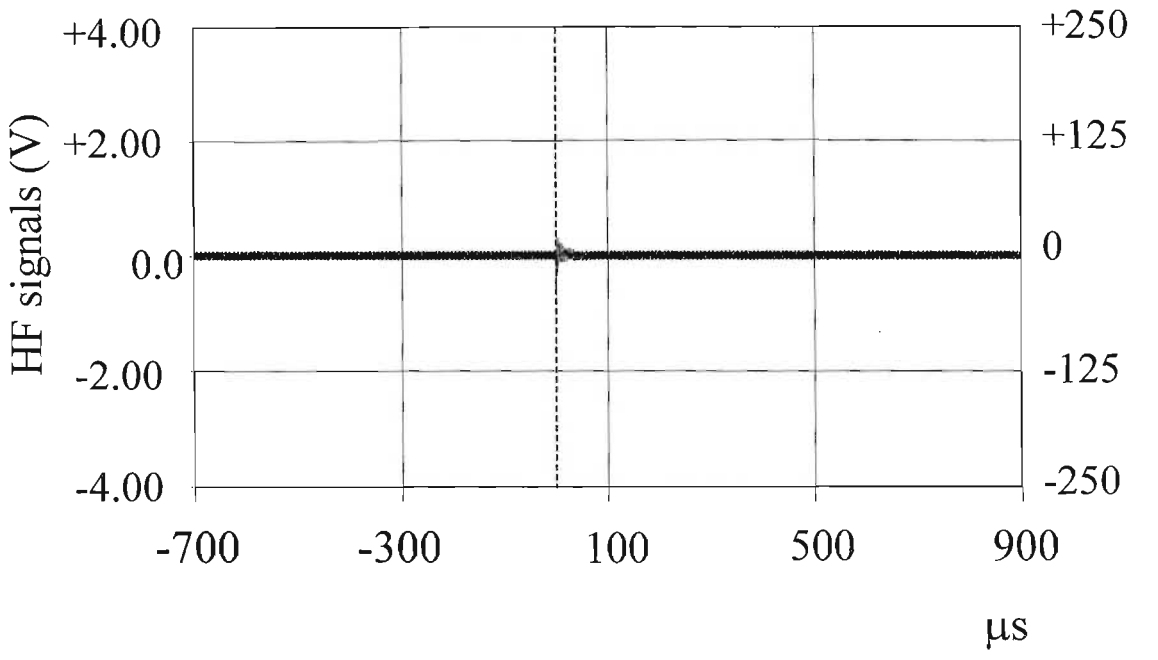

Figure 6. 57: Dry conditions on the twin Zebra bundle prior to a sugar cane fire test.

The spectrum in figure 6.58 was virtually identical to the spectrum when only the background noise was present. Around 293 kHz a slight increase in the noise indicated the presence of the single pulse.

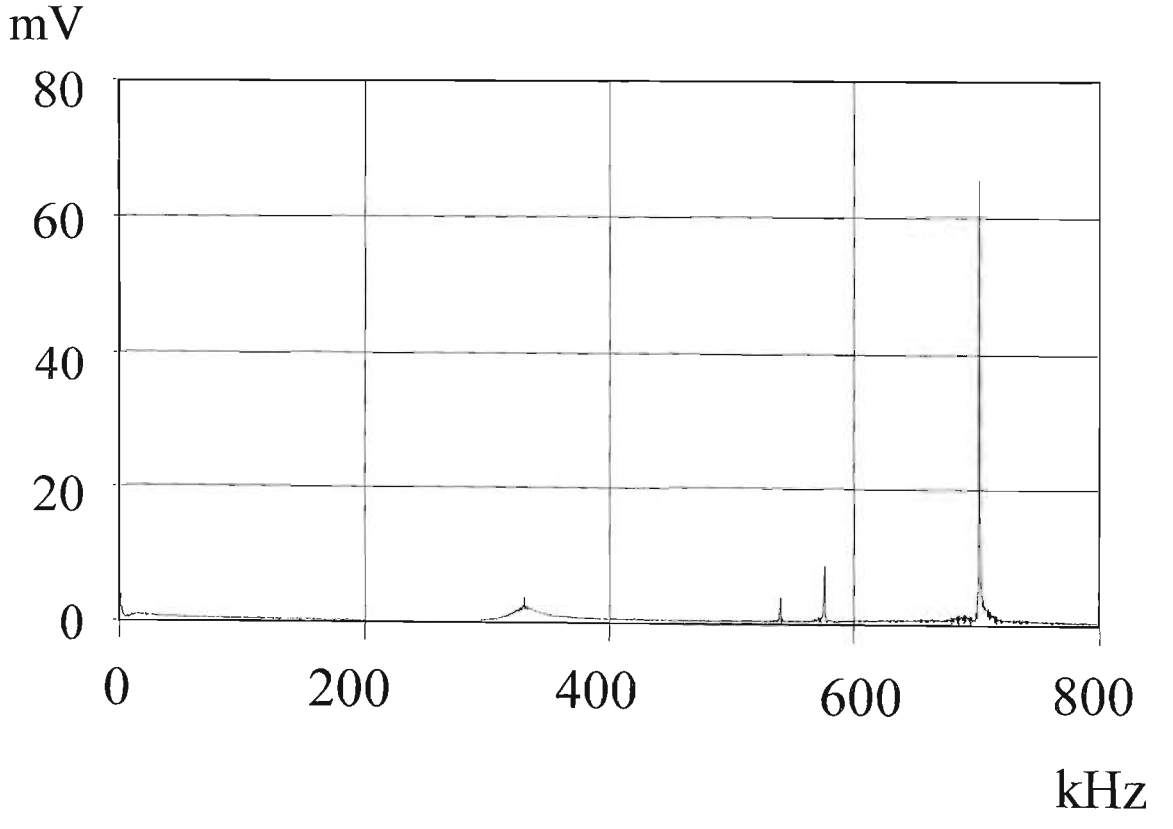

Figure 6. 58: Frequency spectrum of the dry condition noise with a single pulse present.

6.3.4.2 Twin Zebra - Rain conditions

A segment from the data in figure 6.10 on page 92 is given in figure 6.59 below. Since the sugar cane fire could only be tested up to a gradient of 10 kV/cm, the gradient selected for the rain test for comparison to the fire tests was therefore also 10 kV/cm. The pulses were visibly smaller than those captured in figure 6.47 on page 119 where the data was captured with the line stressed to 17 kV/cm.

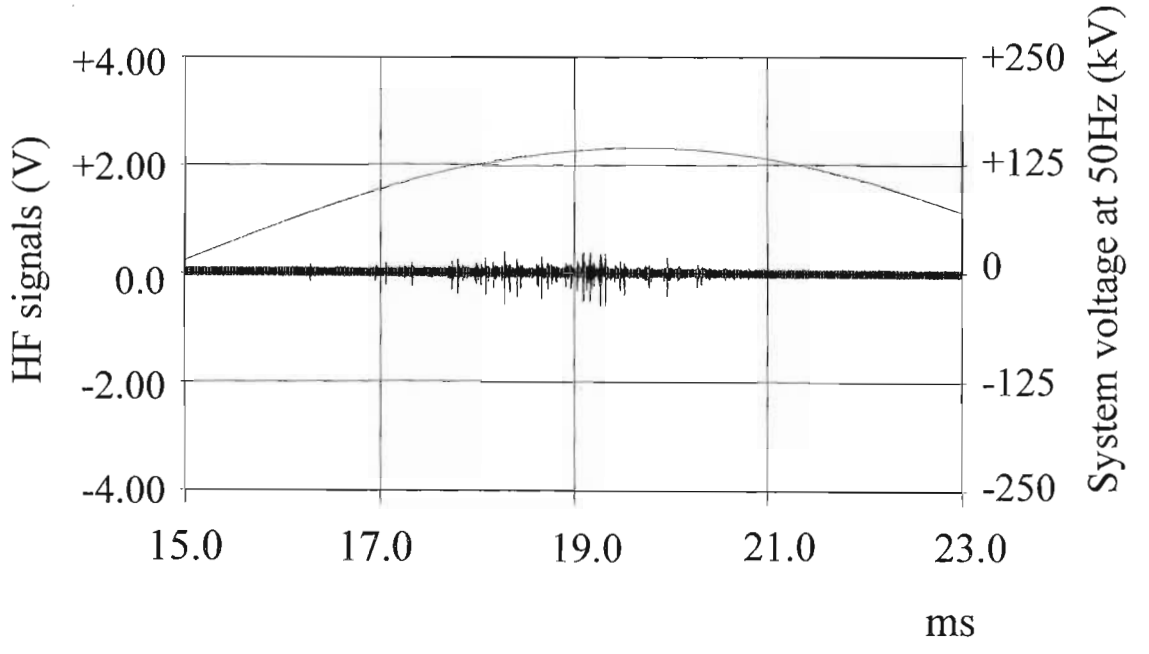

Figure 6. 59: Twin Zebra bundle in wet conditions at 10kV/cm.

A segment from the above rain-induced corona noise was captured in figure 6.60 and the FFT shown in figure 6.61. The spectral calculations from the data segment generated similar information to that previously calculated.

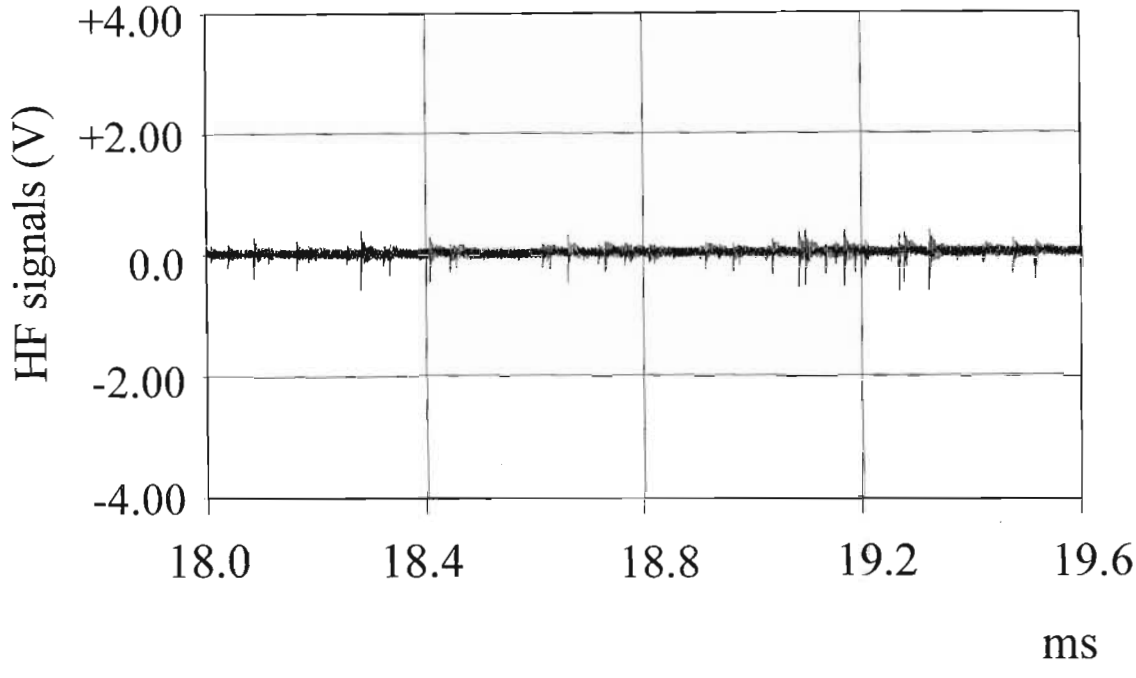

Figure 6. 60: Twin Zebra bundle in rain conditions prior to a sugar cane fire test.

The only difference was the lower amplitudes over the frequency spectrum. The broadcasting level of Radio 702 was unchanged since the broadcasting stations' signals are independent of the operating voltage on our transmission line test section.

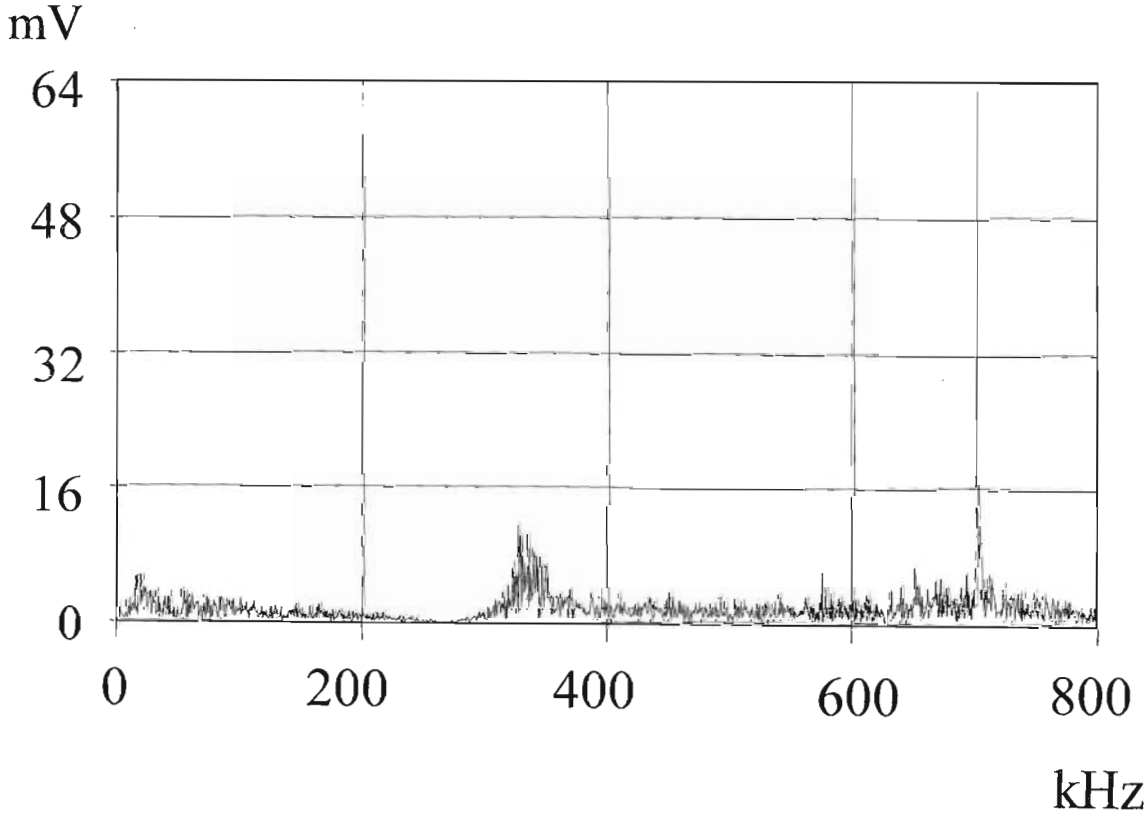

Figure 6. 61: Frequency spectrum of the rain condition noise under lower stresses.

6.3.4.3 Twin Zebra - Sugar cane fire conditions

The following data shown in figure 6.62 below was cut from the data shown in figure 6.11 on page 93. The first significant factor noticeable was the large fire-induced pulses occurring in both half cycles of the 50 Hz power signal. In the gas fire, activity in the negative half cycle was only observed at any comparable amplitude to that in the positive half cycle when conditions were extreme. Secondly, the pulses observed were extremely large when the applied voltage and surface gradient of 10kV/cm were taken into account.

The surface gradient was in fact less than 10kV/cm as the voltage had to be adapted according to the distorted conditions. The corona cage operator initially increased the voltage but had to reduce it in order to obtain a stable 50Hz power supply voltage undistorted by the load demand from the fire-induced corona activity. At 10 kV/cm the gradient corresponded to an applied voltage of 104 kV_{RMS} and 147 kV_{PEAK}. The 50 Hz signal in the graph below had a peak value of approximately 125 kV. Therefore the induced corona activity taking place here was actually initiated at less than 10 kV/cm and the factors mentioned above were therefore even more significant.

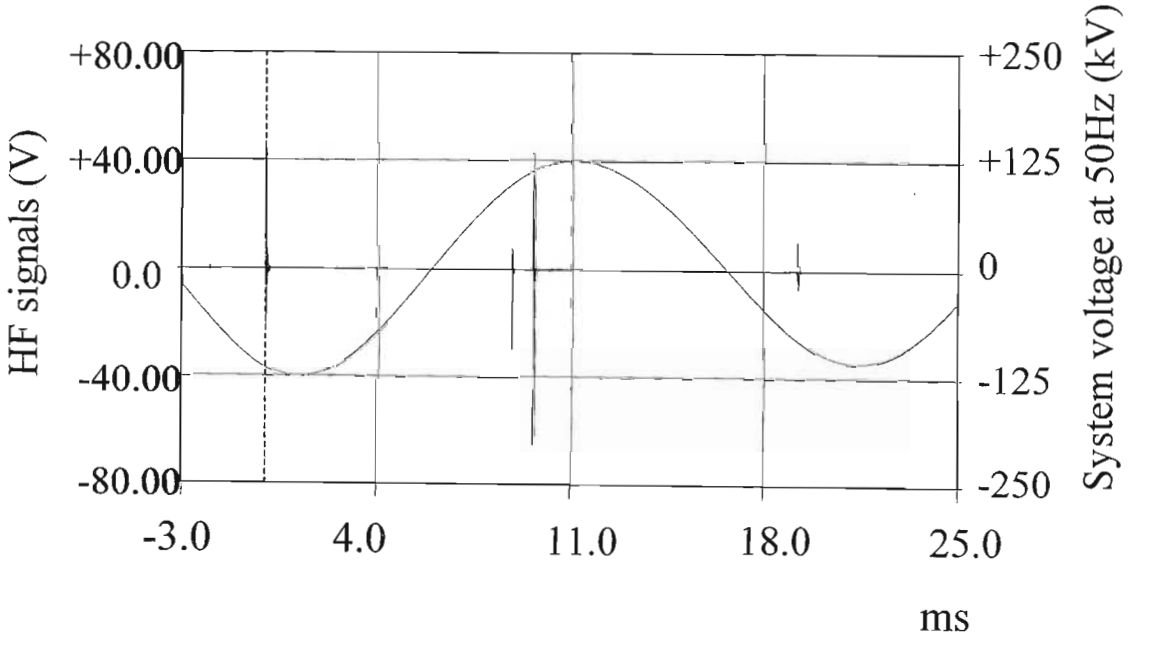

Figure 6. 62: Twin Zebra bundle over sugar cane fire conditions at less than 10kV/cm.

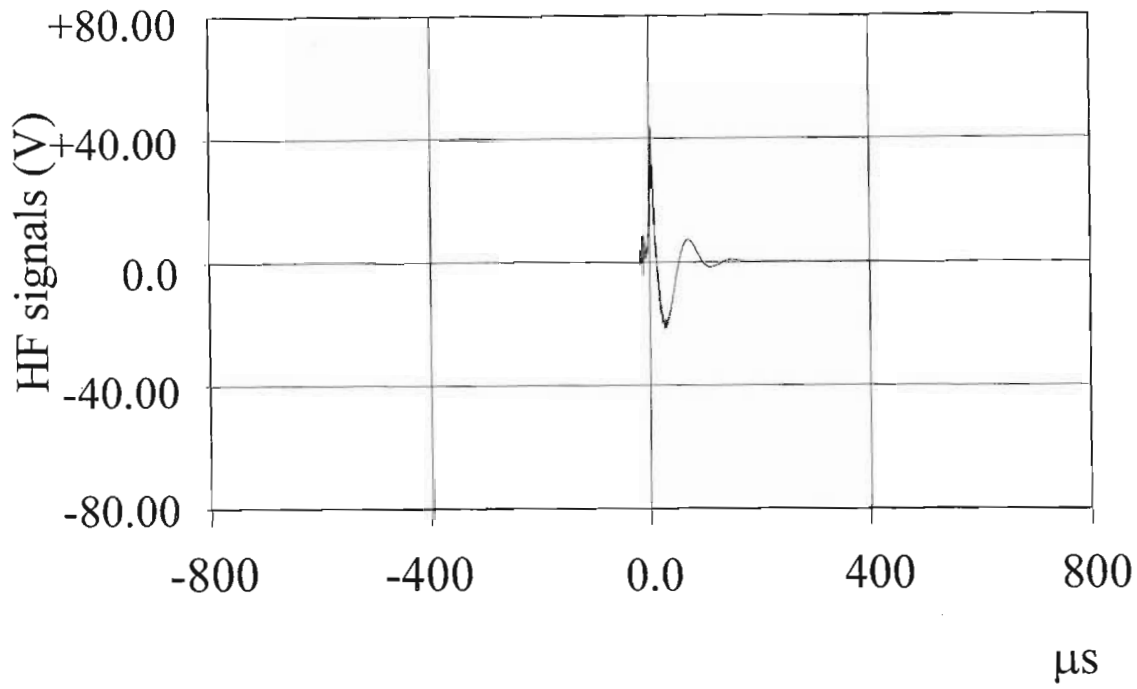

Figure 6. 63: Expanded view of the negative polarity fire-induced pulse.

The fire-induced corona activity in the negative half cycle expanded from figure 6.62 had similar trends to that of it's positive counterpart. The polarity of the impulse and the ensuing ringing was observed as opposite to that of the streamers induced in the positive half cycle.

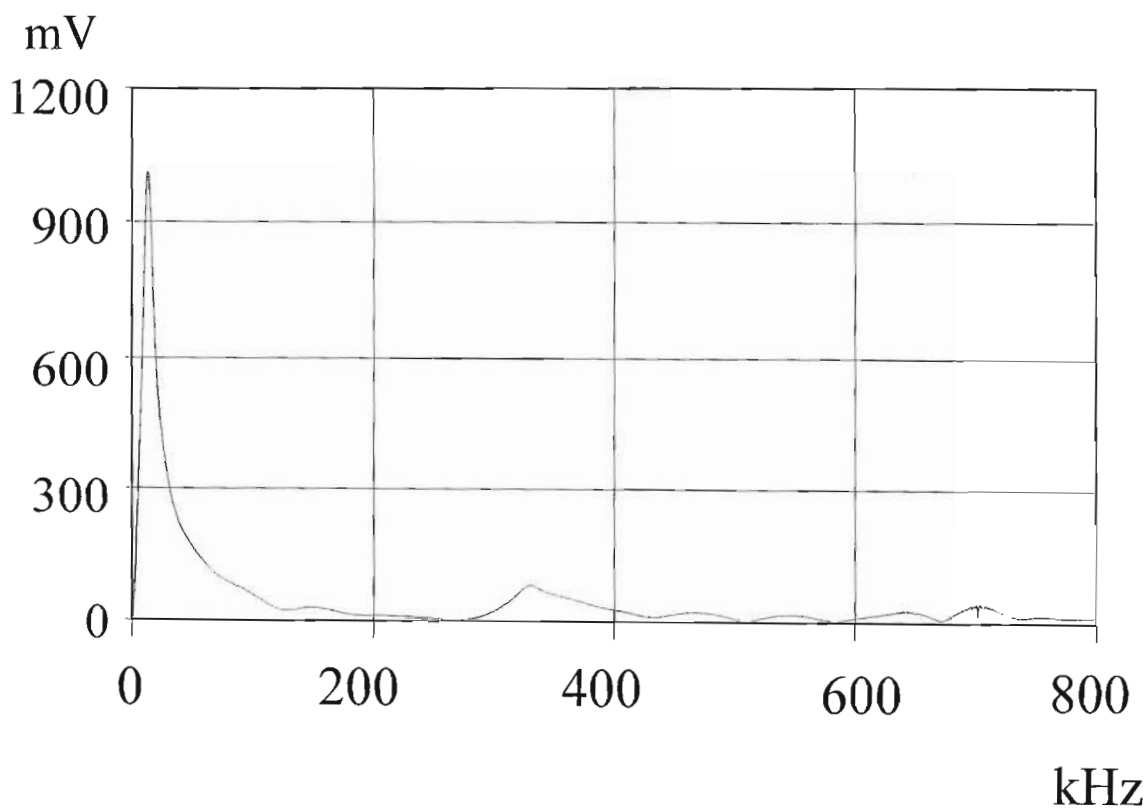

Figure 6. 64: Frequency spectrum of the negative polarity fire related noise.

The frequency spectrum in figure 6.64 again revealed a very strong low frequency component.

The development of the negative streamers was also slightly different. A growth in the electrical current was observed prior to the pulse or transient event. This was followed by a longer dissipation period during which an underdamped affect was noticed.

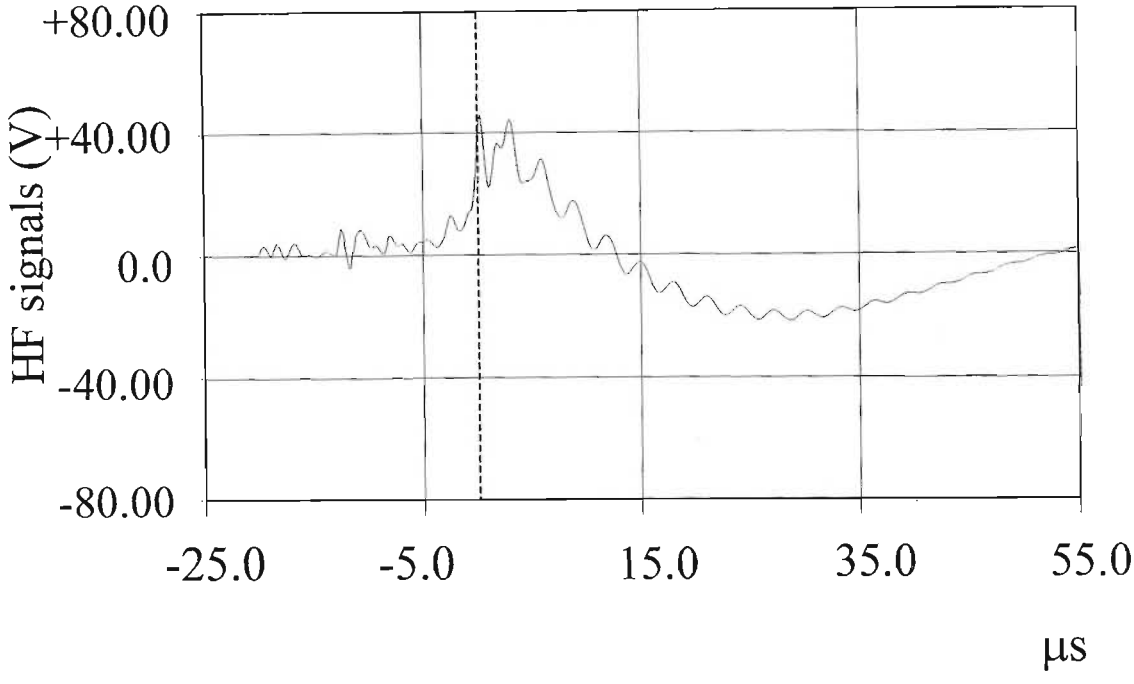

Figure 6. 65: First large sugar cane fire-induced pulse (negative half cycle).

In comparison, the positive corona pulses increased from virtually zero volts to the peak of the current surge. This was observed in the expanded views of the two pulses shown in the positive half cycle of figure 6.62. In the graphs of figures 6.66 and 6.67 below, (with the same vertical axes as for the negative corona pulse), the pulses do not have any significant activity before the surge starts. These characteristics were clear indicators to the development of corona through the universally recognised corona modes.

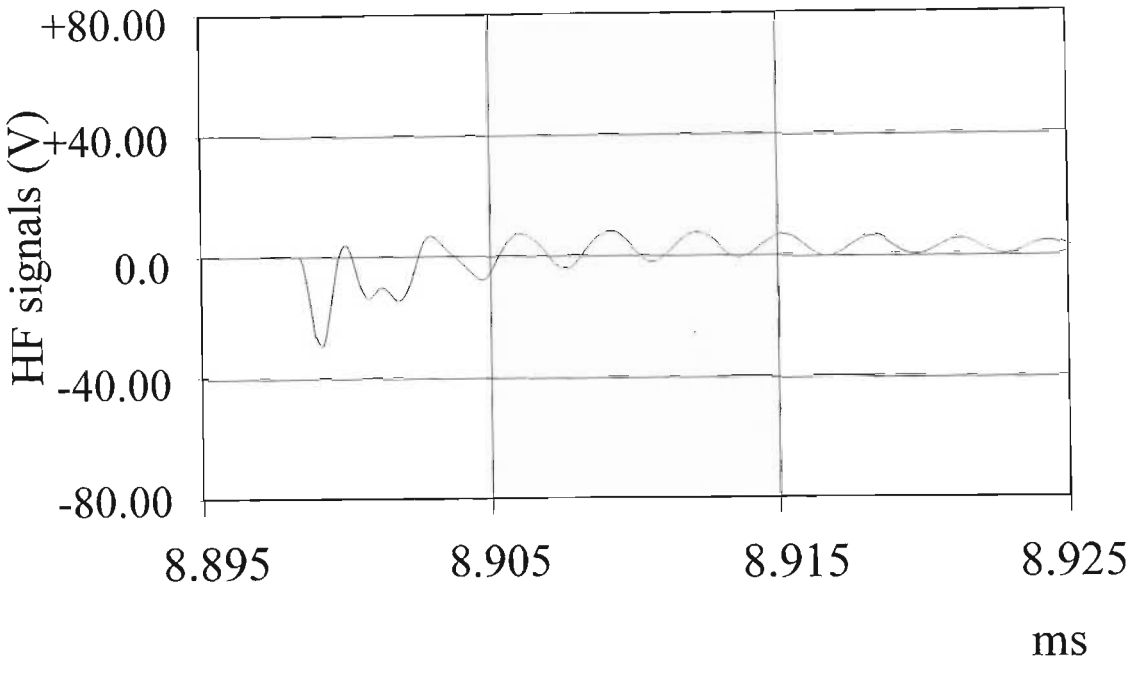

Figure 6. 66: Second large sugar cane fire-induced pulse (positive half cycle).

The scales were set extremely large for the dry condition and rain condition measurements so that an extremely large pulse arising from appropriate fire conditions could be observed in context, but figure 6.67 shows that under the "ideal" circumstances those scales were still too small. The dynamic range of the oscilloscope was set to approximately a factor of 10 greater than the maximum levels measured for the corresponding rain condition tests. An additional complicating factor was the repeatability of the fire tests. On some occasions only small amounts of corona was generated due to the size of the fire and wind direction and in these instances the scales should have been set to a lower level. As the objectives were to fully describe the fire-induced corona activity relative to the other major sources of induced corona noise, the size of the pulses required for such a description was a minor criteria. Hence the clipping recorded for this particular pulse was not critical (although the actual maximum amplitude would allow for more accurate predictions). A projected maximum peak arising from the pulse was measured at approximately -174.6 volts by graphical means. Under gas fire conditions at 10 kV/cm, such large pulses were not present and the pulse in figure 6.66 would have been more typical. The combination of heat which creates the channels of low density air and particles therefore induced a higher level of corona activity than when only heat and the reduction in air density was considered.

The pattern of the two positive corona pulses was also very similar to that discussed in the twin Dinosaur bundle results on page 110 where the pattern of the dry and rain condition corona

pulses were analysed and compared. The deduction therefore followed that the fundamental process by which the streamers occur was similar, which was the process of ionisation by electron impact followed by corona regions followed by the development of new streamers and ultimately leader breakdown if the conditions were sustained.

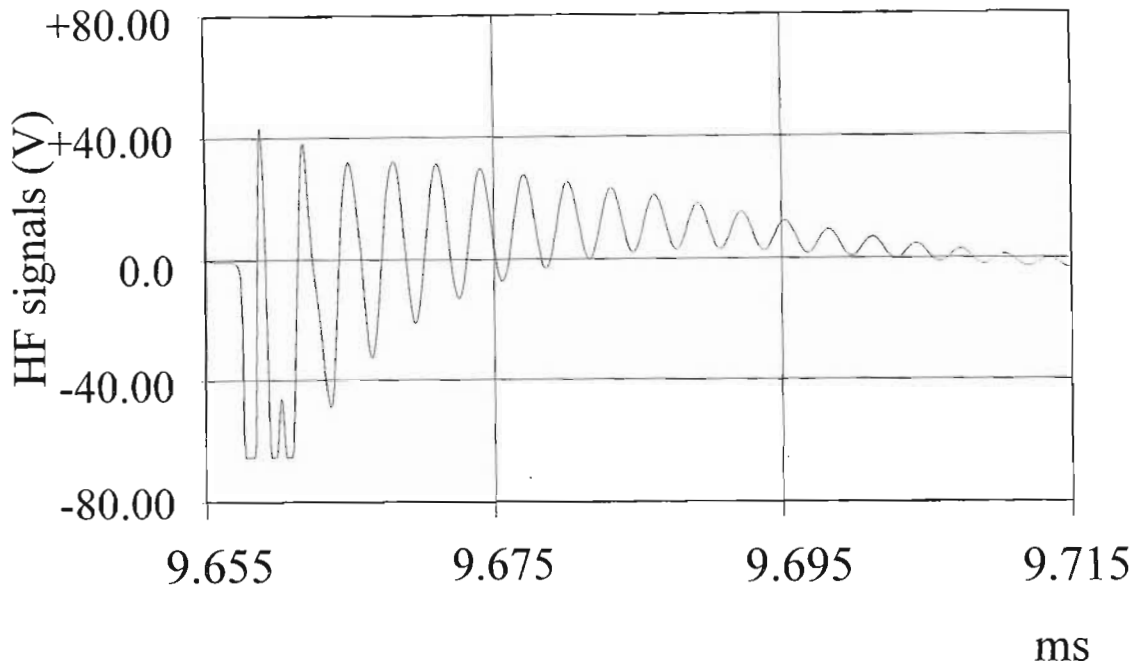

Figure 6. 67: Third large sugar cane fire-induced pulse (positive half cycle).

The maximum amplitude recorded for the equivalent rain-induced pulse at 17 kV/cm was -3.594 volts and was listed in the statistics data in appendix G from page 238.

The effective increase in the noise generated in a direct comparison of rain-induced and sugar cane fire-induced noise was then 33.73 dB (as measured on the twin Zebra conductor bundle). Note that this increase in noise was the result of a comparison of what was considered to be high levels of rain-induced corona noise generated at 17 kV/cm to low levels of fire-induced corona noise generated at less than 10 kV/cm. Therefore an adjustment had to be made to the rain-induced corona noise for an accurate comparison.

The rain-induced corona noise generated on the twin Zebra conductor bundle was recorded in the quasi peak measurements on page 62. A 15 dB increase in noise was recorded when increasing the gradient from 11 kV/cm to 17 kV/cm in rain conditions and approximately 3 dB was measured for every kV/cm increase in gradient made. Therefore the rain-induced corona noise at 10 kV/cm may be estimated at approximately 18 dB lower than that measured at 17 kV/cm.

Hence the projected increase in noise from the rain-induced corona noise pulse recorded, to the sugar cane fire-induced noise pulse was an effective 51.73 dB.

In the second series of tests in the corona cage, rain-induced corona noise was recorded at 10 kV/cm. The maximum peak for rain-conditions at 10 kV/cm from figure 6.10 on page 92, was recorded on that particular day as -688 mV. The increase in noise was therefore 48.09 dB.

The 3 dB discrepancy was most likely due to the approximations which took place when the noise levels were converted to a quasi-peak level. When considering that the quasi-peak measurement included the total activity through the 50 Hz cycle, the approximation was reasonably accurate. The projection to obtain the largest peak of the fire-induced corona noise pulse may also have contributed to the error. However, the projected voltage would have to be reduced to -114.84 volts to account for the 3 dB error. As the main pulse initiated in all previous cases did not have a rounded (or attenuated) turning point, the reduction of 60 volts is unlikely and this may therefore not have been the sole cause of the error.

It is therefore safe to state that when comparing the actual rain-induced noise pulses with the equivalent sugar cane fire-induced noise pulses, the equivalent components of the fire-induced noise was at least up to 48 dB higher than the equivalent rain-induced noise.

The corona activity occurring when the polarity of the charge on the conductor bundle was negative, was more unstable than that occurring in the positive half cycle. It appeared to develop at higher gradients when higher stresses exist since the pulses in the negative half cycle were the exception rather than the norm when tests were done with the gas fire and in the rain conditions. This is a common phenomena with the universally recognised characteristics of the positive and negative corona processes playing the dominating role [t].

Firstly the Trichel pulses have a much smaller amplitude than the positive "onset" pulses, therefore the positive onset pulses would totally dominate this phase with the negative Trichel pulses barely visible.

Secondly, the Hermstein Glow is initiated at a lower gradient than the negative "pulseless" glow with the same result. What was observed in the sugar cane fire results (at the lower gradients)

---

[t] See pp 170-175 [35]

was probably the initiation of the pulseless glow due to the higher fields created by particles and the lower critical field for the onset of the Townsend process (ionisation by electron impact), created by the reduction in air density as a result of the higher temperatures.

Thirdly, the negative streamers are both smaller in amplitude and also require higher gradients than the positive streamers.

6.4 MEASUREMENTS COMPILED FROM POLLUTED INSULATOR TESTS

6.4.1 Overview

Two pollution procedures were attempted in the corona cage to measure the induced corona noise levels generated from polluted insulators. The first was the salt fog test and the second was the clean fog test as laid out in the IEC publication 507 [34].

6.4.2 Polluted insulator test assembly

A string of insulators were assembled vertically at one end of the cage on the outer edge of one of the earthen outer cylinders with all the necessary metal fittings. This ensured that the fields generated by the stressed conductor bundle were generating minimal corona under the normally dry conditions. The number of insulators in the string were selected with an appropriate creepage length to ensure that the insulators would experience stresses very near the limit, thereby generating corona as soon as any form of increased stress took place on the insulators. A pipeline was strung along the perimeter of the cage cylinder about the insulators and jets were appropriately located to ensure the finest of sprays reaching the insulators. Via an electric pump, the applicable liquid mixture was pumped through the pipes and onto the stressed insulators. It was absolutely essential that the spray did not generate a flowing stream of liquid over the surfaces of the insulators, thereby allowing a path for current flow. The flow of current would reduce the surface tension on the insulators and prevent the generation of corona. A current measurement was made by bypassing the last insulator to earth through the digital storage oscilloscope, thus making it possible to ensure that a leakage current was flowing. From the description of the leakage current, it would then also be possible to establish whether or not the basic simulation of insulator pollution-induced corona activity had been successful.

6.4.3 Salt fog test

The salt fog test involves the spraying of a salt solution onto the insulators which are stressed to the normal operating gradient of the conductor bundle with the particular number of insulators in the string. The voltage was held constant for several minutes before the spray was applied. The insulators were then subjected to a defined ambient of pollution. Level of ambient pollution was measured by the salinity, in kg/m3, which is the concentration of salt (NaCl of commercial purity) in tap water.

Four levels of ambient pollution were selected for the tests. Very light pollution (2.5 to 10 kg/m3), light pollution (14 to 28 kg/m3), medium pollution (28 to 56 kg/m3) and heavy pollution (112 to 224 kg/m3). The temperature of the water was between 5 and 30 °C.

Following the aforementioned procedures and starting with very light pollution, as high levels of corona activity were expected, the pollution mixtures were applied to the conductor bundle. The results were an anti-climax as no corona activity was observed above the normal amounts observed for the conductor bundle under normally dry conditions. One of two options could have occurred. Either the liquid mixture was arriving at the insulators in a droplet form instead of a mist or an insufficient amount of moisture was reaching the insulators. The former was considered more likely.

6.4.4 Clean fog test

In the clean fog test, the insulators were coated with an even layer of a composition of kaolin, tap water and a suitable amount of salt measured in mg/cm2 as the salt deposit density (SDD). The insulators were then baked to dry the deposit and assembled in position for the test. The insulators were then wetted with the insulators stressed to the normal operating gradient of the conductor bundle with the required number of insulators in the string. A finer set of jet nozzles were selected to minimise the size of the droplets arriving on the insulators.

The induced corona noise measurements were recorded (600 000 points per waveform) with the Nicolet 500 series digital storage oscilloscope. Each sample contained two bytes of information. At a sampling rate of 10 MHz, each channel had the capability to capture a total 60 ms of data. Sufficient channels were available to capture both the induced corona noise and the 50 Hz signal

simultaneously and to cascade the information over two sets of channels. The two sets were combined ("joined") in the figure below.

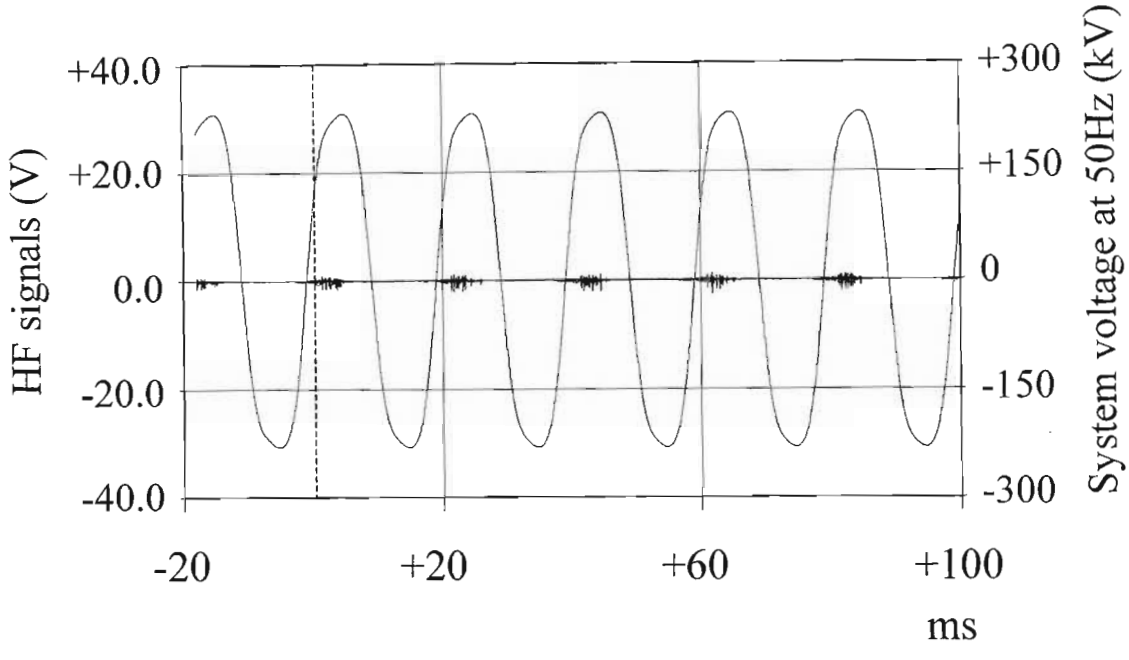

Figure 6. 68: Polluted insulator attached to the twin Zebra conductor bundle.

Figure 6.68 showed a very low overall level of polluted insulator-induced corona noise activity (less than impressive) when compared to figure 6.5 on page 89. There the stress on the conductor was 17 kV/cm and the noise was only marginally different in pattern. The expected pattern was one similar to the fire-induced corona noise activity but with a higher degree of predictability. That is, the pulses should have been larger and reasonably proportional to the applied voltage at that instant, more so than was observed in the fire tests.

In addition to the corona noise, the leakage current as measured as a voltage across a 10 Ω high-power resistance, was recorded. The leakage current in figure 6.69 indicates that insulator corona losses were present on the system.

The noise levels however, were much lower than expected. In earlier work [u], indicated that the polluted insulator-induced noise levels should have been on a par with the fire-induced noise.

---

[u] See p14 [1]

In sub-contacted work performed at the University of Stellenbosch [v], the polluted insulator-induced corona noise pulses generated were significantly more severe than those measured here. However, in the earlier field work, the data was not recorded in detail and several projected deductions were necessary.

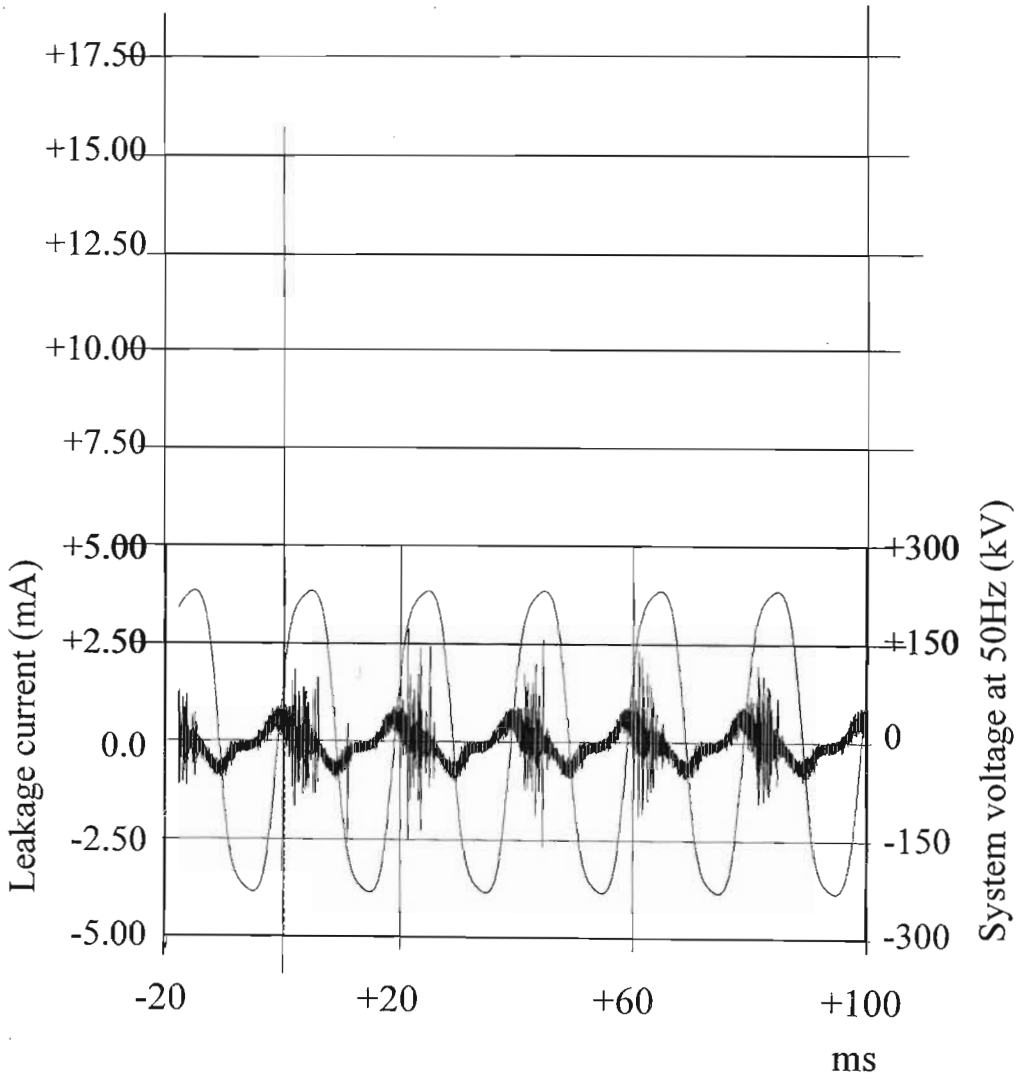

Figure 6. 69: **Leakage current from the twin Zebra conductor bundle.**

In the work performed by the University of Stellenbosch, the affects of the severe scaling of the laboratory cage were not fully evaluated and the polluted insulator measurement method was not consistent with that of the other induced corona noise measurements, making a comparison as attempted in the document ambivalent.

[v] See pp 152-173 [10]

6.5 CORONA CAGE RESEARCH RESULTS IN PERSPECTIVE

In summary of the results obtained in the corona cage:

6.5.1 Complexity Of Measurements

"Research on corona phenomena must be based on experiments. However, the number of parameters associated with the problem is so high that a systematic ordering and separation of affects, as well as the application of reliable theories, is indispensable" – author unknown.

Separation of the fire-induced corona noise from ALL other possible noise sources - within reason - was therefore essential. Theories developed and documented in universally recognised books and papers such as the "Red book" ("Transmission Line Reference Book [35] - 345kV and Above" which was prepared by Project UHV of the General Electric Co. for the Electric Power Research Institute) have been extensively applied in the work done in the corona cage. The separation of affects was successfully completed and as a result a much better understanding of the corona activity process was possible.

Further motivation to do a sugar cane fire series of tests was possible as a result of the very positive results achieved in the gas fire tests. By avoiding the extra time and work required to identify the processes taking place, many assumptions would have been necessary and incorrect assumptions would have led to the derailing of this research as many theories were being bandied around and either no funds were available to test them or inadequate equipment and no incentive to do so prevented this from happening. Therefore to date, very little progress had been made towards developing a cost effective means by which to actively avoid faults due to flashovers from fires.

Similar tests were performed at the mini test corona cage at the University of Stellenbosch to ascertain the development of corona with various components of the sugar cane fire[10]. The information provided from this work shed some light on the direction required. The implementation of a sugar cane fire test series in the large Eskom corona cage also drew attention to the affects of smoke on the levels of induced corona generated and corrected information obtained from the Stellenbosch work due to the dimensional limitations of the smaller cage. This is an assumed cause for the error as the university did not venture to determine the limitations of the dimensions of it's cage. A more complete understanding has

therefore also been developed by an overall conglomeration of the work performed in the corona cage.

6.5.2 No Flashover Due To The Sugar Cane Fire

Several tests were completed with the sugar cane stacked under the test line in the corona cage and high voltages were applied in line with the appropriate normal operating gradients for the particular conductor bundle. In each case audible corona was produced and increased with increasing voltage. High levels of corona and radio noise were recorded. However, the supply voltage regulation was poor and the voltage dropped with increasing corona currents and no flashover occurred.

Energy was necessary to start a disruption of the air insulation and it was reasonably safe to assume that additional energy was also necessary for an increase in that disruption. The gas fire accentuated the affects of increased heat and the reduction in air density in a very small portion of the conductor bundle. The result in the gas fire was a "single" path to ground with only a small amount of current flowing in the path as graphically represented in figure 6.70 (condition A) by the current flow "i". The small current required at the applied voltage was not excessive and as a result the power supply was able to maintain the applied voltage.

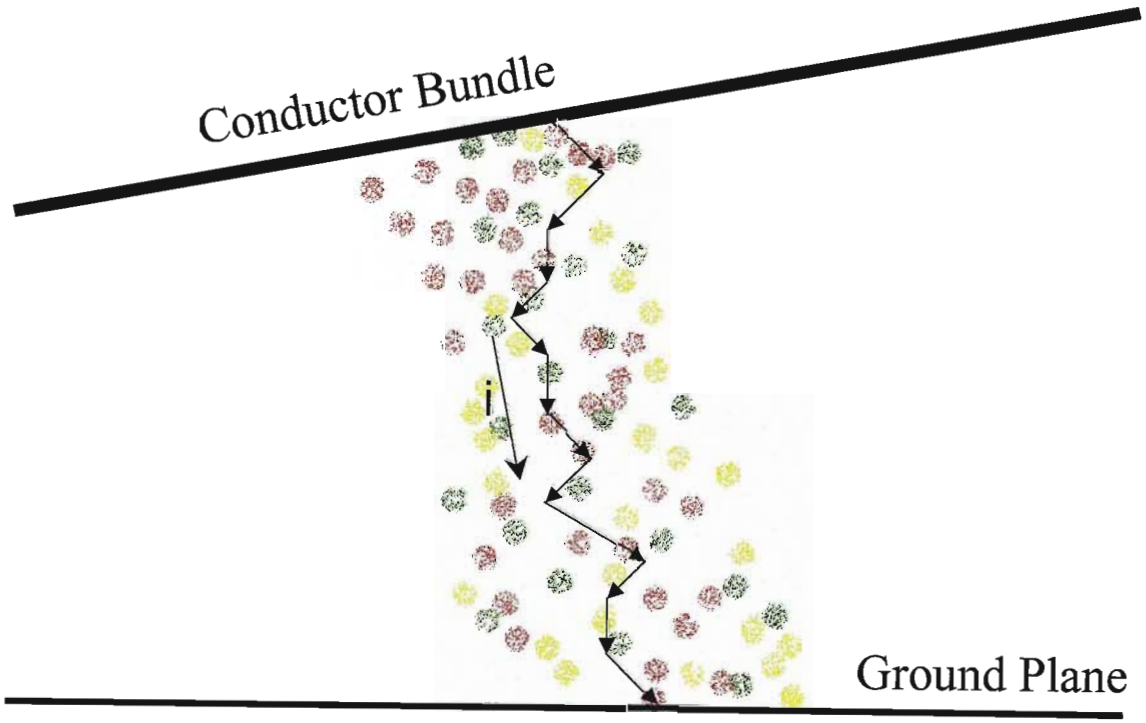

Figure 6. 70: Corona development in the gas flame [condition A].

On several occasions the applied voltage was increased creating a gradient about the conductors very near the critical field required for ionisation by electron impact to develop (example:

17kV/cm with the installed twin Dinosaur conductor bundle). Then igniting the gas burner resulted in large increases in the audio noise level and an arc developed across the gap between the conductor bundle and the grounded cylinder through the heated plasma. As the flashover occurred the breakers opened removing the high flashover sustaining gradient and eliminating the arc.

In the case of the sugar cane fire under the conductor bundle the area of the bundle exposed to the fire was considerably larger. A high applied voltage equal to that applied when the gas fire was tested did however not create the same affects as that created by the gas fire.

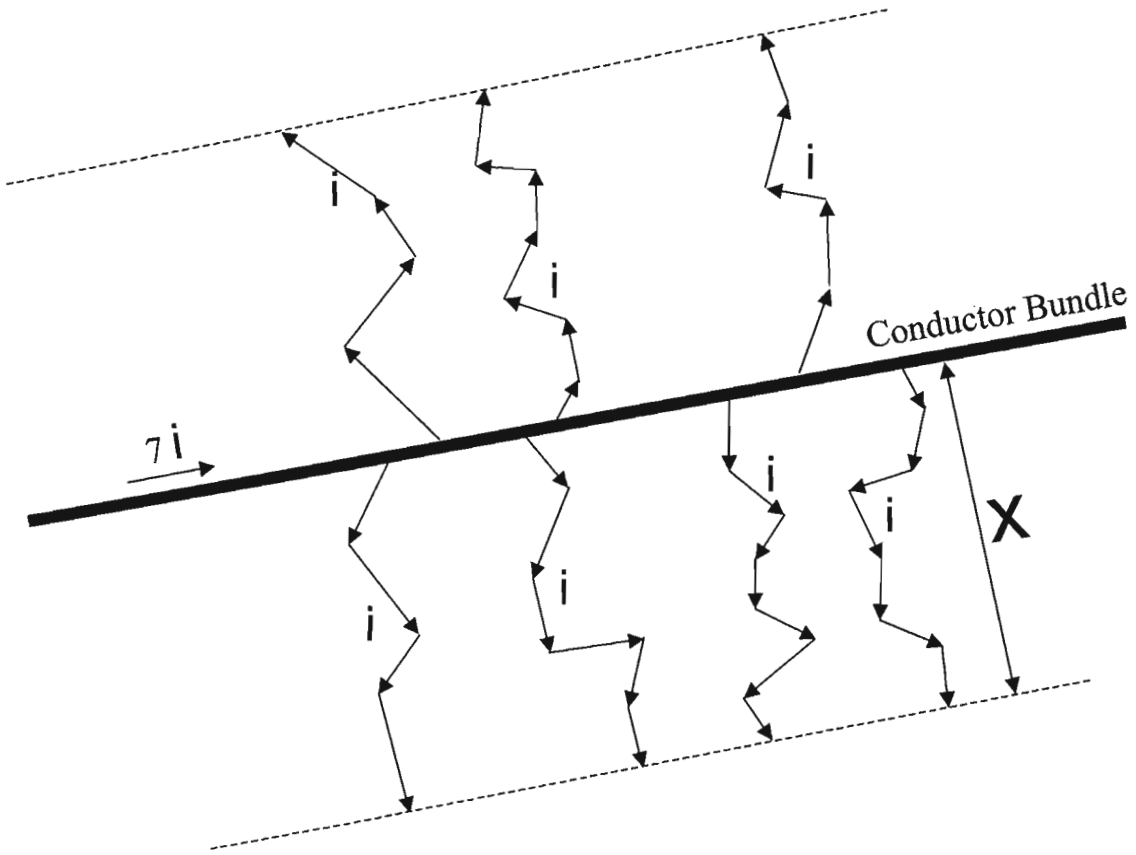

Figure 6. 71: Corona development in the sugar cane fires [condition B].

Firstly, condition B as illustrated in figure 6.71, did not result in a flashover. The sum of the currents in the streamers could have been considerably larger than that experienced in condition A. The typical stresses on the operational line required a high applied 50 Hz voltage in the single phase system to simulate the operational gradient in the three phase system.

With many points along the conductor already active with corona due to the larger size of the sugar cane fire (three to four meters as opposed to less than one meter of focused heat from the gas burner), the disruption demanded more energy. Due to the limited power supply, not enough

power was available to supply the additional energy required. Consequently the voltage dropped proportionately to the increase in streamer current.

$$P = VI$$

where I is the total current supplied to the line and

$$I = I_{std} + i_{TOTAL}$$

where I_{std} is the typical load current of the system with no or very little corona and corona losses (μA) and

$$i_{TOTAL} = \sum i_{streamer}$$

with $i_{streamer}$ being the current in each streamer.

In condition B i_{TOTAL} increased with each new streamer. P was constant, therefore V, the applied voltage was reduced to accommodate the increased current.

A reduction in voltage reduced the stress on the conductors and a reduction in corona followed. Finally a point was reached at which the voltage and current were quasi-stable each trading with the other. A reduction in voltage reduced the gradient on the conductor bundle and the conditions for ionisation by electron impact were limited to a distance "x" from the conductors. That is, the corona region existed only to a distance "x" from the conductors. At this point E_{local} was no longer greater than E_{crit}. In the catch-22 situation, the increased voltage resulted in increased corona which resulted in increased current which resulted in decreased voltage which resulted in decreased corona which resulted in decreased current - power rating of the transformer then forced the voltage up and the cycle was repeated. As a result the sugar cane fire in the corona cage with the present transformer supply could not produce a flashover.

Using condition A as an isolated streamer simulating the action of an individual streamer in a sugar cane fire, it was possible to analyse and describe the overall destructive pattern occurring. In the power transmission network, large currents were available to source the sinking of the streamer currents, and hence P = VI was no longer a constraint. As the voltage did not decrease

with an increase in current, the condition $E_{local} > E_{crit}$ persisted and the gap between electrodes was rapidly bridged with the leader breakdown process.

In the corona cage, it was found that when the conditions were appropriate (correct gradient, temperature, humidity and thermal positioning of the flame - dependent on the wind), flashover was nearly instantaneous. Projecting this phenomena onto the three phase system, time to flashover was not dependent on the build-up of conditions at the conductors. The nature of the fire was such that the appropriate conditions were available in a near-binary fashion. That is, either they were appropriate or they were not.

However, the definition of "instantaneous" is dependent on the "dynamic" range of the time measurement. A faster measuring process was therefore considered necessary to allow the detection mechanism sufficient time for analysis.

6.5.3 Streamer Characteristics

The pulses documented in this chapter exhibited the same characteristics as those found by Kip (1938) [36]and Foggo and Whitcombe (1968) [23]. Kip discovered that there were two types of pulses, burst pulses and streamers, occurring with a highly stressed positive electrode with negligible cathode influence.

Oscillograms recorded by Kip show the streamers and these were virtually identical to those documented in this report. However, the data captured here was captured at a faster rate than that captured by Kip where the initial negative trace was lost in Kip's oscillograms. The oscillations, present in the data documented in this report, occurring directly after the fall of the pulse was as a result of the transfer function of the filters and capacitive and inductive affects of the insulators and the conductors in the cage.

Foggo and Whitcombe showed similar trends in the pulse pattern and also determined that with an increase in voltage the pulse repetition frequency increased. A maximum of approximately 240 000 pulses per second was recorded before the discharge lost it's pulsating character. Hence in the detection of fire-induced corona, the limit when monitoring the pulse repetition rate would have to be less than 240 kHz (note that this is not the same parameter as the frequency at which the noise was being measured).

6.5.4 Processes of Measurement

As no measure of the activity of fires under power lines had yet been quantified, it was necessary to define the character of fire-induced corona noise with the aim of using this information for detection purposes. Therefore measurements had to be taken of the noise propagated along the transmission line rather than noise transmitted radially from the transmission line.

Quasi-peak measurements are the more common means of measuring "radio noise". However, the measurement favours rapid repetitions of pulses. As A.H. Davis [7] stated, the meter "must have an appropriate leak, for the loudness of a slow series of repetitions is less than that of a rapid series".

The results obtained in the corona cage have shown that the ability to detect fires is dependent on the ability of the detection device to select appropriate frequency and amplitude thresholds and thereby appropriate windows and to combine the 50 Hz initiating voltage with the noise signal emanating from the appropriate windows.

An indication of the information lost in the quasi-peak measurement was the actual fire measurements taken from the twin Zebra conductor bundle. A quasi-peak measurement recorded an approximate 7 dB average increase in noise from rain-induced noise to fire-induced noise with increasing gradient. The gas fire-induced noise was limited to an absolute voltage of -65.73 volts and the rain-induced noise attained a maximum absolute voltage of -3.594 volts. In dB the increase of noise when comparing "apples with apples" was therefore 25 dB. This new result is much more significant than the quasi-peak measurement, especially considering that the fire-induced noise absolute voltage was higher than the -65.73 volts recorded.

6.6 CONCLUDING REMARKS ON LARGE CORONA CAGE RESEARCH

Two types of measurements were made in most of the tests performed in the corona cage; quasi-peak measurements (universally recognised as the more popular method of measuring radio interference voltages), and instantaneous time-domain measurements. The quasi-peak measurement process clearly showed in all cases - for the given dimensions - that fire-induced corona noise generated higher levels of noise than rain-induced corona noise. However, the time-domain measurements, recorded on digital storage oscilloscopes, showed that much of the

information available in the fire-induced noise was lost when only performing quasi-peak measurements.

The time-domain measurements recorded several useful characteristics of the rain- and fire-induced corona noise patterns. The amplitude of the rain-induced corona noise pulses varied with the applied local fields and hence proportionately with the applied voltages on the conductor bundle. The amplitude of the fire-induced corona noise pulses were primarily influenced by the changing environmental conditions - changing air density and particulate activity - within the secondary influence of the applied voltage. Due to the probability parameter introduced by the ionisation by collision phenomena, a large number of sample measurements were taken in the corona cage (totalling more than 281 megabytes of data) thereby ensuring a high level of confidence in the conclusions made. The detail of each and every result obtained during these stringent tests have not been included in this dissertation to reduce the overall size of the document. These records have been documented and are available [37],[38].

The result was that fire-induced corona noise pulses consisted of long and short pulses depending on the air density (and the electron mean free path λ_e) and the proximity of particles. Hence the fire-induced pulses were described as existing in a quasi-random fashion whereas the rain-induced pulses existed in a very predictable pattern as was universally recognised by many authors.

The amplitude of fire-induced corona noise pulses were recorded at values of up to 48 dB higher than the rain-induced corona noise pulses. The number of rain-induced pulses captured in a particular half cycle were up to three times higher than the equivalent number of gas fire-induced pulses recorded. However, the number of fire-induced pulses increased with the volatile nature of the fire in the proximity of the conductor bundle. Therefore the repetition rate of the fire-induced pulses was also less predictable than the repetition rate of the rain-induced corona noise.

Several conductor bundles used by Eskom in the transmission of power over long distances were tested and all the results described similar trends in the rain- and fire-induced corona noise characteristics. Only the twin Dinosaur and twin Zebra bundles were discussed extensively in this report. Results of the remaining conductor bundles will be published at a later date in either Eskom internal reports or other publications.

The environment in the corona cage was inappropriate for the clean and salt fog tests performed on insulator strings. The density and molecular size of droplets required to adequately create a "fog" could not be developed and the tests were terminated.

To observe the characteristics of the fire-induced corona, the electrical discharges as a result of the flames need to be tracked strictly with the flames when they are present at the energised conductor only.

To track the flames, the flames need to be visually monitored. Simultaneously, the channel needs to be monitored for electrical discharges. During the periods when the flames are consistently in the vicinity of the energised conductors the detected electrical discharges are relevant. When the flames are not consistently present at the energised conductors the associated electrical discharge patterns will be that related to a combination of dry conditions and fire conditions.

Note that the power cycle is critical to the tracking process and must therefore also be recorded throughout the tracking process. When the voltage has dropped to zero there is a limited electric field stress present and no corona activity will exist at this point in time as a result of the applied electric field. Some corona may be initiated near the zero crossover as a result of residual space charge from the previous half cycle.

When the flame conditions are quasi-steady at the conductors, the fire-induced corona grows rapidly in amplitude, occurs more frequently in the half cycle and is present in both the positive and negative half cycles.

Finally, tracking the flames as they induce corona to a more accurate degree in the corona cage may not be a financially viable exercise as the results achieved in this research already provide the author with sufficient information to both develop an elementary detector and move testing to the operational main transmission system (MTS) with confidence.

CHAPTER 7

Laboratory – Modelled Corona Cage

7.1 BACKGROUND

Eskom has facilities within which to study the overall affects of fires on the changes in the electric field about a high voltage transmission line and has been discussed in chapters 4, 5 and 6 above. However, the fundamental components of a fire - typically sugar cane or brush fires - could not be studied in the facilities available to Eskom. This task was sub-contracted to the University of Stellenbosch. An understudy at the university undertook to build up a miniature quasi-replica of the Eskom facility and had the technical resources (fellow colleagues) available to study these fundamental components.

The cage was 1.5 m in diameter and 2 m in length. The cage was entirely enclosed in order to measure the factors such as humidity and temperature and a gas burner was used to generate the flames. The conductor used in this cage was a single Hare conductor which has an overall diameter of 14.21 mm with 30 aluminium strands and 7 steel strands each with a diameter of 2.03 mm.

A combination of the gas burner, sugar cane and flow rate through a "smoke generator" was used to create the different conditions of fire with no particles, fire and smoke and only smoke with no large particles. The details of the test procedures and measurement methods and techniques are described in detail in the final report of this sub-project which was also presented as a thesis at the University of Stellenbosch [10].

7.2 CONCLUSIONS REACHED

The research work investigating the modular components of the sugar cane fire was sub-contracted to the University of Stellenbosch with very positive results. These results were extensively discussed in a thesis presented by a post-graduate student in the Electrical department [10].

7.3 RELATING MODELED CORONA CAGE TO LARGE CORONA CAGE

An interesting development was the affect of modelling the parameters at such a small scale that the influences of very small particles (smoke) started playing a major role in the amount of noise generated. The influence of smoke was measured as comparable to the affects of the reduction in air density due to the fire with no particles.

CHAPTER 8

Operational Conditions

8.1 BACKGROUND

The induced corona noise results observed in the corona cage have been correlated with the specific noise source, namely normal dry condition high voltage stresses, heavy rain and fires.

In the operational environment, the power line is a conduit for both intentional high frequency communications and high frequency transients emanating from high voltage partial and complete electrical discharges. Due to the high operating voltage, the conduit for the electrical discharges cannot be accessed without specialised equipment which will provide the necessary isolation between the high voltage on the power line and the low voltage electronic equipment used to interpret the signals. The options are to measure the high frequency signals at high voltage or to extract them to low voltages and measure them "on the ground". The alternatives are numerous, including fibre optic or radio communication links to equipment on the conductor on the one hand, and high insulation filtering equipment on the other.

The high insulation filtering equipment presently forms part of the installed equipment and as such would present the more cost effective solution. For 220kV and above, line voltages are measured via capacitive voltage transformers (CVT). These units consist of stacked capacitors making up a capacitance potential divider from which a secondary step-down transformer further reduces the measuring voltage to 63.5 volts. At all voltages in the power utility, a current transformer (CT) is used to measure the current flowing in a particular bay. These units generally have capacitively graded insulation which presents the same electrical circuit as a CVT. However, these units do not always have a dedicated path to ground. Some units have a "test tap" which provides the tester with an access point to measure the insulation condition. The majority of CTs in Eskom do not have test taps and as such do not have a single point from which a high frequency signal can be extracted. For that reason, the work in this particular research will focus on the CVT and in principle poses the same circuit as applied in the corona cage with a coupling capacitor of known value.

8.2 POWER LINE CARRIER CIRCUITS

In the CVT, the stacked capacitance to ground is also used for high speed protection communications. The CVT provides a means to inject high frequency signals onto the overhead power lines and to extract these signals at remote locations for high speed protection protocols. A control signal is modulated onto a carrier signal and demodulated to inject and extract the information respectively.

The carrier band ranges from 50 kHz to 500 kHz but the data on any particular line utilises a bandwidth of only 4 kHz in each direction - a total of 8 kHz. The filters used by the carrier system and essential for the measurement of high frequency noise and signals on the transmission line are similar in concept to those used in the corona cage supply circuit. Figure 8.1 illustrates the concept. A "line trap" serves as the band-stop filter preventing the high frequency components on the transmission line from evading the measuring circuit by passing through the substation to earth. Coupling capacitors, line matching units and hybrids make up the bandpass filter circuitry allowing the high frequency components to pass through into the measurement circuits.

The presence of carriers on the relevant line implies that the measurement of fire-induced corona noise on that particular line is dependent on the detector's ability to filter out carrier signals within the band. The carrier signal is itself amplified to ensure that "noise" cannot disrupt the link and initiate a false trip procedure. The frequencies where these carriers exist must therefore be avoided entirely.

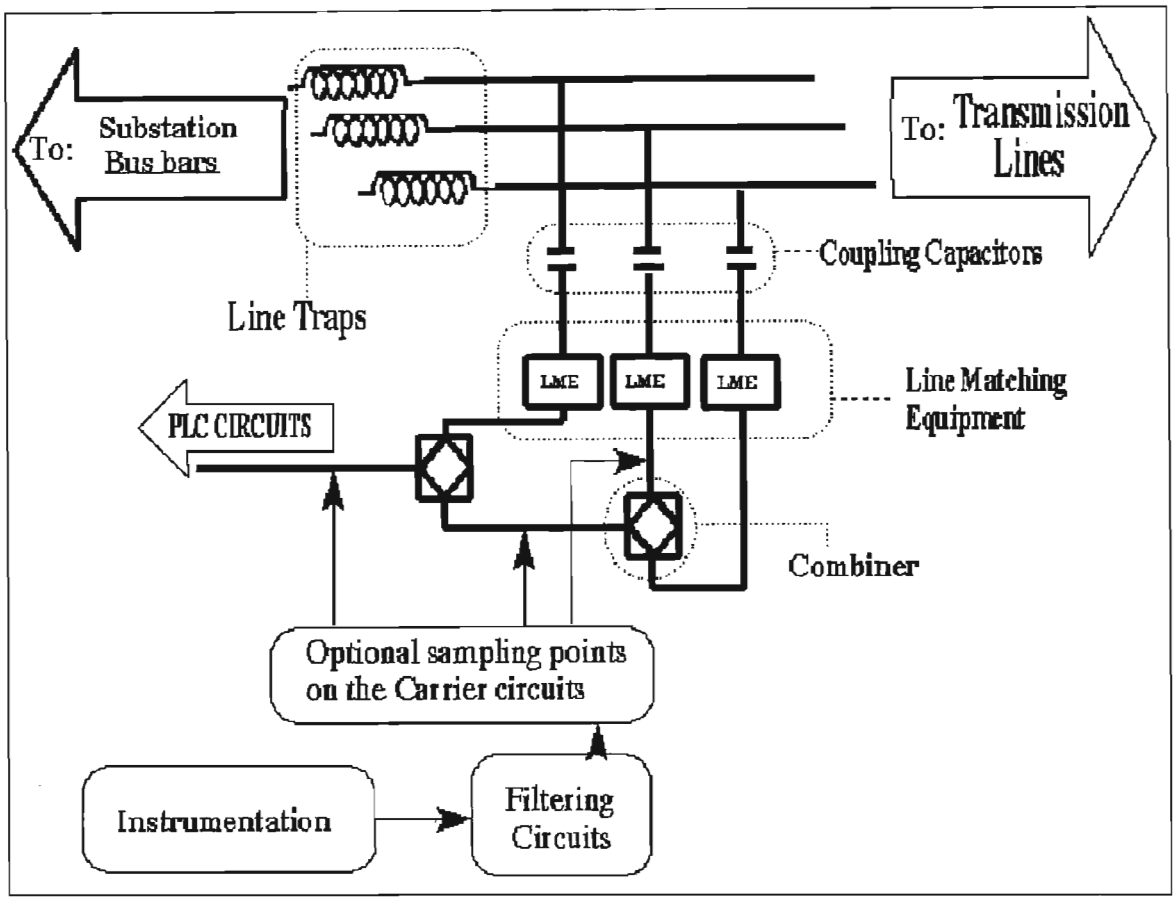

Figure 8. 1: PLC filtering and noise measurement circuitry

In addition to the main carriers, adjacent carrier circuits on other transmission lines leaving the same substation also have an affect on the measurements. The line trap provides significant attenuation of the carriers and any adjacent carrier must pass through two line traps before that carrier signal reaches the measurement point. The attenuation is not sufficient to reduce these signals to the same level as normal background noise. It is standard Eskom practice to have the same frequencies used at no less than 3 substations apart to ensure that an adjacent carrier does not interfere with the protection of a particular line. The adjacent carriers in a substation are therefore additional "frequency band users" to avoid.

The bandpass filters used within the power line carrier equipment has a bandwidth of 4 kHz. With sensible selection of the particular centre frequency of the device, they were used when doing measurements at various substations.

8.3 ACCESS TO FIRE-INDUCED CORONA

The main objective in the operational line measurements was to monitor the power line carrier channel when a fire incident exists. That is, from the time a fire approaches the overhead transmission line to the time that the particular fire leaves the area, the carrier channel had to be monitored.

Several important issues had to be considered in order to accomplish the above objectives. Firstly, in order to observe the affects of the fire on induced corona levels, it was essential that the background noise levels be considered "normal", that is, with minimal abnormal activity such as switching surges, lightning surges, insulator spark gap noise and rain-induced corona noise.

Secondly, in order to monitor weather conditions to ensure that the above "abnormal" activities - in particular rain-induced corona noise -were minimal, the selection of transmission lines was critical. In some geographical regions the weather patterns can vary substantially over very short distances. Traction stations have severe loading affects on the network and similar environments need to be avoided for these research measurements.

Thirdly, the occurrence of a fire under the particular transmission line selected for the research was essential.

The first two issues were rudimentary problems but the third placed the team at the mercy of both the elements and the network control policies.

Fires are seldom planned and when sugar cane fires are planned in the region where the "unplanned" fires cause the most problems, those transmission lines are de-energised in order to maximise the quality of supply to major consumers of electricity in the entire region. Any flashover occurring due to fires would not only disrupt supply to the end-user of that line but the gap breakdown would decrease the voltage of the entire network in the region - in utility terms this is known as a "voltage depression" or "voltage sag". Additional lines in the MTS region of Kwazulu Natal provide a "ring-feed" network in which more than one power line serves as a supply to a group of customers. The end-user would therefore not lose the supply of electricity in the event of an incident. Although the precautions taken all point to good management of the

network and essential to meeting the needs of the consumer, it severely inhibits any efforts to confirm results obtained in the experimental work performed under controlled conditions. Veld and brush fires usually fall into the category of "unplanned" fires.

The Nelspruit/Komatipoort 275 kV transmission line in Mpumalanga has its servitude running through several kilometres of sugar cane plantations and does not get de-energised when a "planned" sugar cane burn is to take place. The major thrust of our research work under operational conditions was therefore to be done here. However, sugar cane plantations are burnt on an annual basis and as only several kilometres of this line run through such plantations, only two or three burns occur under this line per year. The team then had to rely heavily on the relevant farmers and the sugar mills to inform Eskom of these burns well in advance. As the equipment used - digital storage oscilloscope described previously - is both expensive and extremely useful in other work, the availability of this equipment also had to be taken into consideration. The mills manage the sugar cane plantation burning according to which farmers are available, the availability of harvesting staff and the condition of the plantations. An additional consideration was the possibility of a farmer cancelling the planned burn at the last minute due to changing weather conditions. This results in the mill selecting the next farmer not yet scheduled in the roster and the relevant farmer with a transmission line through the harvestable plantation, is sometimes selected. Under these conditions the scheduling of a research test on Eskom's network is usually not of any significant priority to either the farmer or the sugar mill.

Three sets of operational fire experiments were completed. The abovementioned 275kV transmission line test with one fire in Mpumalanga, a series of controlled tests with flammable material transported to a test site in Gauteng and finally with a detector, three fires were generated under controlled conditions in Kwazulu Natal.

8.4 FILTERING

Initially a passive filter (by BBT then known as Brown Boveri Technologies) normally used for the PLC equipment, was used to filter out the bulk of the carrier signals on the relevant transmission line. For the later work, an active filter was added to virtually completely eliminate the carrier signals from the measurement. The frequency response of the BBT filters were

measured and is shown in appendix H. Two filters were used to test the spectrum of the fire signals. One with a centre frequency at 52 kHz and the other at 428 kHz.

All measurements completed in this section were collected with the aid of a quasi-computer controlled digital storage oscilloscope with a maximum waveform capacity of 62 000 sample points per waveform in the artificial fire tests and 256 000 sample in the sugar cane plantation fire (the extra memory capacity only becoming available at a later stage in the project).

CHAPTER 9

Operational Line – Controlled Fuel

9.1 OVERVIEW

In order to create an opportunity for fire tests in the operational environment it was necessary to "take the fire to the transmission line". The gas burner was used to complete the simulation of fire tests in the corona cage. By testing the same fire source in both the cage and on the operational network a tentative comparison could then be made between the isolated environment and the noisy environment. For the sugar cane and grass fires, a framework of scaffolding was prepared to contain sugar cane and grass. In order to compensate for wind directions the centre phase was selected for the placement of this structure for the sugar cane and grass fire tests. For the gas burner a mobile, extendable platform was used. The gas burner was mounted on the platform which made it possible to test the gas fire under all three phases and at separations between phase conductor and burner, similar to those in the corona cage.

Due to unfortunate circumstances, the sugar cane and grass fire tests were unsuccessful. The gas fire, being independent of "flaws" in the weather patterns and the inabilities of available personnel, was tested under all three phases and the centre phase in particular, with success. The fire in each case was started and the instruments operator at the substation was notified continually of the progress of the fire via radio communication.

The transmission line selected for these tests was the 275 kV Craighall / Lepini transmission line with a quad-Zebra conductor bundle. Monitoring a shorter transmission line (22.86 km) made it possible to determine the weather conditions over the whole length of the line. The geographical location at which the fires were burnt was approximately 12 km from Lepini substation where all the measurements were made.

This chapter documents the tests done under the Craighall/Lepini 275kV transmission line.

9.2 NORMAL CONDITIONS AND FILTERING AFFECTS

The power line carrier signals existing on the transmission line overwhelm any noise and therefore had to be eliminated from the measurement. The carrier signals on the transmission line can be seen in figure 9.1 where the sampling rate was set to 2.0 MHz, the slower sampling rate captures a larger portion of the waveform, and figure 9.2 with sampling rate set at 10.0 MHz, the faster sampling rate captures data in a better resolution format for comparison purposes.

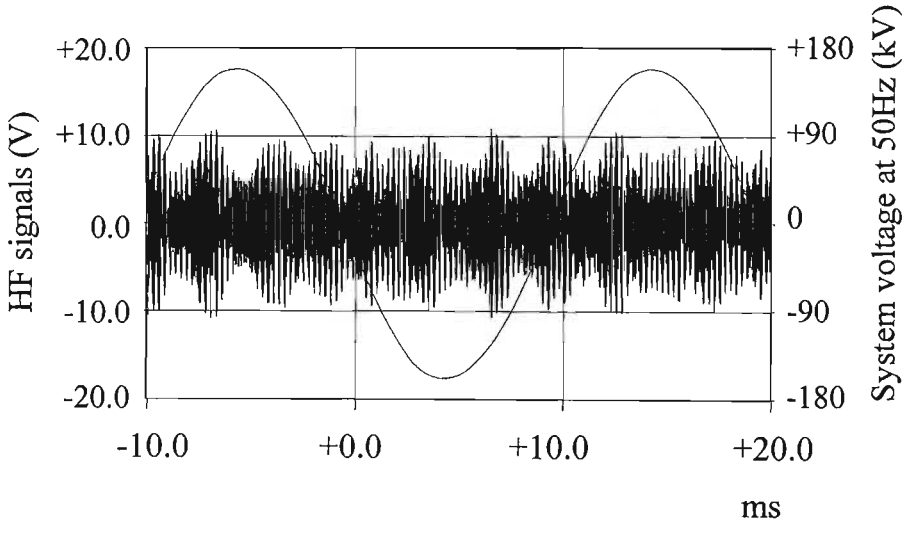

Figure 9. 1: Signals on transmission line at higher frequencies (sampling rate = 2MHz).

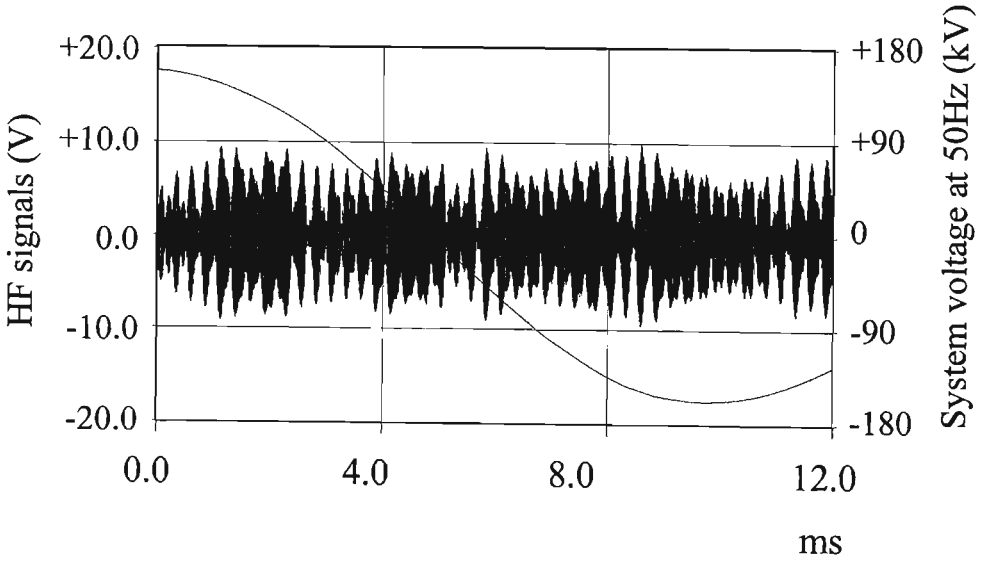

Figure 9. 2: Signals on transmission line at higher frequencies (sampling rate = 10MHz).

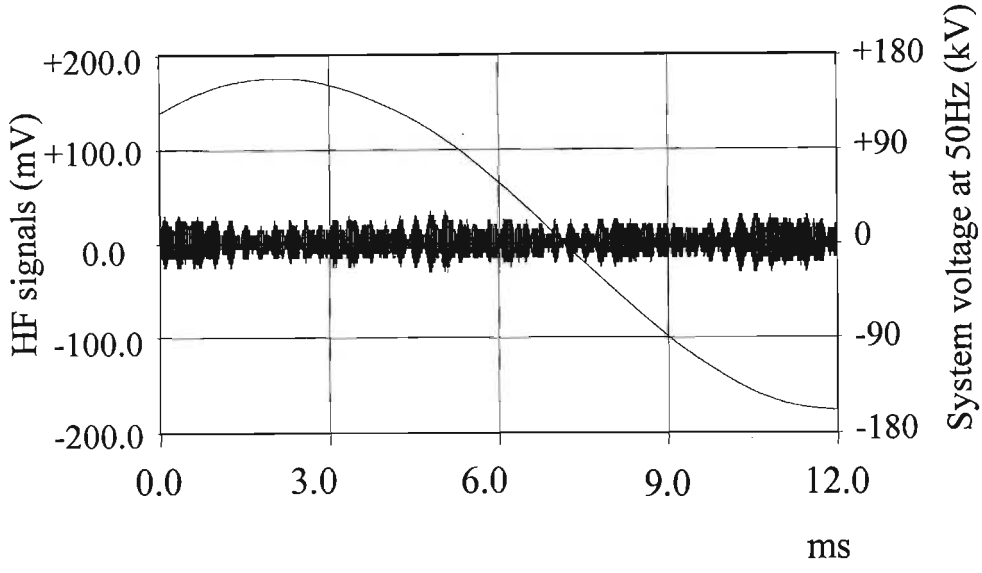

Figure 9. 3: Dry condition; monitoring the noise levels with the 52 kHz filter.

The BBC filter from BBT with a centre frequency of 52 kHz was selected, since this filter was normally used in the BBT PLC equipment, making it possible to minimise the above carrier signals as shown in figure 9.3 above. The filter had a high input impedance and did therefore not load (and t herefore i nterfere w ith) t he P LC c ommunication s ystem i n a ny w ay. A lso, u sing a BBC filter with a higher centre frequency, 428 kHz, the response at the higher end of the carrier channel range was recorded.

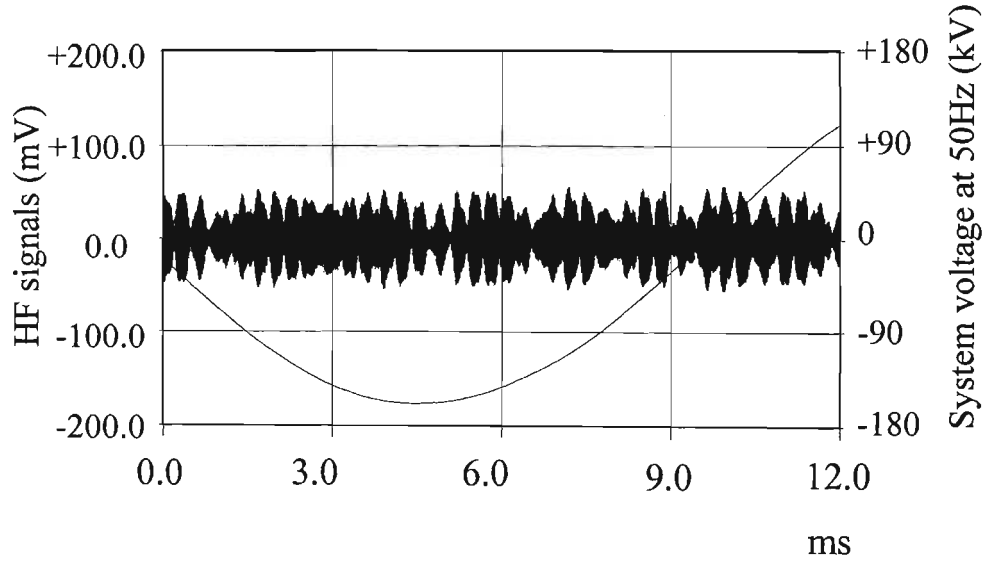

Figure 9. 4: Dry condition; monitoring the noise levels with the 428 kHz filter.

The sampling rate for the dry conditions in figures 9.3 and 9.4 was at 10 MHz. The PLC carrier signal levels received from the two filters were now much lower but neighbouring carriers were clearly visible through the 428 kHz filter. These levels therefore indicated that it may be more favourable to monitor the lower end of the carrier frequency range with amplitudes of ± 25 mV background voltage levels through the 52 kHz filter as opposed to ± 50 mV through the 428 kHz filter, and that further filtering was required for an extra reduction in the interfering affects of the carrier signals.

9.3 GAS FIRE UNDER THE TRANSMISSION LINE

The gas burner used was activated by means of a remote radio signal received which activated the main gas feeder to the burner. A pilot flame then ignited the large influx of gas.

With the gas burner assembled approximately three (3) meters below the centre phase and taking the wind direction and wind speed into account - placing the burner two (2) meters north of centre, the following burst of noise in figure 9.5 was captured at a sampling rate of 5 MHz.

The fire-induced corona activity was visible in the negative half cycle of the 50 Hz power signal.

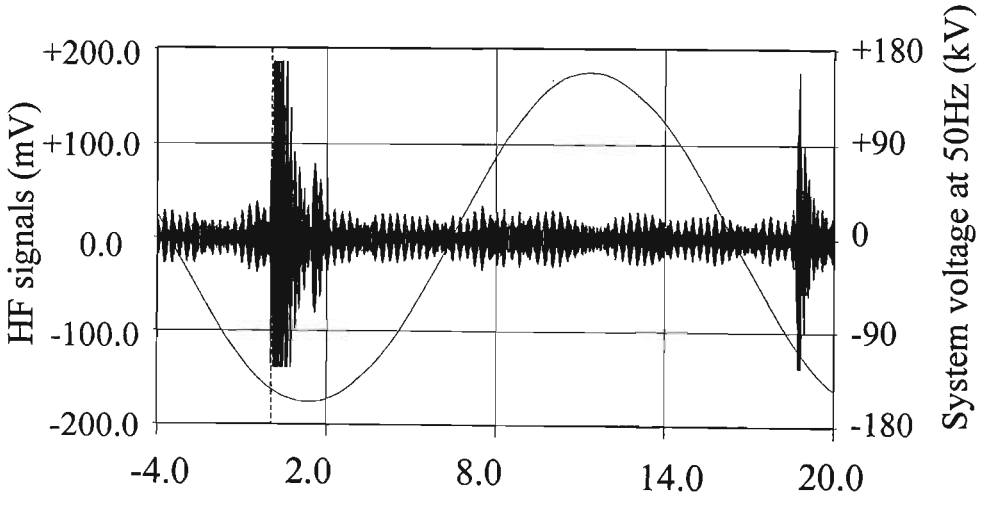

Figure 9. 5: Gas fire under the center phase.

On several occasions when no fire was present under the transmission line, unexpected surges were monitored.

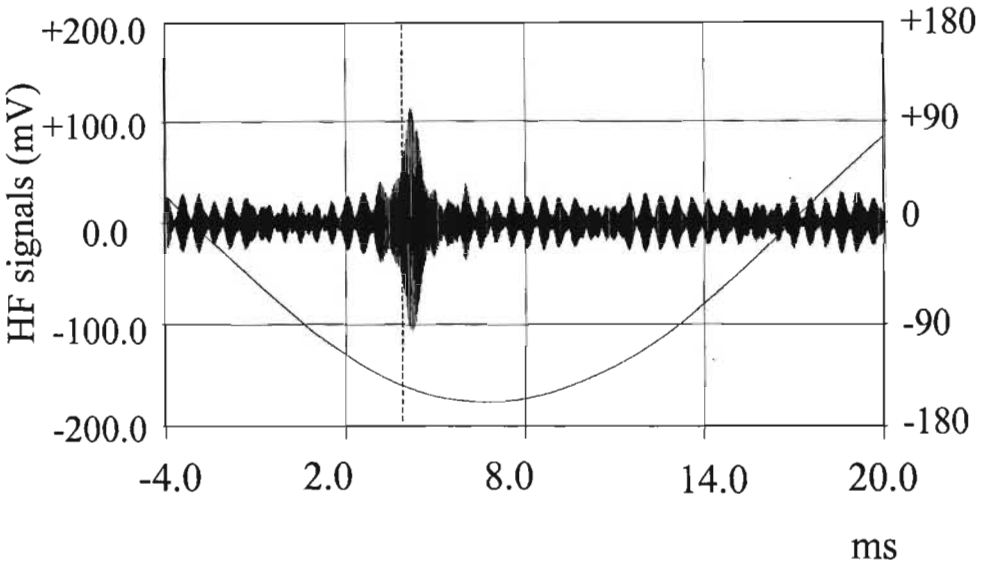

Figure 9. 6: Spurious surges detected on the transmission line.

With the gas burner mounted 3 meters below one of the outer phases, 3 meters north of the phase due to stronger winds, the following induced corona noise was recorded.

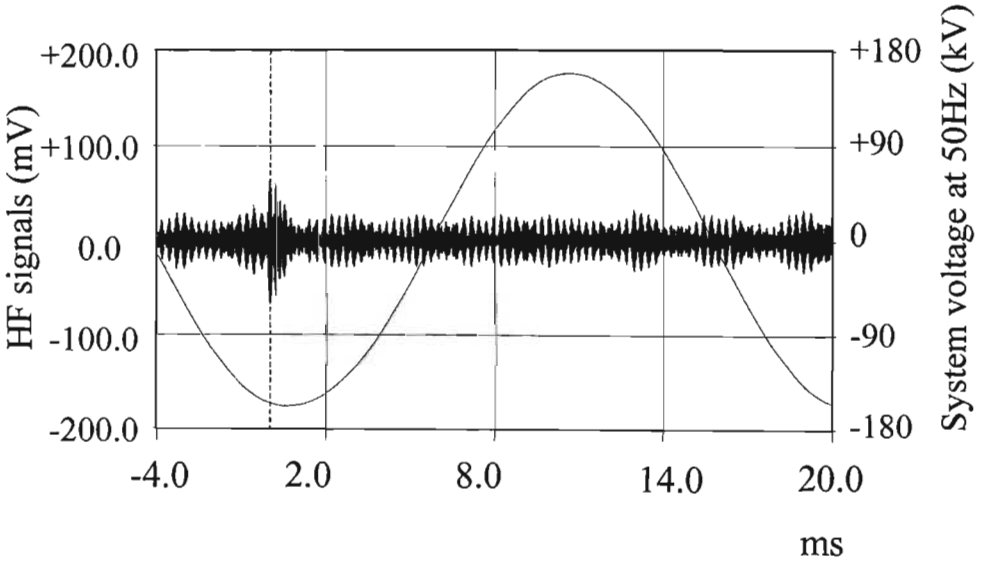

Figure 9. 7: Gas fire burning under an adjacent phase.

It should be recognised however, that the strong wind probably played a major role in diluting the affects of the flame on the electric field about the conductor bundle.

A segment from the waveform captured in figure 9.5 was used in the calculation to determine what affects the huge burst of noise had on the frequency spectrum. Note that these levels measured in figure 9.8 below, were clipped at +186 mV and -140 mV.

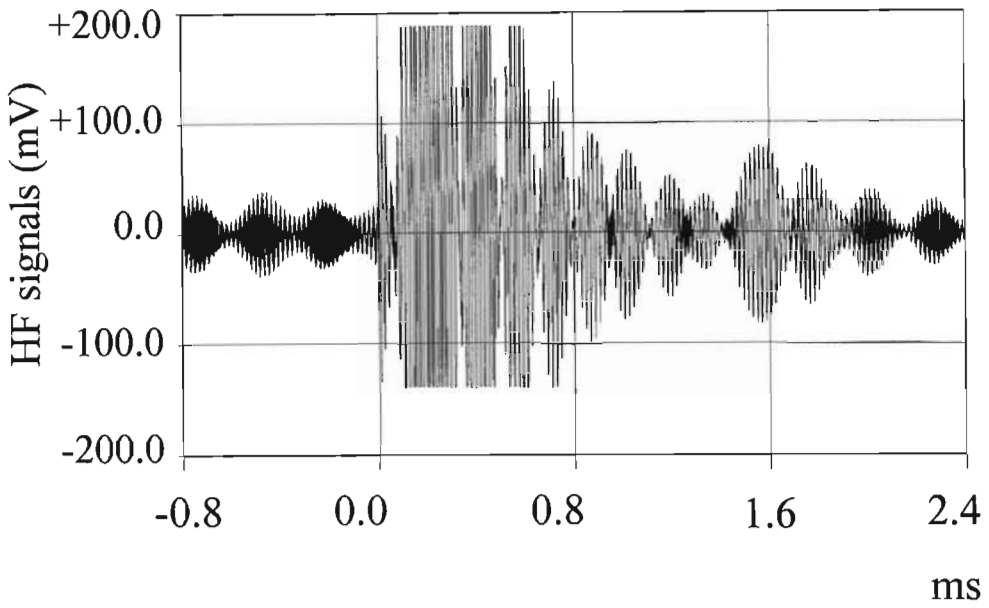

Figure 9. 8: Gas Noise burst with the gas fire ignited (Quad Zebra conductor bundle).

The expected levels were lower than the measured levels and as such the dynamic range limited the measurement. The precautions taken were to ensure that some form of the fire data had to be captured in order to be able to process such information. If the dynamic range was set too high, the resolution of the recorded data would not have been acceptable. As this kind of information captured on a sensitive network was not easily repeated, the data had to be captured the first time it existed on the line.

The opportunity could not be assumed to be available for a second time as the line could have tripped and not been re-energised until the problem (created by the experiments) was cleared. Naturally, more than three or four trips on the network could not be tolerated and as such any data captured on the transmission line had to be protected.

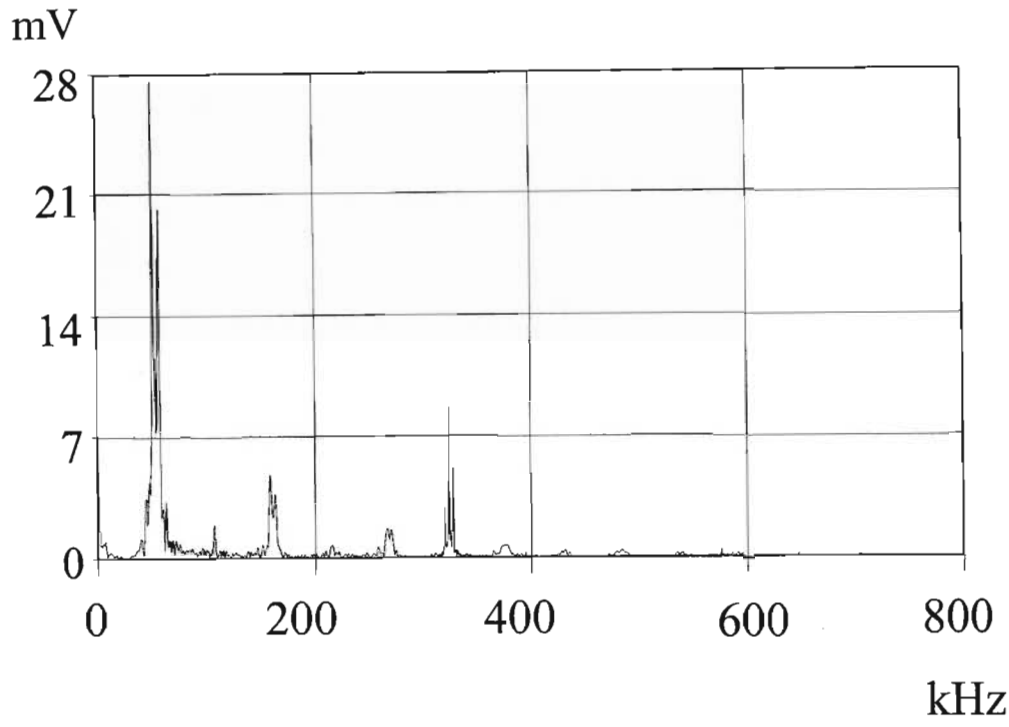

Figure 9. 9: Frequency spectrum of the fire induced noise on 275kV transmission line.

Due to the longer sample duration the levels of the strong frequency components in figure 9.9 could not be directly compared to those registered in figures 9.13 and 9.14 presented in section 9.6 from page 165. However, the ratio of the noise levels at 52 kHz to that at 324 kHz could be and was compared to the result in figure 9.13. The amount of carrier signal which leaked through the filter remained unchanged in both measurements. The only component which was changed to give the frequency spectrum of the carrier a lower amplitude was the change in sample time and hence the different sample weighting from which the spectrum was calculated. Therefore the carrier signal was used as a reference by which to calculate the increase in background noise from normally dry conditions to a gas fire in dry conditions.

The total increase in noise was the sum of the dB difference (dB_1) of carrier signal to background noise and the dB difference (dB_2) of the fire noise to the carrier signal.

$$dB_{(TOTAL)} = dB_1 + dB_2$$

$$dB_1 = 20 \log \frac{14.433}{2.2}$$

$$= 16.34 \text{ dB}$$

$$dB_2 = 20 \log \frac{27.577}{8.66}$$

$$= 10.06 \text{ dB}$$

Therefore $dB_{(TOTAL)} = 16.34 + 10.06$

$$= 26.40 \text{ dB}$$

The additional frequency components visible in figure 9.9 between 52 kHz and 324 kHz were more than likely harmonics due to the clipping in the data. The components above 324 kHz were harmonics of the 52 kHz signal added onto the carrier signal.

The frequency spectrum calculation has an averaging affect, and hence an attenuation of the change in the increase in noise had to be considered. To understand the full extent to which the averaging affect attenuated the noise, a complete analysis of the time domain noise levels was necessary. A projected maximum peak in the waveform in figure 9.8 following the trigger (at 0 ms) was measured at approximately ±600 mV by graphical means. The background noise before the fire affected the noise levels, was ±25 mV. Therefore the increase in noise from the carrier signal leakage level to the fire-induced noise was approximated to:

$$dB = 20 \log \frac{600}{25}$$

$$= 27.6 \text{ dB.}$$

The affects of the carrier leakage "voltage" then had to be added. However, the actual background noise in the time domain could not be measured. Therefore the loss through the frequency spectrum information was approximately 1 dB plus the actual increase in level from the background noise to the carrier leakage "voltage".

9.4 SUGAR CANE FIRE UNDER THE TRANSMISSION LINE

The sugar cane was set up vertically in a scaffolding structure. An earth strap was attached between the structure and the nearest pylon (for a better earth). The cane was set alight. The progress of the flames was radioed through to the corona activity observer at Lepini substation

who then recorded any significant corona activity in accordance with the information supplied to him from the burn site.

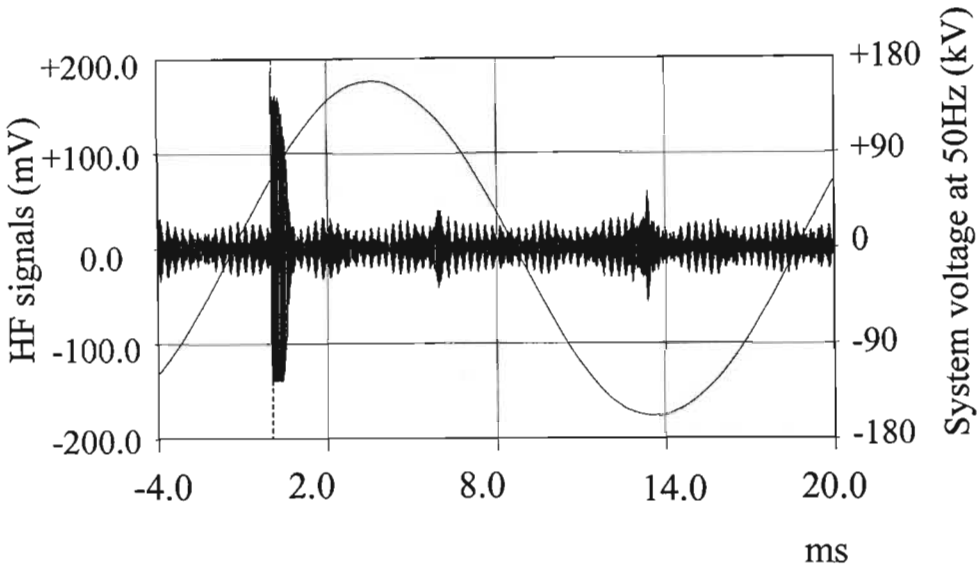

Figure 9. 10: Sugar cane fire under the center phase (cold condition).

The large burst observed in figure 9.10 was recorded with the information of a "cold burn" taking place. That is, the flames were low relative to the height of the conductors. A lot of smoke was present but due to the strong wind none of it came near the conductors and hence the probability of the corona activity being initiated by the presence of particles was excluded. The fire fluctuated over a reasonably long period and some thirty minutes later flames erupted from the smoke and the surge in figure 9.11 below was captured at a sampling rate of 10 MHz.

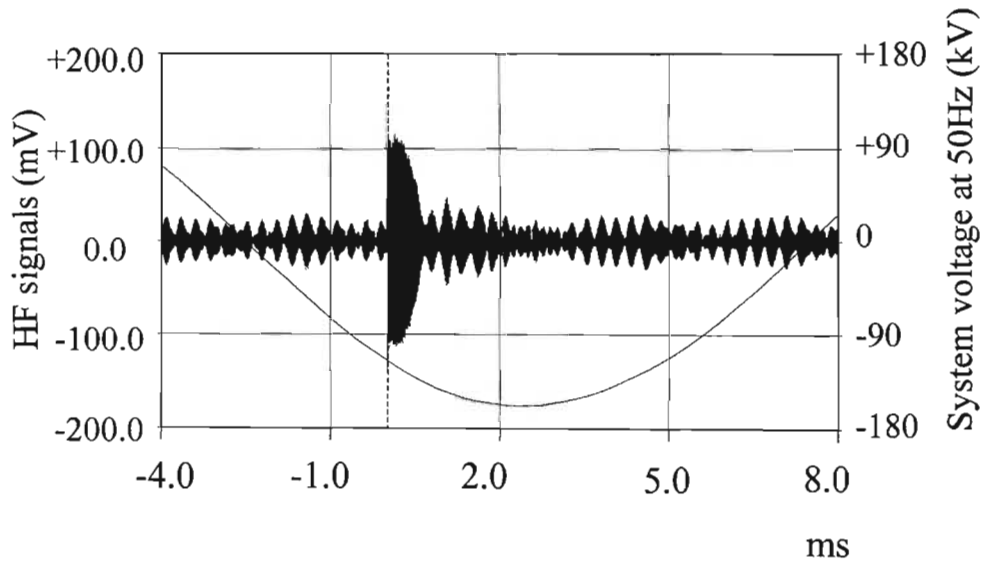

Figure 9. 11: Sugar cane fire under the center phase (matched flames present).

When comparing these bursts of noise with the spurious burst observed in figure 9.6, it was obvious (from our earlier findings of the affects of corona activity on the background noise levels), that the increase in noise occurred rapidly in accordance with that of induced corona noise and was therefore not characteristic of the unexpected surges observed from time to time. Positive recognition of these signatures would be possible.

9.5 GRASS FIRES UNDER THE TRANSMISSION LINE

Grass bales were used for this test. Failure to mount the bales for sufficient draft amplified the problems created by wind and only one set of data of any value was captured.

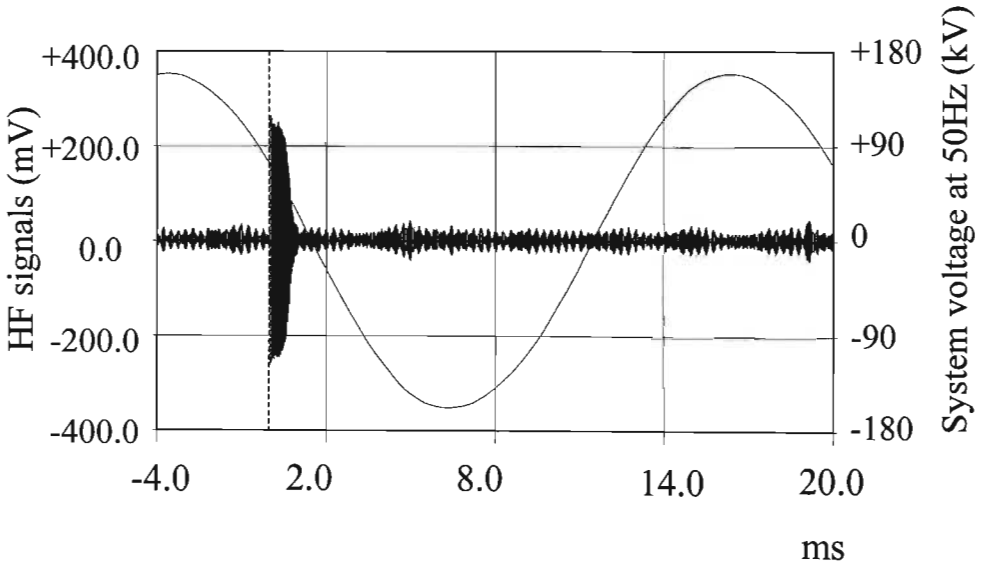

Figure 9. 12: Grass fire under the center phase (poor fire condition).

The flames were again well below the conductors with no particles reaching the height of the conductors due to the high winds. Only an intense heat was generated which may have influenced the generation of corona about the conductors. The almost instantaneous rise in noise level was again an indication that the noise generated was as a result of induced corona activity at the conductors.

9.6 AFFECT OF THE FILTERING CIRCUIT

The frequency spectrum of the background noise levels from the two BBC filters used were calculated from a segment of the data and is shown in the two graphs below.

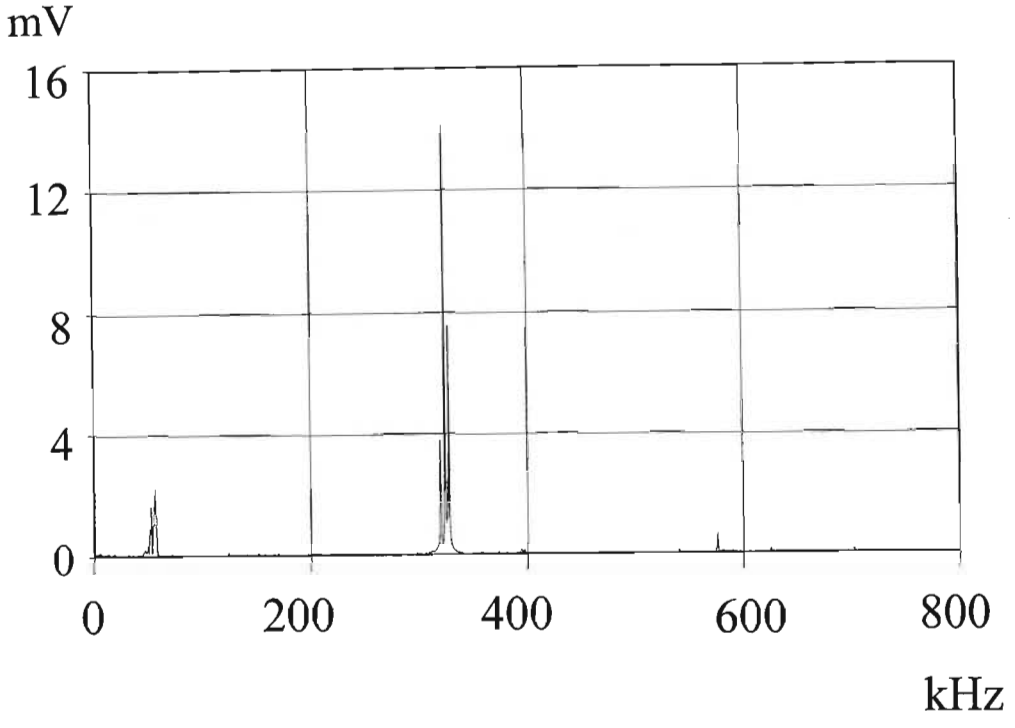

Figure 9. 13: Frequency spectrum of noise on the transmission line via a 52kHz filter.

The remainder of the carrier signal not attenuated by the 52 kHz filter was clearly seen breaking through the background level in figure 9.13 whilst the true background level of noise at the filter centre frequency of 52 kHz was determined at approximately 2.2 mV for the sample used.

The remainder of the carrier signal not attenuated by the 428 kHz filter was clearly seen breaking through the background level in figure 9.14. Due to the proximity of the filter centre frequency to the carrier frequencies both on the Craighall/Lepini line and the neighbouring lines, these signals leaked through. Higher levels were measured here (where the centre frequency is in fact at approximately 390 kHz) than at the 52 kHz centre frequency of the first filter. The carrier frequencies used on the Craighall/Lepini line was 320 kHz and 324 kHz with the stronger 324 kHz component being transmitted from Lepini substation where the measurements were being made. Therefore the 52 kHz filter was preferred. Another reason for the selection of only one filter was the limited data memory capacity on the digital storage oscilloscope used, which at

the time was considered to have the highest memory capacity on the local market. In addition, on a national level most frequencies used for the carriers are higher than 100 kHz.

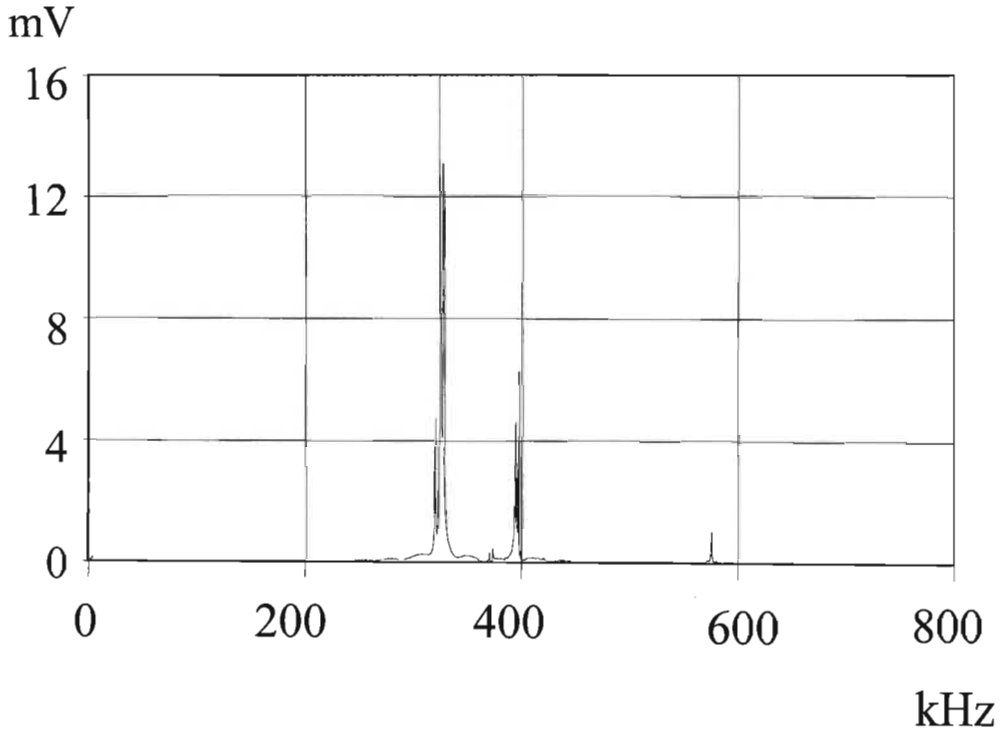

Figure 9. 14: Frequency spectrum of noise on the transmission line via a 428kHz filter.

9.7 SUMMARY

The relative increase from dry condition corona noise to that generated by a gas fire under a transmission line in the three phase power system was

$$27.6dB + 20\log\frac{carrier\_leakage(V)}{background\_noise(V)}$$

The relative increase from rain-induced corona noise to that generated for the same gas fire under a test section in the simulated single phase corona cage system was 48.09 dB.

Therefore it was assumed that the increase from background noise to the carrier signal leaking through the filter was less than 10.49 dB. As already previously discussed, under isolated conditions in the corona cage the magnitude of corona pulses generated in normally dry conditions was only marginally smaller than the rain-induced corona pulses. The relative increases in induced corona noise activity due to fires under a controlled single phase system or an operational three phase system were similar and at least of the same order of magnitude.

CHAPTER 10

Operational Lines – Sugar Cane Plantation Fuel

10.1 BACKGROUND

The two transmission lines selected from the main transmission system (MTS) were the Marathon – Komatipoort and the Avon – Impala 275kV feeders.

Planned sugar cane fires under the Marathon/Komatipoort 275 kV transmission line - with a twin Bear conductor bundle and a length of 115.65 km - usually occur approximately 40 km to 80 km from the Komatipoort substation. The Bear conductors have an overall diameter of 23.47 mm with 30 aluminium strands and 7 steel strands each with a diameter of 3.35 mm.

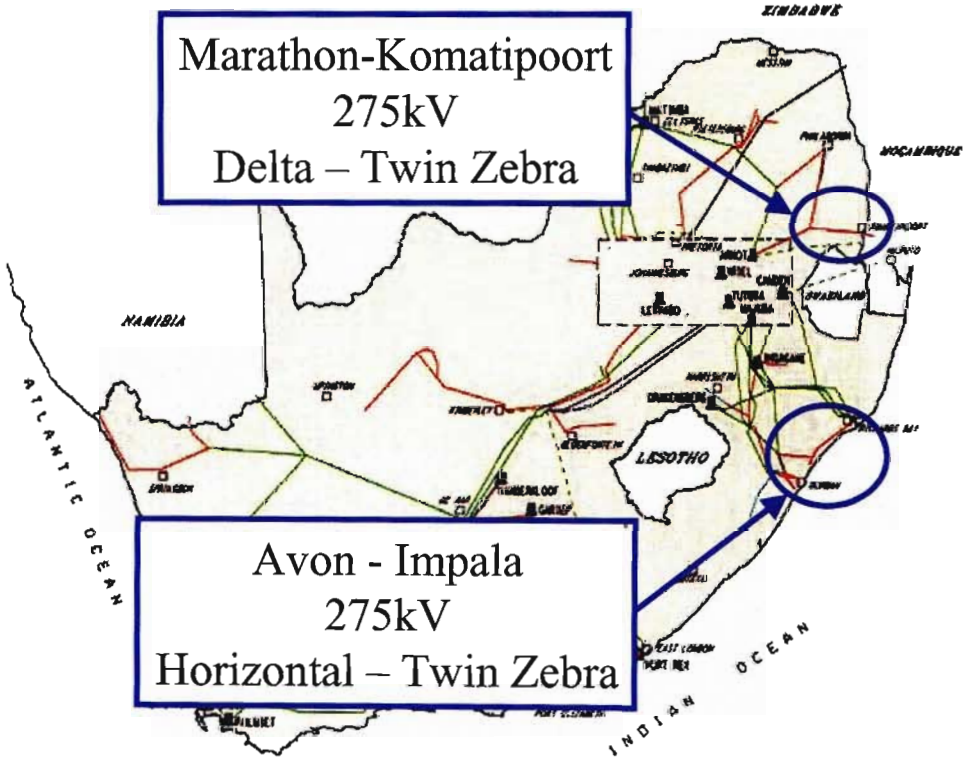

Figure 10. 1: Location of the two MTS transmission lines under test.

10.2. SUGAR CANE FIRE TESTS - MARATHON / KOMATIPOORT

10.2.1 Test Conditions And Results

Although the Marathon substation may be closer to the burn site in some cases, the radio communication link between the plantation and the substation was restricted by a mountain range approximately 30 km from Nelspruit. The additional benefit although a forced risk, is the confirmation that the fire-induced corona noise can be measured over the longer distances. In November 1992, induced corona noise from a planned fire was recorded at a distance of 70 km from the Komatipoort substation.

First phase proto-type detector testing was also carried out here. The digital storage equipment was preset to a trigger level, monitored for over 45 minutes to ensure that non-fire related noise would not trigger the measurement and then set to save the waveforms to disk as soon as they were captured, thereby ensuring no human error could interfere with the capture of the data.

An additional factor to consider was the protection of the supply to the measuring instrumentation. The auxiliary power supply integrity on substations across South Africa are not necessarily the same. The work done on the Craighall/Lepini line led to several flashovers occurring and the substation auxiliary supply adequately ensured the maintenance of the 50 Hz power supply within the station. The Komatipoort substation auxiliary supply was not so well protected and required a generator as an alterantive power supply to the equipment - to ensure that when a flashover occurred, the data in the digital storage oscilloscope's memory could be saved to a stiffy drive (external read/write memory). The available generator could not supply sufficient power to both systems and the risk of losing power on one unit had to be taken.

In addition to the substation measurements, a video camera was installed at the plantation to record the fire activity. Video recordings included time-stamping to correlate the fire activity with the corona noise measured at the substation.

In order to capture sufficient data to determine a trend in the induced corona activity, it was necessary to capture the data at a reasonably high sampling rate and for as long a period as possible.

While the sampling rate of 20 MHz was not extremely difficult to operate at, the maximum available memory for the captured waveform was an inhibiting factor. At the time the Nicolet 500 computer-controlled digital storage oscilloscope was not available and the quasi-computer controlled Nicolet 400 digital storage oscilloscopes shown in figure 10.1 below were utilised.

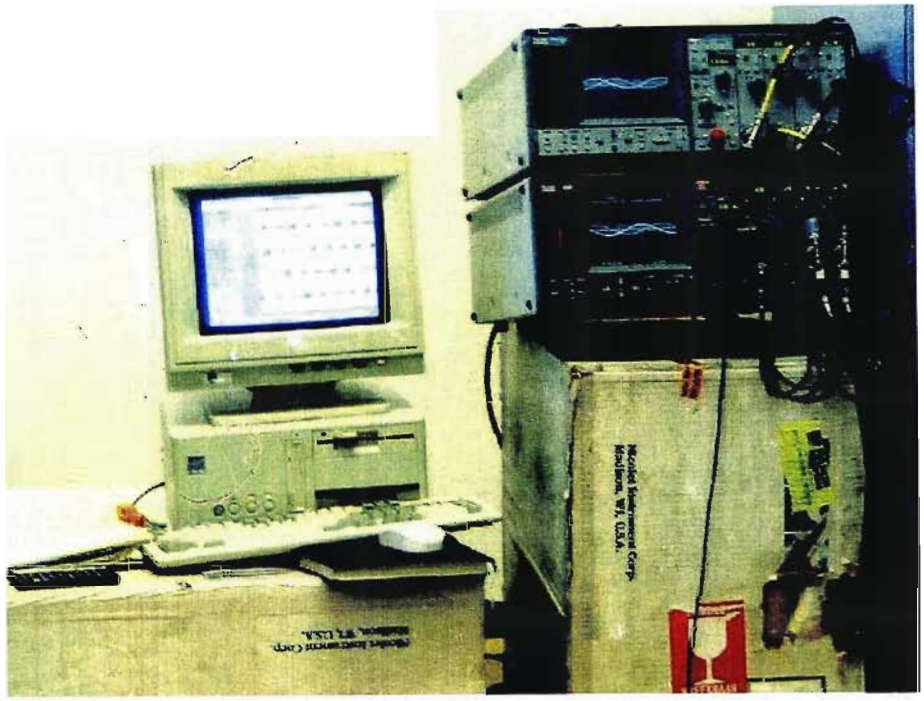

Figure 10. 2: Measurement equipment in the Komatipoort substation.

A maximum waveform capacity of 256 000 sample points per channel was available with these units. Two units were available and by cascading the triggering of each channel of the available eight channels, it was possible to capture a total of 100 ms, or five 50 Hz power cycles, of data from the time at which a trigger takes place.

By establishing the levels at which no trigger will take place due to other random noise sources before the controlled fire tests, the level for safe and determined triggering could be established. "Safe and determined" implies in our case - "if a trigger takes place coinciding with the presence of a fire about the conductors at the site of the burn, then such triggering will be as a result of the fire and not due to any other noise source occurring randomly at the same time" although some level of probability must still be considered if a strange and unrecognised level of activity does take place.

The following work was performed in Mpumalanga in conjunction with the Eskom Telecommunication staff from the region and the farmer owning the plantations.

Due to the findings in the tests of the previous section an active filter, used in conjunction with the passive BBC filter was added forming part of the prototype detector developed from this work, to eliminate the carrier signals which were present on the transmission line.

The plantation to be burnt was situated some 70 km from Komatipoort substation where the equipment was set up for monitoring the corona noise levels. As the burning usually takes place either very early in the morning or late afternoon - in order to minimise the probability of a runaway fire developing - the fire was scheduled to start at 16h30. At 16h28, a temperature of 31 C and a relative humidity of 43 % was recorded at Komatipoort with clear weather conditions recorded for the entire length of the transmission line.

Figure 10. 3: Delta configuration 275kV twin Zebra Transmission Line.

Figure 10.3 above shows the site of the transmission line crossing sugar cane plantation to be burnt. The thermal video camera was positioned on top of the water tank visible in the photo to record fire temperatures. The twin Zebra conductors in the bundle are visible in the Delta configuration with two phases of the feeder directly above each other and the third separated off to the right midway between the other two.

At approximately 16h50 the fire was started and with the aid of handheld and vehicle radios the progress of the fire was continuously reported back to Komatipoort substation. Figure 10.4 below shows the development of the fire.

Figure 10. 4: Sugar cane fire approaching the transmission line.

At 16h56 the first significant noise activity (shown in figure 10.5 below) was recorded on the transmission line.

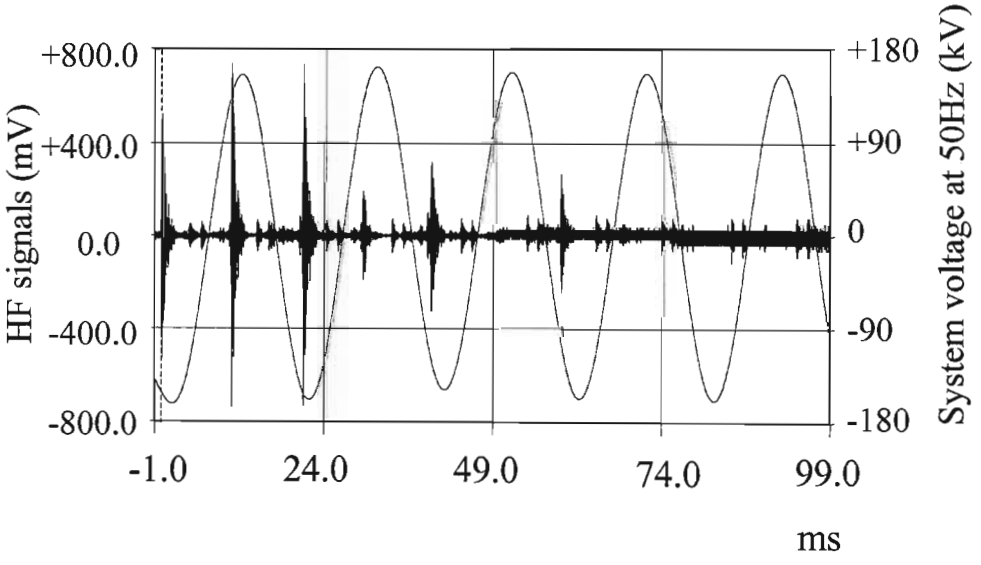

Figure 10. 5: Sugar cane fire induced corona noise activity.

As only a 5% pre-trigger was set on the first channel, only 1 ms of information was recorded before the trigger occurred. The corona activity was quite apparent in both positive and negative half-cycles. At the time, the fire moved away from the conductors and no further such vociferous activity followed immediately.

Some five minutes later, the fire moved back towards the overhead power line (progress shown in figure 10.5 above) and at 17h01 a flashover took place shown in the photo in figure 10.6 below. The photo below was captured using a Minolta Dynax 7000i with high speed shutter enabled to 3 photos per second. The high audible corona activity was used as an indicator by the cameraman to start taking photos. Of the three photos taken at the time of the flashover, only the photo shown in figure 10.6 held evidence of the fault.

Figure 10. 6: Sugar cane fire flashover.

The electrical breakdown of the air gap was phase to ground with the arcing current travelling through the flames and particles to ground in the plantation.

The data shown in figure 10.7 below was recorded on one storage oscilloscope at the time the air gap was bridged with the arc. The second oscilloscope was disabled due to loss of power supply in the substation.

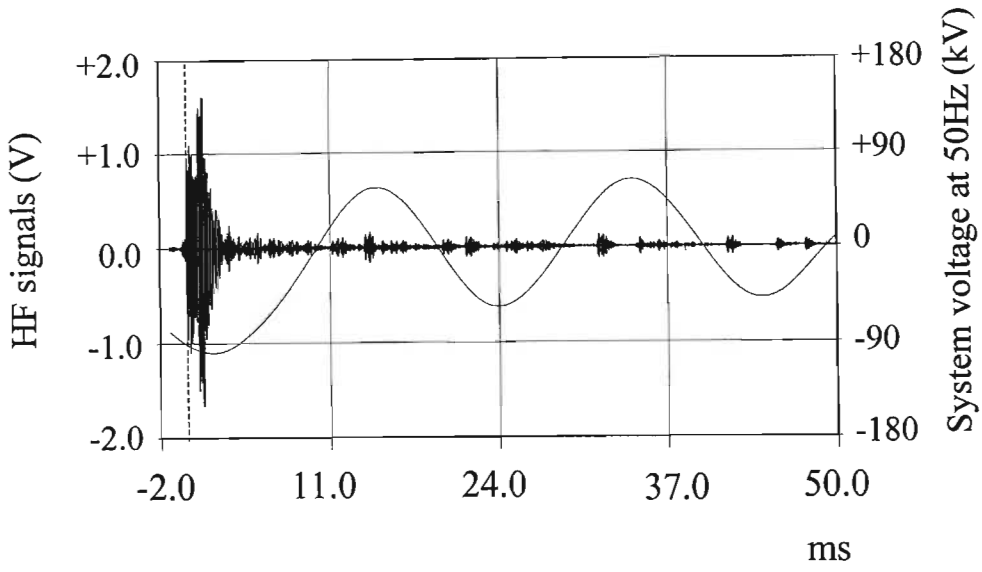

Figure 10. 7: Sugar cane fire induced noise activity at time of flashover.

Exactly what occurred on the channel between the two captured events of figure 10.5 and figure 10.7 was uncertain as the digital storage oscilloscopes were occupied with the task of transferring data from the memory registers to external memory (stiffy drive) storage. This was one of the main setbacks of having neither sufficient memory available nor fast downloading facilities.

From 17h29, several spurious bursts of noise of large amplitude were observed. The electricity control centre for Mozambique in Maputo reported that they were experiencing severe over-voltages from the South African supply at about the same time as these measurements were recorded. It seemed apparent that the bursts were therefore as a result of the over-voltages. The surge down the line inevitably pushes the voltage up above its normal design levels. At the point at which the voltage rises above those stress criteria, the increased gradient on the conductors would then result in the increase in local fields over the entire length of the bundle at the points along which the surges are travelling. The local fields would rise above the critical field at which ionisation by electron impact takes place and corona would be initiated.

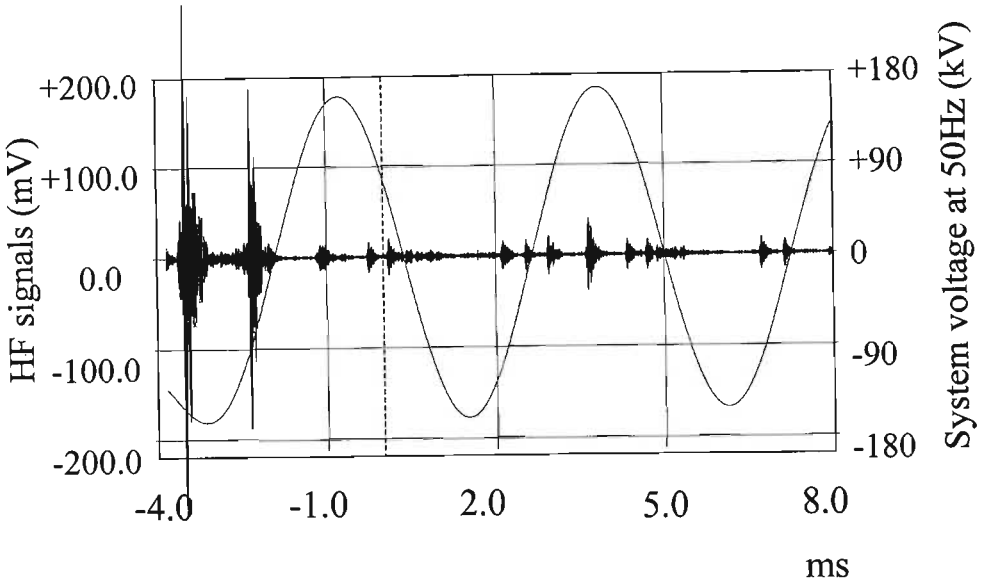

Figure 10. 8: Induced corona noise due to over-voltages on the transmission line (1).

At 17h35, the following burst was observed.

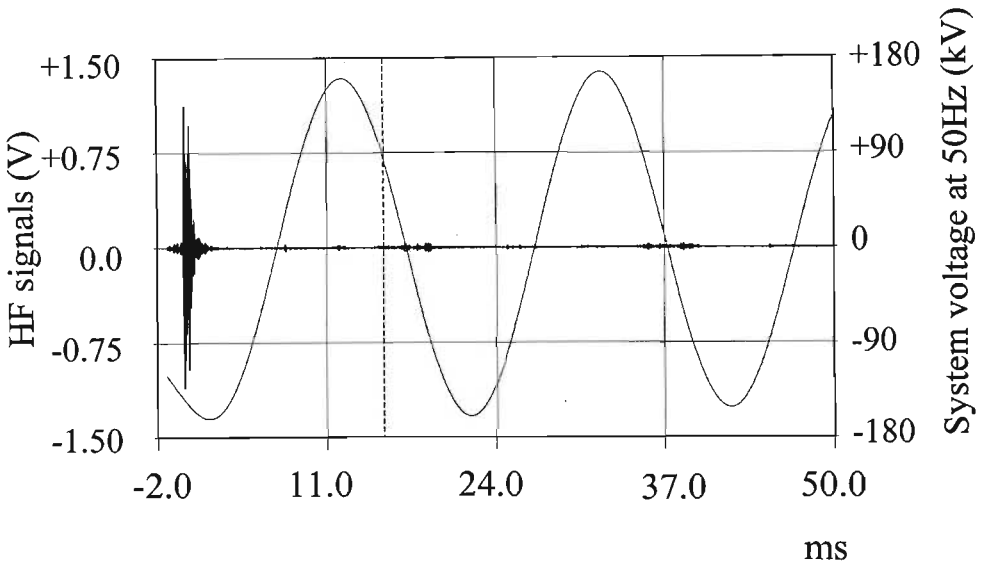

Figure 10. 9: Induced corona noise due to over-voltages on the transmission line (2).

In figure 10.9 the induced corona activity seemed to have been extinguished over the first cycle implying that the over-voltage (not clearly discernable in the 50 Hz waveform shown) existed for not more than that single cycle (that is, less than 20 ms).

At 17h39, the following burst was observed.

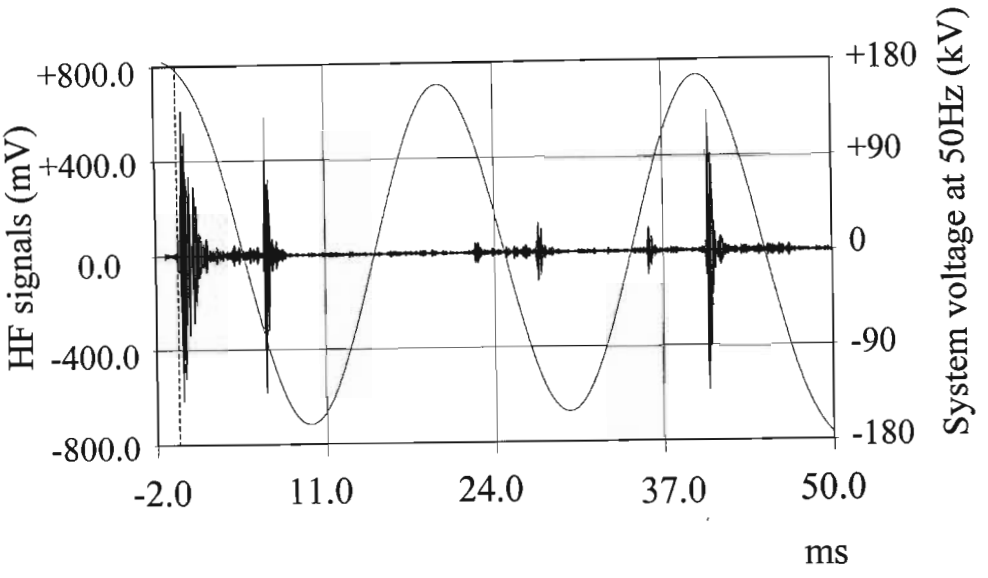

Figure 10. 10: Induced corona noise due to over-voltages on the transmission line (3).

In figure 10.10 the induced corona noise activity persisted for a longer period but the peak values of the pulses were smaller than previously experienced. This information was consistent with high voltage surges which are at first large but are of short duration and then the following surges are smaller in amplitude and are longer in duration. The corona activity should have and did reflect this phenomena provided the over-voltage occurring was large enough to ensure that the local field was larger than the critical field for ionisation by electron impact to occur.

10.2.2 Cane Fire Test Results Analysed

10.2.2.1 Fire Induced Corona Burst

The active filters included as a second stage before measurement took place, significantly attenuated the carrier signals present on the transmission lines (including neighbouring carriers). Some attenuation in the passband also took place and in order to emphasise the corona generated signals in the passband, a small component of gain was added to the active filter design.

A limitation of the results was the necessity to set a high trigger level and as such a high level selection for the dynamic range. As previously discussed, an extensive amount of approximation was required to determine the actual increases in noise occurring from rain and dry conditions to

the fire-induced noise levels developed. The main reasons for this was the low level of dynamic range selected. In order to accurately measure the maximum signal levels present on the transmission line due to the fire, a repeat of previous measurement methods was avoided. The limitation arising as a result of the high trigger levels was the limited description of the development of the sugar cane fire-induced corona noise activity up to the peak noise level generated. If the trigger level was set to a lower voltage, a larger portion of the corona development would have been captured. A limited percentage (up to a maximum 100%) of the first channel was available for pre-trigger data. The additional cascaded channels could therefore not be utilised for pre-trigger data.

The signal burst in the first positive half cycle of figure 10.5 was expanded in figure 10.11 below. The background noise was measured at approximately 15 mV while the fire induced corona currents produced voltage peaks of the order of 737 mV.

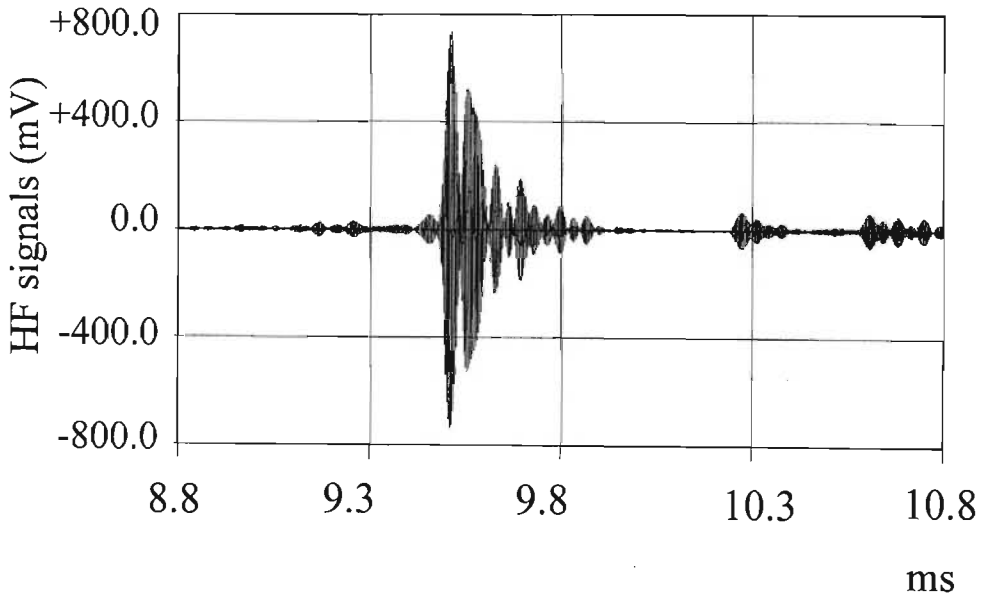

Figure 10. 11: Expanded view of the sugar cane plantation fire induced corona noise.

Therefore for the sugar cane plantation fire under an operational transmission line, the minimum increase in directly measured noise was

$$dB_{direct} = 20Log\frac{737}{15}$$

$$= 33.83 \text{ dB}$$

This value can be directly compared to the 27.6 dB obtained for the gas fire tests.

10.2.2.2 Background Noise Level

An expanded view of the background noise in figure 10.12 below revealed the enveloping affect of a carrier signal. However, from figure 10.13 below, it was clear that the "carrier" observed was in fact the influence of the bandpass filter circuitry.

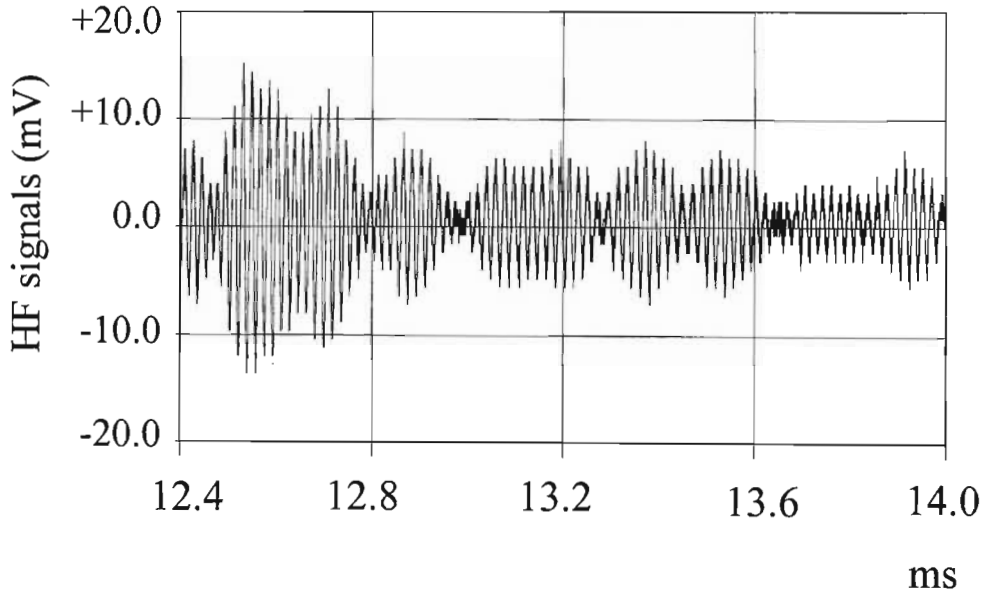

Figure 10. 12: View of the background noise only.

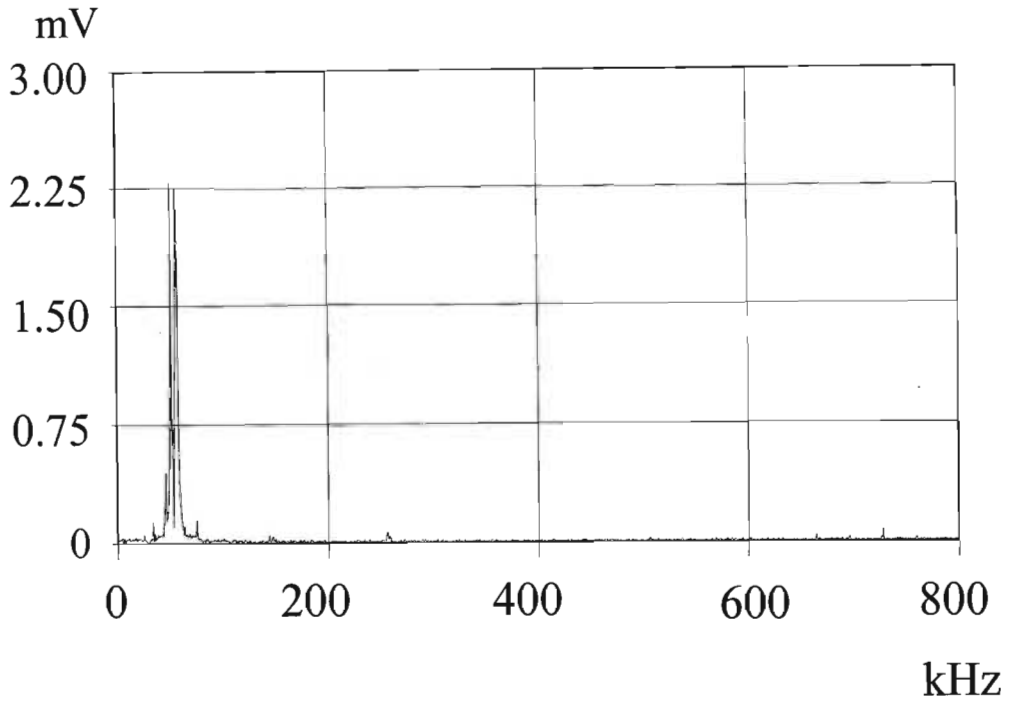

Figure 10. 13: Frequency spectrum of the background noise.

The frequency spectrum in figure 10.13 above showed the strong component at approximately 52 kHz and with the given sample period and time between points (of 100 ns), the amplitude of the noise at this frequency was 2.253 mV.

10.2.2.3 Fire Induced Corona Characteristics

The corresponding sample of the fire-induced corona activity had a similar noise pattern at higher amplitudes. The noise which passed through the filter appeared in strong bursts and seemed to be due to additional factors not present in the background noise. The first seven packets from figure 10.11 are shown in figure 10.14 below.

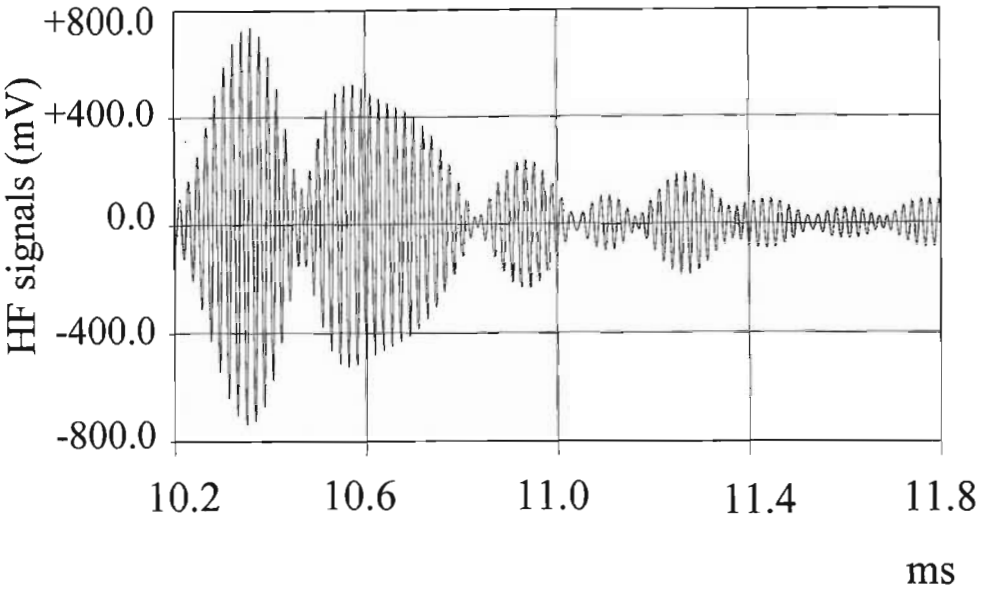

Figure 10. 14: View of the fire induced noise only.

The frequency spectrum was also calculated for 100 ns intervals between points and the same sample period as that of the background noise calculation and is shown in figure 10.15 below. The maximum amplitude of the noise calculated at around 52 kHz with the fire-induced noise component present in the sample space, was 130.87 mV.

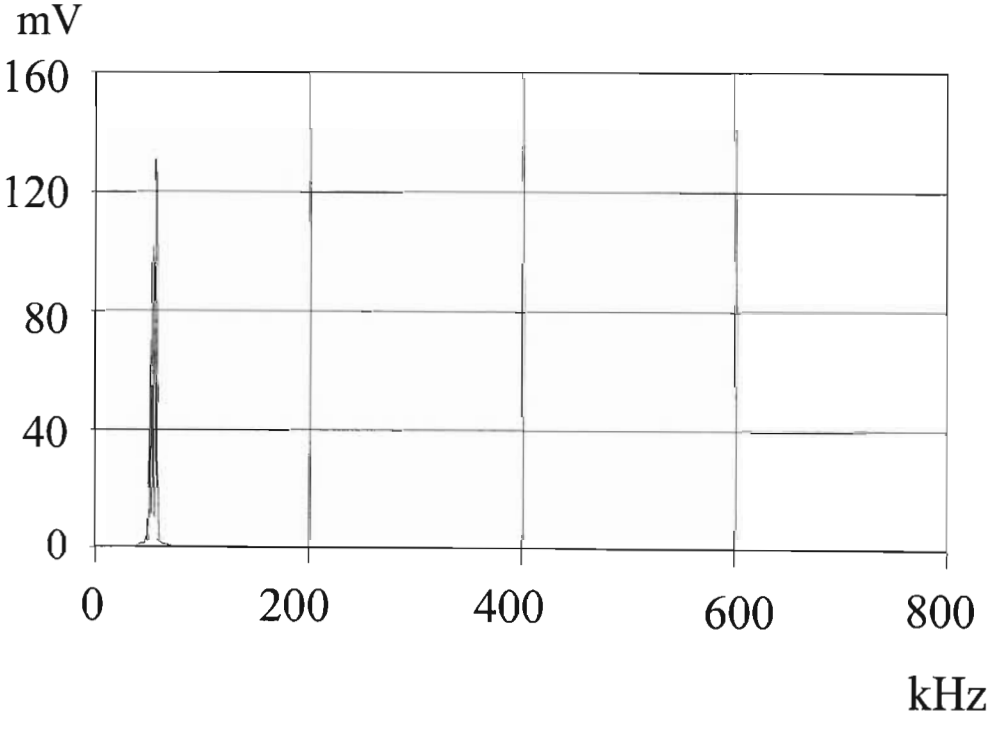

Figure 10. 15: Frequency spectrum of the cane plantation fire induced corona noise.

$$dB_{spec} = 20Log\frac{130.87}{2.253}$$

$$= 35.28 \text{ dB}$$

The increase in induced corona noise from dry conditions to fire conditions was approximately the same whether calculated directly from captured data or from the relevant frequency spectrum data [$dB_{direct} \approx dB_{spec}$].

The main factor creating the increase in noise levels of the 52 kHz component was the induced corona impulses which were essentially modulated up to 52 kHz. For each pulse or streamer induced from the overhead transmission line, a series of burst packages were measured through the tuning equipment. The implication was that for every pulse or streamer generated in the corona cage under any conditions, the method of measurement and the existing constraints in the operational environment dictated that the induced corona would generate a burst of noise in the form of a modulated "carrier" signal. The carrier was the passband frequencies of the filtering or tuning circuit and the modulation information was the induced corona pulses generated by whatever sources on the line.

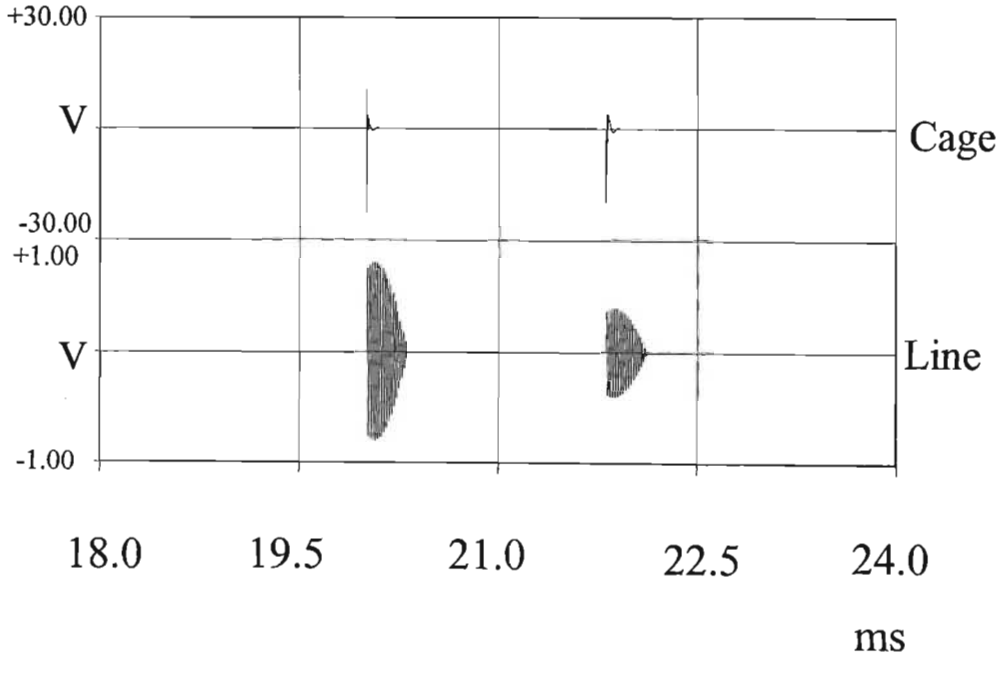

Figure 10. 16: Corona cage induced noise vs transmission line induced noise.

Therefore the number of streamers created by the sugar cane fire, rain or any other conditions could be expected to be converted to a burst package as illustrated in figure 10.15 with the comparison to the corona cage data. For a consecutive series of streamers that occurred rapidly, the envelope of the burst package either fluctuated according to the streamers existing or overwhelmed them depending on their size. This hypothesis will need further research work and may be dependent on the variation in tuning equipment through which the measurements are done.

The level for "safe and determined" triggering was adequate to detect the fire-induced pulses over the distance of 70 km from point of origin to the substation point of detection. The overvoltage reaction of the system occurring thereafter was analysed as "a strange and unrecognised level of activity". The presence of burst packages after the sugar cane fire had dissipated clearly indicated "a strange and unrecognised level of activity". With the aid of the radio communication made between the Maputo control centre and the South African regional control centre, it was possible to identify the source of these unexpected burst packages. With adequate analysis and sufficient additional information, the source of other strange and unrecognised levels of activity may also be identified.

10.3. SUGAR CANE FIRE TESTS - AVON / IMPALA

10.3.1 Prototype Detector Modifications

Fires may be detectable from a distance of at least 70km from a substation as was shown from the operational results obtained in section 10.2.

The passive filters used in those tests were considered to be a limitation and an active filter was designed to replace the passive filter to produce a passband with a sharper roll-off to eliminate more of the carrier signals present on the transmission line. This design work was done by a team of Eskom research personnel of which the author was a minor contributing member. Special appreciation must be expressed for the efforts put in by the task leader Pat de Klerk and the design technician, Carl van der Berg. Figure 10.17 below defines the passband characteristics of the new active filter.

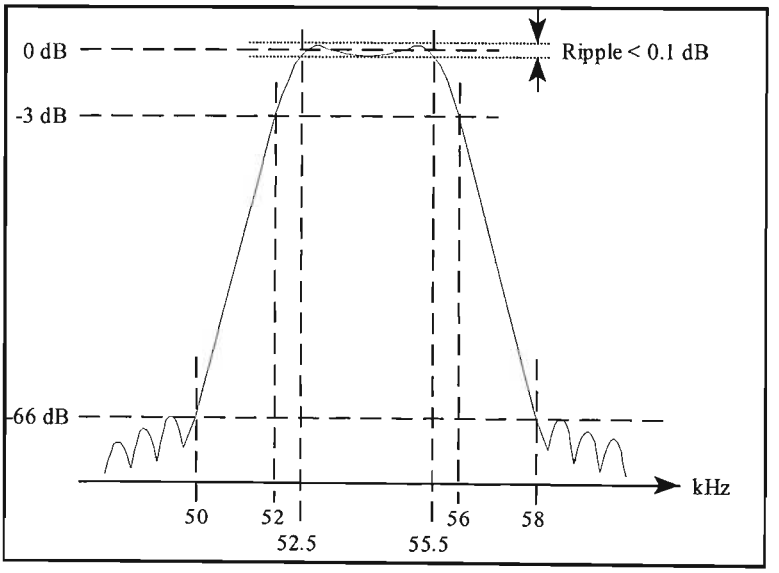

Figure 10. 17: Narrowband 16th order elliptic filter.

10.3.2 Test Equipment Set Up

A considerable portion of the Avon / Impala 275kV transmission lines cross over sugar cane plantations. A series of controlled burns were planned for the 3rd of August 1997 approximately 10km from Avon substation. Details of the tests have been prepared by the author and documented in the power utility's research archives [39]. Figures 10.18 and 10.19 below show

the block diagrams of the testing circuits from the existing power network to track the new detectors capabilities and to record more electrical discharges induced by the presence of the sugar cane fires.

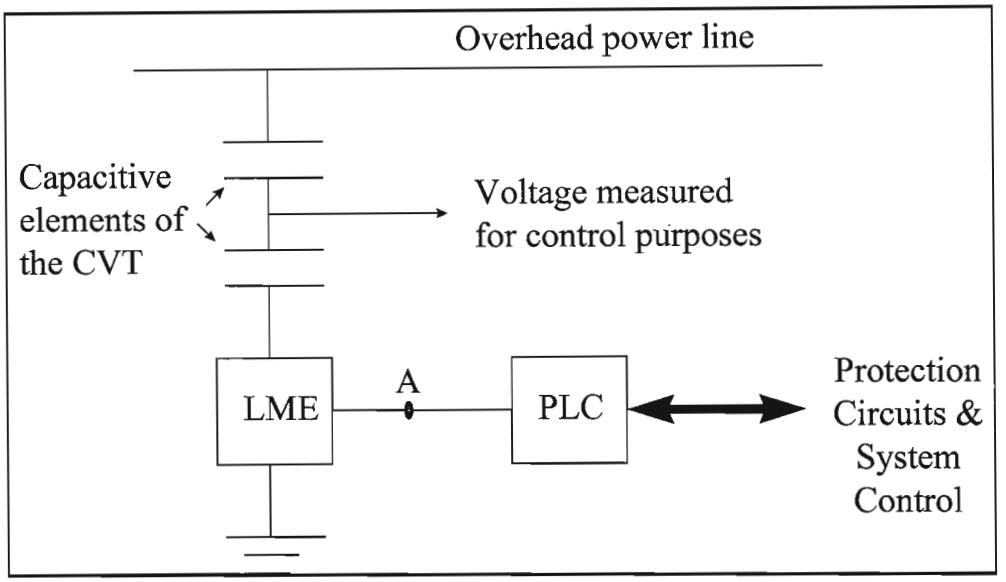

Figure 10. 18: Access to the power system.

Review chapter 8 for more detail on the access circuits.

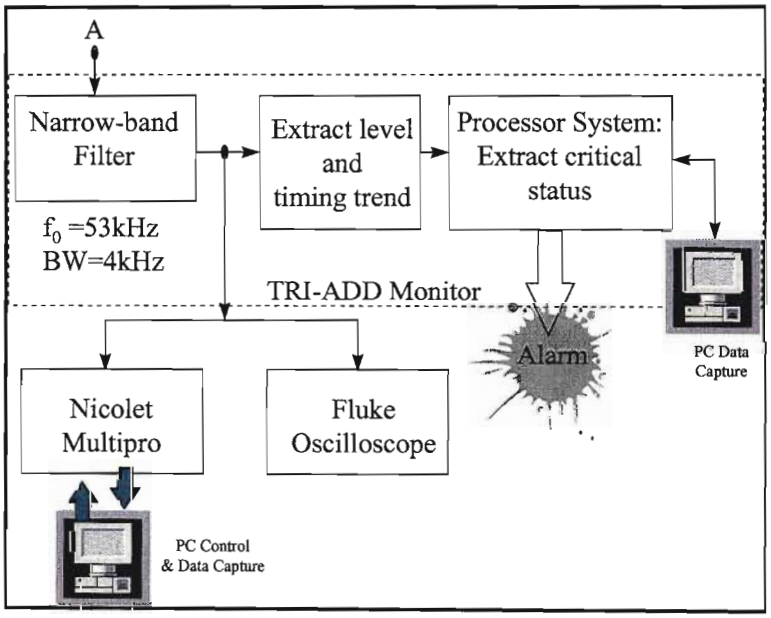

Figure 10. 19: Test Equipment Configuration.

The point A on the block diagrams above are common and indicate the point in the substation control room cabinets linked to the incoming signal shown in figure 10.20 below.

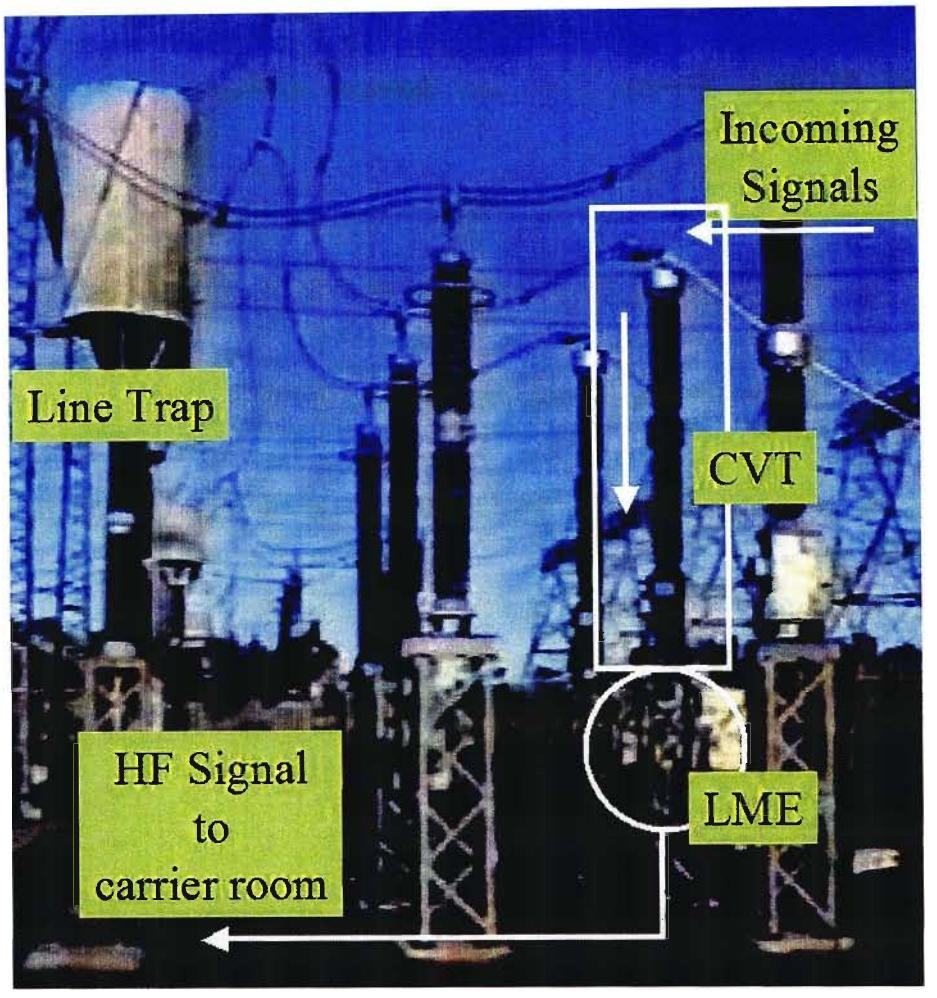

Figure 10. 20: High Voltage apparatus in the substation 275kV yard.

The new narrow-band filter discussed in section 10.3.1 above was included in the interface to the newer Nicolet MultiPro digital storage oscilloscope for review of the individual induced corona pulses from the fires. A second oscilloscope (Fluke analogue oscilloscope) was installed to obtain a view of any activity which may take place whilst the Nicolet is processing any incoming data.

The details of the following stages of the detection device has been documented in other Eskom reports and does not form part of the dissertation [40].

The equipment was set up as shown in figures 10.21 and 10.22 below.

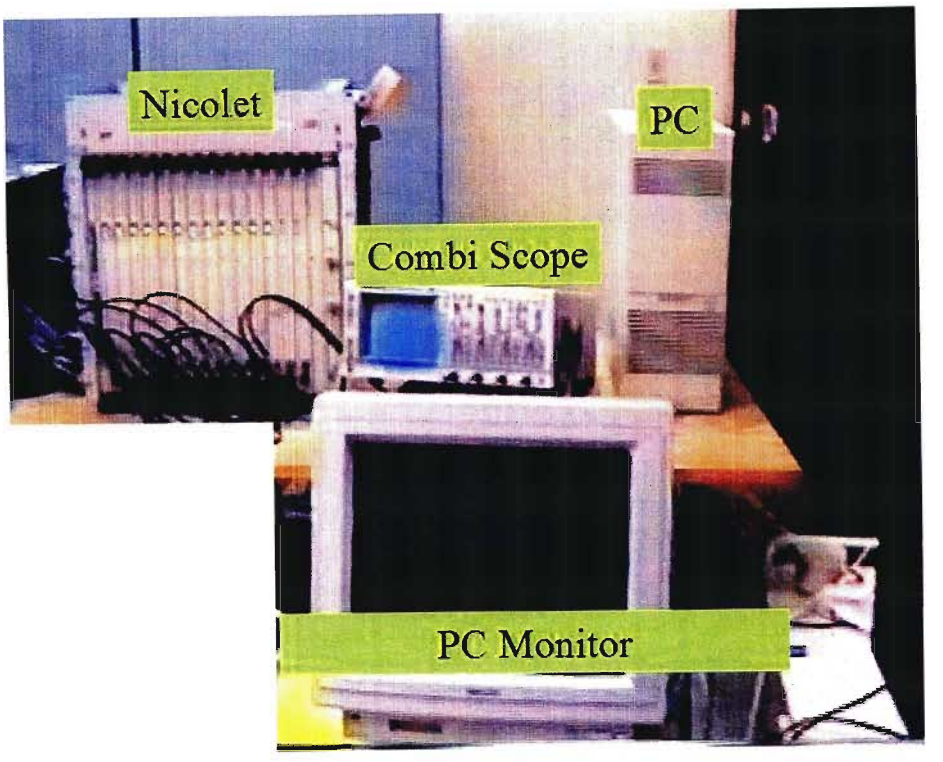

Figure 10. 21: **Digital Storage Oscilloscope with analogue oscilloscope backup.**

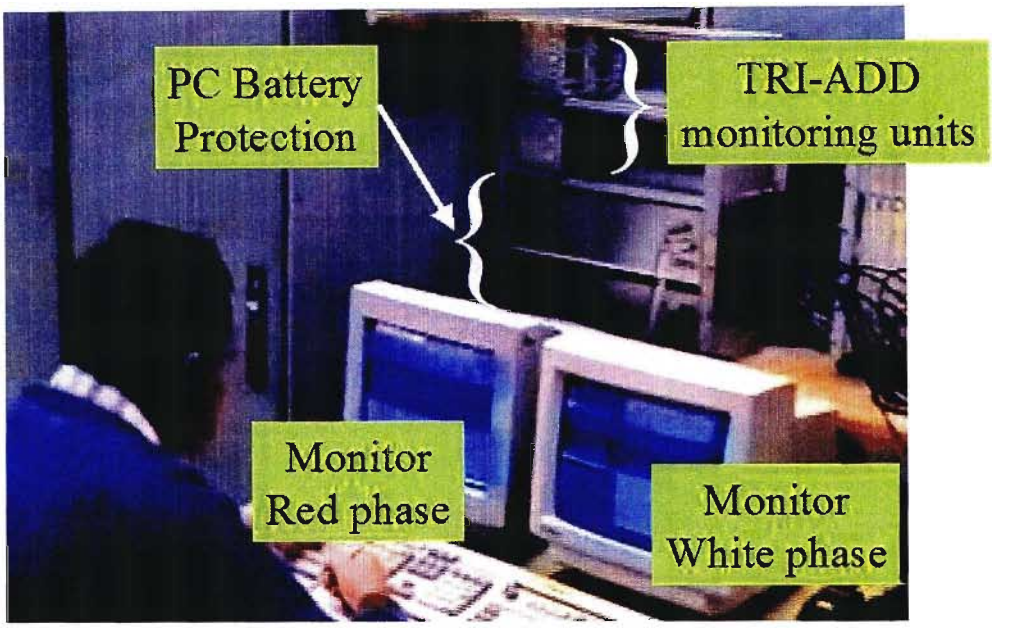

Figure 10. 22: **Detection system with developer in position for the fires.**

10.3.3 Fire Testing Conditions

A total of three fires were arranged with the farmer who generously separated the plantation into segments which could be burnt as separate fires from one plantation.

Figure 10. 23: Separated plantations for two arranged Eskom fire tests.

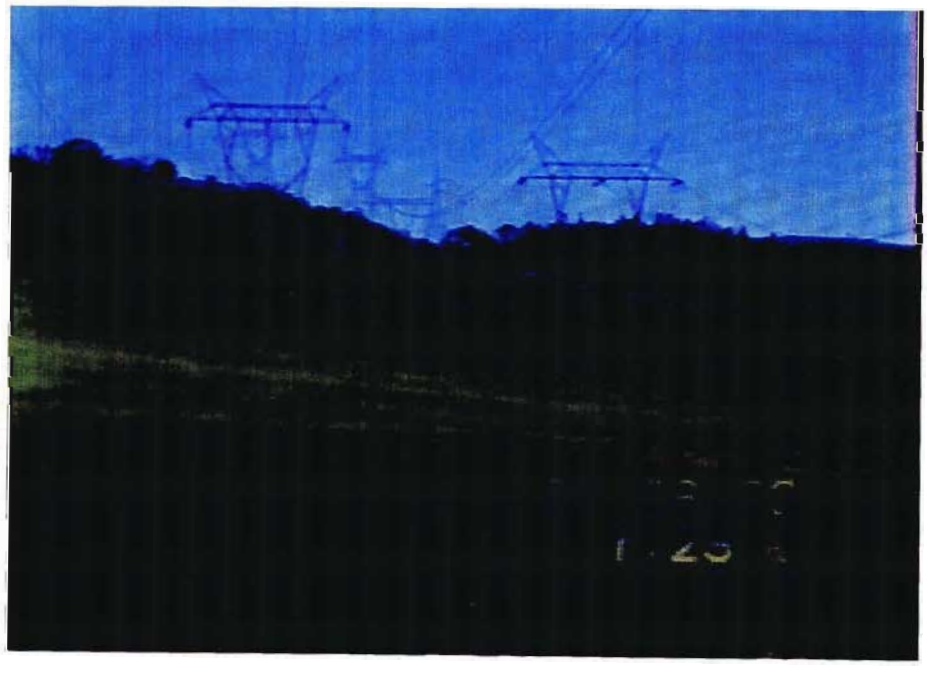

Figure 10. 24: Third plantation for arranged Eskom fire tests.

The following figures are photos from each of the three planned and controlled fires.

Figure 10. 25: First controlled fire.

Figure 10. 26: Second controlled fire.

Figure 10. 27: Third controlled fire.

In order to adequately record the fire conditions at the conductors, several video cameras and a thermal video camera were used to document the progress of each fire. In figure 10.28 below, a cameraman was located in a raised platform to record the fires.

Figure 10. 28: Personnel on site to record the fires.

A fire-induced flashover took place during the second fire and the following photos show a sequence of the incident.

Figure 10. 29: Cane fire induced breakdown sequence in fire 2.

The following figure contains temperature readings captured during the fire tests.

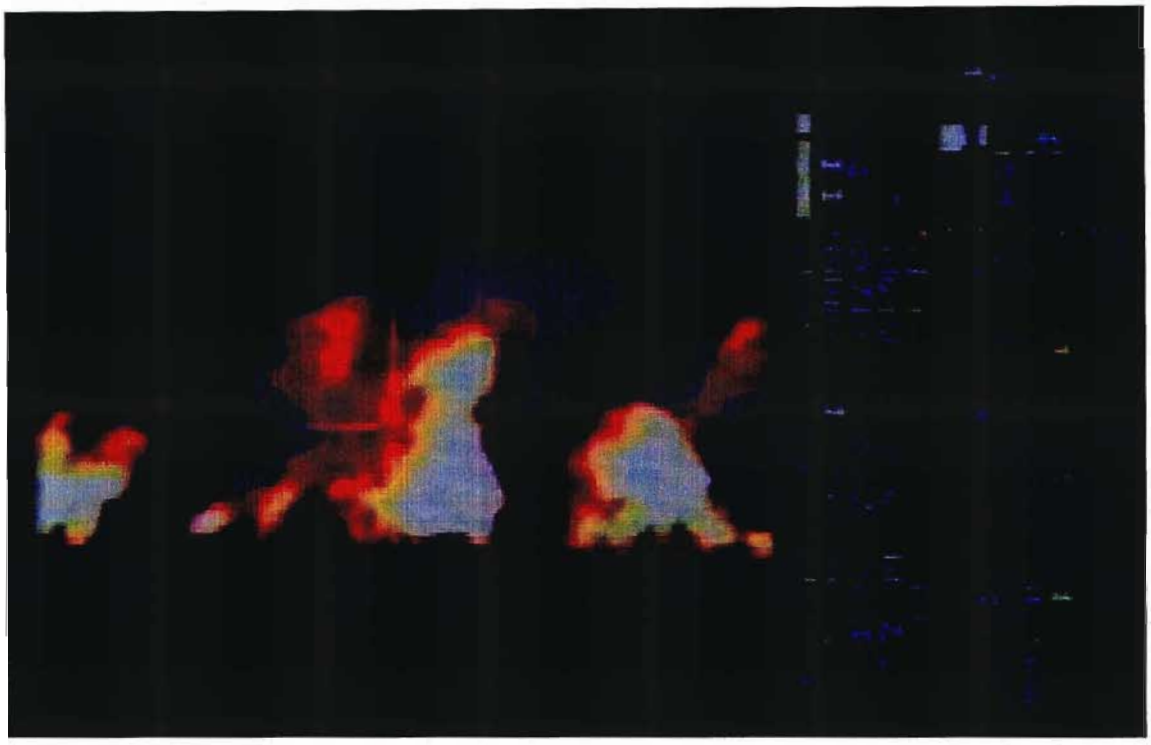

Figure 10. 30: **Thermal readings from the cane fires (1025°C at the cross hair).**

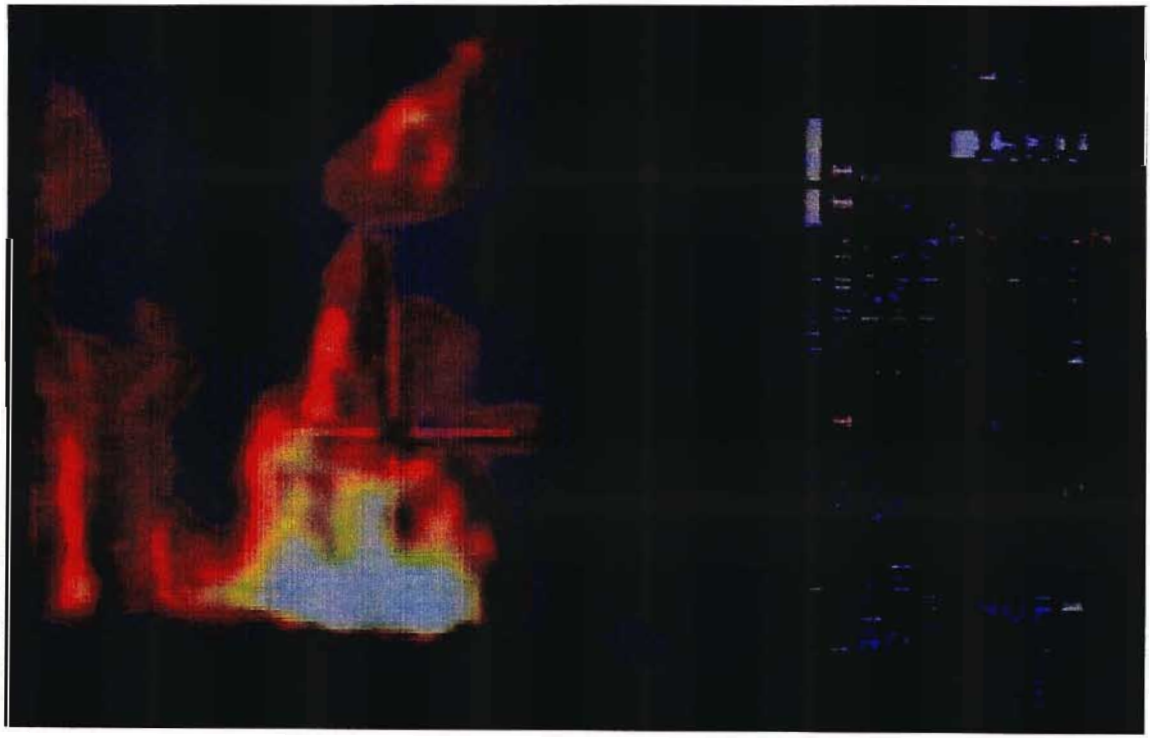

Figure 10. 31: **Thermal readings from the cane fires (1531°C at the cross hair).**

From figures 10.30 and 10.31, several momentary temperature readings were recorded above 1000°C at the overhead conductors indicating that some thermal ionisation may be possible during the ionisation process.

10.3.4 Fire Testing Results

Several additional monitoring systems were installed for these tests and were used to verify the presence of electrical discharges from the fires and which were observable at the substation 10km from the fire testing site.

10.3.4.1 RMS Level Detection

An RMS level detection scheme was prepared and is illustrated in figure 10.30 below.

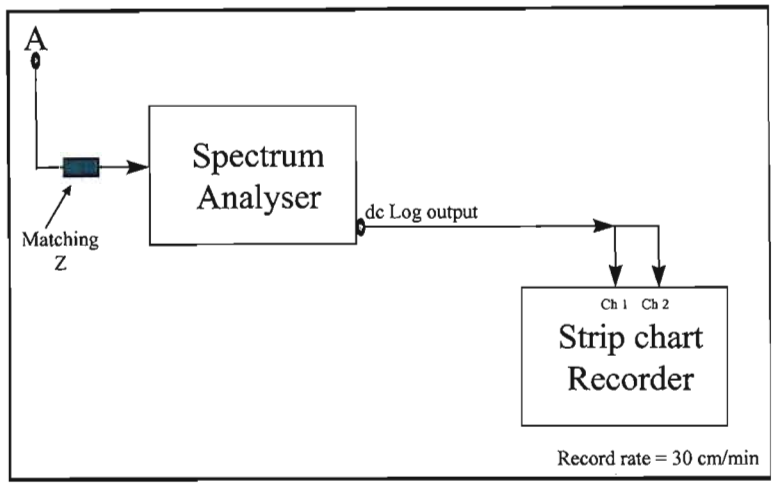

Figure 10. 32: RMS level detection block diagram.

Point A in the above block diagram matches that shown in figures 10.18 and 10.19 with the spectrum analyser therefore in parallel with the narrow band filter described in figure 10.19.

The details of this test method are described in an Eskom research report and special thanks must go to Tony Britten for his support in preparing this test set up [41].

From this measurement, several instances of electrical activity was detected coinciding with the presence of the fires under the power lines. Some of the data is shown in the figures below.

Although it has been shown from the corona cage research work that this type of measurement is not an optimum technique to detect fires, it does confirm the presence of significant electrical activity which we could correlate to a fire by the video footage of the fires.

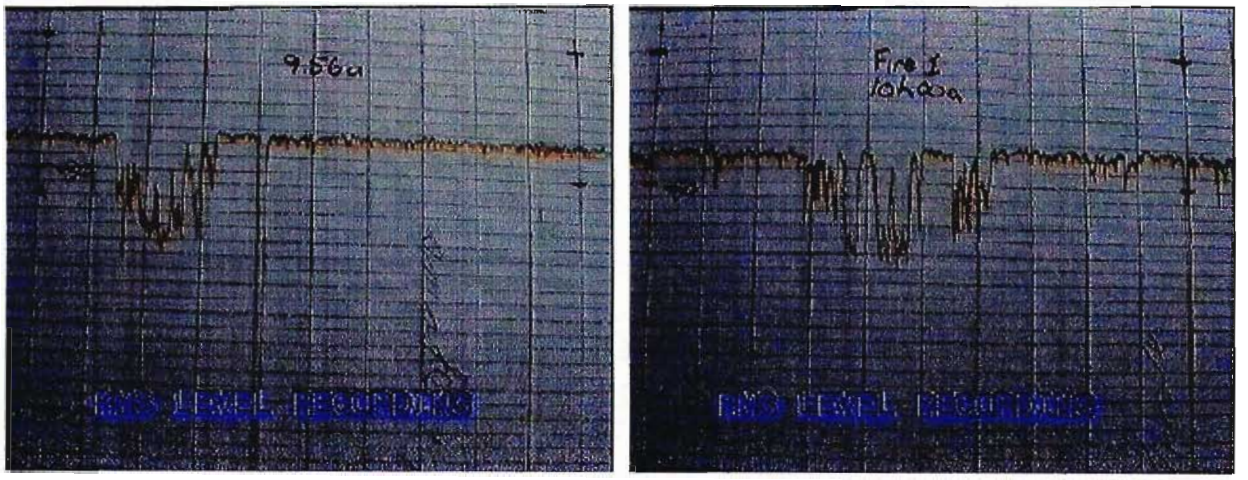

Figure 10. 33: RMS level detection - induced electrical activity (fire 1).

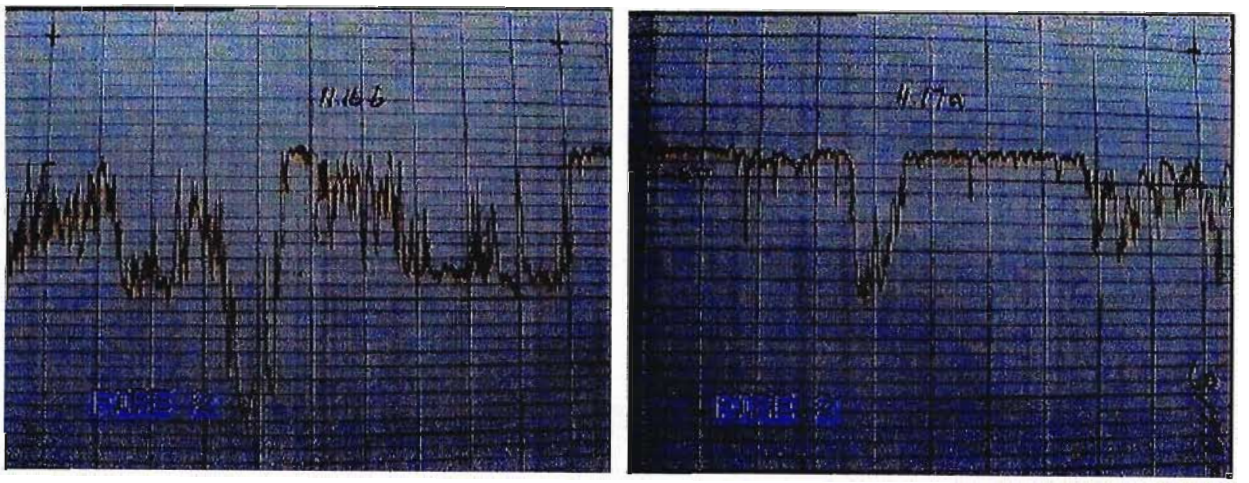

Figure 10. 34: RMS level detection - induced electrical activity (fire 2).

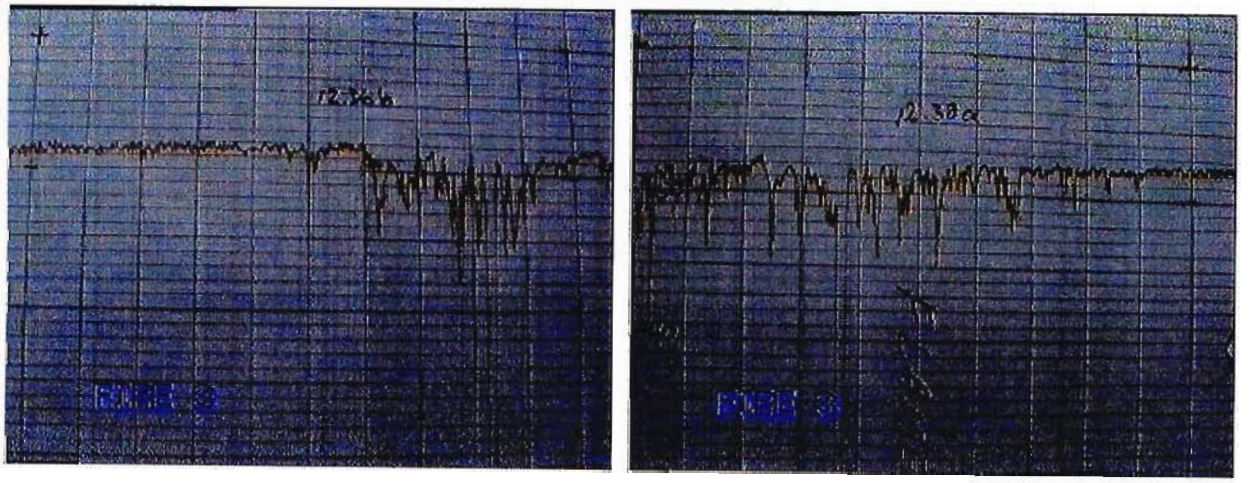

Figure 10. 35: RMS level detection - induced electrical activity (fire 3).

10.3.4.2 Fire Test Results (Time Domain Dominant)

No fire induced electrical discharges were observed in either the Nicolet DSO or the TRI-ADD detection unit.

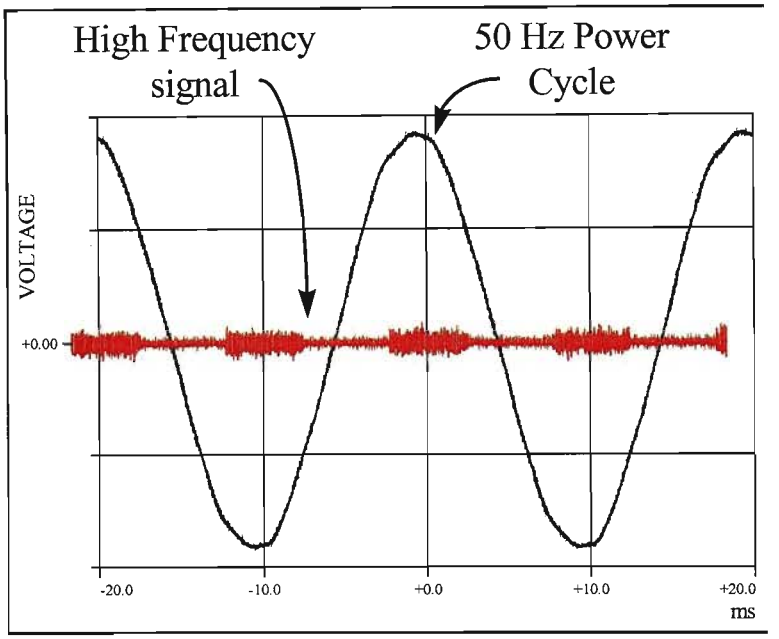

Figure 10. 36: Pattern recognition measurements.

The electrical activity observed in figure 10.34 above do not correlate to the presence of the sugar cane fire but rather show steady state background signal levels which may exist as a result of some other plant related partial discharges or normal operating conditions.

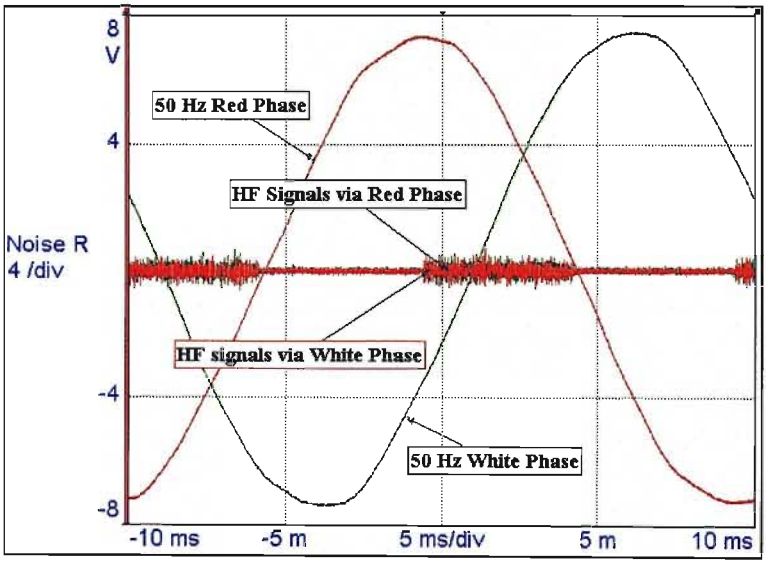

Figure 10. 37: Pattern recognition measurements – two phases.

There were two phases on the feeder equipped with monitoring equipment and figure 10.35 shows the data from the two inputs. By superimposing the two inputs, the source of electrical

activity can be seen at both inputs and it can be concluded that this data is being generated from the same source.

However, no fire induced electrical activity was recorded from any of the three fires. Reviewing the results from the RMS level detection circuit, the signal amplitudes measured, the lack of data from both the systems connected downstream from the 16^{th} order elliptic filter, the conclusion was that the devices should have picked up the activity from the fires. The fire amplitudes were large enough to produce significant RMS voltage fluctuations. The error was determined to be present in the new filter design. After investigating the design parameters and testing the unit with high speed transients, the response time of the electronic components used in the device was identified as the problem. Pulses with a high enough repetition rate remain present on the system and pass through the filter. Pulses that exist in isolation (as has been repeatedly observed in earlier fire testing) rise and fall before the filter can respond to the changes.

10.4 OPERATIONAL LINES PLANTATION FUEL SUMMARY

The research work performed in the transmission network was broken into two phases. Firstly, a short transmission line was identified for testing and fires were created under this line. This made it possible to "control" the environment during the tests. A gas fire, sugar cane fire and a grass fire test was performed. In all cases fire-induced corona activity was recorded and hence was detectable.

Secondly, with the co-operation of the field staff and sugar cane farmers, four sugar cane plantation fires under 275 kV transmission lines were monitored and fire-induced corona noise was detected. With the original passive filters, high frequency signals were captured from the fire 70 km from the substation. Most transmission lines are shorter than 140 km in length and with the above information any fire may therefore be detectable, irrespective of distance from substation provided a detection device is placed at both ends of the transmission line.

The characteristics of the fire-induced corona noise recorded on the transmission line was a modulated version of the noise measured in the corona cage. The filtering equipment and the singular events of induced corona pulses resulted in a modulated measurement at the centre frequency of the filtering equipment.

Several sugar cane plantation fires were monitored and visual recordings were made. Depending on the environmental elements, flames of the sugar cane fires reached heights of several meters above the earth wires of any configuration. With no wind present, the vertical heights obtainable from a continuous flame should therefore not be underestimated. Recordings have captured flames at heights of 25 to 30 meters. Therefore attempting to solve the problem of fires under power lines by changing the dimensions of the transmission line structures will require appropriate investigation. Similarly, the approach to remove sugar cane from the servitude may be a positive reaction to eliminate the problem. However, the cost of such a venture will inevitably mean that less rather than more land will be purchased. Some findings from the University of Queensland indicate that "any transmission line within 25 metres of a cane crop can be considered as subject to cane fire induced faults". If the selected width is only marginally too small, a flashover from fires under the correct conditions will still be possible. Should this occur the whole venture will be uncertain. With appropriate servitude widths purchased, Eskom will probably not be able to treat all sensitive lines in the same manner.

Temperatures in excess of 1500°C were measured during these tests indicating that the influence of thermal ionisation cannot be ignored in the electrical process. However, this dissertation does not focus on the research into the breakdown mechanism but rather on the detection of the induced high frequency signals being generated from that source.

The active filtering device developed to eliminate more of the carrier signals always present on many of the transmission lines failed to take response time into consideration. The same device however, is adequate for passing plant deteriorating electrical partial discharges through and may yet be useful in the early detection of high voltage apparatus failure such as current transformer insulation deterioration.

CHAPTER 11

Fire Detection Prototype Proposals

Several options were available with implementation possible both individually and in parallel.

Of significance when determining a suitable methodology for the detection of fires (and preferably any fires with the potential to disrupt the transmission of power through the national transmission grid) were;
Firstly; the identification and characterisation of fire-induced corona activity in all its forms (within reason).
And secondly the identification and characterisation (to a lesser degree) of the varying alternative noise sources which may generate significant amounts of noise and be confused with the fire-induced noise.

11.1 DETECTION OF FIRES IN PERSPECTIVE

The process of detection should be seen in the context of its application in the national grid. Factors which will influence the development of the detector will be firstly, the technology based environment within which the device must be implemented. Secondly, the personnel involvement in the problem and the solution both obscures the development and also assists the development of the device. Thirdly, the expected output of such a device. And finally, the pace with which such a device is implemented as a "final detection device".

11.1.1 Implementation

The face of the current technology within Eskom is continuously changing according to the demands made on it to supply an ever increasing consumer load with a reliable and preferably excellent quality of supply. As a result the protection mechanisms currently in place are improving with faster and faster response times. The implementation of phase III protection will naturally imply very fast reaction or response times to problems in the network. The fire detection device has to be directed at immediate implementation into the current technology with the view to developing within Eskom technology. This would imply that the options available

from the detection device should only be limited by the available technology within Eskom and not limited by the technology used for the device.

The action required from the device will therefore have to be directed towards obtaining a balance between providing information to regional and national control centres and automatic control of parts of the network. Reaction time and turn-around times from time of detection to time to take preventative action is crucial. The algorithmic methods to handle, maintain and implement the information provided by the detector would be helpful in not only recognising the presence of fires and its role in the cause of particular faults, but also in the prevention of faults due to fires. A straight forward "plug-it-in-and-see-if-it-works" approach would most likely lead to an unsuccessful result.

Several other sources of noise have been identified as possible "interfering" noise which may induce false alarms. This negative information could be turned to positive results with appropriate action. If these noise sources can interfere with our detection device's received noise levels it also means that those noise sources are detectable. A detectable noise source is usually also a source of power cycle losses with a potential to causing load disruption. Appropriate identification and characterisation of these noise sources would therefore also lead to an additional means by which the generation and transmission of power can be optimised. Therefore the device has to be implemented with the flexibility to include further innovations when necessary. An example of such a noise source is the development or build-up of pollution on insulators.

The main emphasis and criteria when considering the implementation of the detection device is not how "clever" the device can be but how should it be implemented to maximise its benefit to the system operations departments within the utility. That is, the departments with the most experience with regard to the network should be involved in its implementation. The final implementation of the device should be orchestrated by those departments who would benefit the most from it. With this concept in mind, it is therefore also necessary to ensure that the fundamental task the device is requested to perform is performed to the standards required.

Like any device which may have a significant impact on its environment, the fire detection device will have to go through a prototype phase during which a level of confidence must be established - p ercentage o f f ires i dentified, p ercentage o f f ires not detected and percentage of

false alarms. This information must be documented and any deficiency must be identified and eliminated. It would be pointless to implement such a detection device throughout the transmission network if fundamental errors are present in the device. Such problems would create a poor sense of conviction (with a resulting "cry wolf" syndrome) and finally the concept would be shelved. Not due to the inadequacy of the technology but simply due to inadequate design and development strategies. Most utilities with fire related problems cannot afford such indulgences. The current plan to purchase the servitudes along which the transmission lines run will cost millions of rand and will not be implemented along all affected lines. In addition, the "safe" width of the purchased servitude can only be calculated (and guaranteed) after long periods of time when detailed analysis will be useful. Some findings from the University of Queensland indicate that "any transmission line within 25 metres of a cane crop can be considered as subject to cane fire induced faults" [2] which is not an encouraging factor when the cost of purchasing the extended servitude per meter in width is considered. Already some of these cane free servitudes in Eskom have produced cane fire induced faults.

11.1.2 Timing

The changing technology goes along with a particular pattern of planning and maintenance of the network. Standard operating procedures dictate the manner in which work is performed and creates an element of stability in the workplace. If the detection device is inappropriate for both the technology and the acceptable operating procedures, the device will not be successful. However, an appropriate device will have exactly the opposite affect. Therefore the manner in which the device is introduced and the orientation of the design is critical.

11.1.3 System requirements

The requirements from the system operations departments within Eskom is to supply the consumers with electricity according to the customer's needs in a cost-effective manner. In order to achieve this goal, factors such as total number of line faults per 100 km, automatic successful load resumption and the line protection performance index are considered primary factors by which to measure the optimum performance of the network. Failure to reach acceptable standards is considered to be inadequate and therefore any detection device implemented in the network may not generate false alarms or be installed in a critical decision making position until the extent of its abilities are fully tested.

Consequently the systems operations departments must be prepared for a prototype development phase in the build up to a viable detection device. This device should not be expected to have irrevocable decision making capabilities from its inception into the system. Naturally, the process to achieve such expectations will be carried out as rapidly as the environmental conditions and system conditions will allow.

11.1.4 Development

The environmental conditions on a transmission line are not ideal laboratory conditions and hence cannot be controlled in the same manner. The real implication is the time duration taken for appropriate testing procedures.

The more volatile the system is the quicker the tests, defining the device as an appropriate tool for optimising the network, will be completed. Since the system operations departments endeavour to keep the system as stable as possible, the opposite occurs. The development and improvement of the detection device will suffer from the same limitations. Provided these limitations are well understood, the development of the device will not suffer strategic setbacks.

11.2 DETECTION CONSIDERATIONS

The main parameters identifying fires were the high amplitudes of the corona pulses (measured in volts) - and interpreted as the streamers surging from the conductor bundle - and the random manner in which those pulses occurred.

The fundamental requirement was therefore to detect the high pulses via an appropriate measuring circuit (with pre-set threshold levels) and to identify the random development of the noise pulses.

11.2.1 Sampling

The process of viewing the induced corona on the transmission line requires a selective amount of information. The field results and knowledge of the PLC operation dictates that a frequency window is necessary. The corona cage findings have shown that the selection of a window must

be done at the lowest available frequencies. In addition the majority of the power line carrier communication links operate at frequencies higher than 100 kHz. The exceptions are those lines which are transposed (which are very few in number). Hence the lowest frequencies in the PLC band are preferable. A multi-stage frequency filtering system is therefore necessary before any measurements can be performed. Any detection system needing access to higher frequencies than those available through the high voltage apparatus will require additional equipment for filtering at an additional cost. The alternatives for such a solution did not form part of this research.

11.2.2 Analysis

The process of analysing the noise measured must be performed in conjunction with the phases of the 50 Hz signal. The rain induced noise and all the other noise sources have characteristics predominantly significant in relation to the 50 Hz power cycle. The creation of the corona noise is fundamentally dependent on the existence of the high surface gradients created by the high applied voltages. Each parameter has its own manner in which the corona is created from it and therefore the electric fields are modified according to the characteristics unique to that parameter.

11.2.3 Intelligence

The information created from further research work will essentially create a more "informed" database from which appropriate decisions can be extracted. The efficiency with which the detection unit can process this information will define whether it is the "ideal" design for the application.

11.3 DETECTION METHODOLOGIES

11.3.1. Threshold detection

Threshold detection requires the selection of appropriate voltage, time and frequency threshold levels for creating a window within which the magnitude, phase and frequency of the fire-induced corona noise can be identified.

A carrier circuit tuning filter was used in collaboration with additional filters to minimise the influence of the power line carrier (PLC) signals. A similar approach may create the required frequency window. The centre frequency and bandwidth of such a cascaded filtering unit must be appropriately selected for the relevant lines along which the detection device is to be implemented. The 50 Hz power cycle is then combined with the induced noise signals received to create a time domain window. The final voltage threshold level must be appropriately selected according to expected noise from other sources on the relevant line in both time and frequency.

The resulting information must then be combined into an algorithm identifying the trends described when a fire is present under the line. A neural network or a standard expert system would provide a flexible environment within which such an algorithm may be implemented. The additional information discovered from future research work will continually improve the implemented algorithm and enhance the selected voltage, time and frequency windows.

The method by which this concept can be implemented can be either analogue hardware or digital hardware. The digital option would be preferable, thereby allowing on-board processing to speed up the reaction time from time of detection. Of necessity, an interface would be required between the analogue noise received and the digital processing taking place.

A significant consideration was the sampling rate to capture the affects of individual streamers and duration of the total sample from which the final calculations are to be performed. The concepts from this proposal have been implemented and have shown successful results.

11.3.2 Zero crossing

Test for high levels of noise when the 50 Hz power signal is zero. The characteristics of corona induced due to fires indicate that no fire-induced noise exists when there is no electric field at the conductors. Inclusion of all three phases or appropriate calculations made regarding the nodal propagation of the induced noise may be necessary. Noise on one phase will induce noise on the other phases by the nodal propagation concept and a calculation determining the phase of the noise in relation to the specific phase monitored may be necessary.

11.3.3 Threshold Register

Test for any noise generated greater than the threshold level set and increment a counter in the digital signal processing component of the detector. This will be of use in both positive and negative half cycles of the 50 Hz power signal. The development of the noise in both half cycles on the operational transmission line has been observed but more research is required here.

11.3.4 Critical threshold

Test for the existence of high noise levels in both half cycles of the 50 Hz power signal. Most of the findings to date indicate that this case is evidence that a flashover is imminent. More research is required to comprehensively quantify this concept.

11.3.5 Half Cycle Segmentation

Segmentation of the induced-noise with respect to the development of the 50 Hz signal appears to result from the tuning circuitry used. This information can therefore also be used to eliminate surges from the analysis. The induced noise due to fires appears primarily in the first half of the half cycle. The presence of noise in the first half and the lack of noise in the second half (relative to the selected threshold voltage) should then result in a confirmation of this test.

11.3.6 Probability Distribution Function

The characteristics of the noise recorded in a segmented fashion can be of some use when considering the statistical development of the streamers. Development of corona and ionisation

by electron impact is a probability phenomena discussed extensively in chapter 3, section 3.1 from page 21.

11.3.7 Spectral Analysis

Sample the data and determine the frequency spectrum of that data. Then compare the result to results determined in the laboratory. This will however require several frequency windows (parallel filtering stages) and cannot be replaced by a broadband measurement.

11.3.8 Quasi-peak level

While the standard measurement for radio interference has been extensively discredited as a means of detecting fires, the output of a quasi-peak measuring hardware component can provide an additional test mechanism. This however, is an option which will firstly, point to the presence of fires only in conjunction with other information, and secondly, will not be able to confirm that there is no fire under the line. It is therefore only partially useful in the system.

11.3.9 Cluster analysis

Relate information obtained in the positive half cycle to information obtained in the negative half cycle. This is a form of the probability distribution function and was recommended from findings in the mini-corona cage at the University of Stellenbosch. This method requires a large sample of data to enable recognition of zoning. Simultaneously, it requires an extensive feedback system whereby the main transmission system information and environmental information related to specific noise events can be combined with the actual noise event occurring. This avenue had been thoroughly investigated and the costs involved to examine each affected line were found to be extremely high in both manpower and equipment with very little positive results to show. The time required for all possible alternatives to be sampled and categorised would be high and no immediate results would be imminent. This process would have to be repeated for each affected line. The implication is therefore that on lines which are considered "not crucial", this method would not be implemented. Further research is necessary to make this alternative a viable option.

11.4 PROTOTYPE DETECTION SPECIFICATIONS

The following specifications are the absolute minimum requirements for a prototype detection device and was specified for the design team working within T-R-I. The TRI-ADD discussed in section 10 was developed based on these specifications [40].

11.4.1 Input Specification:

11.4.1.1 Tuned channel noise from power line carrier channel;
11.4.1.2 Power signal (50 Hz) = 63.5 volts from protection voltage transformers;
11.4.1.3 High input impedance > 1MΩ.

11.4.2 Output Specification:

11.4.2 1 Output for local indication (LED and audible alarm);
11.4.2 2 Output to modem for remote analysis.

11.4.3 Trigger Conditions:

11.4.3.1 Filter

$f_c = 60$ kHz
$f_B = 20$ kHz
Roll off = 100dB over 50 kHz

11.4.3.2 Threshold

Instantaneous voltage initial setting 100mV

11.4.3.3 Pre-trigger

2 seconds

11.4.3.4 Reaction time

15 seconds

Note: This applied when one minute is considered to be the minimum time to flash-over with smoke present

11.4.3.5 Discrimination

Rain vs fire = 15dB

11.4.4 Hardware:

11.4.4.1 Power Supply

220Vac with UPS supply;

11.4.4.2 Detection Device Adaption

As the above specifications were applied for the minimum information available, it was clearly understood that the device will need to be adjusted as per requirements.

11.5 PROTOTYPE DETECTION RESULTS

From a research point of view the detection device worked very well. A sugar cane plantation fire was detected before it could cause a breakdown of the air gap to ground (tests completed on the Marathon / Komatipoort 275kV transmission line) using the passive filtering units.

Fundamentally, this meant that if no immediate action were taken, it would still be possible to log exactly how many faults occurred due to flashovers from fires. The procedures in the event of faults due to fires are currently not clearly defined but with some additional investigation it would be possible to establish a standard operating procedure (SOP) for a fire event. This will minimise the number of depressions occurring on the MTS network.

In addition to the above positive aspects, the rather "primitive" specifications provided a positive result. Now further development of the prototype into a quality product with outputs to an expert system with possible neural network abilities holds realistic opportunities to minimise the affects of fires.

The development of an active filtering device was partially successful. The device was able to track events with a high repetition rate. As a fire detection device the filtering unit requires a faster response time to pass short term isolated events.

CHAPTER 12

Conclusions

12.1CORONA CAGE TEST RESULTS

Without the work performed in the corona cage, the results obtained on operational transmission lines would have been meaningless and would have existed with unsubstantiated hypotheses. With the corona cage work, the activity as created by fires have been adequately identified. The developments of the fire may be described by many scientists as "obvious". However, until theories are substantiated with factual information the process of analysis remains a purely theoretical one. The fact that fires under power lines have been a problem for so many years substantiates this philosophy.

Fire under power lines are detectable over long distances through measurement of the propagated corona noise induced by the fire. Fire-induced corona noise is distinguishable from rain-induced corona noise. With adequate characterisation, most noise sources generating corona on the transmission line may have different characteristics to the characteristics of fire-induced corona noise.

The quasi peak values of fire induced corona is higher than the values for both dry and heavy rain conditions. These values are not sufficiently high to make detection by means of quasi peak values alone, reliable. Individual corona occurring as a result of fires is considerably higher in amplitude than the same activity in dry and heavy rain conditions by an average of 35dB. The repetition rate of fire induced corona is lower than that for rain under average fire conditions but grows with fire intensity by way of heat and particle content.

Smoke does not produce significant amounts of corona and does not produce flashovers unless accompanied by intense heat and / or a high number of particles.

12.2 ESKOM TEST RESULTS AND FUTURE WORK

The development of a fire was not very accurately defined in previous work. The perception that smoke and the flame created the same level of corona noise implied that when the smoke was

present at the conductors, induced corona noise would be measurable at the substation. As a result all information was based on the proximity of the smoke to the conductors. Hence minimum time to flashover was initially specified as 60 seconds. The operational line work indicates that this information could in fact not be described as the "minimum time to flashover". While the detection of fires is not dependent on this minimum time, the reaction time of the control circuitry and control staff has to be taken into account if the detection philosophy is to be graduated to a control level or high priority action device with the aim of being pro-active rather than reactive.

Objectives in future work was laid out as follows:

i) Determine typical amplitudes of fire-induced corona noise in the context of the operational environment,

ii) Characterise the modified pattern of fire-induced corona noise as a function of the 50 Hz transmitted power in the context of the operational environment (for improved confidence in the data),

iii) Define the activity of fire-induced corona noise in the duration of one half-cycle of the 50 Hz transmitted power in the context of the operational environment, and

iv) Determine the duration of corona activity at conductors before full breakdown of the gap occurs and define how the corona activity develops in terms of the high frequency noise measured.

Without this information, the fire detector currently in development may not command the authority that it will eventually require and the anticipated expert systems approach to the detection of fires, heavily polluted insulators and possibly the cutting of overhead transmission lines will be severely impeded.

Work planned for immediate action was stipulated as follows:

1) Establish correspondence links with sugar cane farmers, municipalities and any other useful individuals with land over which the Eskom transmission network is installed where the probability of a fire (sugar cane, veld or any other) is reasonably high and may be anticipated beforehand.

2) Capture fire-induced data on operational transmission lines in conjunction with visual material, recording the progress of the fires in relation to the overhead transmission lines, with time-stamping on both.
3) Process fire-induced data and supply the results to an expert systems team, and make recommendations on the development of the prototype fire detector.

In addition, further temperature recordings should be made to capture more information about the actual temperatures under which corona is being generated at the conductors. This data will provide more information about the physical breakdown process and the influence thermal ionisation may have on that breakdown process.

The developed detection device (TRI-ADD), works but with limited effectiveness due to the influence of the carrier signals which overwhelm other electrical activity. The attempted active filtering method does not work due to the slow response time from the circuit.

The passive analogue filter process functioned adequately providing some means of identifying fire-induced corona activity.

CHAPTER 13

Recommendations

The detection of fires under power lines by means of the corona generation characteristics of the fire in the proximity of high fields about a high voltage overhead transmission line has opened up a complete new field of research. Any high voltage activity generating higher frequency "radio noise" may or may not be detected by monitoring the propagated noise through an appropriate tuning circuit. This avenue of research must be exploited to further the understanding and elimination of corona losses and gap discharges or partial electrical discharges (pd) - usually an indication of equipment deterioration.

The detection mechanism also enables the researcher to "look" at corona activity and with the aid of system information better analysis of the network status may be possible.

Detection of other common sources of system disruption may also be possible. On the eastern Natal coastline where major problems exist due to the levels of pollution injected onto the insulators, indications show that this method would be appropriate to identify when actions such as spray washing may be necessary. Monitoring and evaluating the performance of different insulator strings under similar pollution conditions will then also become possible. This option has already been considered and will be taken further in conjunction with the development of the detector. The possibility of detecting hardware faults is also currently being researched.

As the option of reactive and proactive decision making has not yet been fully discussed in the broader spectrum of Eskom system management, the method by which the detector will interact with the system has yet to be decided. The protection and communication environments are evolving into faster response time systems, and the detection process should therefore be evaluated in terms of reactive and proactive processes. The goal would be to develop from a reactive system to a proactive system as the protection and communication technologies within Eskom progress.

The possibility of detecting field interference on lower voltage distribution lines also needs further research. The necessity for expensive tuning equipment may make this option prohibitive

but research into the transmission of corona noise through current transformers may provide a viable and efficient means of detecting such infamous activities as conductor theft which currently leads to losses in the order of millions of South African rand to the utility. With adequate insight, additional tuning equipment may yet be considered to be a reasonable expense.

CHAPTER 14

PUBLICATIONS BY AUTHOR

The following publications have been produced as a result of this research work. These publications have not been referenced in the document but are included for completeness.

1. Evert,C.R.; Britten,A.C.; Van Coller,J.M.; Analysis of Fire-induced Corona on Power Lines, South African Universities Power Engineering Conference, 13-14 July 1992, University of Natal, Durban, South Africa.

2. Evert, C.R.; De Klerk, P.J.; Measurement and Detection of Fires under High Voltage Power Lines, Third Symposium on Modern Measurement Techniques, 8 June 1993, Randburg, Johannesburg, South Africa.

3. Evert,C.R.; Britten,A.C.; Analysis of Fire-induced Corona on Power Lines, Eighth International Symposium on High Voltage Engineering, 23 – 27 August 1993, Pacifico Yokohama, Yokohama, Japan.

4. Evert, C. R; Vosloo, W.L; Holtzhausen, J.P; Britten, A.C; Discrimination Between Electromagnetic Noise Generated By Sugar Cane Fires, Conductor Corona and Polluted Insulators on Overhead Lines; Southern African Universities Power Engineering Conference, 13-14 January 1994, Cape Town, South Africa.

5. Evert, C.R; De Klerk, P.J; Fire-Induced Corona on High Voltage Power Lines – An Opportunity for detection and Prevention of Flashover; 2nd Cigre Southern African Regional Conference Electrical Power Systems in Sub-Equatorial Africa, 25-26 May 1994, Durban, South Africa.

6. Evert, C.R; De Klerk, P.J; Corona Noise as a Diagnostic Tool; 4th International Conference on Properties and Applications of Dielectric Materials; 3-8 July 1994, University of Queensland, Brisbane, Australia.

7. Evert, C.R; Swift, D.A; Britten, A.C; Analysis of Plant Deterioration Related EM noise; 9th International Symposium on High Voltage Engineering, August 1995, Graz, Austria.

8. Evert, C.R; Britten, A.C; Swift, D.A; Fire Induced Corona on Power Lines; 7th Southern African Universities Power Engineering Conference, 20-21 January 1998, University of Stellenbosch, Cape Town, South Africa.

9. Evert, C.R; Britten, A.C; An Early Warning Mechanism To Detect Fires Under High Voltage Transmission Lines; Cigre Third Southern Africa Regional Conference, 20-21 May 1998, Midrand, Johannesburg, South Africa.

APPENDIX A

Statistical distribution of fires present under high voltage transmission lines in the Eskom network only.

1989	275 kV		400 kV	
	Percentage of Total Faults (%)	No. of Faults: Fires vs Total	Percentage of Total Faults (%)	No. of Faults: Fires vs Total
August	62	16 - 26	30	8 - 27
September	11	17 - 150	28	22 - 78
October	12	3 - 26	10	3 - 30
November	7	4 - 56	0	0 - 32
December	0	0 - 58	0	0 - 31
Totals	**13**	**40-316**	**17**	**33-198**

1990	275 kV		400 kV	
	Percentage of Total Faults (%)	No. of Faults: Fires vs Total	Percentage of Total Faults (%)	No. of Faults: Fires vs Total
January	0	0 - 40	0	0 - 13
February	0	0 - 33	0	0 - 22
March	0	0 - 38	0	0 - 27
April	0	0 - 26	4	1 - 23
May	3	1 - 40	40	6 - 15
June	11	3 - 28	32	7 - 22
July	21	8 - 39	31	9 - 29
August	30	9 - 30	22	5 - 23
September	39	13 - 33	52	14 - 27
October	44	15 - 34	4	1 - 26
November	7	2 - 34	3	1 - 38
December	0	0 - 37	0	0 - 37
Totals	**12**	**51-412**	**15**	**44-302**

1991	275 kV		400 kV	
	Percentage of Total Faults (%)	No. of Faults: Fires vs Total	Percentage of Total Faults (%)	No. of Faults: Fires vs Total
January	0	0 - 57	0	0 - 31
February	0	0 - 49	6	1 - 16
March	3	2 - 71	6	3 - 48
April	2	1 - 41	0	0 - 28
May	8	2 - 25	9	3 - 34
June	36	8 - 22	4	1 - 24
July	20	9 - 44	36	14 - 39
August	43	31 - 72	40	19 - 47
September	30	10 - 33	55	32 - 58
October	28	11 - 40	41	20 - 49
November	20	7 - 35	4	1 - 27
December	0	0 - 48	11	3 - 27
Totals	**15**	**81-537**	**23**	**97-428**

Summary of the total faults and percentages from August 1989 to December 1991:

Operating Voltage (kV)	Fire Faults	Total Fault	Percentage of Total caused by fires
400	174	928	19 %
275	172	1265	14 %

Note that these were minimum figures since there were cases in which the cause of a fault was not established and may have been as a result of a fire.

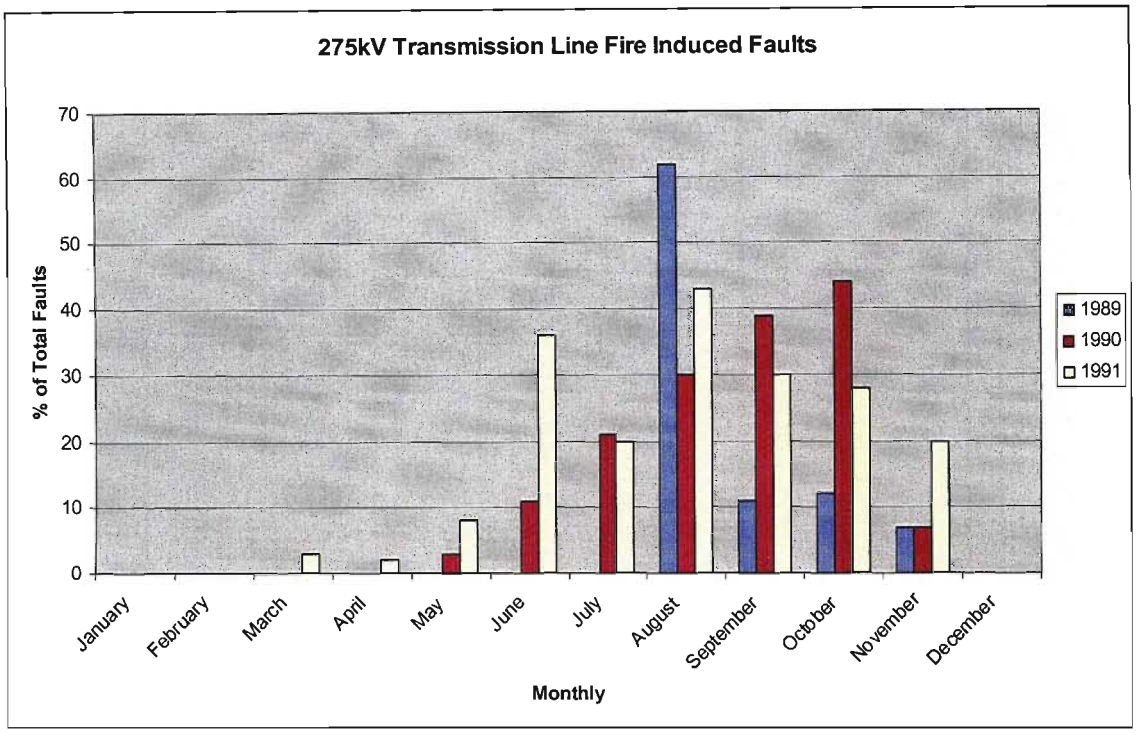

Figure A 1: Statistics of the 275kV faults from 1989 to 1991

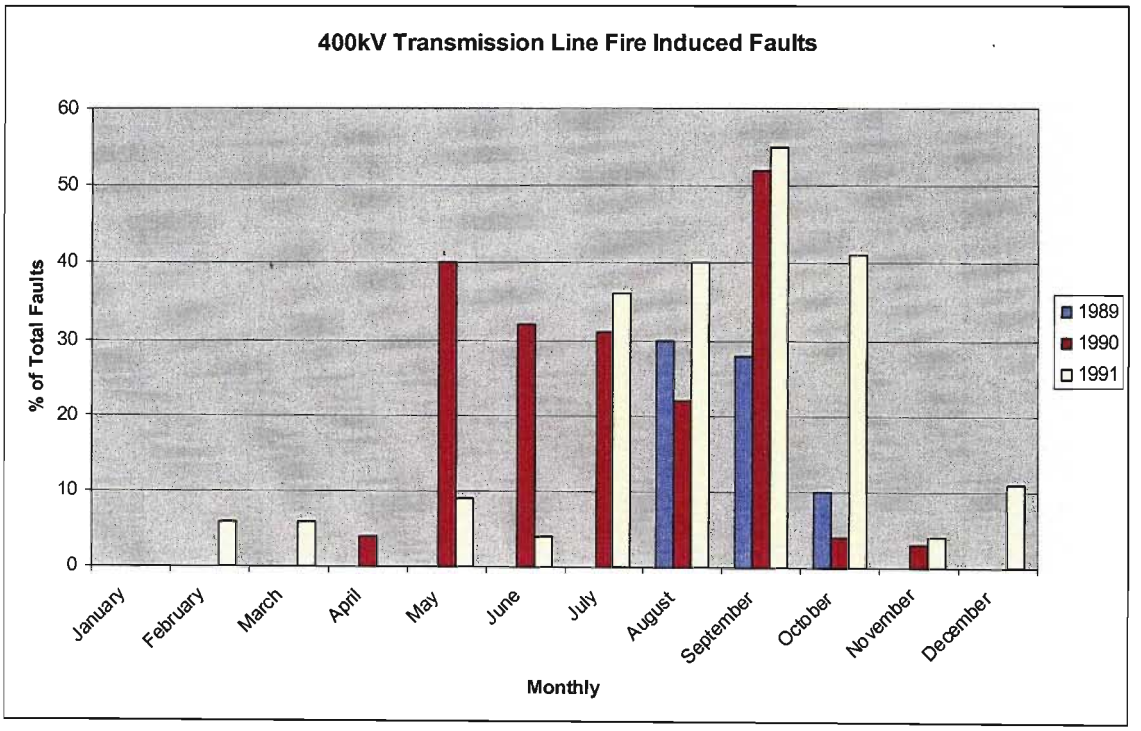

Figure A 2: Statistics of the 400kV faults from 1989 to 1991

APPENDIX B

Calculations: Characteristic Impedance for each conductor bundle tested in the corona cage.

The characteristic impedance for a particular conductor bundle is $Z_c = \sqrt{\frac{L}{C}}$ where C is the characteristic capacitance $C = \frac{2\pi\varepsilon_0}{\ln\frac{R}{r''}}$ and L is the characteristic inductance $L = \frac{\mu_0}{2\pi}\ln\frac{R}{r''}$ of the bundle. The GMR (geometric mean radius) of the conductor bundle is $r'' = \sqrt[n]{nr'a^{n-1}}$ (equation 20) and the GMR of the individual conductors in the bundle is $r' = e^{-\frac{\mu_r}{4}} r$ (equation 19). For a detailed explanation, refer to page 52.

r	= conductor radius
r'	= GMR (geometric mean radius) of each conductor
r''	= overall GMR of the conductor bundle
μ_r	= permeability taken as approximately equal to one for aluminium and copper
ε_0	= permittivity of a vacuum or approximately the permittivity of air ($\varepsilon_0 = 8.859 \times 10^{-12}$ F/m)
μ_0	= permeability of a vacuum or approximately of air ($\mu_0 = 1.275 \times 10^{-6}$ H/m)
n	= number of conductors in the conductor bundle
a	= bundle radius calculated as a function of s
s	= separation between the conductors in a conductor bundle
R	= radius of the cylindrical cage (Eskom corona cage radius = 3.5 m)
C	= capacitance of a conductor bundle (in Farads per meter F/m)
L	= inductance of a conductor bundle (in Henry per meter H/m)
Z_c	= characteristic impedance of the conductor bundle

1) Twin Dinosaur conductor bundle

Bundle construction: The dinosaur conductor has an overall diameter of 35.56 mm with 54 aluminium strands each with a diameter of 3.95 mm and 19 steel strands each with a diameter of 2.36 mm. Separation between the two conductors (s) was 380 mm.

Calculation: $\mu_r \approx 1$ (for the inductance calculation), $\mu_r = \mu_0$ (for the capacitance calculation), r = 17.78 mm for the Dinosaur conductor and $(na^{n-1}) = s = 380$mm

Capacitance:

$$r' = e^{-\frac{\mu_r}{4}} r$$

r′ = r

= 17.78mm

Overall GMR:

$$r'' = \sqrt[n]{nr'a^{n-1}}$$

$$r'' = \sqrt{(17.78)(380)}$$

= 82.20 mm

$$C = \frac{2\pi\varepsilon_0}{\ln\frac{R}{r''}}$$

$$C = \frac{(55.66\times10^{-12})}{\left(\ln\frac{3.50}{82.20\times10^{-3}}\right)}$$

= 14.84 pF/m

Inductance:

$$r' = e^{-\frac{\mu_r}{4}} r$$

r′ = 0.779r

= (0.779)(17.78)

= 13.85 mm

Overall GMR:

$$r'' = \sqrt[n]{nr'a^{n-1}}$$

$$r'' = \sqrt{(13.85)(380)}$$

= 72.55 mm

$$L = \frac{\mu_0}{2\pi}\ln\frac{R}{r''}$$

$$L = (200.06\times10^{-9})\ln\left(\frac{3.50}{72.55\times10^{-3}}\right)$$

= 775.49 nH/m

Characteristic impedance:

$$Z_c = \sqrt{\frac{L}{C}}$$

$$Z_c = \sqrt{\frac{775.49\times10^{-9}}{14.84\times10^{-12}}}$$

$$= \underline{228.60\Omega}$$

2) Twin Zebra conductor bundle

Bundle construction: The Zebra conductor has an overall diameter of 28.56 mm with 54 aluminium strands and 7 steel strands each with a diameter of 3.17 mm. Separation between the two conductors (s) was 380 mm.

Calculation: $\mu_r \approx 1$ (for the inductance calculation), $\mu_r = \mu_0$ (for the capacitance calculation), r = 14.28 mm for the Zebra conductor and $(na^{n-1}) = s = 380$mm

Capacitance:

$r' = e^{-\frac{\mu_r}{4}} r$

r′ = r

= 14.28mm

Overall GMR:

$r'' = \sqrt[n]{nr'a^{n-1}}$

$r'' = \sqrt{(14.28)(380)}$

= 73.66 mm

$$C = \frac{2\pi\varepsilon_0}{\ln\frac{R}{r''}}$$

$$C = \frac{(55.66\times10^{-12})}{\left(\ln\frac{3.50}{73.66\times10^{-3}}\right)}$$

= 14.42 pF/m

Inductance:

$r' = e^{-\frac{\mu_r}{4}} r$

r′ = 0.779r

= (0.779)(14.28)

= 11.12 mm

Overall GMR:

$r'' = \sqrt[n]{nr'a^{n-1}}$

$r'' = \sqrt{(11.12)(380)}$

= 65.02 mm

$$L = \frac{\mu_0}{2\pi}\ln\frac{R}{r''}$$

$$L = (200.06\times10^{-9})\ln\left(\frac{3.50}{65.02\times10^{-3}}\right)$$

= 797.41 nH/m

Characteristic impedance:

$$Z_c = \sqrt{\frac{L}{C}}$$

$$Z_c = \sqrt{\frac{797.41\times10^{-9}}{14.42\times10^{-12}}}$$

$$= \underline{235.16\Omega}$$

3) Triple Wolf conductor bundle

Bundle construction: The wolf conductor has an overall diameter of 18.13 mm with 30 aluminium strands and 7 steel strands each with a diameter of 2.59 mm. Separation between the three conductors (s) was 450 mm.

Calculation: $\mu_r \approx 1$ (for the inductance calculation), $\mu_r = \mu_0$ (for the capacitance calculation),

r = 9.07 mm for the Zebra conductor and $a = \frac{\frac{s}{2}}{\cos 30°} = 0.577s = (0.577)(450) = 259.81$ mm

Capacitance:

$r' = e^{-\frac{\mu_r}{4}} r$

$r' = r$

$= 9.07$mm

Overall GMR:

$r'' = \sqrt[n]{nr'a^{n-1}}$

$r'' = \sqrt[3]{3(9.07)(259.81)^2}$

$= 122.46$ mm

$C = \frac{2\pi\varepsilon_0}{\ln\frac{R}{r''}}$

$C = \frac{(55.66\times10^{-12})}{\left(\ln\frac{3.50}{122.46\times10^{-3}}\right)}$

$= 16.60$ pF/m

Inductance:

$r' = e^{-\frac{\mu_r}{4}} r$

$r' = 0.779r$

$= (0.779)(9.07)$

$= 7.07$ mm

Overall GMR:

$r'' = \sqrt[n]{nr'a^{n-1}}$

$r'' = \sqrt[3]{3(7.07)(259.81)^2}$

$= 112.68$ mm

$L = \frac{\mu_0}{2\pi}\ln\frac{R}{r''}$

$L = (200.06\times10^{-9})\ln\left(\frac{3.50}{112.68\times10^{-3}}\right)$

$= 687.39$ nH/m

Characteristic impedance:

$$Z_c = \sqrt{\frac{L}{C}}$$

$$Z_c = \sqrt{\frac{687.39\times10^{-9}}{16.60\times10^{-12}}}$$

$$= \underline{203.49\Omega}$$

4) Twin Wolf conductor bundle

Bundle construction: The wolf conductor has an overall diameter of 18.13 mm with 30 aluminium strands and 7 steel strands each with a diameter of 2.59 mm. Separation between the two conductors (s) was 380 mm.

Calculation: $\mu_r \approx 1$ (for the inductance calculation), $\mu_r = \mu_0$ (for the capacitance calculation) and r = 9.07 mm for the Wolf conductor and $(na^{n-1}) = s = 380$mm

Capacitance:

$$r' = e^{-\frac{\mu_r}{4}} r$$

r′ = r

= 9.07mm

Overall GMR:

$$r'' = \sqrt[n]{nr'a^{n-1}}$$

$$r'' = \sqrt{(9.07)(380)}$$

= 58.71 mm

$$C = \frac{2\pi\varepsilon_0}{\ln\frac{R}{r''}}$$

$$C = \frac{(55.66\times10^{-12})}{\left(\ln\frac{3.50}{58.71\times10^{-3}}\right)}$$

= 13.62 pF/m

Inductance:

$$r' = e^{-\frac{\mu_r}{4}} r$$

r′ = 0.779r

= (0.779)(9.07)

= 7.07 mm

Overall GMR:

$$r'' = \sqrt[n]{nr'a^{n-1}}$$

$$r'' = \sqrt{(7.07)(380)}$$

= 51.83 mm

$$L = \frac{\mu_0}{2\pi}\ln\frac{R}{r''}$$

$$L = (200.06\times10^{-9})\ln\left(\frac{3.50}{51.83\times10^{-3}}\right)$$

= 842.75 nH/m

Characteristic impedance:

$$Z_c = \sqrt{\frac{L}{C}}$$

$$Z_c = \sqrt{\frac{842.75\times10^{-9}}{13.62\times10^{-12}}}$$

$$= \underline{248.75\Omega}$$

5) Single Wolf conductor bundle

Bundle construction: The wolf conductor has an overall diameter of 18.13 mm with 30 aluminium strands and 7 steel strands each with a diameter of 2.59 mm. Separation between the two conductors was 380 mm.

Calculation: The GMR of each conductor (as opposed to the GMR of the whole conductor bundle) was given by equation 19 with $\mu_r \approx 1$ (for the inductance calculation), $\mu_r = \mu_0$ (for the capacitance calculation) and r = 9.07 mm for the Wolf conductor.

Capacitance:

$$r' = e^{-\frac{\mu_r}{4}} r$$

$$r' = r$$

$$= 9.07\text{mm}$$

$$C = \frac{2\pi\varepsilon_0}{\ln\frac{R}{r''}}$$

$$C = \frac{(55.66\times10^{-12})}{\left(\ln\frac{3.50}{9.07\times10^{-3}}\right)}$$

$$= 9.35\ \text{pF/m}$$

Inductance:

$$r' = e^{-\frac{\mu_r}{4}} r$$

$$r' = 0.779r$$

$$= (0.779)(9.07)$$

$$= 7.07\ \text{mm}$$

$$L = \frac{\mu_0}{2\pi}\ln\frac{R}{r''}$$

$$L = (200.06\times10^{-9})\ln\left(\frac{3.50}{7.07\times10^{-3}}\right)$$

$$= 1241.30\ \text{nH/m}$$

Characteristic impedance:

$$Z_c = \sqrt{\frac{L}{C}}$$

$$Z_c = \sqrt{\frac{1241.30\times10^{-9}}{9.35\times10^{-12}}}$$

$$= \underline{364.36\Omega}$$

APPENDIX C

Quasi peak corona induced noise values measured in the corona cage.

---

1) Twin Dinosaur conductor bundle

Surface Gradient (kV/cm)	RIV Measurement (dBμV)		
	Dry Conditions	Rain (2 mm/min.)	Fire (In dry condition)
9	4	53	80
10	5	57	85
11	7	61	90
12	11	65	95
13	47	68	95
14	44	72	98
15	50	75	95
16	55	77	95
17	58	79	Flashover
18	65	81	
19	68	82	
20	73	83	
21	75	83	
22	78	84	
23	80	85	
24	82	86	

2) Twin Zebra conductor bundle

Surface Gradient (kV/cm)	RIV Measurement (dBμV)			
	Dry Conditions	Rain (2 mm/min.)	Fire (Measured)	Fire (Projected)
11	45	60	59	65
12	54	63	69	69
13	54	66	69	72
14	61	68	69	75
15	63	71	65	77
16	65	74	79	79
17	67	75	66	83
18	71	76	85	85
19	74	77	75	90

* Shading in the cell indicates the modified figures

APPENDIX D

Calculated Excitation Function Of The Induced Corona Noise Values Measured in the Corona Cage.

1) Twin Dinosaur conductor bundle

Surface Gradient (kV/cm)	Excitation Function dB (1μA/ m)		
	Dry Conditions	Rain (2 mm/min.)	Fire (In dry condition)
9	-21.87	27.13	54.13
10	-20.87	31.13	59.13
11	-18.87	35.13	64.13
12	-14.87	39.13	69.13
13	21.13	42.13	69.13
14	18.13	46.13	72.13
15	24.13	49.13	69.13
16	29.13	51.13	69.13
17	32.13	53.13	Flashover
18	39.13	55.13	
19	42.13	56.13	
20	47.13	57.13	
21	49.13	57.13	
22	52.13	58.13	
23	54.13	59.13	
24	56.13	60.13	

2) Twin Zebra conductor bundle

Surface Gradient (kV/cm)	Excitation Function dB (1μA/ m)		
	Dry Conditions	Rain (2 mm/min.)	Fire (In dry condition)
11	19.13	34.13	39.13
12	28.13	37.13	43.13
13	28.13	40.13	46.13
14	35.13	42.13	49.13
15	37.13	45.13	51.13
16	39.13	48.13	53.13
17	41.13	49.13	57.13
18	45.13	50.13	59.13
19	48.13	51.13	64.13

APPENDIX E

Instantaneous Data Captured in the Corona Cage - Twin Dinosaur Conductor Bundle

---

The data here is a sample record of the electrical discharge activity captured on the twin dinosaur conductor bundle for a variety of surface gradients for three environmental conditions. The three conditions were

1) Dry conditions with average humidity and low wind speeds;
2) Wet conditions with a constant rain rate of 2mm/minute; and
3) Fire conditions with a localised point source of fire generated from a balloon gas burner.

The set of data shown was the reference used in chapter 6. The surface gradient was set to 16kV/cm and the next three graphs are duplicates of those shown in that chapter but magnified for better inspection of the discharge.

Experiments were repeated with an increasing surface gradient from 14 kV/cm up to 19kV/cm for dry and rain conditions. The fire tests could only be carried out up to 17kV/cm at which point flashover was consistently achieved.

Twin dinosaur with applied surface gradient of 16kV/cm (*DRY CONDITIONS*)

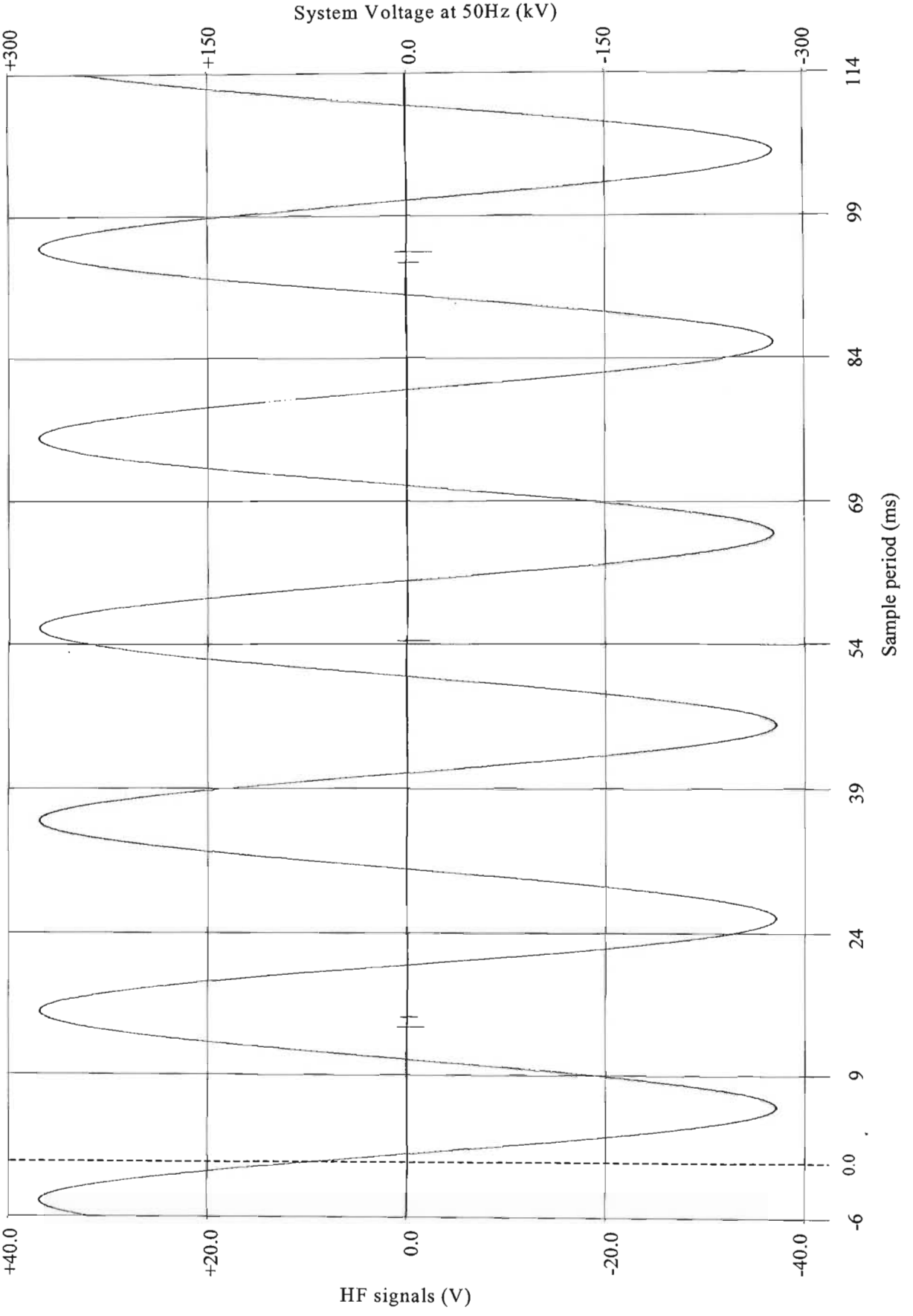

Figure E 1: Dry conditions at 16kV/cm.

Twin dinosaur with applied surface gradient of 16kV/cm (*RAIN / WET CONDITIONS*)

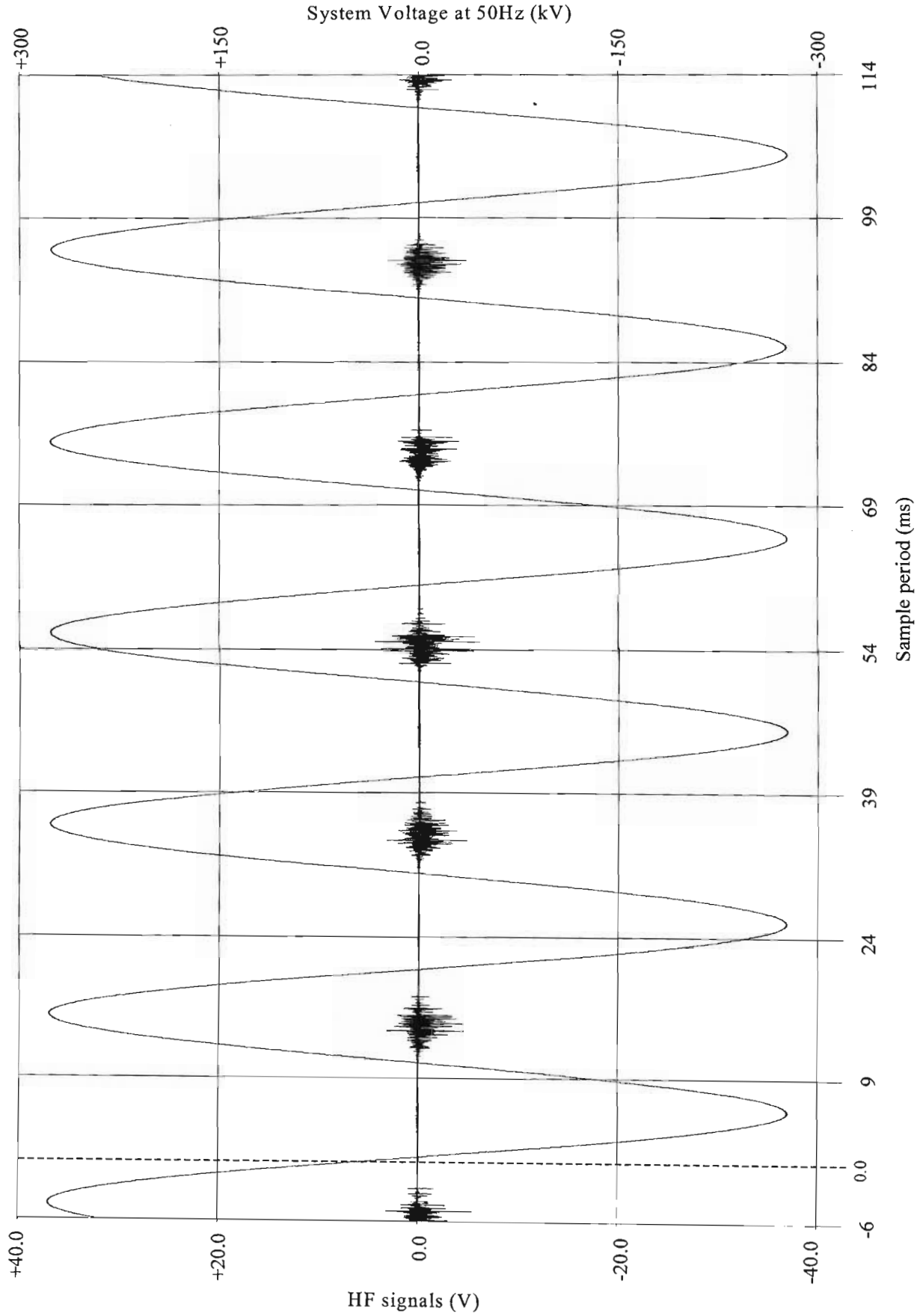

Figure E 2: Rains conditions at 16kV/cm

Twin dinosaur with applied surface gradient of 16kV/cm (*GAS FIRE CONDITIONS*)

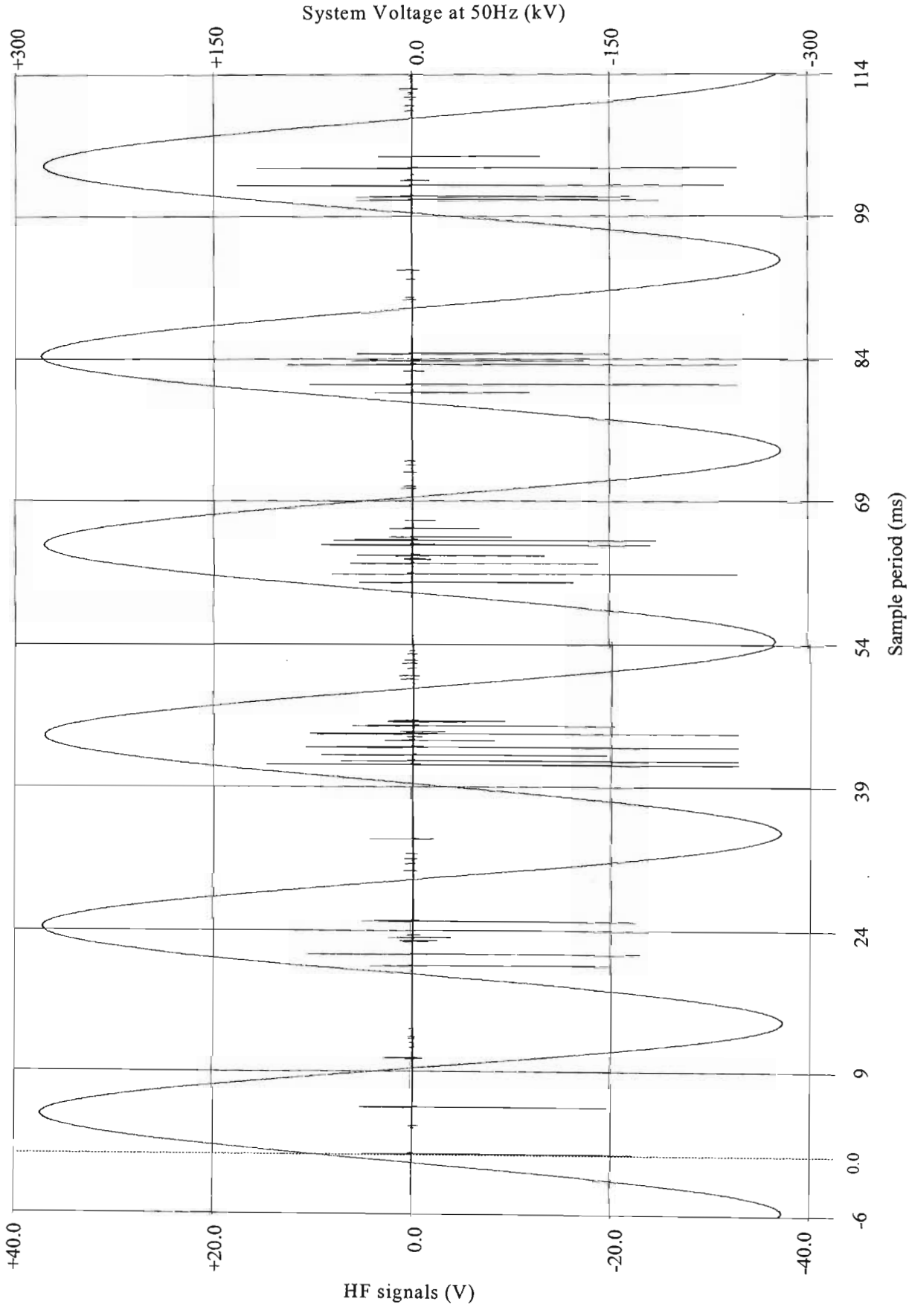

Figure E 3: Gas fire conditions at 16kV/cm (Sample 1 of 2)

Twin dinosaur with applied surface gradient of 16kV/cm (*GAS FIRE CONDITIONS*)

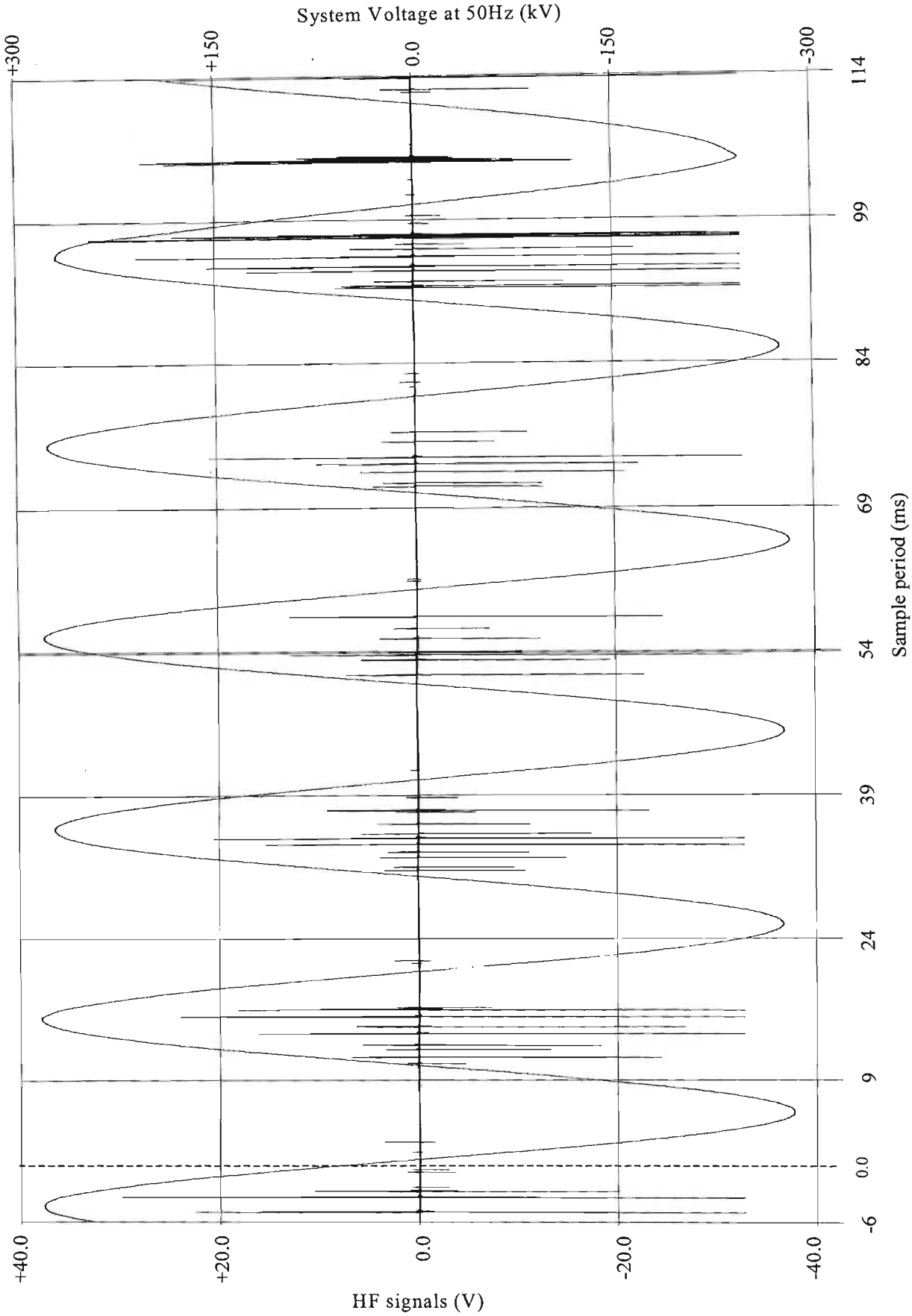

Figure E 4: Gas fire conditions at 16kV/cm (Sample 2 of 2)

APPENDIX F

Instantaneous Data Captured in the Corona Cage - Twin Zebra Conductor Bundle - Gas Fire Testing

---

The data here is a sample record of the electrical discharge activity captured on the twin zebra conductor bundle for a variety of surface gradients for three environmental conditions. The three conditions were

1) Dry conditions with average humidity and low wind speeds;
2) Wet conditions with a constant rain rate of 2mm/minute; and
3) Fire conditions with a localised point source of fire generated from a balloon gas burner.

The set of data shown, was the reference used in chapter 6. The surface gradient was set to 17kV/cm and the next three graphs are duplicates of those shown in that chapter but magnified for better inspection of the discharge.

Experiments were repeated with an increasing surface gradient from 16 kV/cm up to 20kV/cm for the three conditions.

Twin zebra with applied surface gradient of 17kV/cm (*DRY CONDITIONS*)

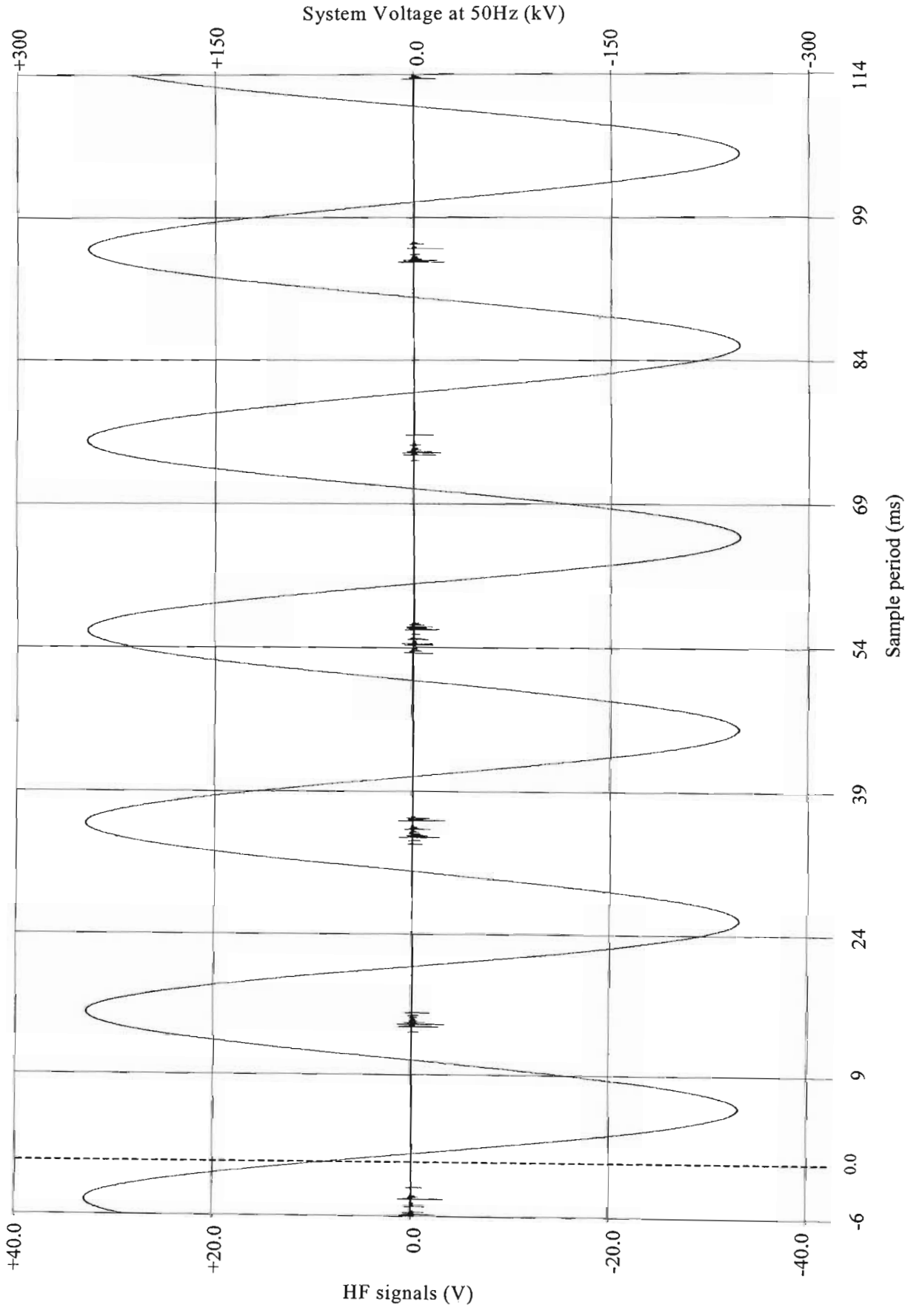

Figure F 1: Dry conditions at 17kV/cm.

Twin zebra with applied surface gradient of 17kV/cm (*RAIN / WET CONDITIONS*)

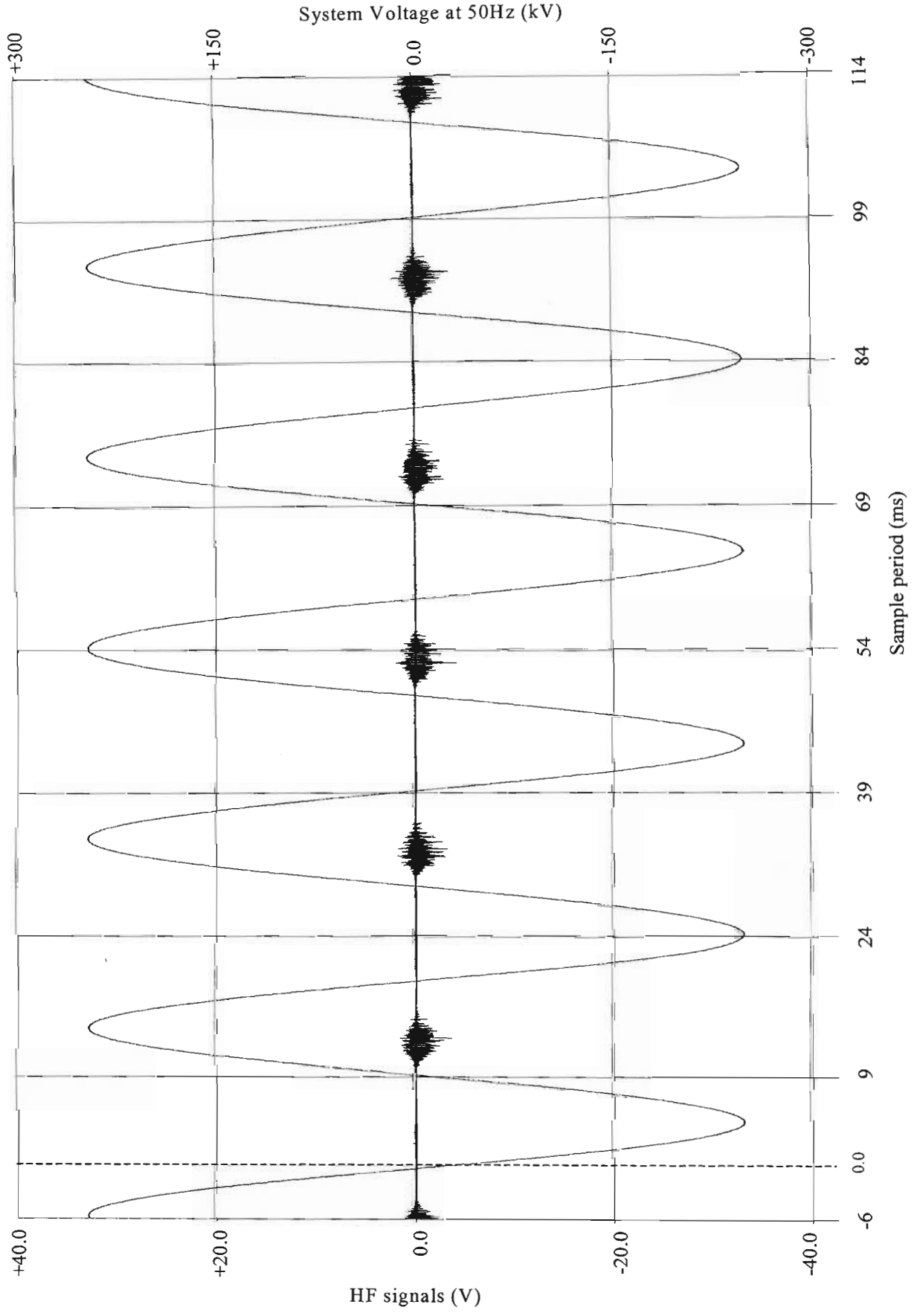

Figure F 2: Rain conditions at 17kV/cm.

Twin zebra with applied surface gradient of 17kV/cm (*GAS FIRE CONDITIONS*)

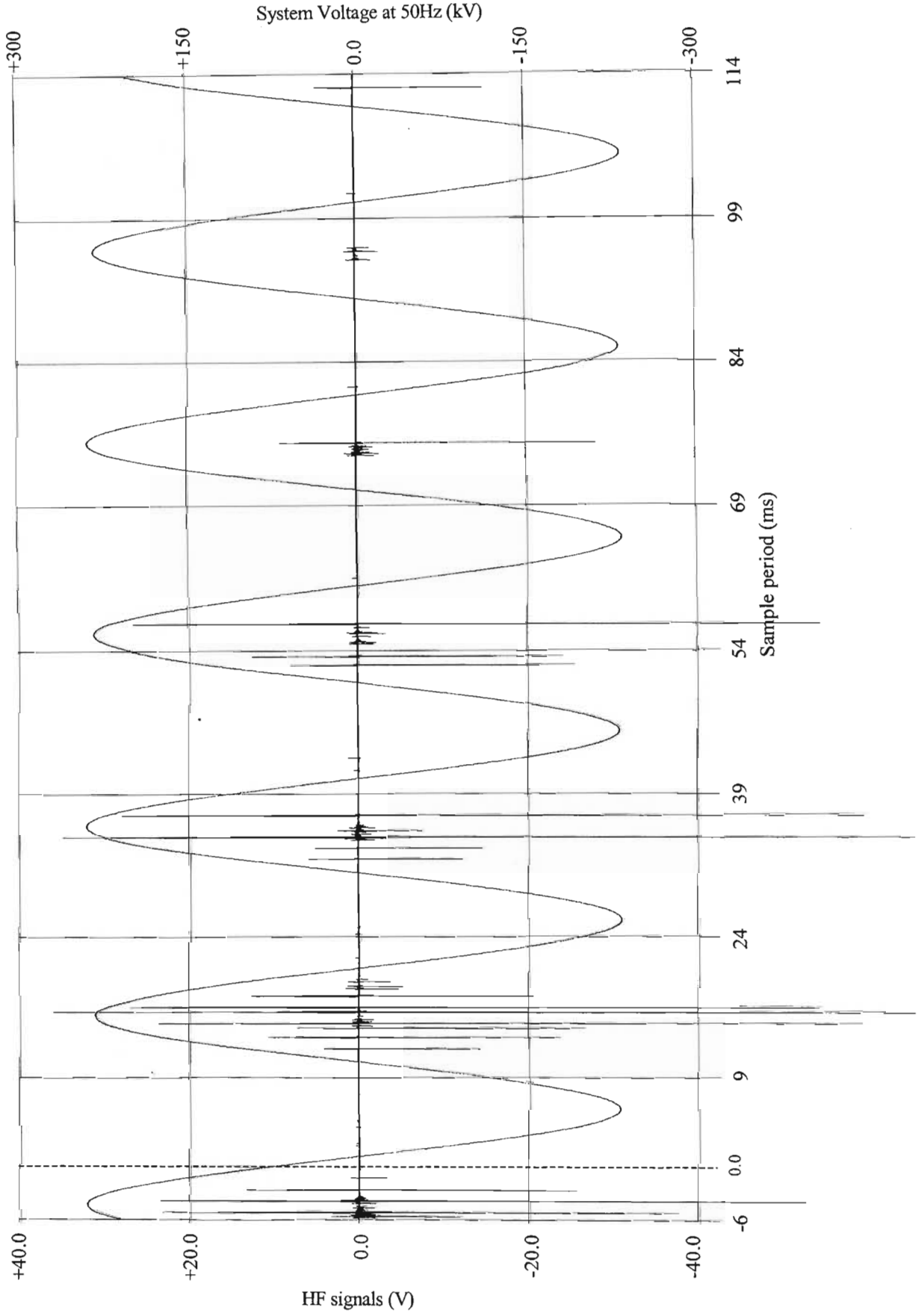

Figure F 3: Gas fire conditions at 17kV/cm

APPENDIX G

Statistical Calculation Of The Trend In The Induced Corona Noise Patterns.

The statistical data is calculated for the corona noise generated in a particular 50 Hz half cycle. The statistical data includes the following:

1) The minimum voltage measured at any point during the half cycle,
2) The maximum voltage measured at any point during the half cycle,
3) The arithmetic mean of the voltage levels measured during the given half cycle (sum of all the data points divided by the total number of points),
4) The standard deviation between the data points and the mean value - calculated by the following [where M = the mean value (given in point 3 above), p_i is the i_{th} data point and n is the total number of data points] :-

$$Std.DEV = \sqrt{\frac{\sum_{i=1}^{n}(p_i - M)^2}{n-1}} \qquad (26)$$

5) The RMS value of the voltage levels measured during the given half cycle,
6) The number of pulses occurring in that half cycle, measured as follows:
   Dry condition: Any activity greater than the radio station "noise" measured,
   Rain condition: Any activity greater than that occurring in normally dry conditions,
   Fire conditions: Any activity greater than that occurring in normally dry conditions and as additional information, any activity greater than that occurring in rain conditions,
7) The number of pulses occurring in that half cycle, measured for all three conditions relative to a reference voltage of ± 1 volt - the number of pulses with amplitudes greater than this reference was then recorded. A direct quantifiable comparison of pulse information is then more practical.
8) The frequency with which the pulses as recorded in 6) and 7) above, are repeated

All data analysed in this appendix was captured in the corona cage and has been discussed in the earlier chapters 4 and 6. The whole positive half cycles in each series of data was considered and shown with the statistical data in tabular form directly after all the graphs.

The conductor bundles are presented in the following order:

1. Twin Dinosaur conductor bundle: Sample data was at a gradient of 16 kV/cm

1.1 Normal dry conditions

1.2 Rain conditions

1.3 Fire conditions

1.4 Summary of statistics on the twin Dinosaur

2. Twin Zebra conductor bundle: Sample data was at a gradient of 17 kV/cm

2.1 Normal dry conditions

2.2 Rain conditions

2.3 Fire conditions

2.4 Summary of statistics on the twin Zebra

Note: P_n and P_r were determined measuring all pulses occurring with greater amplitude than the amplitude of the next noise source. P_{nl} and P_{rl} were determined measuring all pulses occurring with greater amplitude than a reference amplitude (Reference of ± 1 V).

Dinosaur conductor Bundle limits for P_n and P_r:

For dry conditions the limits were set by the background radio noise (± 100 mV);

For rain conditions the limits were set by dry conditions (-2.662V and +1.171 V);

For gas fire conditions the limits were set by the heavy rain conditions (-6.122V and +4.435V).

Zebra conductor Bundle limits for P_n and P_r:

For dry conditions the limits were set by the background radio noise (± 100 mV);

For rain conditions the limits were set by dry conditions (-3.318V and +1.581V);

For gas fire conditions the limits were set by the heavy rain conditions (-3.594V and +2.154V).

G1. TWIN DINOSAUR CONDUCTOR BUNDLE: SAMPLE DATA AT 16 kV/cm.

G1.1 Normal Dry Conditions

Corona noise data presented with respect to the positive half of the applied 50Hz power signals as shown in figure 6.1 on page 85.

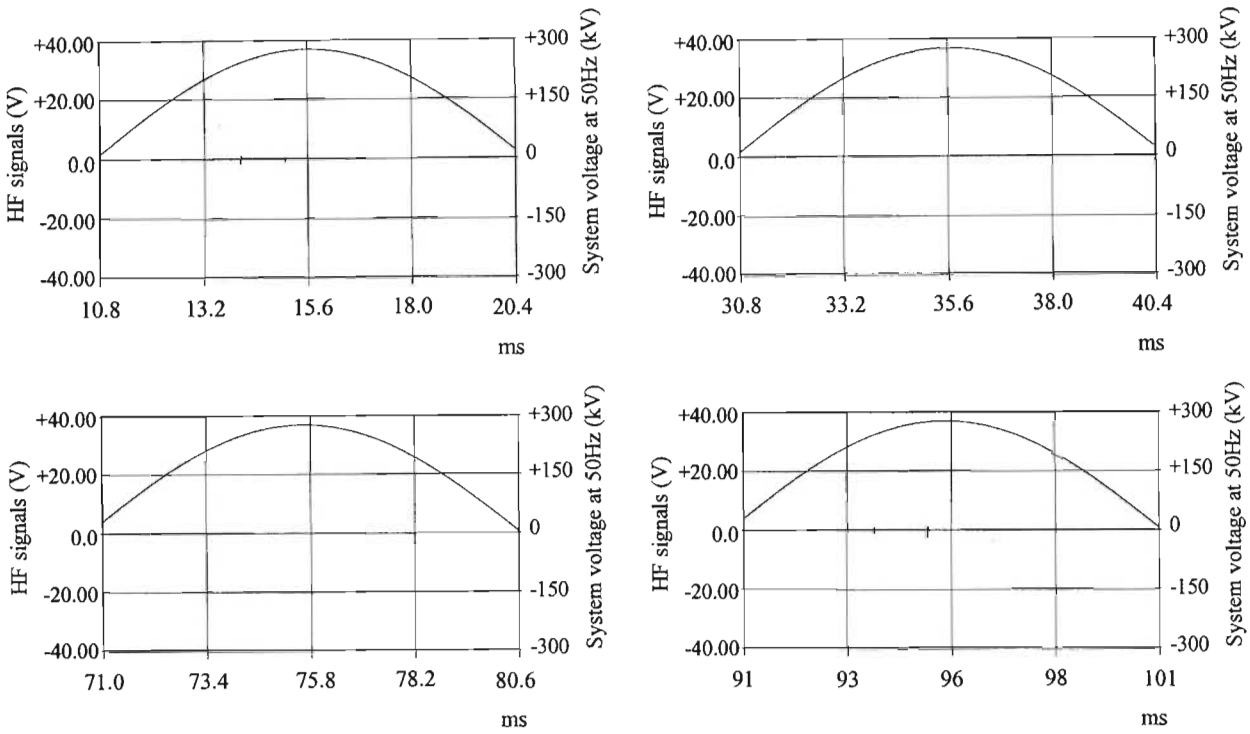

Figure G 1: Statistics for the first four positive half cycles of corona in dry conditions.

Statistics	Positive half cycles			
	First	Second	Third	Fourth
Min. (V)	-1.755	- 0.0992	- 0.0912	- 2.662
Max. (V)	1.042	0.088	0.0928	1.171
Mean (mV)	-2.65	- 2.59	- 1.20	- 1.13
Std. Dev (mV)	41.06	35.98	35.73	55.77
RMS (mV)	41.15	36.07	35.75	55.78
# of pulses (P_n)	6.5	0	0	7
Pulse reps. (P_r)	677	0	0	729
# of pulses (P_{nl})	1	0	0	1.5
Pulse reps.(P_{rl})	104	0	0	156

G1.2 Heavy Rain conditions

Corona noise data presented with respect to the positive half of the applied 50 Hz power signals as shown in figure 6.2 on page 85.

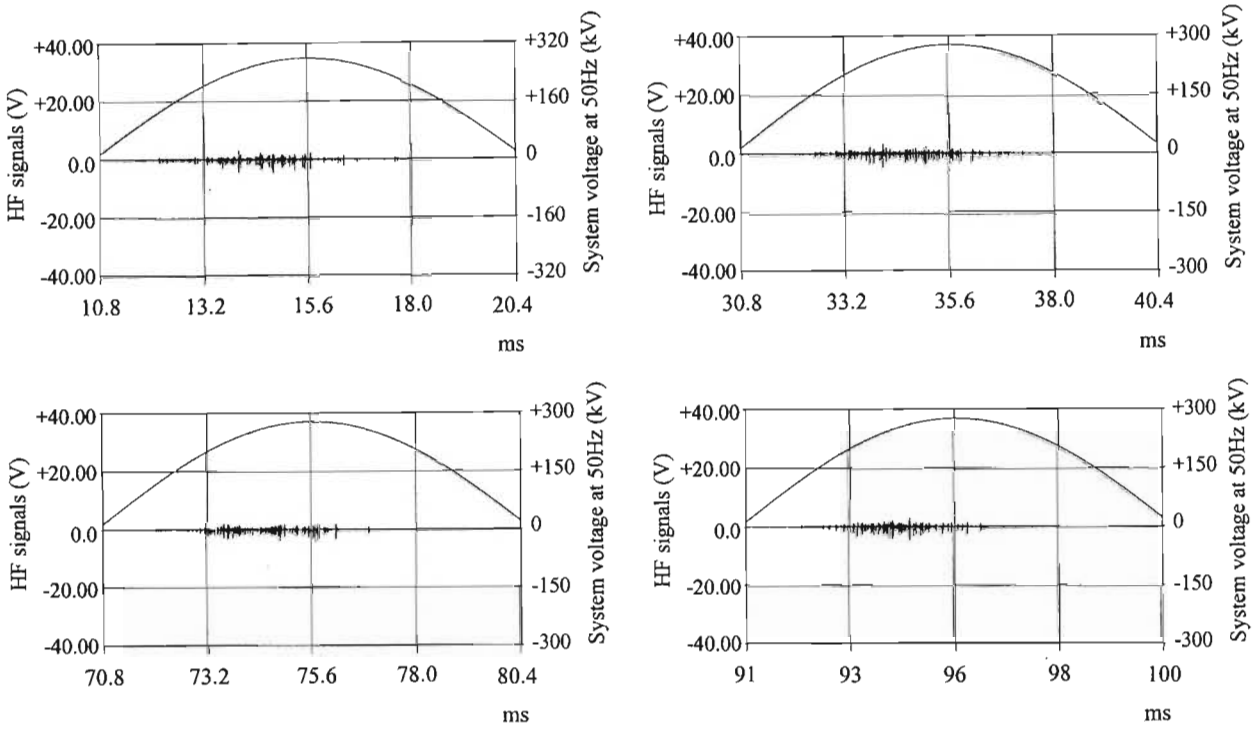

Figure G 2: Statistics for the first four positive half cycles of corona in heavy rain conditions.

Statistics	Positive half cycles			
	First	Second	Third	Fourth
Min. (V)	- 4.566	- 4.768	- 6.122	- 4.006
Max. (V)	3.171	3.274	4.435	2.215
Mean (mV)	- 4.559	-4.405	-9.25	0.243
Std. Dev (mV)	204.4	205.6	209.6	195.4
RMS (mV)	204.4	205.6	209.8	195.4
# of pulses (P_{nd})	12.5	11.5	11.5	10.5
Pulse reps. (P_{rd})	1302	1198	1198	1094
# of pulses (P_{nl})	38	39	49	42
Pulse reps.(P_{rl})	3958	4063	5104	4375

G1.3 Gas Fire Conditions

With a low pressure gas source. Corona noise data presented with respect to the positive half of the applied 50 Hz power signals as shown in figure 6.3 on page 86.

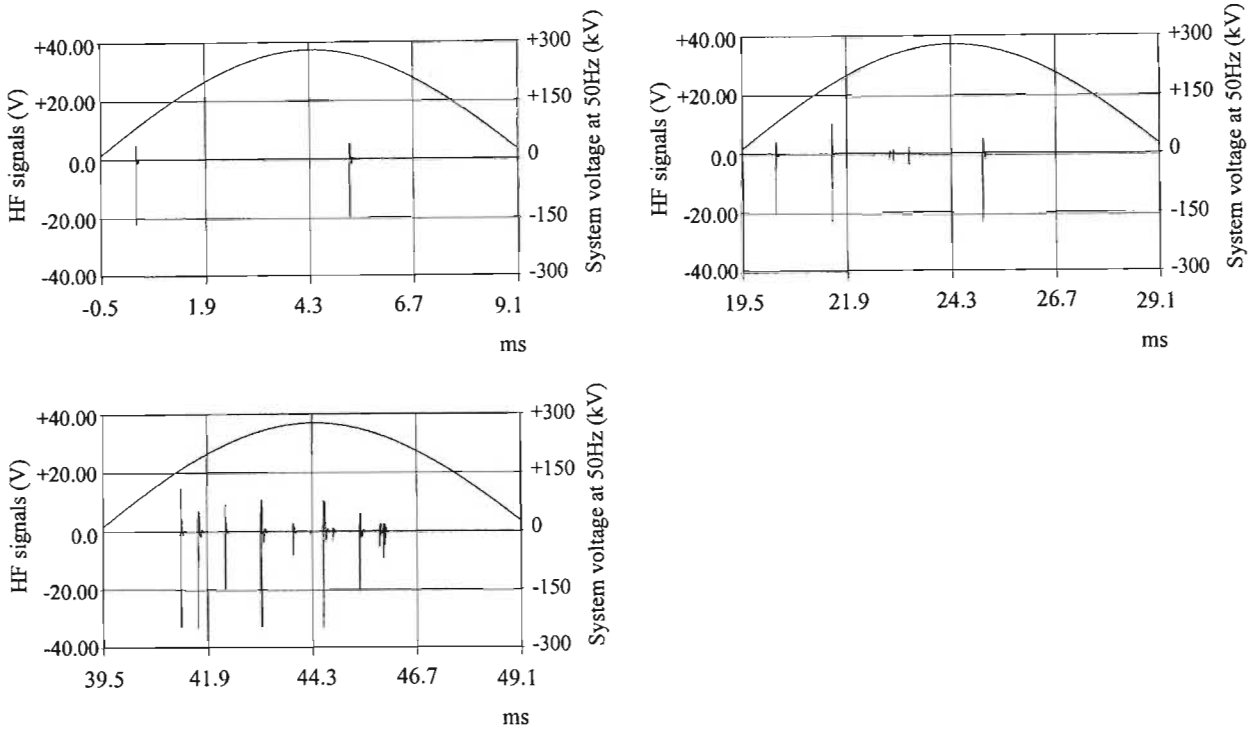

Figure G 3: Statistics for the first three positive half cycles of corona over a gas fire.

Statistics	Positive half cycles (Table 1 of 2)		
	First	Second	Third
Min. (V)	-22.2	-22.99	-32.78
Max. (V)	5.328	10.5	14.74
Mean (mV)	-14.89	-14.87	-13.73
Std. Dev (mV)	439.0	455.6	1161
RMS (mV)	439.3	455.9	1161
# of pulses (P_{nw})	1.5	1.5	11
Pulse reps. (P_{rw})	156	156	1146
# of pulses (P_{nl})	4	11	25.5
Pulse reps. (P_{rl})	416	1146	2656

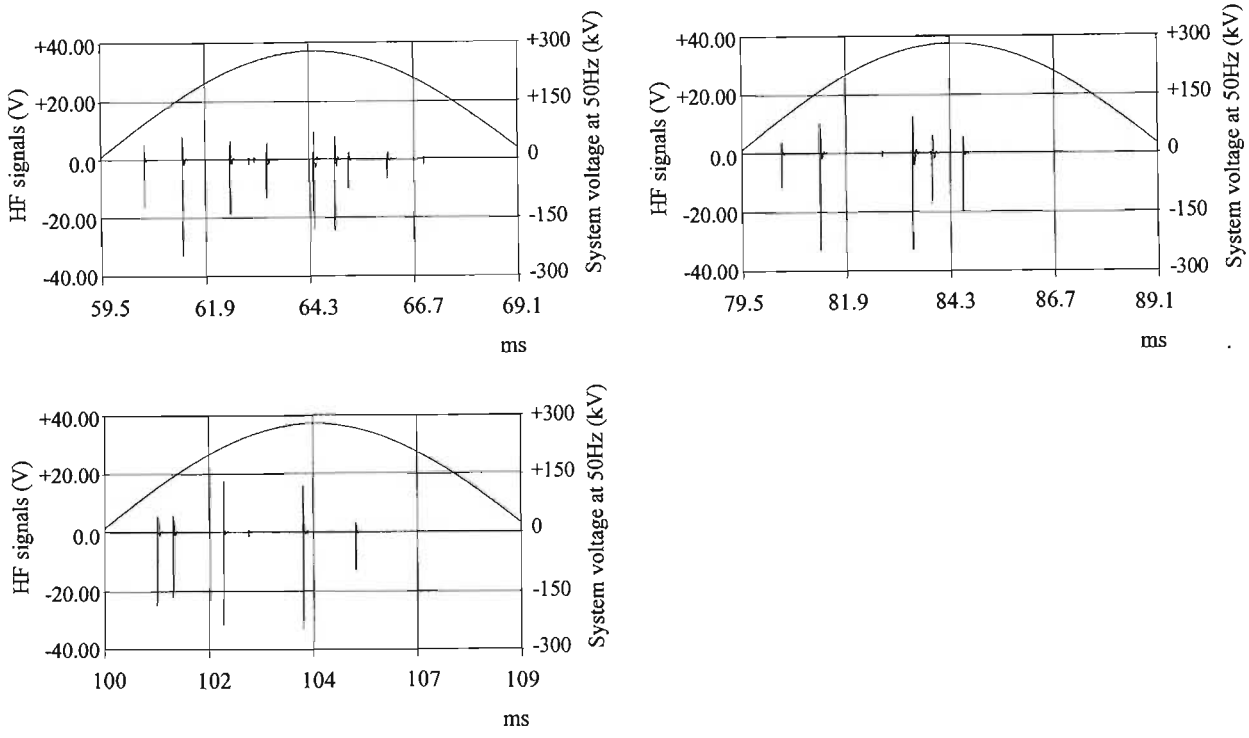

Figure G 4: Statistics for the second three positive half cycles of corona over a gas fire.

Statistics	Positive half cycles (Table 2 of 2)		
	Fourth	Fifth	Sixth
Min. (V)	-32.88	-32.88	-32.88
Max. (V)	9.296	12.61	17.63
Mean (mV)	0.57	0.81	1.46
Std. Dev (mV)	976.4	976.0	602.2
RMS (mV)	976.4	976.0	602.2
# of pulses (P_{nw})	7	5	7
Pulse reps. (P_{rw})	729	521	729
# of pulses (P_{nl})	19	12.5	16.5
Pulse reps. (P_{rl})	1979	1302	1719

G1.4 Summary of statistics on the twin Dinosaur

Statistical Variables	Normally Dry Conditions	Rain Conditions (2 mm/min.)	Fire in Normal Dry Conditions
Min. (V)	- 2.662	-6.122	-32.88*
Max. (V)	1.171	4.435	17.63
Mean (mV)	- 1.89	-4.49	-6.78
Std. Dev. (mV)	42.14	203.75	768.37
RMS (mV)	42.19	203.75	768.47
# of Pulses**	0.63	42	14.75
Pulse Rep. Rate**	65	4375	1536.33

In the above table, all values (except minimum and maximum which are the overall minimum and maximum voltages) were obtained by averaging the information of each positive half cycle per condition.

* The range selected for the measurement of the pulse voltages limited the voltage to the negative voltage of 32.88 volts (the noise pulses were therefore clipped at this value).

** The pulse data was determined from P_{nl} and P_{rl} respectively.

G2. TWIN ZEBRA CONDUCTOR BUNDLE: SAMPLE DATA AT 17 kV/cm.

G2.1 Normal Dry Conditions

Corona noise data presented with respect to the positive half of the applied 50 Hz power signals as shown in figure 6.5 on page 89.

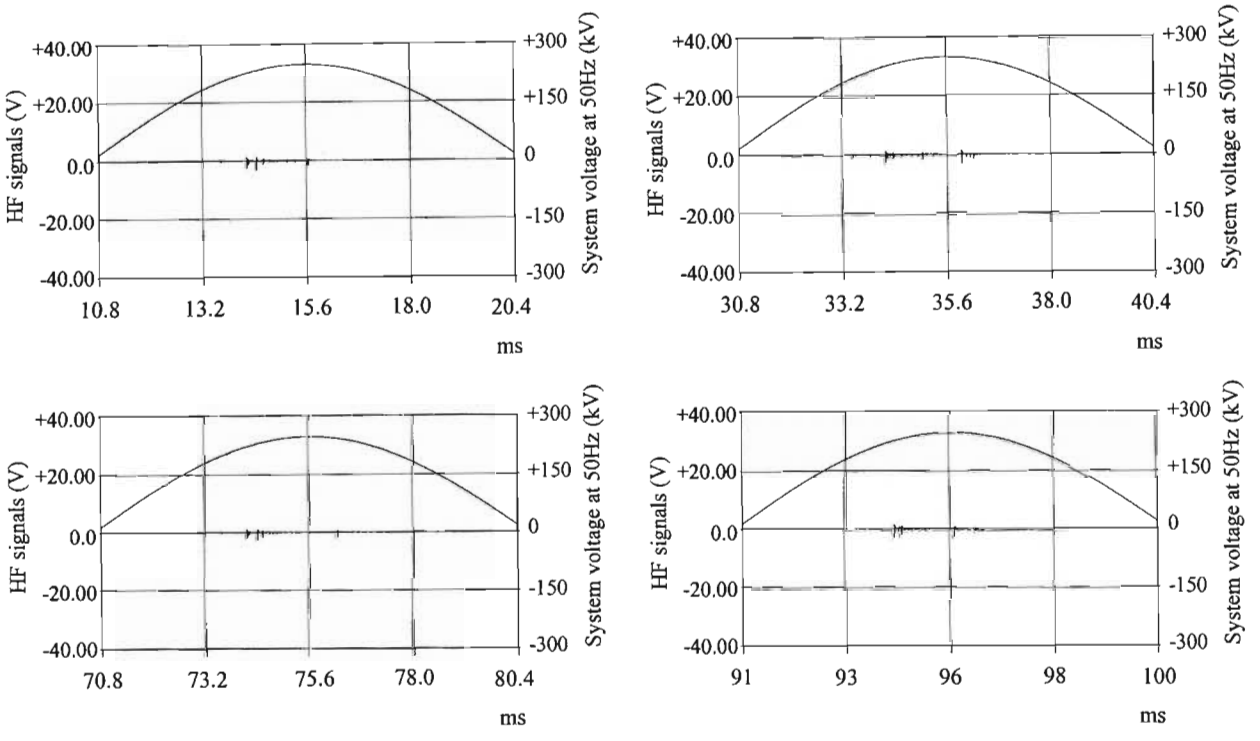

Figure G 5: Statistics for the first four positive half cycles of corona in dry conditions.

Statistics	Positive half cycles			
	First	Second	Third	Fourth
Min. (V)	-3.296	-3.318	-2.755	-3.171
Max. (V)	1.478	1.44	1.203	1.581
Mean (mV)	-2.46	-2.36	1.32	1.43
Std. Dev (mV)	71.78	80.99	67.77	76.15
RMS (mV)	71.82	81.03	67.78	76.16
# of pulses (P_n)	109	140	109	116
Pulse reps. (P_r)	11354	14583	11354	12083
# of pulses (P_{nl})	3	2	3	3
Pulse reps.(P_{rl})	312.5	208	312.5	312.5

G2.2 Heavy Rain conditions

Corona noise data presented with respect to the positive half of the applied 50 Hz power signals as shown in figure 6.6 on page 90.

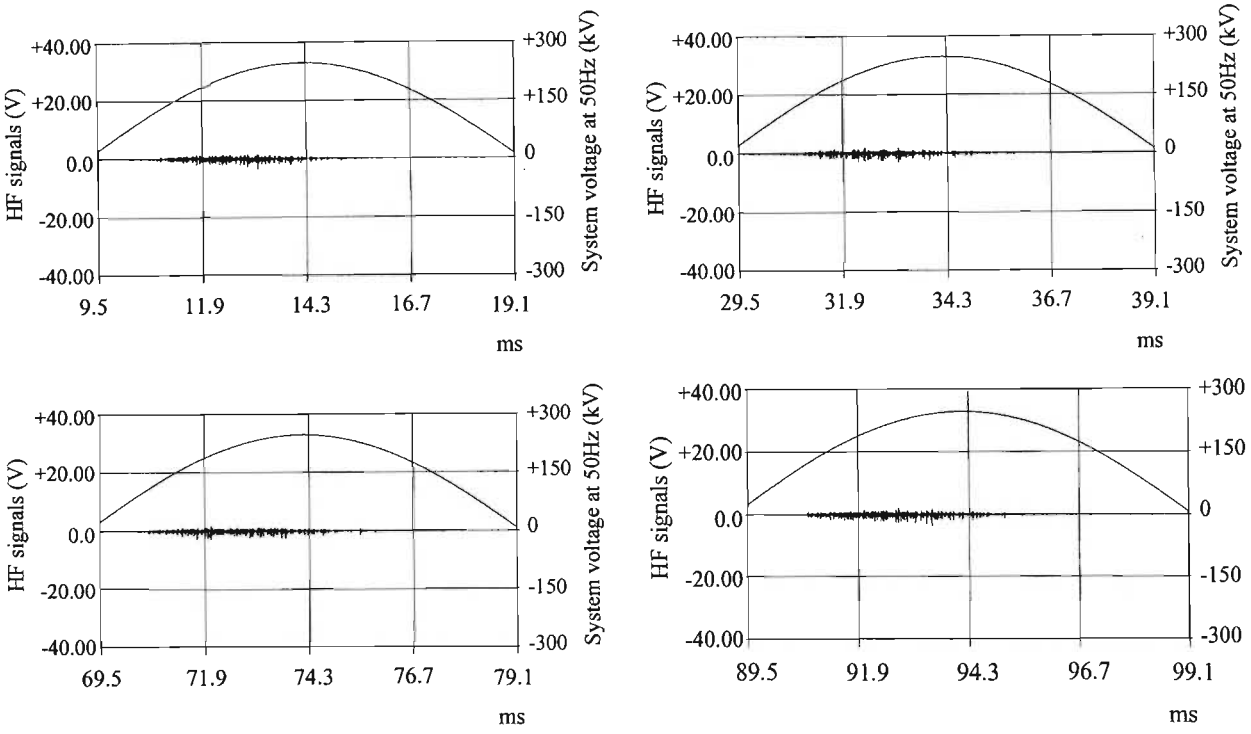

Figure G 6: Statistics for the first four positive half cycles of corona in heavy rain conditions.

Statistics	Positive half cycles			
	First	Second	Third	Fourth
Min. (V)	-3.594	-3.267	-3.005	-3.587
Max. (V)	1.568	1.85	1.626	2.154
Mean (mV)	-3.55	-3.61	-0.47	-0.51
Std. Dev (mV)	207.3	213.8	203.2	221.1
RMS (mV)	207.3	213.8	203.2	221.1
# of pulses (P_{nd})	0	5.5	0.5	1.5
Pulse reps. (P_{rd})	0	52	52	156
# of pulses (P_{nl})	29	38	21	35
Pulse reps. (P_{rl})	3021	3958	2188	3646

G2.3 Gas Fire Conditions

With a low pressure gas source. Corona noise data presented with respect to the positive half of the applied 50 Hz power signals as shown in figure 6.7 on page 90.

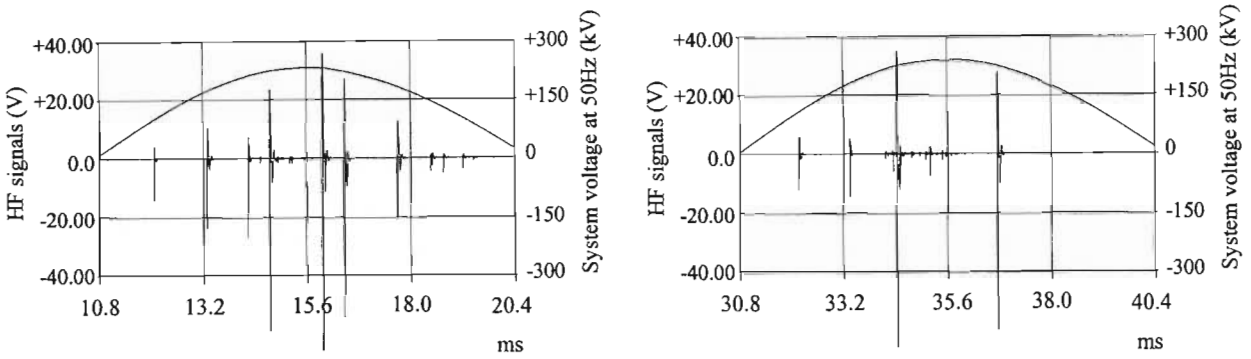

Figure G 7: Statistics for the first two positive half cycles of corona over a gas fire.

Statistics	Positive half cycles (Table 1 of 2)	
	First	Second
Min. (V)	-65.73	-65.73
Max. (V)	35.94	34.94
Mean (mV)	-6.53	-4.83
Std. Dev (mV)	2002	2690
RMS (mV)	2002	2690
# of pulses (P_{nw})	13	8.5
Pulse reps. (P_{rw})	1354	885
# of pulses (P_{n1})	22	14.5
Pulse reps. (P_{r1})	2292	1510

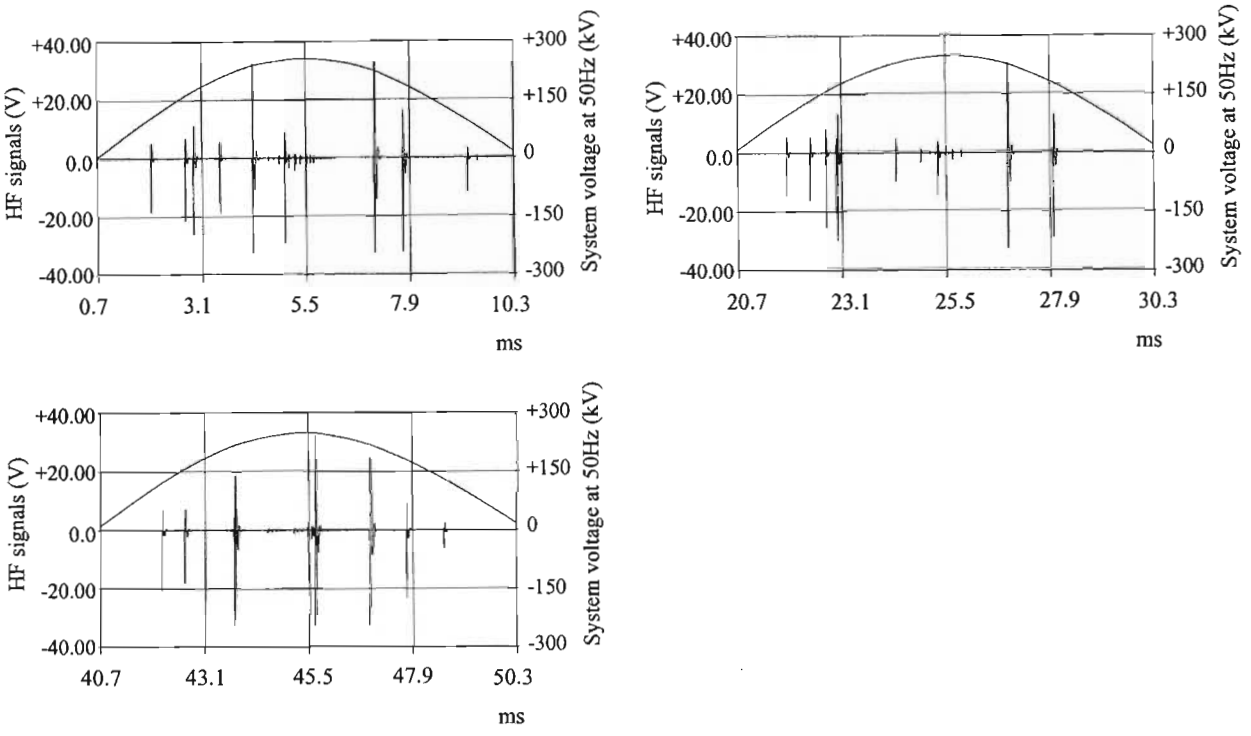

Figure G 8: Statistics for the last three positive half cycles of corona over a gas fire.

Statistics	Positive half cycles (Table 2 of 2)		
	Third	Fourth	Fifth
Min. (V)	-32.67	-32.67	-32.67
Max. (V)	32.85	30.99	32.34
Mean (mV)	23.54	0.23	7.68
Std. Dev (mV)	2766	1943	2450
RMS (mV)	2766	1943	2450
# of pulses (P_{nw})	16.5	16	9.5
Pulse reps. (P_{rw})	1719	1667	989.5
# of pulses (P_{nl})	35.0	28.5	16.5
Pulse reps. (P_{rl})	3646	2969	1719

G2.4 Summary of statistics on the twin Zebra

Statistical Variables	Normally Dry Conditions	Rain Conditions (2 mm/min.)	Fire in Normal Dry Conditions
Min. (V)	-3.318	-3.594	-65.73*
Max. (V)	1.581	2.154	35.94
Mean (mV)	-0.52	-2.04	4.02
Std. Dev. (mV)	74.17	211.35	2370.2
RMS (mV)	74.20	211.35	2370.2
# of Pulses**	2.75	30.75	23.3
Pulse Rep. Rate**	286.38	3203.25	2427.2

In the above table, all values (except minimum and maximum which are the overall minimum and maximum voltages) were obtained by averaging the information of each positive half cycle per condition.

* The range selected for the measurement of the pulse voltages limited the voltage to the negative voltage of 65.73 volts (the noise pulses were therefore clipped at this value).

** The pulse data was determined from Pn1 and Pr1 respectively.

APPENDIX H

Filter Response of the BBC Filters

These filters are standard filters available for use in the power line carrier equipment and are therefore ideal filters for use in the measurement of the carrier channel background noise.

Filter 1:

Manufacturer's Specification:
Centre Frequency: 52 kHz
Bandwidth: 4 kHz

In the table on the next page, the output of the 52 kHz BBC filter was measured when a 0 dB signal was provided - at the given frequency - at the input. The graphical representation is shown in figure H1 below.

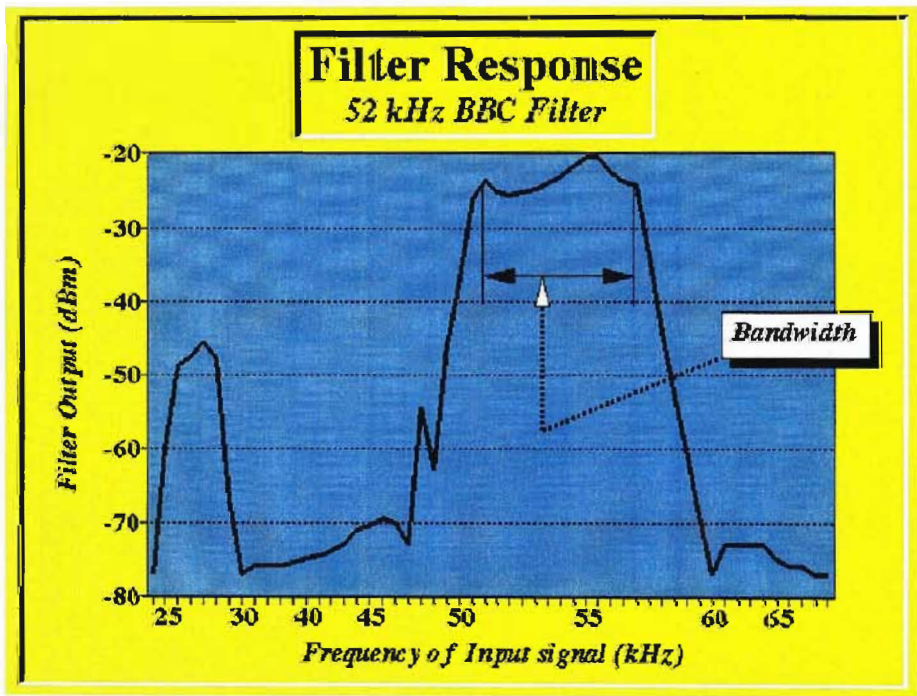

Figure H 1: 52kHz Bandpass Filter Response.

Response data of the 52 kHz BBC filter with a 0dB input signal at the frequency shown

Frequency (kHz)	dBm (OUT)	Frequency (kHz)	dBm (OUT)
24.0	-77.0	51.5	-25.2
25.0	-60.0	52.0	-25.6
26.0	-49.0	52.5	-25.4
27.0	-47.6	53.0	-24.9
27.5	-45.5	53.5	-24.1
28.0	-48.0	54.0	-23.1
29.0	-67.0	54.5	-21.9
30.0	-77.0	55.0	-20.7
36.0	-76.0	55.5	-20.7
37.0	-76.0	56.0	-22.6
38.0	-76.0	56.5	-23.9
39.0	-75.5	57.0	-24.2
40.0	-75.0	57.5	-33.6
41.0	-74.5	58.0	-44.0
42.0	-74.0	58.5	-53.0
43.0	-73.0	59.0	-61.0
44.0	-71.0	59.5	-69.0
45.0	-70.5	60.0	-77.0
46.0	-69.5	61.0	-73.0
47.0	-70.0	62.0	-73.0
48.0	-73.0	63.0	-73.0
48.5	-63.0	64.0	-73.0
49.0	-54.5	65.0	-75.0
49.5	-46.0	66.0	-76.0
50.0	-36.8	67.0	-76.0
50.5	-26.4	68.0	-77.0
51.0	-23.8	69.0	-77.0

Filter 2:

Manufacturer's Specification:

Centre Frequency: 428 kHz

Bandwidth: 4 kHz

In the table on the next page the output of the 428 kHz BBC filter was measured when a 0 dB signal was provided - at the given frequency - at the input. The graphical representation is shown in figure H2 below.

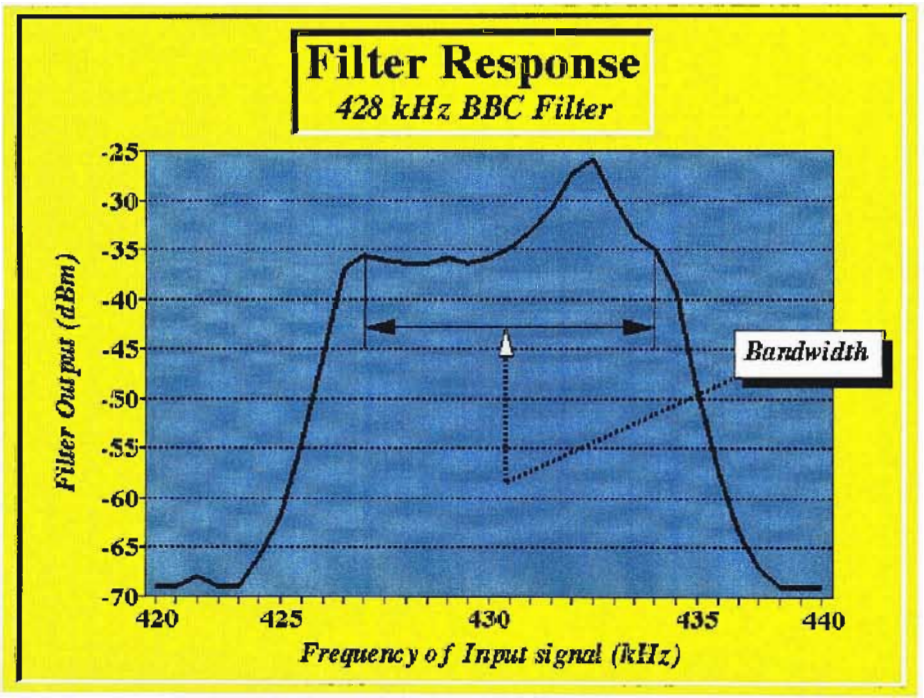

Figure H 2: 428kHz Bandpass Filter Response.

Response data of the 428 kHz BBC filter with a 0dB input signal at the frequency shown.

Frequency (kHz)	dBm (OUT)	Frequency (kHz)	dBm (OUT)
420.0	-69.0	430.5	-30.8
421.0	-69.0	431.0	-27.4
422.0	-68.0	431.5	-26.0
423.0	-69.0	432.0	-30.0
424.0	-69.0	432.5	-33.6
424.5	-66.0	433.0	-35.0
425.0	-62.0	433.5	-39.2
425.5	-54.5	434.0	-49.0
426.0	-45.8	434.5	-57.4
426.5	-37.0	435.0	-63.5
427.0	-35.6	435.5	-67.0
427.5	-36.2	436.0	-69.0
428.0	-36.5	437.0	-69.0
428.5	-36.4	438.0	-69.0
429.0	-35.9	439.0	-69.0
429.5	-34.9	440.0	-69.0
430.0	-33.2		

REFERENCES

[1] Cowan, P.; Britten, A.C.; Natal Cane Fires Transmission Line Fault Research, Eskom Internal Report TRR/E89/P010, EEI, Power Equipment, October 1989.

[2] Bird, J.T.; A study of transmission line outages due to cane fires, Bachelor of Engineering Thesis, Faculty of Engineering, University of Queensland, 20 May 1978.

[3] Eskom in Perspective. A survey of Eskom and its plans for the future, Supplement with the Eskom Nineteen Ninety One Annual Report, March 1992, Leadership Publications.

[4] Cowan, P.; Britten, A.C.; Natal Cane Fires Transmission Line Fault Research, Eskom Internal Report TRR/E89/P010, EEI, Power Equipment, October 1989.

[5] Sadurski, K.J.; Robertson, E.W.J.; Effects of Bush, Grass and Cane Fires Below Transmission Lines, Eskom Internal Report 123/2/97, New Works Dept., ERD, May 1977.

[6] Cowan, P.M.; Dunn, J.A.; Naidoo, P.; Masters, J.D.; Sugar cane fire induced transmission line flashovers, Elektron, SAIEE, January 1991, pp 12-15.

[7] Davis, A.H.; An Objective Noise-meter for the Measurement of Moderate, Loud, Steady and Impulsive Noises, cited by Comber, M.G.; Nigbor, R.J.; in the Transmission Line Reference Book - 345 kV and Above, Chapter 5 "Radio Noise".

[8] Protective Relays Application Guide; Third Edition Reprinted September 1990; GEC Alsthom Measurements; Published by GEC ALSTHOM Protection & Control Limited, England.

[9] Gary, Claude H.; The theory of the excitation function: A demonstration of its physical meaning, IEEE transactions on Power Apparatus and Systems, Volume 91, Jan/Feb 1972, pp 305 - 310.

[10] Vosloo, W.L.; A study into the effect of sugar cane fires on ac corona noise, Thesis for the degree Master of Engineering Science, Institute of Electrical Technology, University of Stellenbosch, sponsored and supported by Eskom, January 1992. Supervised by Holtzhausen, J.P.

[11] Sadurski, K.J.; Reynders, J.P.; High voltage AC breakdown in presence of fires, Sixth International Symposium on High Voltage Engineering, New Orleans, LA, USA, August 28 - September 1, 1989.

[12] Countryman, C.M.; Mass fires and fire behaviour, U.S. Forest Service Research Paper PSW-19, 1964, cited by West, H.J.; McMullan, D.W.; Fire induced flashovers of EHV transmission lines, IEEE PES Winter meeting, New York, NY, 4-9 February 1979.

[13] Kuffel, E.; Zaengl, W.S.; High Voltage Engineering Fundamentals, Pergamon Press, First Ed. 1984, Reprinted 1986, 1988.

[14] Kraus, J.D.; Carver, K.R.; Electromagnetics, McGraw-Hill International Book Company, International Student Edition, Second edition, 9th printing 1981.

[15] Townsend, J.S.; Electricity in Gases, Oxford, Clarendon Press, 1915, Chapters 1 and 8

[16] Raether, H.; Electron Avalanches and Breakdown in Gases, Butterworths, London, 1964 cited by Kuffel,E.; Zaengl, W.S.; High Voltage Engineering Fundamentals, Chapter 5 "Electrical breakdown in gases, solids and liquids".

[17] Meek,J.M.; Craggs,J.D.; Electrical Breakdown of Gases, Clarendon Press, Oxford, 1953 cited by Kuffel,E.; Zaengl, W.S.; High Voltage Engineering Fundamentals, Chapter 5 "Electrical breakdown in gases, solids and liquids".

[18] Loeb, L.B.; Electrical Coronas - Their Basic Physical Mechanisms, University of California Press, USA, 1965.

[19] Peek, F.W.; The law of corona and the dielectric strength of air, Vol. I - 28th Annual Convention of the American Institute of Electrical Engineers, Chicago, Ill., June 29, 1911; and published in Trans. A.I.E.E.,Vol. XXX, 1911, pp 1889 - 1965

[20] Peek, F.W.; The law of corona and the dielectric strength of air, Vol. II - 29th Annual Convention of the American Institute of Electrical Engineers, Boston, Mass., June 25, 1912; and published in Trans. A.I.E.E.,Vol. XXXI, 1912, pp 1051 - 1092

[21] Peek, F.W.; The law of corona and the dielectric strength of air, Vol. III - 30th Annual Convention of the American Institute of Electrical Engineers, Cooperstown, N.Y., June 27, 1913; and published in Trans. A.I.E.E.,Vol. XXXII, 1913, pp 1767 - 1785 respectively.

[22] Peek, F.W.; Dielectric Phenomena in High-Voltage Engineering, McGraw-Hill Book Company, Inc., Third Edition, New York and London, 1929

[23] Foggo, S.M.; Whitcombe, L.C.; Techniques for determining the characteristics of corona pulses, Central Electricity Research Laboratories, Leatherhead, Surrey, England published in Electronics Letters, 12th July 1968, Vol. 4, No 14, pp 284 -288.

[24] Von Engel, A; Ionized Gases; Second Edition, Oxford University Press, 1965.

[25] Compton; K.T.; Trans. A.I.E.E. p.882,1927 cited by Peek, F.W.; Dielectric Phenomena in High-Voltage Engineering, pp 45-46

[26] IEEE Standard Procedures for the Measurement of Radio Noise from Overhead Power Lines. New York, N.Y.: Institute of Electrical and Electronic Engineers (IEEE), 1976. Std. 430-197.

[27] Macky, W.A.; Proc. Roy. Soc. (London) A133, 565 (1931) cited by Loeb, L.B.; Electrical Coronas - Their Basic Physical Mechanisms, p 248

[28] Juette, G.W.; Zaffanella, L.E.; Radio Noise, Audible Noise, and Corona Loss of EHV and UHV Transmission Lines Under Rain: Predetermination Based on Cage Tests, IEEE Transactions on Power Apparatus and Systems, Vol. PAS-89, No. 6, July/August, 1970, pp 1168 - 1178

[29] Boulet, L.; Jakubczyk, B.J.; AC Corona in Foul Weather I-Above Freezing Point, IEEE Trans. on Power Apparatus and systems, vol. 83, pp 508 - 512, May 1964.

[30] Kuffel, E.; Zaengl, W.S.; High Voltage Engineering Fundamentals; Pergamon Press, 1984.

[31] Britten,A.C.; Van Der Westhuizen,C.; Eskom's corona cage as a tool for research into corona phenomena at high altitudes, May 1989, EI '89 Conference, Eskom, Rosherville, Johannesburg.

[32] Demichelis, F.; Magistris, G.C.; Mantini, A.; Report on the study and implementation of a measuring system for radio interference and corona losses supplied to "Escom-Evkom" (South Africa) for EHV cage unit investigations, ENEL, Electrical Research Centre Report CRE1.DSR 608.410/2; Automatica Research Centre Report CRA.DSR 754.983/-, February 1981.

[33] Gary, C.H.; Moreau, M.R.; L'Effet de Couronne en Tension Alternative, Paris, Eyrolles, 1976.

[34] Artficial pollution tests on high-voltage insulators to be used on a.c. systems, International Electrotechnical Commission (IEC) Report Publication 507, first edition 1975, followed by draft publication in 1987 under the technical committee No. 36 on insulators.

[35] Transmission Line Reference Book - 345kV and Above; Prepared by Project UHV, General Electric Co. for the Electric Power Research Institute; 2nd Edition; 1982.

[36] Kip, A.F.; Phys. Rev. 54, 139, 1938 cited by Loeb, L.B.; Electrical Coronas - Their Basic Physical Mechanisms, Chapter 3 "True Coronas: I".

[37] Evert, C.R; The detection of sugar cane fires (or other fires) under high voltage transmission lines; Final project report for the National Energy Council; June 1992.

[38] Evert, C.R; The detection of fires under high voltage transmission lines; Eskom Internal Research report TRR/E/93/EL017, Project 7755P009R, July 1993.

[39] Evert, C.R; Pattern Recognition Test Results For The Early Detection Of Fires; Eskom Internal Research report TRR/E/97/EL120, Project 7755K403R, December 1997.

[40] van den Berg, CFK; Conducted HF Discharge Recognition Monitor - (TRI-ADD) Operational Guide, Report TRR/E/96/EL265; Project No 7755K101R; Eskom, Technology Research and Investigations; December 1996.

[41] Evert, C.R; RMS Level Detection Results For The Early Detection Of Fires; Eskom Internal Research report TRR/E/97/EL121, Project 7755K403R, December 1997.